Universidade de Aveiro Departamento de Química
Université Montpellier II Ecole Doctorale de Sciences Chimiques
2009

Guylhaine Clavel

Impurezas Magnéticas em Materiais Nanoestruturados

Magnetic Impurities in Nanostructured Materials

Universidade de Aveiro Departamento de Química
Université Montpellier II Ecole Doctorale de Sciences Chimiques
Ano 2009

Guylhaine Clavel

Impurezas Magnéticas em Materiais Nanoestruturados

Magnetic Impurities in Nanostructured Materials

Dissertação apresentada à Universidade de Aveiro para cumprimento dos requisitos necessários à obtenção do grau de Doutor em química, realizada sob a orientação científica dos Doutors Nicola Pinna e David Zitoun, Investigadore Coordenadore do Departamento de química da Universidade de Aveiro e Maître de conférences do equipe AIME da Université Montpellier II.

Dedicted to Frugu

o júri

presidente

Prof. João de Lemos Pinto
Professor catedrático da universidade de Aveiro

Prof. Bruno Chaudret
Directeur de recherches CNRS do Laboratoire de Chimie de Coordination de Toulouse

Prof. António Jorge Duarte de Castro Silvestre
Professor coordenador do Instituto Superior de Engenharia de Lisboa

Prof. André Vioux
Professor da Université de Montpellier II

Prof. Tito da Silva Trindade
Professor Associado com Agregação da universidade de Aveiro

Prof. Jacques Rozière
Professor da Université de Montpellier II

Prof. David Zitoun
Maître de conférences na Université de Montpellier II

Prof. Nicola Alessandro Pinna
Investigador coordenador do Laboratório Associado CICECO Universidade de Aveiro

agradecimentos

The works presented in this manuscript had begun at the Martin-Luther-University of Halle (Inorganic Chemistry, Germany) for five months and was then completed at the University of Aveiro (CICECO and Chemistry department, Portugal) in close collaboration with the University of Montpellier II (ICGM, Equipe AIME, France).

First and foremost, I would like to thank my supervisors Dr. Nicola Pinna and Dr. David Zitoun for giving me the opportunity to accomplish my PhD thesis; their support and guidance made my work possible. If it is useless to highlight their scientific qualities, I would like to say that I greatly appreciated their confidence, patience, enthusiasm, help, advice, friendship and understanding during these four years. Prof. Jacques Rozière is also acknowledged for tacking part of my PhD advisor board.

I am very grateful to Dr. Bruno Chaudret and Prof. António Jorge Silvestre for agreeing to be the external examiners and referees of my thesis and looked critically at my work. I also thank the other members of the examination committee, Prof. João Lemos Pinto, Prof. André Vioux and Dr. Tito Trindade, for contributing to the reviewing of this work.

I am indebted to people that contribute to this work; Dr. Serge Ravaine for sharing his secret about Langmuir-Blodgett technique and his welcoming at the CRPP of Bordeaux and Dr. Mato Knez (Max-Planck Institute, Halle) for the ALD deposition of ZnO. C. Reibel is acknowledged for technical assistance on EPR and SQUID measurements.

Dr. Marc Willinger has provided assistance in numerous ways; thank you for your help in microscopy and physics and also for your support, friendship and astonishing discussions. Be sure, I will miss you!

I would like also to thank the people from the group, in particular Andrea and Catherine for their contributions to the ZrO_2 study and ALD deposition, respectively, but also for their support. Good luck on the next steps.

Finally, thanks to the people that helped me in my daily life in Germany and in Portugal; Lilly, André, Paula, Penka and Marc (once again!). Special thank to Céline, who took care of me providing food and bed and support during the writing of this dissertation (keep it up; you will finish your thesis!).

This work received financial support from the Martin-Luther-University of Halle, CICECO (Centro de Investigação em Materiais Cerâmicos e Compósitos), FCT (Fundação para a Ciência e a Tecnologia) and FAME Network of Excellence.

palavras-chave

Óxidos magnéticos, Sol-gel não-hidrolitico, Semicondutores magnéticos diluídos, Hetero-estruturas, Nanopartículas, Films.

resumo

Os resultados apresentados aqui foram alcançados no âmbito do programa de doutoramento intitulado “Impurezas Magnéticas em Materiais Nano-estruturados”. O objectivo do estudo foi a síntese e caracterização de óxido contendo impurezas magnéticas. Durante este trabalho, sínteses de sol-gel não-aquoso têm sido desenvolvidos para a síntese de óxidos dopados com metais de transição (ZnO e ZrO_2). A dopagem uniforme é particularmente importante no estudo de semicondutores magnéticos diluídos (DMSs) e o ponto principal deste estudo foi verificar o estado de oxidação e a estrutura local do dopante e para excluir a existência de uma fase secundária como a origem do ferromagnetismo. Para alargar o âmbito da investigação e explorar plenamente o conceito de "impurezas magnéticas em materiais nanoestruturados" estudamos as propriedades de nanopartículas magnéticas dispersas em uma matriz de óxido. As nanopartículas (ferrita de cobalto) foram depositadas como um filme e cobertas com um óxido metálico semicondutor ou dielétrico (ZnO, TiO_2). Estes hetero-sistemas podem ser considerados como a dispersão de impurezas magnéticas em um óxido. As caracterizações exigidas por estes nanomateriais têm sido conduzidas na Universidade de Aveiro e Universidade de Montpellier, devido ao equipamento complementar.

keywords

Magnetic oxides, Non-hydrolytic sol-gel, Diluted magnetic semiconductors, Hetero-structures, Nanoparticles, Films.

abstract

The results presented here have been achieved under the PhD program entitled “Magnetic Impurities in Nanostructured Materials”. This study had as purpose the synthesis and characterization of oxidic semiconductor containing magnetic impurities. During this work we have developed non-aqueous sol-gel routes, leading to well controlled oxide nanomaterials, to the synthesis of transition-metal doped oxides (ZnO and ZrO_2). Homogeneous doping is particularly important in the comprehensive study of diluted magnetic semiconductors (DMSs), and the main point of this study was to ascertain the oxidation state and local structure of the dopant, as well as to exclude the existence of secondary phase as the origin of ferromagnetism. To enlarge the field of research and fully explore the concept of “magnetic impurities in nanostructured materials” we have studied the magnetic properties of nanoparticles embedded in an oxide matrix. The nanoparticles (cobalt ferrite) were deposited as a film and coated by a semiconducting or dielectric metal oxide (ZnO, TiO_2). These hetero-systems can be regarded as dispersion of magnetic impurities in oxides. The characterizations needed by these nanomaterials were performed at the University of Aveiro and University of Montpellier because of complementary available equipments.

Table of Contents

List of Figures

List of Tables

Acronyms & Symbols

List of Acronyms:

.

ALD	Atomic Layer Deposition.
BA	Benzyl Alcohol.
CVD	Chemical Vapor Deposition.
DMS	Diluted Magnetic Semiconductor.
EDX	Energy Dispersive X-ray Spectrometry.
EELS	Electron Energy Loss Spectroscopy.
GC-MS	Gas Chromatography-Mass Spectrometry.
HRTEM	High-Resolution Transmission Electron Microscopy.
ICP-AES	Inductively Coupled Plasma-Atomic Emission Spectrometry.
IR	InfraRed.
LB	Langmuir-Blodgett.
MBE	Molecular Beam Epitaxy.
NHSG	non-hydrolytic sol-gel.
NMR	Nuclear Magnetic Resonance.
NPs	Nanoparticles.
PLA	Pulsed Laser Ablation.
PLD	Pulsed Laser Deposition.

RT	Room temperature.
SAED	Select Area Electron Diffraction.
SEM	Scanning Electron Microscopy.
SPM	Surface Phonon Mode.
SV	Solid-Vapor process.
TEM	Transmission Electron Microscopy.
VSL	Vapor-Liquid-Solid process.
XRD	X-Ray Diffraction.
XRR	X-ray Reflectometry.
ZFC-ZC	Zero-field cooled - field cooled.

List of Symbols:

.

χ	Susceptibility.
μ_B	Bohr magneton, $\mu_B = 9.27400915\text{x}10^{-24}$ J.T^{-1}.
A	Hyperfine coupling constant, A(cm^{-1}) = gμ_Ba/hc.
a	Hyperfine splitting (T).
g	g-factor (dimensionless), hν = gμ_B.
Hc	Coercive field.
Ms	Magnetization at saturation.
T_B	Blocking temperature.
T_C	Curie temperature.

Introduction

Spin-transport electronics (spintronics) is an emerging field of electronics which aims to exploit the electron spin in addition to its charge. Spintronics promises to offer several advantages over traditional charge-based devices, for instance, improved information processing power, faster response, lower power consumption and increased levels of miniaturization.

The aim of the study presented in this thesis was the synthesis and characterization of materials that can be relevant to spintronics application, i.e. materials combining magnetic and semiconducting properties. We focused on oxides materials that were synthesized by soft chemistry routes and especially by non-hydrolytic sol-gel processes. We principally investigated diluted magnetic semiconductors (DMSs); a class of semiconductors for which a small fraction of the cations has been replaced by magnetic ions in order to make them magnetic. We made use of NHSG routes, leading to well controlled oxide, to the synthesis of transition-metal-doped ZnO and ZrO_2 which are both promising materials to obtain ferromagnetism at room temperature. Homogeneous doping is particularly important in the comprehensive study of DMSs, and the main point of theses works was to ascertain the local structure of the dopant to exclude the existence of secondary phase as the origin of magnetism. Beside the work on DMSs, we have studied the magnetic properties of hetero-structures materials composed of a film of magnetic nanoparticles embedded in an oxide matrix. The elaboration of hetero-system is another strategy for combining multiple properties and functionalities in a material. Here, the resulting films can be regarded as magnetic impurities, the nanoparticles, dispersed in an oxide.

The manuscript is organized as the following:

The first chapter starts with an overview of the field of spintronics and some generalities on diluted magnetic semiconductors. The chapter then concludes by an introduction to non-hydrolytic sol-gel. The results obtained during the PhD will be presented and discussed in four different chapters. Chapter II and III are allocated to the doping of ZnO by manganese and cobalt. The first part is devoted to the synthesis, the morphological and structural characterizations. The second part presents the assessments of the dopant environment and the magnetic results with a discussion on the influence of the solvent used during synthesis on the magnetic properties. Chapter IV deals with the doping of ZrO_2, its synthesis, characterizations and magnetic properties. Finally, the experimental results obtained on hetero-structures are given and discussed in chapter V. The materials studied are cobalt ferrite nanoparticles distributed into a semiconducting or dielectric film, namely ZnO or TiO_2. The synthesis of theses films has needed three distinct steps: (i) the synthesis of uniform magnetic nanoparticles, (ii) deposition of the particles as a film on substrate by Langmuir-blodgett technique and (iii) the covering of the particles by an oxide matrix deposited by atomic layer deposition (ALD).

Chapter I:

Introductive part

Contents

I.1 Spintronics and DMS

Electronics demands constantly more efficient and smaller devices motivated by the need to process and store information in greater quantities and at higher speed. However the constant miniaturization of conventional electronic devices begins to show the limits of traditional materials used, their highest performances being almost reached. This fact has stimulated intense researches in diverse fields in order to elaborate more efficient systems. The prospect of a new generation of electronic devices passes by the search for alternative materials that possess better performance or higher potential of miniaturization, and by the development of multifunctional devices. Among the potential technologies to provide new devices, spintronics has many advantages.

I.1.1 Spintronics

Basically, in conventional electronics, the information is encoded and manipulated by the electron charge while data are stored magnetically. Spintronics exploits the spin of electron rather than its charge. Thus, based on spin-polarized current, spintronics offers the possibility to combine the computing power of semiconductor technology and the storage capacity of magnetic memory together on the same device. Additionally, spin can be manipulated by magnetic and electric field but also optically, offering new perspectives. Furthermore, as spin results from quantum mechanics, no limit to miniaturization is foreseen while for traditional materials the problem of quantum tunneling, resulting in leakage currents, increases as sizes become smaller. For same reasons, spintronic components can be good candidates for quantum computation. All in all, using the spin as a new degree of freedom alone or in addition to the electron charge will add significantly more capability and performance to electronic products[1–7].

The beginning of spintronics goes back to the discovery of giant magnetoresistance (GMR) in metallic multilayer at the end of the 80s[8,9]. GMR-based systems as spin valve and later on magnetic tunneling junction (based on tunneling magnetoresistance

(TMR)) have demonstrated the interest that represents the manipulation of itinerant polarized electrons in magnetic materials, finding rapidly applications in magnetic sensors, hard-disk read heads and MRAM (magnetic random access memory). Albert Fert and Peter Grünberg, who discovered GMR phenomena, received the Nobel Prize in physics in 2007 for the technological breakthrough that represents GMR in today's electronics[4,10]. The next generation of spintronic devices is expected to be based on semiconductor materials, in order to use the potential of spin in processing techniques and obtain in the future an electronics wholly based on spin. However to do so, major challenges have to be addressed and overcome such as injection, transport, manipulation, long coherence times and detection of spin[1,4,5,7,11–14]. Indeed, first spin-polarized current (electrons that are predominantly in a spin-aligned state "up"or "down") has to be produced. Then, the itinerant spins need to be transferred efficiently across interfaces between different semiconductor materials. This transfer must proceed without appreciable loss of spin polarization. Finally their polarization must be preserved long enough for the desired operation to be carried out.

A variety of new materials must be found to meet the different demands[7,11,15]. Robust spin polarization arises naturally in ferromagnetic materials, which can serve as a stable source of spin-polarized carriers. In particular, half-metallic ferromagnets, such as chromium dioxide, Heusler alloys, magnetite and some manganites or double perovskites, are of special interest[5,11]. Indeed, these materials have only one occupied spin direction at the Fermi level giving rise to 100% polarization. Semiconducting and magnetic properties coexist in magnetic semiconductors (see next section). If they could be used as a spin injector (instead of metallic ferromagnets) into a nonmagnetic semiconductor it would facilitate the integration of spintronics in traditional semiconductor-based electronics; they will overcome the problem of conductivity mismatch encountered between metal and semiconductors[16]. Other interesting materials for spintronics are multiferroics[15,17–19]. These materials display both electrical and magnetic orders that can be connected through strong magneto-electric effect giving the possibility

of inducting and controlling the polarization by a magnetic field or the magnetization by an electric field. Thus multiferroics are foreseen for electric field-controlled magnetic data recording. Alternatively, there is also increasing researches on controlling spin-polarization on non-magnetic semiconductor through spin-orbit coupling[20] (spintronics without magnetism) and on molecular materials[21–23].

I.1.2 (Diluted) magnetic semiconductors

Magnetic semiconductors (MS) are materials that exhibit both magnetic and semiconducting properties. MS is key to the development of spintronic devices such as non-volatile memories, spin valve transistors, optical switches, spin-FETs and spin-LEDs[1,7,14,24,25]. Encouraged by the realization of such devices[26–35], the study of MS gave rise to intensive research activities. Requirements for functional MS are: ferromagnetic properties at room temperature (Curie temperature must be superior to 500 K[36]), possibility of n- and p-type semiconducting behaviors and the ferromagnetic properties should be mediated by carriers. Furthermore, they should be compatible to existing semiconductor to be readily integrated.

Natural ferromagnetic semiconductors do exist but are scarce. For example europium and chromium chalcogenides present both properties; unfortunately they possess a low Curie temperature[37,38]. Furthermore the majority of native ferromagnetic semiconductors are difficult to grow and their crystal structures are very different from traditional semiconductors (Si and GaAs)[11,39]. Semiconductors are commonly doped by impurities to tune their properties. The same approach can be follow to make them magnetic, i.e. by doping with magnetic impurities[39,40]. These materials, called diluted magnetic semiconductors (DMSs), are typically II-VI or III-V semiconductors in which a small fraction of their cations have been randomly substituted by magnetic ions such as transition-metal ions (Fig.1).

DMS based on II-VI and IV-VI semiconductors have been widely studied in the 80s; however these materials mainly present paramagnetic, spin-glass or antiferromagnetic

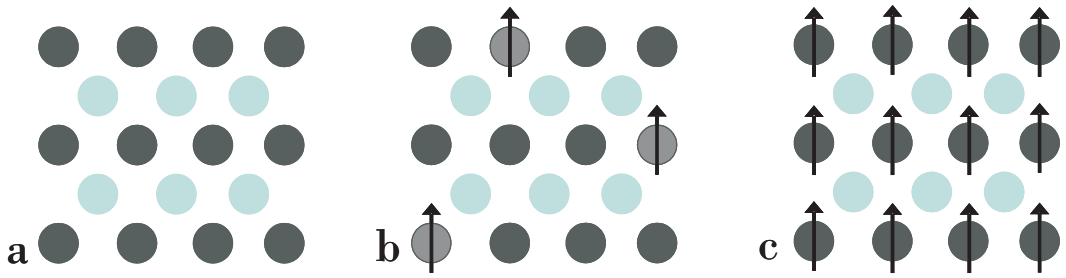

Figure I.1: Schematic representation of a) a non-magnetic semiconductor, b) a diluted magnetic semiconductors made from a non-magnetic semiconductor doped by magnetic elements and c) a magnetic semiconductor which contains periodic array of magnetic elements.

behaviors[40,41]. The study of III-V DMS some years later led to the achievement of ferromagnetic compounds[39,42] but their low Curie temperature prevents them to be used for application (i.e. at room temperature). The revival of this already old field mainly occurs due to the assumption that ferromagnetism is actually promoted by the semiconductor charge carriers and that room temperature ferromagnetism can be reached. Indeed, in an extremely quoted paper Dietl et al. proposed, based on the so-called Zener model, that the wide band-gaps GaN and ZnO doped by manganese would be ferromagnetic with a Curie temperature exceeding room temperature[43]. Additional advantages for the investigation of ZnO and GaN as DMSs are their optoelectronic properties, their possible readily incorporation in existing semiconductor technology and an encouragingly long spin coherence time of their undoped counterpart[25,44,45]. Since the prediction of Dietl et al in 2000, a lot of theoretical[46–52] and experimental works were published on zinc oxide[41,53–57] and gallium nitride[25,58–60]. Furthermore, these materials have led to the investigation of other oxides[36,55,61–64]. In particular, TiO_2 have attracted much attention due to the achievement of room temperature ferromagnetism[58,65].

However the search of high temperature DMS have led to contrasted results. While significant progress has been made in the synthesis and improvement of semiconducting and magnetic properties of these compounds, questions remain; especially significant controversy exists over the origin of ferromagnetism in DMS. First, the discrepancy on

the reported Curie temperature of DMS implies problem of reproducibility, contamination and/or magnetic secondary phase separation and the doubt is placed on the nature, intrinsic or extrinsic, of the ferromagnetism[36,41] (see also introduction of chapter III). The second major concern is about the mechanism relative to the magnetic interactions present in such materials. The type of exchange mechanism which stabilizes the ferromagnetic phase is not well understood and the link between carrier concentration and ferromagnetism has not yet been clearly established[36,46,48,54,62]. In fact, the magnetic properties in such alloys are not trivial especially for highly diluted materials in which the distance between magnetic atoms is enormous. The ferromagnetic properties of DMSs result from a spin interaction between the electrons or holes in the sp bands of the semiconductor host and those of the localized d shells of the magnetic impurities. The collective interaction of atomic magnetic moments, responsible for magnetic order, can arise from one or several types of indirect exchange interactions such as double exchange interaction, RKKY interaction (like in metals) or Zener mechanism. The latest two are carriers-mediated interactions over relatively large distances. Based on these possible interactions, different models have been proposed to account for the magnetic behaviors of DMSs. For example, we can cite the Zener, impurity band and bound magnetic polarons model[25,43,46,48,62,66,67].

I.2 The non-hydrolytic sol-gel

I.2.1 Sol-gel and non-hydrolytic sol-gel syntheses

Sol-gel processes have successfully been used for several decades for the synthesis of bulk oxides as well as films, fibers and particles[68,69]. Advantages such as a low process temperature, homogeneity of multi-component systems and the possibility of easy shape processing explain the high scientific interest in sol-gel approaches. Because the rates of the hydrolysis and condensation steps determine the nature (gel, colloids or particles), size and shape of the final compound, both reactions have been extensively studied[68,69].

While the sol-gel approach is extremely successful in the case of silica, it is less attractive for the synthesis of transition metal oxides. This drawback mainly arises from the fact that transition metal oxide precursors are generally much more reactive towards water, resulting in a loss of control over the size and shape of metal oxides[68]. Different strategies, such as the use of alternative water sources[70–72] and/or the reduction of the precursor reactivity by chemical modification[73] were developed in order to overcome this problem.

During the last decade, the use of non-aqueous conditions, called non-hydrolytic sol-gel (NHSG) or non-aqueous sol-gel, has proven to be an elegant alternative approach. It eliminates the main drawbacks of aqueous sol-gel chemistry and offers advantages such as high reproducibility and a better control of the composition and homogeneity of multi-component oxides[74–77]. These non-aqueous routes were extensively applied to the synthesis of nanoparticles because the as-synthesized oxides are generally characterized by a high crystallinity[78,79]. Furthermore, the process offers the ability to control the crystal growth without the use of any additional ligands[76–81].

I.2.2 Reaction mechanism

In NHSG approaches, the M-O-M bonds of the oxide are formed without a hydrolysis step and the oxygen is provided by other molecular species such as alcohols, ethers or metal alkoxides[74,76,77,81]. As NHSG involves the cleavage of a carbon-oxygen bond, the chemistry of these processes is based on reactions at the frontier of organic and inorganic chemistries[82].

The synthesis of metal oxides based on NHSG routes can be divided into two classes: In the first, the formation of the metal oxide network involves only a condensation step. This is achieved by a reaction between the ligands coordinated to two different metal centers as described by the reaction schemes given in Eq. 1-3 (Fig.1). The M-O-M bond formation directly takes place under the elimination of organic molecules. The alkyl halide elimination (Eq. 1) was the first NHSG reaction introduced for the formation

of metal oxides and it is probably the most studied one. The ether elimination (Eq. 2) takes place during the direct condensation of two metal alkoxides and the ester elimination (Eq. 3) involves the condensation between metal carboxylates and alkoxides. It is important to notice that in the case of these direct condensation reactions no intermediate formation of an OH group is involved.

The second class of reactions based on NHSG engages the reaction between a metal precursor and an organic solvent. In fact, the most common metal complexes, namely, metal halides, alkoxides, carboxylates, and diketonates, react with common organic solvents such as alcohols, ethers, ketones, aldehydes, anhydrides, carboxylic acids, and amines. A classification of the different possible mechanisms involved[76,77,79,80] can be made according to the following general trends: (i) The metal precursors react with the solvent by a ligand exchange, followed by one of the condensation reaction given in figure 1. (ii) The solvolysis of the metal complex leads to the formation of a hydroxyl group (non-hydrolytic hydroxylation reactions[74]) which further reacts with a metal precursor or another hydroxyl group forming M-O-M bonds. (iii) Finally, more complex mechanisms such as Guerbet-like reactions or aldol condensations can take place. These reactions imply several steps and/or require a concerted mechanism of many molecular species. They have recently been evidenced in the formation of several metal oxides[80].

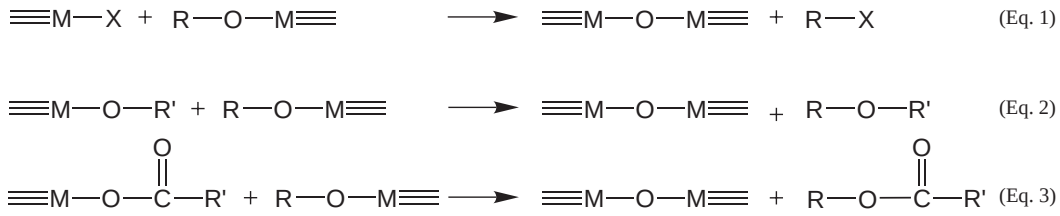

Figure I.2: Condensation steps leading to M-O-M bond formation in NHSG processes. Eq. 1) Alkyl halide elimination, Eq. 2) ether elimination, Eq. 3) ester elimination. X stands in for halide species, R and R' indicate alkyl groups.

I.2.3 Non-hydrolytic sol-gel and doping

As we said before, an advantage of non-hydrolytic sol-gel processes, especially in comparison to aqueous systems, is the accessibility of multi-metal oxide nanoparticles [76,77,79]. One reason is that, in general, the reactivity of metal oxide precursors is significantly reduced under water exclusion, allowing to control the metal oxide formation and more importantly, makes easier to match the reactivity of different metal precursors to obtain single-phase multi-component oxides. In addition, the large number of available precursors and organic solvents offers many possible combinations for the synthesis of a specific system. As a matter of fact, non-hydrolytic sol-gel has been successfully employed for the synthesis of various binary, ternary and multi-metal oxides such as $BaTiO_3$, $InNbO_4$, $ZnGa_2O_4$, $NaNbO_3$, $NaTaO_3$, $BaZrO_3$, $SrTiO_3$, and $(Ba,Sr)TiO_3$ [77,79]. Therefore, this approach appears particularly promising for the synthesis of doped oxide nanoparticles.

As a typical example, solid solution of indium tin oxide nanoparticles, for a large range of compositions, could be synthesized in benzyl alcohol starting from Sn(IV) alkoxides and In(III) acetylacetonate [83,84]. The same could not be achieved using In(III) alkoxides instead, because the different reactivity of the two metal complexes does not permit the formation of a solid solution [84,85]. It is important to note that, unfortunately, it is not yet possible to predict the reactivity of metal complexes in a particular solvent as the metal oxide formation is influenced by various additional effects such as intermediate products formed during the reaction, side reactions and catalytic effects of the metal centers, the metal oxide seeds and early formed nanoparticles.

I.2.4 Non-hydrolytic sol-gel in atomic layer deposition

Atomic Layer Deposition (ALD) is a form of chemical vapor deposition (CVD) in which the reaction between precursor materials is separated into successive surface reactions. In this manner, the precursor materials are kept separate until the adsorbed species

react at the surface in a self-limiting process[86–88], i.e. without the presence of a gas phase reaction. As a consequence, ALD offers excellent surface conformity. Inherent to the process, is the possibility to accurately control the thickness of the deposited film at almost atomic level simply by counting the number of deposition cycles. Finally, ALD is an elegant and versatile procedure for the formation of oxide thin films.

Usually, ALD of metal oxides involves the reaction of a metal oxide precursor with an oxygen source. Water is the most commonly used oxygen source and it is generally admitted that water hydrolyzes the surface molecular species which results, at reasonable temperature, in the formation of -OH groups[89–91]. The resulting hydroxyl groups will further react with the metal oxide precursors supplied by a new pulse forming the M-O-M bond. Therefore, the formation of the oxide is obtained through hydrolysis and condensation steps as in traditional sol-gel process used in solution. Recently, inspired by the success of nonaqueous sol-gel, similar nonaqueous conditions were developed in[92–97]. An exhaustive list of nonaqueous sol-gel approaches applied to ALD can be found in Table 1 of Ref[98]. It is interesting to note that similar chemistry is responsible for the metal oxide formation in ALD and in solution[95,97–100].

However, notable differences have to be pointed out. First of all, the nature of reactions is obviously different. In sol-gel, the reactions occurring in solution are step growth condensation polymerizations. The precursor-monomers and already-formed dimers and oligomers condense to give larger colloidal species under the elimination of simple molecules. In ALD, the metal oxide growth is based on subsequent self-terminating heterogeneous reactions between the surface species and the monomers coming from the gas phase. The latter thereby undergo irreversible chemisorption. Another important difference concerns the time scales of these two processes. Non-hydrolytic conditions were introduced in sol-gel chemistry because the reactions are slow and therefore allow better control of the metal oxide formation. On the contrary, in ALD, fast reactions are sought after in order to obtain short deposition times. Although this suggests that non-hydrolytic conditions are not favorable for ALD of metal

oxides, they bring some important benefits. Notably, they were firstly proposed with the aim of reducing the growth of an interfacial layer (silica or silicates) in the case of metal oxides grown on silicon[95]. In NHSG reactions, the metal oxide formation can in certain cases be achieved without intermediate formation of hydroxyl groups. Finally, the growth per cycle can be twice as large as compared to traditional depositions since both reactants can contain a metal center[95].

Bibliography

[1] D. D. Awschalom, M. E. Flatte, "Challenges for Semiconductor Spintronics", *Nat. Phys.*, **3**, 153 (2007). http://dx.doi.org/10.1038/nphys551. 5, 6, 7

[2] P. Ball, "Meet the Spin Doctors...", *Nature*, **404**, 918 (2000). http://dx.doi.org/10.1038/35010132. 5

[3] C. Chappert, A. Fert, F. N. Van Dau, "The Emergence of Spin Electronics in Data Storage", *Nat. Mater.*, **6**, 813 (2007). http://dx.doi.org/10.1038/nmat2024. 5

[4] A. Fert, "Nobel Lecture: Origin, Development, and Future of Spintronics", *Rev. Mod. Phys.*, **80**, 1517 (2008). http://dx.doi.org/10.1103/RevModPhys.80.1517. 5, 6

[5] G. A. Prinz, "Magnetoelectronics", *Science*, **282**, 1660 (1998). http://dx.doi.org/10.1126/science.282.5394.1660. 5, 6

[6] M. L. Roukes, "Electronics in a Spin", *Nature*, **411**, 747 (2001). http://dx.doi.org/10.1038/35081213. 5

[7] S. A. Wolf, D. D. Awschalom, R. A. Buhrman, J. M. Daughton, S. von Molnar, M. L. Roukes, A. Y. Chtchelkanova, D. M. Treger, "Spintronics: A Spin-Based Electronics Vision for the Future", *Science*, **294**, 1488 (2001). http://dx.doi.org/10.1126/science.1065389. 5, 6, 7

[8] M. N. Baibich, J. M. Broto, A. Fert, F. N. Van Dau, F. Petroff, P. Etienne, G. Creuzet, A. Friederich, J. Chazelas, "Giant Magnetoresistance of (001)Fe/(001)Cr Magnetic Superlattices", *Phys. Rev. Lett.*, **61**, 2472 (1988). http://dx.doi.org/10.1103/PhysRevLett.61.2472. 5

[9] G. Binasch, P. Grunberg, F. Saurenbach, W. Zinn, "Enhanced Magnetoresistance in Layered Magnetic Structures with Antiferromagnetic Interlayer Exchange", *Phys. Rev. B*, **39**, 4828 (1989). http://dx.doi.org/10.1103/PhysRevB.39.4828. 5

[10] P. A. Grunberg, "Nobel Lecture: From Spin Waves to Giant Magnetoresistance and Beyond", *Rev. Mod. Phys.*, **80**, 1531 (2008). http://dx.doi.org/10.1103/RevModPhys.80.1531. 6

[11] C. Felser, G. H. Fecher, B. Balke, "Spintronics: A Challenge for Materials Science and Solid-State Chemistry", *Angew. Chem., Int. Ed.*, **46**, 668 (2007). http://dx.doi.org/10.1002/anie.200601815. 6, 7

[12] I. Malajovich, J. J. Berry, N. Samarth, D. D. Awschalom, "Persistent Sourcing of Coherent Spins for Multifunctional Semiconductor Spintronics", *Nature*, **411**, 770 (2001). http://dx.doi.org/10.1038/35081014. 6

[13] M. Oestreich, "Materials Science: Injecting Spin into Electronics", *Nature*, **402**, 735 (1999). http://dx.doi.org/10.1038/45406. 6

[14] I. Zutic, J. Fabian, S. D. Sarma, "Spintronics: Fundamentals and applications", *Rev. Mod. Phys.*, **76**, 323 (2004). http://dx.doi.org/10.1103/RevModPhys.76.323. 6, 7

[15] M. Bibes, A. Barthelemy, "Oxide Spintronics", *IEEE T. Electron. Dev.*, **54**, 1003 (2007). http://dx.doi.org/10.1109/TED.2007.894366. 6

[16] G. Schmidt, D. Ferrand, L. W. Molenkamp, A. T. Filip, B. J. van Wees, "Fundamental Obstacle for Electrical Spin Injection from a Ferromagnetic Metal into a Diffusive Semiconductor", *Phys. Rev. B*, **62**, R4790 (2000). http://dx.doi.org/10.1103/PhysRevB.62.R4790. 6

[17] C. Binek, B. Doudin, "Magnetoelectronics with Magnetoelectrics", *J. Phys.: Condens. Matter*, **17**, L39 (2005). http://dx.doi.org/10.1088/0953-8984/17/2/L06. 6

[18] M. Gajek, M. Bibes, S. Fusil, K. Bouzehouane, J. Fontcuberta, A. Barthelemy, A. Fert, "Tunnel Junctions with Multiferroic Barriers", *Nat. Mater.*, **6**, 296 (2007). http://dx.doi.org/10.1038/nmat1860. 6

[19] R. Ramesh, N. A. Spaldin, "Multiferroics: Progress and Prospects in Thin Films", *Nat. Mater.*, **6**, 21 (2007). http://dx.doi.org/10.1038/nmat1805. 6

[20] D. Awschalom, N. Samarth, "Spintronics Without Magnetism", *Physics*, **2**, 50 (2009). http://dx.doi.org/10.1103/Physics.2.50. 7

[21] M. Affronte, "Molecular Nanomagnets for Information Technologies", *J. Mater. Chem.*, **19**, 1731 (2009). http://dx.doi.org/10.1039/b809251f. 7

[22] J. Camarero, E. Coronado, "Molecular vs. Inorganic Spintronics: the Role of Molecular Materials and Single Molecules", *J. Mater. Chem.*, **19**, 1678 (2009). http://dx.doi.org/10.1039/b819594n. 7

[23] J. Ferrer, V. M. Garcia-Suarez, "From Microelectronics to Molecular Spintronics: an Explorer's Travelling Guide", *J. Mater. Chem.*, **19**, 1696 (2009). http://dx.doi.org/10.1039/b810617g. 7

[24] Y. Ohno, F. Matsukura, H. Ohno, "Semiconductor Spin Electronics", *JSAP International*, **5**, 4 (2002). http://www.jsapi.jsap.or.jp/number05.html. 7

[25] C. Liu, F. Yun, H. Morkoc, "Ferromagnetism of ZnO and GaN: A Review", *J. Mater. Sci.: Mater. Electron.*, **16**, 555 (2005). http://dx.doi.org/10.1007/s10854-005-3232-1. 7, 8, 9

[26] S. Datta, B. Das, "Electronic Analog of the Electro-optic Modulator", *Appl. Phys. Lett.*, **56**, 665 (1990). http://dx.doi.org/10.1063/1.102730. 7

[27] M. Tanaka, Y. Higo, "Large Tunneling Magnetoresistance in GaMnAs /AlAs /GaMnAs Ferromagnetic Semiconductor Tunnel Junctions", *Phys. Rev. Lett.*, **87**, 026602 (2001). http://dx.doi.org/10.1103/PhysRevLett.87.026602. 7

[28] Y. Ohno, D. K. Young, B. Beschoten, F. Matsukura, H. Ohno, D. D. Awschalom, "Electrical Spin Injection in a Ferromagnetic Semiconductor Heterostructure", *Nature*, **402**, 790 (1999). http://dx.doi.org/10.1038/45509. 7

[29] D. Chiba, F. Matsukura, H. Ohno, "Electrical Magnetization Reversal in Ferromagnetic III-V Semiconductors", *Journal of Physics D: Applied Physics*, **39**, R215 (2006). http://dx.doi.org/10.1088/0022-3727/39/13/R01. 7

[30] D. Chiba, M. Yamanouchi, F. Matsukura, H. Ohno, "Electrical Manipulation of Magnetization Reversal in a Ferromagnetic Semiconductor.", *Science*, **301**, 943 (2003). http://dx.doi.org/10.1126/science.1086608. 7

[31] T. Gruber, M. Keim, R. Fiederling, G. Reuscher, W. Ossau, G. Schmidt, L. W. Molenkamp, A. Waag, "Electron Spin Manipulation using Semimagnetic Resonant Tunneling Diodes", *Appl. Phys. Lett.*, **78**, 1101 (2001). http://link.aip.org/link/?APL/78/1101/1. 7

[32] F. Matsukura, D. Chiba, T. Omiya, E. Abe, T. Dietl, Y. Ohno, K. Ohtani, H. Ohno, "Control of Ferromagnetism in Field-Effect Transistor of a Magnetic Semiconductor", *Physica E*, **12**, 351 (2002). http://dx.doi.org/10.1016/S1386-9477(01)00275-2. 7

[33] R. Fiederling, M. Keim, G. Reuscher, W. Ossau, G. Schmidt, A. Waag, L. W. Molenkamp, "Injection and Detection of a Spin-Polarized Current in a Light-Emitting Diode", *Nature*, **402**, 787 (1999). http://dx.doi.org/10.1038/45502. 7

[34] S. Chakrabarti, M. A. Holub, P. Bhattacharya, T. D. Mishima, M. B. Santos, M. B. Johnson, D. A. Blom, "Spin-Polarized Light-Emitting Diodes with Mn-Doped InAs Quantum Dot Nanomagnets as a Spin Aligner", *Nano Lett.*, **5**, 209 (2004). http://dx.doi.org/10.1021/nl048613n. 7

[35] G. Kioseoglou, A. T. Hanbicki, J. M. Sullivan, O. M. J. van 't Erve, C. H. Li, S. C. Erwin, R. Mallory, M. Yasar, A. Petrou, B. T. Jonker, "Electrical Spin Injection from an n-type Ferromagnetic Semiconductor into a III-V Device Heterostructure", *Nat. Mater.*, **3**, 799 (2004). http://dx.doi.org/10.1038/nmat1239. 7

[36] J. Coey, "Dilute Magnetic Oxides", *Curr. Opin. Solid State Mater. Sci.*, **10**, 83 (2006). http://dx.doi.org/10.1016/j.cossms.2006.12.002. 7, 8, 9

[37] P. K. Baltzer, P. J. Wojtowicz, M. Robbins, E. Lopatin, "Exchange Interactions in Ferromagnetic Chromium Chalcogenide Spinels", *Phys. Rev.*, **151**, 367 (1966). http://dx.doi.org/10.1103/PhysRev.151.367. 7

[38] M. D. Regulacio, K. Bussmann, B. Lewis, S. L. Stoll, "Magnetic Properties of Lanthanide Chalcogenide Semiconducting Nanoparticles", *J. Am. Chem. Soc.*, **128**, 11173 (2006). http://dx.doi.org/10.1021/ja0620080. 7

[39] H. Ohno, "Making Nonmagnetic Semiconductors Ferromagnetic", *Science*, **281**, 951 (1998). http://dx.doi.org/10.1126/science.281.5379.951. 7, 8

[40] J. K. Furdyna, "Diluted Magnetic Semiconductors", *J. Appl. Phys.*, **64**, R29 (1988). http://dx.doi.org/10.1063/1.341700. 7, 8

[41] R. Seshadri, "Zinc Oxide-Based Diluted Magnetic Semiconductors", *Curr. Opin. Solid State Mater. Sci.*, **9**, 1 (2005). http://dx.doi.org/10.1016/j.cossms.2006.03.002. 8, 9

[42] H. Ohno, H. Munekata, T. Penney, S. von Molnar, L. L. Chang, "Magnetotransport Properties of p-type (In,Mn)As Diluted Magnetic III-V Semiconductors", *Phys. Rev. Lett.*, **68**, 2664 (1992). http://dx.doi.org/10.1103/PhysRevLett.68.2664. 8

[43] T. Dietl, H. Ohno, F. Matsukura, J. Cibert, D. Ferrand, "Zener Model Description of Ferromagnetism in Zinc-Blende Magnetic Semiconductors", *Science*, **287**, 1019 (2000). http://dx.doi.org/10.1126/science.287.5455.1019. 8, 9

[44] B. Beschoten, E. Johnston-Halperin, D. K. Young, M. Poggio, J. E. Grimaldi, S. Keller, S. P. DenBaars, U. K. Mishra, E. L. Hu, D. D. Awschalom, "Spin Coherence and Dephasing in GaN", *Phys. Rev. B*, **63**, 121202 (2001). http://dx.doi.org/10.1103/PhysRevB.63.121202. 8

[45] S. Ghosh, D. W. Steuerman, B. Maertz, K. Ohtani, H. Xu, H. Ohno, D. D. Awschalom, "Electrical Control of Spin Coherence in ZnO", *Appl. Phys. Lett.*, **92**, 162109 (2008). http://dx.doi.org/10.1063/1.2913049. 8

[46] T. Dietl, "Origin and Control of Ferromagnetism in Dilute Magnetic Semiconductors and Oxides (invited)", *J. Appl. Phys.*, **103**, 07D111 (2008). http://dx.doi.org/10.1063/1.2832613. 8, 9

[47] T. Chanier, M. Sargolzaei, I. Opahle, R. Hayn, K. Koepernik, "LSDA + U versus LSDA: Towards a Better Description of the Magnetic Nearest-neighbor Exchange Coupling in Co- and Mn-doped ZnO", *Phys. Rev. B*, **73**, 134418 (2006). http://dx.doi.org/10.1103/PhysRevB.73.134418. 8

[48] J. M. D. Coey, M. Venkatesan, C. B. Fitzgerald, "Donor Impurity Band Exchange in Dilute Ferromagnetic Oxides", *Nat. Mater.*, **4**, 173 (2005). http://dx.doi.org/10.1038/nmat1310. 8, 9

[49] K. Sato, H. Katayama-Yoshida, "First Principles Materials Design for Semiconductor Spintronics", *Semicond. Sci. Technol.*, **17**, 367 (2002). http://dx.doi.org/10.1088/0268-1242/17/4/309. 8

[50] N. A. Spaldin, "Search for Ferromagnetism in Transition-metal-doped Piezoelectric ZnO", *Phys. Rev. B*, **69**, 125201 (2004). http://dx.doi.org/10.1103/PhysRevB.69.125201. 8

[51] A. Walsh, J. L. F. D. Silva, S.-H. Wei, "Theoretical Description of Carrier Mediated Magnetism in Cobalt Doped ZnO", *Phys. Rev. Lett.*, **100**, 256401 (2008). http://dx.doi.org/10.1103/PhysRevLett.100.256401. 8

[52] Q. Wang, Q. Sun, P. Jena, Y. Kawazoe, "Carrier-mediated Ferromagnetism in N Codoped (Zn,Mn)O $(10\overline{1}0)$ Thin Films", *Phys. Rev. B*, **70**, 052408 (2004). http://dx.doi.org/10.1103/PhysRevB.70.052408. 8

[53] U. Ozgur, I. A. Ya, C. Liu, A. Teke, M. A. Reshchikov, S. Dogan, V. Avrutin, S. J. Cho, H. Morkoc, "A Comprehensive Review of ZnO Materials and Devices", *J. Appl. Phys.*, **98**, 041301 (2005). http://dx.doi.org/10.1063/1.1992666. 8

[54] S. Chambers, T. Droubay, C. Wang, K. Rosso, S. Heald, D. Schwartz, K. Kittilstved, D. Gamelin, "Ferromagnetism in Oxide Semiconductors", *Mater. Today*, **9**, 28 (2006). http://dx.doi.org/10.1016/S1369-7021(06)71692-3. 8, 9

[55] T. Fukumura, H. Toyosaki, Y. Yamada, "Magnetic Oxide Semiconductors", *Semicond. Sci. Technol.*, **20**, S103 (2005). http://dx.doi.org/10.1088/0268-1242/20/4/012. 8

[56] K. R. Kittilstved, W. K. Liu, D. R. Gamelin, "Electronic Structure Origins of Polarity-Dependent High-T_C Ferromagnetismin Oxide-Diluted Magnetic Semiconductors", *Nat. Mater.*, **5**, 291 (2006). http://dx.doi.org/10.1038/nmat1616. 8

[57] M. Snure, D. Kumar, A. Tiwari, "Progress in ZnO-based Diluted Magnetic Semiconductors", *J. Miner. Met. Mater. Soc.*, **61**, 72 (2009). http://dx.doi.org/10.1007/s11837-009-0092-9. 8

[58] S. A. Chambers, "Ferromagnetism in Doped Thin-Film Oxide and Nitride Semiconductors and Dielectrics", *Surf. Sci. Rep.*, **61**, 345 (2006). http://dx.doi.org/10.1016/j.surfrep.2006.05.001. 8

[59] A. Bonanni, "Ferromagnetic Nitride-based Semiconductors Doped with Transition Metals and Rare Earths", *Semicond. Sci. Technol.*, **22**, R41 (2007). http://dx.doi.org/10.1088/0268-1242/22/9/R01. 8

[60] S. J. Pearton, C. R. Abernathy, G. T. Thaler, R. M. Frazier, D. P. Norton, F. Ren, Y. D. Park, J. M. Zavada, I. A. Buyanova, *et al.*, "Wide Bandgap GaN-based Semiconductors for Spintronics", *J. Phys.: Condens. Matter*, **16**, R209 (2004). http://dx.doi.org/10.1088/0953-8984/16/7/R03. 8

[61] M. Calderon, S. D. Sarma, "Theory of Carrier Mediated Ferromagnetism in Dilute Magnetic Oxides", *Annals of Physics*, **322**, 2618 (2007). http://dx.doi.org/10.1016/j.aop.2007.01.010. 8

[62] S. J. Pearton, W. H. Heo, M. Ivill, D. P. Norton, T. Steiner, "Dilute Magnetic Semiconducting Oxides", *Semicond. Sci. Technol.*, **19**, R59 (2004). http://dx.doi.org/10.1088/0268-1242/19/10/R01. 8, 9

[63] W. Prellier, A. Fouchet, B. Mercey, "Oxide-Diluted Magnetic Semiconductors: A Review of the Experimental Status", *J. Phys.: Condens. Matter*, **15**, R1583 (2003). http://dx.doi.org/10.1088/0953-8984/15/37/R01. 8

[64] J. Philip, A. Punnoose, B. I. Kim, K. M. Reddy, S. Layne, J. O. Holmes, B. Satpati, P. R. LeClair, T. S. Santos, J. S. Moodera, "Carrier-Controlled Ferromagnetism in Transparent Oxide Semiconductors", *Nat. Mater.*, **5**, 298 (2006). http://dx.doi.org/10.1038/nmat1613. 8

[65] R. Janisch, P. Gopal, N. A. Spaldin, "Transition Metal-doped TiO_2 and ZnO - Present Status of the Field", *J. Phys.: Condens. Matter*, **17**, R657 (2005). http://dx.doi.org/10.1088/0953-8984/17/27/R01. 8

[66] T. Dietl, H. Ohno, F. Matsukura, "Hole-mediated ferromagnetism in tetrahedrally coordinated semiconductors", *Phys. Rev. B*, **63**, 195205 (2001). http://dx.doi.org/10.1103/PhysRevB.63.195205. 9

[67] B. W. Wessels, "Ferromagnetic Semiconductors and the Role of Disorder", *New J. Phys.*, **10**, 055008 (2008). http://dx.doi.org/10.1088/1367-2630/10/5/055008. 9

[68] J. Livage, M. Henry, C. Sanchez, "Sol-gel chemistry of transition metal oxides", *Prog. Solid State Chem.*, **18**, 259 (1988). http://dx.doi.org/10.1016/0079-6786(88)90005-2. 9, 10

[69] L. L. Hench, J. K. West, "The Sol-Gel Process", *Chem. Rev.*, **90**, 33 (1990). http://dx.doi.org/10.1021/cr00099a003. 9

[70] H. Kominami, M. Kohno, Y. Takada, M. Inoue, T. Inui, Y. Kera, "Hydrolysis of Titanium Alkoxide in Organic Solvent at High Temperatures: A New Synthetic Method for Nanosized, Thermally Stable Titanium(IV) Oxide", *Ind. Eng. Chem. Res.*, **38**, 3925 (1999). http://dx.doi.org/10.1021/ie9901170. 10

[71] M. Ivanda, S. Music, S. Popovic, M. Gotic, "XRD, Raman and FT-IR Spectroscopic Observations of Nanosized TiO_2 Synthesized by the Sol-Gel Method based on an Esterification Reaction", *J. Mol. Struct.*, **480-481**, 645 (1999). http://dx.doi.org/10.1016/S0022-2860(98)00783-2. 10

[72] M. Monge, M. L. Kahn, A. Maisonnat, B. Chaudret, "Room-Temperature Organometallic Synthesis of Soluble and Crystalline ZnO Nanoparticles of Controlled Size and Shape", *Angew. Chem., Int. Ed.*, **42**, 5321 (2003). http://dx.doi.org/10.1002/anie.200351949. 10

[73] C. Sanchez, J. Livage, M. Henry, F. Babonneau, "Chemical Modification of Alkoxide Precursors", *J. Non-Cryst. Solids*, **100**, 65 (1988). http://dx.doi.org/10.1016/0022-3093(88)90007-5. 10

[74] A. Vioux, "Nonhydrolytic Sol-Gel Routes to Oxides", *Chem. Mater.*, **9**, 2292 (1997). http://dx.doi.org/10.1021/cm970322a. 10, 11

[75] V. Lafond, P. H. Mutin, A. Vioux, "Non-Hydrolytic Sol-Gel Routes based on Alkyl Halide Elimination: Toward Better Mixed Oxide Catalysts and New Supports: Application to the Preparation of a SiO_2-TiO_2 Epoxidation Catalyst", *J. Mol. Catal. A: Chem.*, **182-183**, 81 (2002). http://dx.doi.org/10.1016/S1381-1169(01)00487-3. 10

[76] P. H. Mutin, A. Vioux, "Nonhydrolytic Processing of Oxide-Based Materials: Simple Routes to Control Homogeneity, Morphology, and Nanostructure", *Chem. Mater.*, **21**, 582 (2009). http://dx.doi.org/10.1021/cm802348c. 10, 11, 12

[77] M. Niederberger, N. Pinna, *Metal Oxide Nanoparticles in Organic Solvents*, Engineering Materials and Processes (Springer, 2009). ISBN: 978-1-84882-670-0. 10, 11, 12

[78] M. Niederberger, "Nonaqueous Sol-Gel Routes to Metal Oxide Nanoparticles", *Acc. Chem. Res.*, **40**, 793 (2007). http://dx.doi.org/10.1021/ar600035e. 10

[79] N. Pinna, M. Niederberger, "Surfactant-free Nonaqueous Synthesis of Metal Oxide Nanostructures", *Angew. Chem. Int. Ed.*, **47**, 5292 (2008). http://dx.doi.org/10.1002/anie.200704541. 10, 11, 12

[80] M. Niederberger, G. Garnweitner, "Organic Reaction Pathways in the Nonaqueous Synthesis of Metal Oxide Nanoparticles", *Chem. Eur. J.*, **12**, 7282 (2006). http://dx.doi.org/10.1002/chem.200600313. 10, 11

[81] M. Niederberger, G. Garnweitner, N. Pinna, G. Neri, "Non-Aqueous Routes to Crystalline Metal Oxide Nanoparticles: Formation Mechanisms and Applications", *Prog. Solid State Chem.*, **33**, 59 (2005). http://dx.doi.org/10.1016/j.progsolidstchem.2005.11.032. 10

[82] R. J. P. Corriu, D. Leclercq, "Solution Chemistry for the Elaboration of Solids", *Comments Inorg. Chem.*, **19**, 245 (1997). http://dx.doi.org/10.1080/02603599708032739. 10

[83] J. Ba, D. Fattakhova Rohlfing, A. Feldhoff, T. Brezesinski, I. Djerdj, M. Wark, M. Niederberger, "Nonaqueous Synthesis of Uniform Indium Tin Oxide Nanocrystals and Their Electrical Conductivity in Dependence of the Tin Oxide Concentration", *Chem. Mater.*, **18**, 2848 (2006). http://dx.doi.org/10.1021/cm060548q. 12

[84] G. Neri, A. Bonavita, G. Micali, G. Rizzo, N. Pinna, M. Niederberger, J. Ba, "Effect of the Chemical Composition on the Sensing Properties of In_2O_3-SnO_2 Nanoparticles Synthesized by a Non-aqueous Method", *Sens. and Actuators B*, **130**, 222 (2008). http://dx.doi.org/10.1016/j.snb.2007.07.141. 12

[85] G. Neri, A. Bonavita, G. Rizzo, S. Galvagno, N. Pinna, M. Niederberger, S. Capone, P. Siciliano, "Towards Enhanced Performances in Gas Sensing: SnO_2 based Nanocrystalline Oxides Application", *Sens. and Actuators B*, **122**, 564 (2007). http://dx.doi.org/10.1016/j.snb.2006.07.006. 12

[86] M. Leskela, M. Ritala, "Atomic Layer Deposition (ALD): From Precursors to Thin Film Structures", *Thin Solid Films*, **409**, 138 (2002). http://dx.doi.org/10.1016/S0040-6090(02)00117-7. 13

[87] M. Leskela, M. Ritala, "Atomic Layer Deposition Chemistry: Recent Developments and Future Challenges", *Angew. Chem., Int. Ed.*, **42**, 5548 (2003). http://dx.doi.org/10.1002/anie.200301652. 13

[88] R. L. Puurunen, "Surface Chemistry of Atomic Layer Deposition: A Case Study for the Trimethylaluminum/water Process", *J. Appl. Phys.*, **97**, 121301 (2005). http://dx.doi.org/10.1063/1.1940727. 13

[89] S. M. George, A. W. Ott, J. W. Klaus, "Surface Chemistry for Atomic Layer Growth", *J. Phys. Chem.*, **100**, 13121 (1996). http://dx.doi.org/10.1021/jp9536763. 13

[90] K. Kukli, J. Aarik, A. Aidla, H. Siimon, M. Ritala, M. Leskela, "In situ Study of Atomic Layer Epitaxy Growth of Tantalum Oxide Thin Films from $Ta(OC_2H_5)_5$ and H_2O", *Appl. Surf. Sci.*, **112**, 236 (1997). http://dx.doi.org/10.1016/S0169-4332(96)00989-0. 13

[91] L. Niinisto, M. Ritala, M. Leskela, "Synthesis of Oxide Thin Films and Overlayers by Atomic Layer Epitaxy for Advanced Applications", *Mater. Sci. Eng., B*, **41**, 23 (1996). http://dx.doi.org/10.1016/S0921-5107(96)01617-0. 13

[92] K. Kukli, M. Ritala, M. Leskela, "Atomic Layer Deposition and Chemical Vapor Deposition of Tantalum Oxide by Successive and Simultaneous Pulsing of Tantalum Ethoxide and Tantalum Chloride", *Chem. Mater.*, **12**, 1914 (2000). http://dx.doi.org/10.1021/cm001017j. 13

[93] A. Rahtu, M. Ritala, M. Leskela, "Atomic Layer Deposition of Zirconium Titanium Oxide from Titanium Isopropoxide and Zirconium Chloride", *Chem. Mater.*, **13**, 1528 (2001). http://dx.doi.org/10.1021/cm0012062. 13

[94] P. I. Raisanen, M. Ritala, M. Leskela, "Atomic Layer Deposition of Al_2O_3 Films using $AlCl_3$ and $Al(OiPr)_3$ as Precursors", *J. Mater. Chem.*, **12**, 1415 (2002). http://dx.doi.org/10.1039/b201385c. 13

[95] M. Ritala, K. Kukli, A. Rahtu, P. I. Raisanen, M. Leskela, T. Sajavaara, J. Keinonen, "Atomic Layer Deposition of Oxide Thin Films with Metal Alkoxides as Oxygen Sources", *Science*, **288**, 319 (2000). http://dx.doi.org/10.1126/science.288.5464.319. 13, 14

[96] P. J. Evans, P. H. Mutin, G. Triani, K. E. Prince, J. R. Bartlett, "Characterisation of Metal Oxide Films Deposited by Non-hydrolytic ALD", *Surf. Interface Anal.*, **38**, 740 (2006). http://dx.doi.org/10.1002/sia.2305. 13

[97] E. Rauwel, G. Clavel, M.-G. Willinger, P. Rauwel, N. Pinna, "Non-aqueous routes to metal oxide thin films by atomic layer deposition", *Angew. Chem., Int. Ed.*, **47**, 3592 (2008). http://dx.doi.org/10.1002/anie.200705550. 13

[98] G. Clavel, E. Rauwel, M.-G. Willinger, N. Pinna, "Nonaqueous sol-gel routes applied to atomic layer deposition of oxides", *J. Mater. Chem*, **19**, 454 (2009). http://dx.doi.org/10.1039/b806215c. 13

[99] V. V. Brei, V. A. Kaspersky, N. U. Gulyanitskaya, "Synthesis and Study of Boron Phosphate and Titanium Silicate Compounds on Silica Surface", *React. Kinet. Catal. Lett.*, **50**, 415 (1993). http://dx.doi.org/10.1007/BF02062242. 13

[100] A. Rahtu, M. Ritala, "Reaction Mechanism Studies on the Atomic Layer Deposition of $Zr_xTi_yO_z$ Using the Novel Metal Halide-Metal Alkoxide Approach", *Langmuir*, **18**, 10046 (2002). http://dx.doi.org/10.1021/la026357t. 13

Chapter II:

Cobalt and Manganese Doped ZnO Synthesis

Contents

II.1 Introduction

II.1.1 ZnO

Zinc oxide is a well-know semiconductor that has a Wurtzite crystal structure (hexagonal phase). It is attracting much attention due to its numerous properties combined to its low cost, offering possible applications in various fields such as electronics, optoelectronics and gas sensing[1–11]:

ZnO is an intrinsically n-type, transparent semiconductor having a direct wide band gap at 3.3 eV with a large exciton binding energy (60 meV) and so, have potential applications as transistor[12,13], solar cells electrode[14–19], photodetector[20], nanolaser[21–23], light emitting diode[24–27], field emitter[28–33] and transparent conducting oxide upon doping[34,35]. It rises also some interest as surface acoustic wave device[36], nanogenerator[37,38], and actuator[39,40] due to its piezoelectric properties. ZnO has a high sensitivity to many gases and was proposed as sensor for O_2[41,42], NO_2[43,44], CO[45], H_2[46,47], H_2S[48,49], NH_3[48,50,51] and organic compounds[42,48,50,52]. Furthermore, it is attractive for biological application as biosensors[53,54] or antibacterial/microbial[55,56]. In addition, ZnO is a relevant industrial material, used as additive in rubber, concrete and paint, but also in food and cosmetic as it is nontoxic[4].

II.1.2 Doping

Doping has been performed on ZnO in order to adjust its electrical and optical properties and in fact, for most applications mentioned above, doping is requisite[4,7–10]. For example, doping of ZnO by a group IIIA element, principally Al[35,57] and Ga[58,59], enhances the conductivity (n-type doping). To obtained p-type behavior, the best results are obtained with a group VA element[60] such as As[61], P[62,63], N[64] and by co-doping[65,66]. The emission from the band gap and from the defects can be tuned by Al, Sn, In, rare-earth and transition metal elements[67,68]. The change of electrical property of ZnO with impurities is beneficial also in gas sensors. The dopants used are

Al, In, Sn, Cu, Fe, Pd...[42,44,45,52,69].

Furthermore, doping with paramagnetic ions has certainly found some echo in another scientific area, namely the diluted magnetic semiconductors (DMSs). This domain will be described in the next chapter.

II.1.3 ZnO growth

ZnO has been studied in different form; going from single crystals several mm long[70,71] to quantum dots[72] and colloids[73], including bulk, film, micrometric and nanometric powders. Moreover, zinc oxide presents a large variety of shapes and nanostructures[7,10,67,74]. For example, rod[75–78], wire[79,80], tube[81,82], ellipsoid[83], triangle[84], ring[85,86], donut[87], disk[85,88], cone[89,90], helix[91,92], multipod[28,93], hollow-sphere[94,95], flowerlike[96,97] and branched structure[98,99] have been reported. In particular, nanorod/wire arrays[21,100–105] have attracted much attention because one dimensional structures are easily obtained due to the different polarity of crystal faces[106,107] and are particularly interesting for applications[11,14,74].

Another interesting feature with zinc oxide is that it can be synthesized toward a large variety of methods, ranging from physical/gas-phase processes such as solid-vapor (SV)[21,81,91,93,108], sputtering[34,109], pulsed laser deposition (PLD)[110,111], molecular beam epitaxy (MBE)[27,64], chemical vapor deposition (CVD)[29,31], pulsed laser ablation (PLA)[59,61], ALD[55,112], to solution phase synthesis, i.e. from aqueous solution[77,97,103], sol-gel[54,113,114], hydrothermal[115], from organic solution[76,89], solvothermal[101,116,117] and non-hydrolytic sol-gel[118–120]. Decomposition[121,122], spray pyrolysis[65,123] and microwave assisted synthesis[124–126] were also reported as successful way for nanostructures and films synthesis.

Doped ZnO was mainly studied only as film or bulk synthesized by physical routes[127,128]. In fact, in the beginning of this study, doping of nanostructure prepared by soft chemistry was scarcely reported[129–133]. However as the use of high temperature can promote dopant segregation, the use of liquid phase synthesis can be a good solution to over-

come this problem if it is possible to match the reactivity of the metal and dopant precursors. Furthermore, solution routes allow the synthesis of gram-scale quantities of homogeneous nanostructures. This is an important prerequisite for an in depth analysis and microscopic characterization of the obtained material. Therefore, non-aqueous sol-gel and in particular the use of alcohols may be beneficial as the temperatures used for synthesis are relatively low and many different precursors react with alcohol. Few reports exist on the synthesis of zinc oxide in alcoholic media and in the majority of these cases, either surfactants are used to control the morphology[89,117,118] or basic condition are needed to accomplish hydrolysis of the zinc precursor[72,77,134–136]. In fact, only three different studies involve the syntheses in pure alcohol[90,116,119] and the possibility of doping zinc oxide by this approach had not been explored.

To the authors best knowledge since the beginning of this study other works have been published reporting the doping of zinc oxide nanostructures, using alcohol[137,138] or other solution phase syntheses[139–144].

II.2 Synthesis and morphological study

II.2.1 Synthesis

The nanoparticles were obtained by a solvothermal route involving zinc acetate and different benzyl alcohol/anisole proportions at moderate temperature (250 °C) (table II.1). The dopant precursor was introduced directly in the reaction mixture as cobalt acetate or manganese oleate. Depending on the nature of doping agent used, the resulting nanoparticles are a green (cobalt) or yellow (manganese) powder. The content of organic impurities was estimated by microanalysis. For all samples, less than 0.5% of carbon was found, demonstrating the good purity of the as-synthesized particles.

II.2.2 Morphology

The morphology of the products was examined with scanning electron microscopy (SEM), transmission electron microscopy (TEM) and infrared (IR) spectroscopy. The results are summarized in (table II.1).

Microscopy

The synthesis in pure benzyl alcohol (BA) leads to inhomogeneous samples (Fig.1). Pure ZnO samples are composed of rods and elongated, triangular and hexagonal particles (Fig.1.A). The particles doped with a low content of cobalt (not shown) display similar morphologies and sizes. However, while increasing the cobalt concentration bigger object are formed. They consist, in larger proportion, of rods with different diameter and aspect ratio (Fig.1.C). In contrast, samples doped by manganese (Fig.1.B) appear to be mainly constituted of irregularly shaped particles, slightly smaller than in the case of pure ZnO.

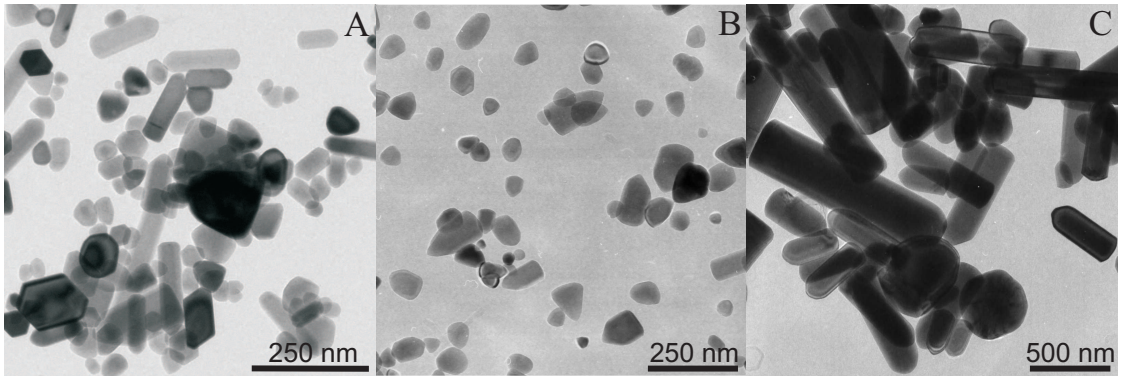

Figure II.1: (A) TEM image of pure ZnO, (B) TEM image of 0.56% Mn-doped ZnO and (C) TEM image of 3.88% Co-doped ZnO synthesized in pure BA.

When decreasing the proportion of benzyl alcohol in the reaction mixture by using a co-solvent, the morphologies obtained are better defined. Using 5% of benzyl alcohol in anisole, rods of approximately 400 x 100 nm are obtained for pure ZnO (Fig.2.A). In the case of Co-doped samples, SEM observations (Fig.2.B) demonstrate that shorter

rods are formed for low doping content. At higher concentration, the formed rods are less homogeneous in size (not shown). The manganese doping leads to the formation of rods with higher average length (Fig.2.C).

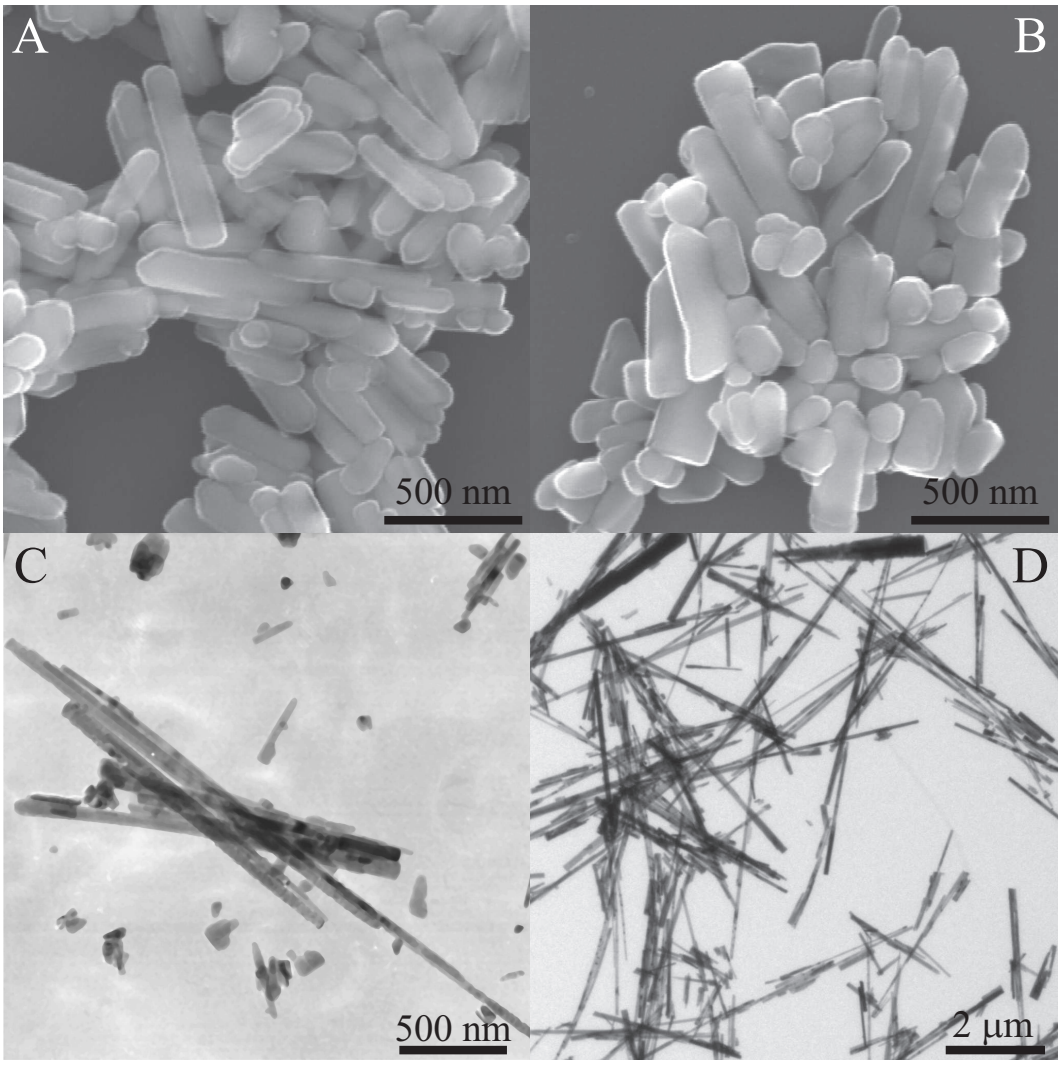

Figure II.2: (A) SEM image of pure ZnO, (B) SEM image of 0.81% Co-doped ZnO and (C) TEM image of 0.56% Mn-doped ZnO synthesized in BA/A (5/95%). (D) TEM image of 0.65% Co-doped ZnO in anisole with traces of BA.

Further decrease of the benzyl alcohol content can improve the aspect ratio; however, a drastic decrease of the synthesis yield is observed. Nevertheless, in order to corroborate the control over the aspect ratio, the synthesis of pure and Co-doped ZnO were

performed with less BA. The highest aspect ratio was obtained in pure anisole using a Teflon cup that was previously used for a synthesis of ZnO in pure benzyl alcohol (Fig.2.D). In fact, we have quantified by GC-MS that a 45 ml Teflon cup can stock and liberate up to 200 μl of solvent inside its walls. As anisole is an inert solvent regarding the sol-gel process, the traces of benzyl alcohol are responsible for the reaction. During the synthesis, the traces of benzyl alcohol which were absorbed by the Teflon at high temperature were slowly released allowing a fine control of the reaction kinetics (Fig.2.D). The larger aspect ratio obtained in this case is certainly due to the continuous and slow supply of the reacting solvent. This method is unconventional and these results are present here only with the purpose to illustrate the decisive role of the solvent and the importance of the kinetics on the growth of ZnO.

Solvents	**Dopants**	**Effective doping(%)**	**Morphology**
pure BA	none	0	Nanoparticles and nanorods
	Co	0.77	Nanoparticles and nanorods
		3.88	Rodlike morphology, inhomogeneous size
	Mn	0.56	Elongated, triangular and hexagonal nanoparticles
A/BA (95/5 %)	none	0	Small rods
	Co	0.81	Small rods
		1.16	Rodlike morphology, inhomogeneous size
		4.09	Rodlike morphology, inhomogeneous size
	Mn	0.66	Rods
		0.86	Rods with inhomogeneous length
A + traces of BA	Co	0.65	Nanowires

Table II.1: Experimental conditions and morphological results for pure and doped ZnO.

IR spectroscopy

IR spectroscopy was performed to confirm the evolution of the morphology at the macroscopic scale. Wurtzite zinc oxide has four IR actives mode; A_1 and E_1 transverse

optical modes (TO) at $\omega_{T\parallel} = 380$ and $\omega_{T\perp} = 410$ cm^{-1} and, A_1 and E_1 longitudinal optical mode (LO) at $\omega_{L\parallel} = 575$ and $\omega_{L\perp} = 590$ cm^{-1}, respectively[8,145,146]. However, typical spectra of small ZnO crystals present up to three bands located between the bulk TO and LO vibrations. These bands are due to surface phonon modes (SPMs) and the values of the frequency of these SPMs depend on the size, shape and dielectric constant of the surrounding medium of the particles. For uniaxial crystal, as ZnO, the effect of the shape on surface phonon has been studied by the theory of average dielectric constant (TADC) that takes into account the anisotropic dielectric constants and the shape of a given materials[147–149]. Furthermore, a collection of spectra vs. morphology can be found in the literature, illustrating the good correlation between band displacement and shape of the crystal[150–155]. Spherical ZnO nanocrystals (c/a=1) give rise to a single band at 430-490 cm^{-1}. A splitting of the absorption band takes place going to the cylinder (c/a$\gg$1) or the slab (c/a$\ll$1)[150–152]. Therefore, this feature can be used to define an average shape of the ZnO particles.

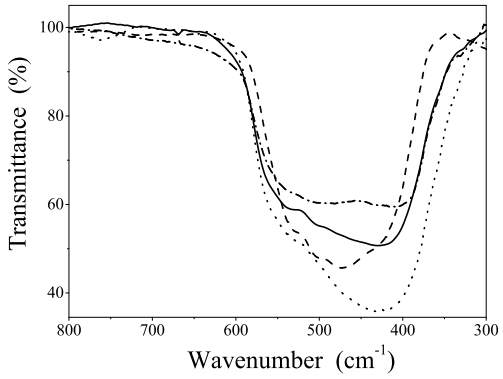

Figure II.3: FT-IR spectra of pure ZnO (—), 0.77% Co-doped ZnO (- - -), 3.88% Co-doped ZnO (·–), 0.56% Mn-doped ZnO (···), synthesized in pure BA.

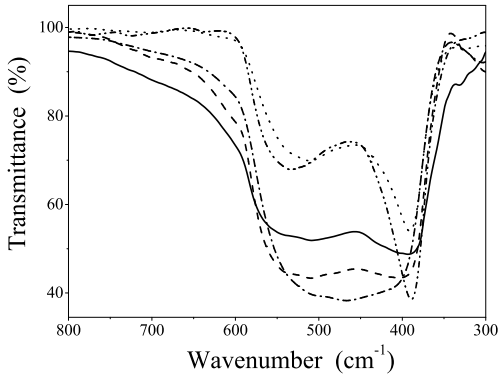

Figure II.4: FT-IR spectra of pure ZnO (—), 0.81% Co-doped ZnO (- - -), 4.09% Co-doped ZnO (·–), 0.66% Mn-doped ZnO (···), synthesized in BA/A (5/95%) and 0.65% Co-doped ZnO synthesized in anisole with traces of BA (··–).

Figure 3 shows the spectra recorded for samples synthesized in pure BA. Pure and

slightly doped ZnO do not present a well-defined morphology as determined by microscopy, and indeed theses samples display similar spectra, i.e. a broad band with three maxima between 415 and 540 cm^{-1} resulting of the overlapping of the three SPM absorptions of ZnO. Sample with high cobalt content (Fig.3 dot-dashed-line) display a similar band that for pure ZnO and Co-doped ZnO made in a mixture of benzyl alcohol/anisole 5/95% (Fig.4 full-line, dashed-line and dot-dashed-line). The broad band is centered at 460 cm^{-1} with and without a small splitting. This is in good agreement with the TEM/SEM findings showing short rods. For the Mn-doped ZnO synthesized with the same benzyl alcohol/anisole quantity the particles present a higher aspect ratio, thus the splitting is better visible and the width of the IR absorptions are much sharper (Fig.4 dotted-line). The same trend is observed in the case of Co-doped sample synthesized in anisole in the presence of traces of benzyl alcohol (Fig.4 dot-dot-dashed-line). A splitting value could be determined for the two latter samples, $\Delta\upsilon$= 120 and 147 cm^{-1} respectively, corresponding to the splitting generally observed for rod-like crystal[150] in good agreement with electron microscopy data.

II.2.3 Mechanism of the reaction

The reaction responsible for the formation of the oxide occurs between the zinc acetate and the benzyl alcohol; the anisole is used as co-solvent and it is inert toward the precursors. In order to understand the crystal growth, the mechanism of the reaction was studied. Nuclear magnetic resonance (NMR) was used to analyze the composition of the solvent mixture after reaction. It contains, quantitatively, benzyl acetate as by-product. Formation of an ester was already observed during the reaction of zinc acetate and ethanol[119], between zinc stearate and 1-octadecanol[118] and in more complex media, between zinc acetate and 1,12-dodecanediol[89]. Such a synthetic approach is well established in the field of nonaqueous sol-gel processes and called ester elimination[156–158]. The formation of zinc oxide following this route engages hydroxylation and condensation reactions (Fig.5).

During hydroxylation, (Fig.5.A) the acetate functions are replaced by hydroxide groups leading to the formation of zinc hydroxide derivative and benzyl acetate. Two competitive condensation reactions can then take place: i) between two freshly formed hydroxide groups (Fig.5.B1) with the formation of water, or ii) between a hydroxide and an acetate function with release of acetic acid (Fig.5.B2). Acetic acid was not detected in final mixture probably because of its immediate reaction with benzyl alcohol producing benzyl acetate and water. Esterification is an equilibrium. However, as it took place in a large excess of alcohol the equilibrium is strongly displaced toward the ester formation, thus explaining the absence of the acid. The water produced in-situ by this side reaction but also during the condensation step B.2 (Fig.5), can hydrolyze zinc precursors increasing the overall reaction kinetics.

Very recently, Bilecka et al. have studied the kinetic of the ZnO formation in this system. Although they principally investigated the reaction under microwave irradiations, they also compared with traditional heating and drew some general conclusions about the mechanism. They particularly demonstrated the role and interconnection of the organic and inorganic condensations for the formation of the oxide[125].

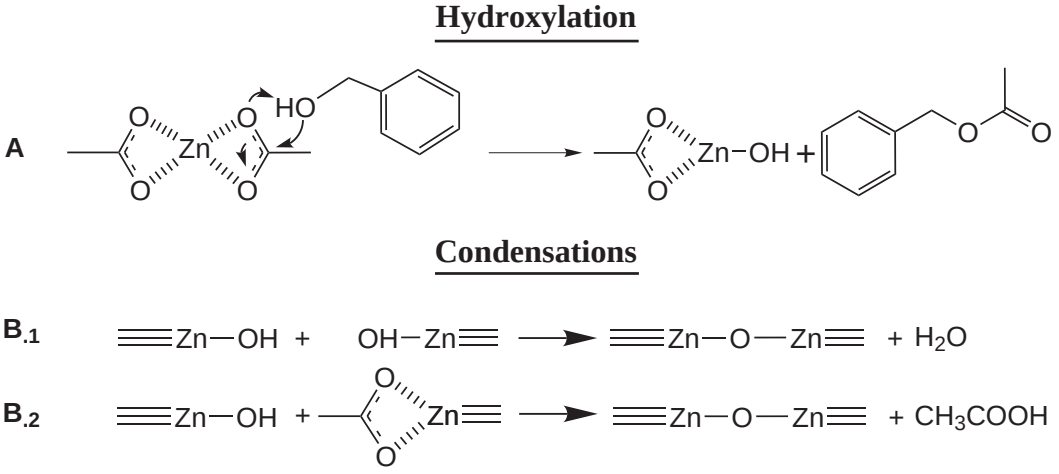

Figure II.5: Scheme of the reaction between benzyl alcohol and zinc acetate. (A) Hydroxylation of zinc acetate, (B) the two possible condensation pathways, ≡ represent any kind of ligand coordinated to the Zn atom (OH, acetate, O-Zn).

II.2.4 Discussion

The poor control over the crystal growth found in the case of ZnO compared to other reactions involving benzyl alcohol[157,158] can be explained by the fact that a lot of water is formed in-situ. Furthermore, NMR quantification points to the complete reaction of acetate species with benzyl alcohol producing two benzyl acetate molecules per Zn atom. It is know that carboxylates act as surfactant in controlling the growth of nanoparticles because they bind to oxide surfaces. For example, it was found that carboxylate species bind so strongly to sub-nanometer thick rare-earth oxide platelets, than they block any further growth[159,160]. In the present case acetates are totally consumed during the esterification reaction and they cannot act as surfactants.

Contrary to other synthesis[76,77,150,161], the size and shape controls are not affected by varying the concentration of zinc precursor. Instead, the concentration of benzyl alcohol plays a role. This is obviously related to the fact that the concentration of zinc precursor is much smaller compared to the one of benzyl alcohol. Reduction of the quantity of alcohol by using an inert co-solvent affects the kinetic of the reaction as the observed aspect ratio increase substantially and a more defined morphology is obtained. However, using anisole leads to a decrease of the synthesis yield. Thus, we have focused this study on samples synthesized with at least 5% of benzyl alcohol in anisole.

Additionally, the nature and the concentration of dopants influence slightly the morphology. In the case of manganese doped particles a better morphological control can be explained by the presence of oleate molecules which behave as a surfactant.

II.3 Strucutral characterizations

II.3.1 XRD

Figure 6 shows the X-ray diffraction (XRD) pattern of the pure ZnO nanoparticles. It can be indexed to the hexagonal Wurtzite structure (Zincite), which is the thermodynamically stable phase. Cobalt and manganese doped samples are plotted in logarithmic scale figures 7 and 8, in order to enhance the presence of any impurity. No additional reflections are observed even for the particles including the largest amount of dopant indicating that there are no additional crystalline structures present in the samples. In all cases, Wurtzite is the only crystalline phase. One would expect a shift of the lattice constant due to the substitution of host atoms, as it is normally the case for solid solution. However, the diffraction peaks do not show any significant shift. This certainly results from the close values of ionic radii in the case of zinc and cobalt ($Zn^{2+} \sim 0.60$ Å, $Co^{2+} \sim 0.58$ Å). Nevertheless, a shift is supposed to occur for manganese doping, which have a higher ionic radius ($Mn^{2+} \sim 0.66$ Å). However, manganese sample studied here are only slightly doped (less than 1%) and probably not enough to induce a detectable shift.

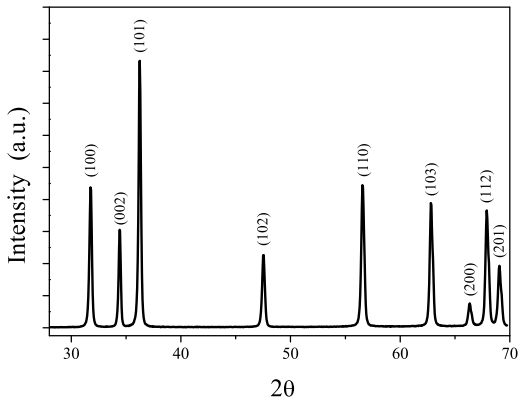

Figure II.6: X-ray diffractogram of pure ZnO synthesized in BA/A (95/5%) the indexation of Wurtzite structure (JCPDS Card No 36-1451) is given.

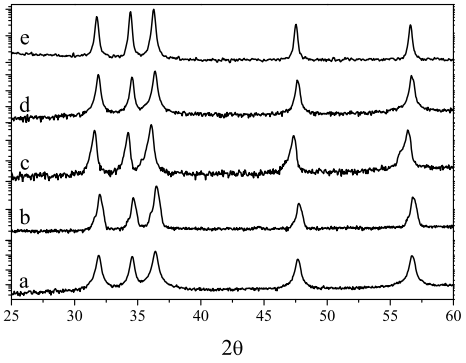

Figure II.7: Log scale XRD patterns of a) 0.77% and b) 3.88% Co-doped ZnO synthesized in pure BA, c) 0.81% and d) 4.09% Co-doped ZnO synthesized in BA/A (5/95%) and e) 0.65% Co-doped ZnO synthesized in anisole with traces of BA.

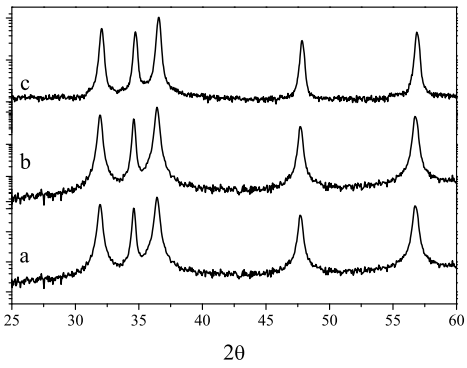

Figure II.8: Log scale XRD patterns of a) 0.56% Mn-doped ZnO synthesized in pure BA, b) 0.66% and c) 0.86 % Mn-doped ZnO synthesized in BA/A (5/95%).

II.3.2 Electron diffraction and HRTEM

Select area electron diffraction (SAED) and high-resolution TEM (HRTEM) were used to investigate the crystallinity and growth orientation. Figure 9.A shows a TEM image of one rod of a cobalt-doped sample. The corresponding diffraction pattern can be indexed to the hexagonal Wurtzite phase of zinc oxide in agreement with XRD. Furthermore, the rods are single-crystalline and elongated in the [001] direction, i.e. along the c axis. This is consistent with the reported preferential orientation growth in solution, based on the different polarity of the crystal planes[106,107]. The presence of forbidden (001) reflections is often observed for ZnO nanoparticles and caused by multiple diffraction[89,122] and defaults. A high resolution TEM image recorded from the tip region of a particle and the corresponding power spectrum is shown in figure 9.B. The tip shows a nice crystallinity and clear lattice fringes can be observed. The separation between the lattice fringes along the wire axis is in agreement with the (002) plane spacing (2.60 Å). In the direction perpendicular to the wire axis, the (110) planes

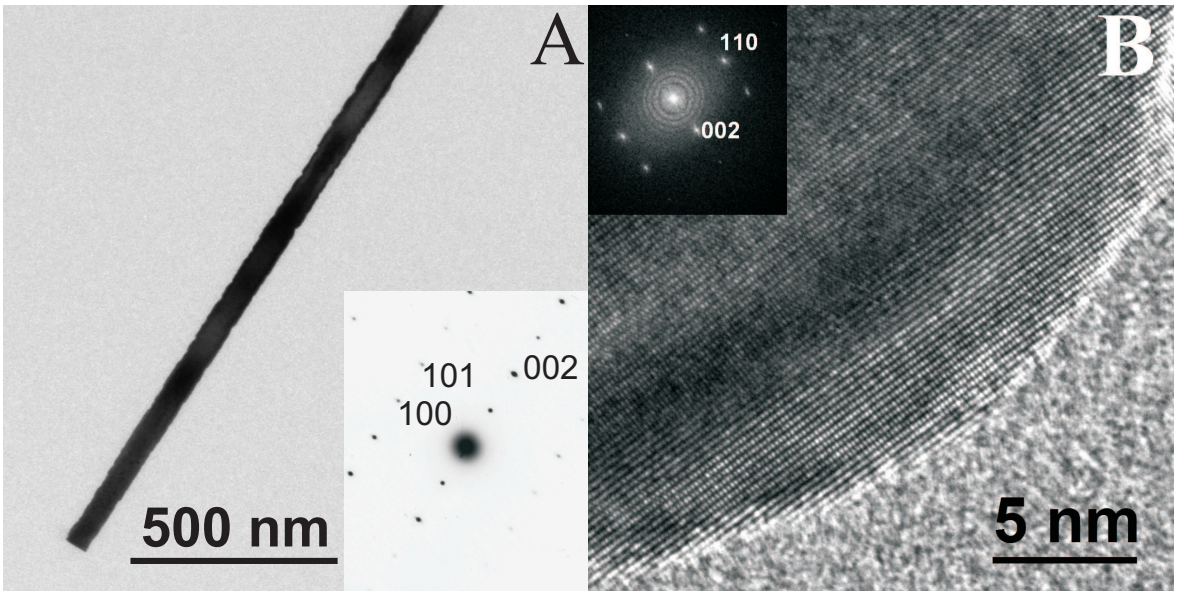

Figure II.9: (A) TEM picture of single rod with in inset the corresponding SAED pattern (0.65% Co-doped sample). (B) HRTEM image of the tip region of a single particle with in inset the corresponding power spectrum (3.88% Co-doped sample).

with a spacing of 1.38 Å are observed. In contrast to the SAED, the power spectrum of the tip only shows the allowed 002 spots. Changes in the contrast are due to the increasing thickness from the tip to the inner part. Furthermore, secondary phases such as precipitates or inclusions were not observed in any samples by microscopy.

II.4 Dopant concentration and homogeneity

After morphologic and structural characterizations, the concentration and homogeneity of the dopant were investigated using inductively coupled plasma-atomic emission spectrometry (ICP-AES) and energy dispersive X-ray spectrometry (EDX). The doping concentration monitored by ICP-AES comes out to be slightly lower than the quantity of precursors introduced, about 30% and 45% less for cobalt and manganese doping, respectively. The cobalt concentration could be varied from 0.5% to larger than 4%, the manganese one from 0.5 to 1%, depending on the amount of precursor added (tableII.2). In order to confirm the homogeneity of the cobalt distribution within the ZnO matrix,

EDX were recorded in the TEM. Figure 10 presents spectra recorded for a small amount of particles as well as when measured at different points along a single particle. The Co concentration seems homogeneous; at least, the variation of the Co concentration lies below the detection limit. In addition to EDX, electron energy loss spectroscopy (EELS) was also used (not shown). Due to the relatively large thickness of the particles, the Co white lines peaked only slightly above the huge background caused by the inelastic scattering processes. Again, the expected variations were below the detection limit. Therefore it can be concluded that the Co is indeed homogeneously distributed in the synthesized particles. This is in agreement with the HRTEM investigations reported above, where no inclusions of a second phase have been observed.

Solvents	**Dopants**	**Nominal doping(%)**	**Effective doping(%)**
BA	Co	1.06	0.77
BA	Co	4.90	3.88
BA	Mn	1.04	0.56
A/BA (95/5 %)	Co	1.22	0.81
A/BA (95/5 %)	Co	1.99	1.16
A/BA (95/5 %)	Co	5.40	4.09
A/BA (95/5 %)	Mn	1.16	0.66
A/BA (95/5 %)	Mn	2.07	0.86
A + traces of BA	Co	0.99	0.65

Table II.2: Nominal doping and effective doping for Co- and Mn-doped ZnO.

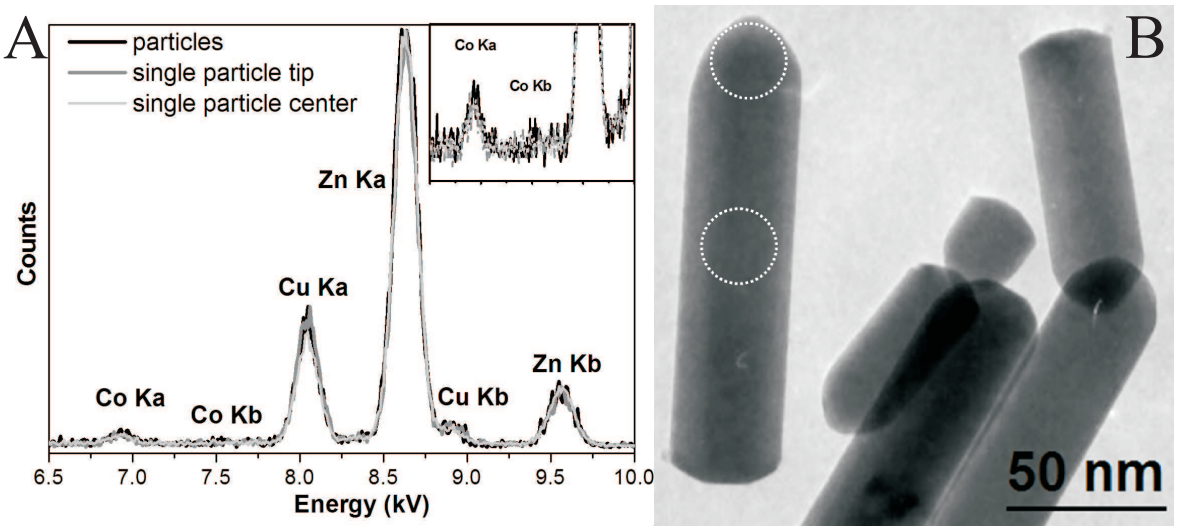

Figure II.10: (A) EDX spectra recorded from regions containing a number of particles and spectra recorded along a single particle reveal a homogeneous distribution of Co. (B) Region from which the EDX spectra shown here were recorded. Circles indicate regions where the spot was focused for the detection of eventual variations in the Co concentration along a single particle (3.88% Co-doped ZnO).

II.5 Conclusion

In summary, we have synthesized cobalt and manganese doped zinc oxide using a non-hydrolytic sol-gel synthesis. The obtained particles are single crystalline presenting a hexagonal structure. ZnO was doped up to 5% for cobalt and 1% for manganese with a good efficiency. No precipitates or inclusions of a secondary phase was observed, hence the dopant is homogeneously distributed in the oxide. Controlling the amount of benzyl alcohol, by using an inert co-solvent, has led to an improvement in size and shape of the particles, producing rods elongated along the [001] direction. However, a decrease in the reaction yield is observed, and thus this study has focused on samples synthesized with at least 5% of benzyl alcohol in anisole.

II.6 Experimental part

Synthesis

Zinc(II) acetate 99.99%, Cobalt(II) acetate anhydrous, Anisole 99% and benzyl alcohol 99%, were purchased from Aldrich, stored in a dessicator (or a glovebox) and used as received. Mn(II) oleate was prepared by reacting Mn(II) chloride and sodium oleate [162]. In a typical reaction, a Teflon cup of 45 ml inner volume was filled with 2.73 mmol of Zinc(II) acetate, 16 ml of anisole and 800 μl of benzyl alcohol for the "benzyl alcohol/anisole (5/95%)" synthesis or with 16 ml of benzyl alcohol for the pure benzyl alcohol route. The "anisole with trace of benzyl alcohol " route was carried out with 16 ml of anisole in an autoclave previously used with benzyl alcohol. Then, the cup was slipped into a steel autoclave, sealed and heated at 250 °C for 2 days. The resulting suspensions were centrifuged, and the precipitates were meticulously washed with ethanol and dichloromethane and then dried in air at 80 °C. The quantity of nanocrystals produced was approximately 170 mg (yield >70%). In the case of the Co(II)- and Mn(II)-doped ZnO x-equivalents of transition-metal precursor were added to the reaction mixture, in that case, green and yellow powder were obtained respectively.

NMR

Nuclear Magnetic Resonance (NMR) was performed with a Brucker instrument at 300MHz using DMSO-d6 as solvent. ^{1}H NMR spectra of final reaction mixture depict: *Benzyl alcohol*, δ(ppm): 4.55 (d, 2H, CH_2, ^{3}JH-H=5.4Hz), 5.27 (t, H, OH, ^{3}JH-H=5.4Hz), 7.34 (m, 5H, C_6H_5). *Benzyl acetate*, δ(ppm): 2.07 (s, 3H, CH_3), 5.1 (s, 2H, CH_2), 7.26 (m, 5H, C_6H_5). *Water*, δ(ppm): 3.54 (s, H_2O).

Experimental details

SEM images were performed using a FEG-SEM Hitachi S4100 microscope operating at 25 kV. The samples were prepared by depositing a drop of a suspension of the particles

in ethanol onto a glass piece, which was then coated by carbon. TEM was carried out on a Hitachi H-9000 microscope operating at 300 kV, high resolution microscopy EDX and EELS measurements were performed on a CM200FEG (Philips) microscope, operated at 200 kV, equipped with a field emission gun and a GATAN Tridiem GIF. Samples were prepared by depositing a drop of a solution of particles in ethanol on a copper grid coated with an amorphous carbon film. FTIR spectra were measured on a Matson 7000 FTIR spectrometer from KBr pellets. XRD data were collected on an X'Pert MPD Philips diffractometer (CuKα X-radiation at 40 kV and 50 mA). ICP-AES was realized in the Analytical Laboratories of University of Aveiro.

Bibliography

[1] Y. Heo, D. Norton, L. Tien, Y. Kwon, B. Kang, F. Ren, S. Pearton, J. LaRoche, "ZnO Nanowire Growth and Devices", *Mater. Sci. Eng., R*, **47**, 1 (2004). http://dx.doi.org/10.1016/j.mser.2004.09.001. 25

[2] V. A. Karpina, V. I. Lazorenko, C. V. Lashkarev, V. D. Dobrowolski, L. I. Kopylova, V. A. Baturin, S. A. Pustovoytov, A. J. Karpenko, S. A. Eremin, *et al.*, "Zinc Oxide - Analogue of GaN with New Perspective Possibilities", *Cryst. Res. Technol.*, **39**, 980 (2004). http://dx.doi.org/10.1002/crat.200310283. 25

[3] C. Klingshirn, "ZnO: From Basics towards Applications", *phys. stat. sol. (b)*, **244**, 3027 (2007). http://dx.doi.org/10.1002/pssb.200743072. 25

[4] C. Klingshirn, "ZnO: Material, Physics and Applications", *ChemPhysChem*, **8**, 782 (2007). http://dx.doi.org/10.1002/cphc.200700002. 25

[5] C. Klingshirn, R. Hauschild, H. Priller, M. Decker, J. Zeller, H. Kalt, "ZnO Rediscovered - Once Again!?", *Superlattices Microstruct.*, **38**, 209 (2005). http://dx.doi.org/10.1016/j.spmi.2005.07.003. 25

[6] D. C. Look, "Recent Advances in ZnO Materials and Devices", *Mater. Sci. Eng., B*, **80**, 383 (2001). http://dx.doi.org/10.1016/S0921-5107(00)00604-8. 25

[7] D. P. Norton, Y. W. Heo, M. P. Ivill, K. Ip, S. J. Pearton, M. F. Chisholm, T. Steiner, "ZnO: Growth, Doping & Processing", *Mater. Today*, **7**, 34 (2004). http://dx.doi.org/10.1016/S1369-7021(04)00287-1. 25, 26

[8] U. Ozgur, I. A. Ya, C. Liu, A. Teke, M. A. Reshchikov, S. Dogan, V. Avrutin, S. J. Cho, H. Morkoc, "A Comprehensive Review of ZnO Materials and Devices", *J. Appl. Phys.*, **98**, 041301 (2005). http://dx.doi.org/10.1063/1.1992666. 25, 31

[9] S. J. Pearton, D. P. Norton, K. Ip, Y. W. Heo, T. Steiner, "Recent Progress in Processing and Properties of ZnO", *Prog. Mater. Sci.*, **50**, 293 (2005). http://dx.doi.org/10.1016/j.pmatsci.2004.04.001. 25

[10] L. Schmidt-Mende, J. L. MacManus-Driscoll, "ZnO - Nanostructures, Defects, and Devices", *Materials Today*, **10**, 40 (2007). http://dx.doi.org/10.1016/S1369-7021(07)70078-0. 25, 26

[11] G.-C. Yi, C. Wang, W. I. Park, "ZnO Nanorods: Synthesis, Characterization and Applications", *Semicond. Sci. Technol.*, **20**, S22 (2005). http://dx.doi.org/10.1088/0268-1242/20/4/003. 25, 26

[12] B. Sun, H. Sirringhaus, "Solution-Processed Zinc Oxide Field-Effect Transistors Based on Self-Assembly of Colloidal Nanorods", *Nano Lett.*, **5**, 2408 (2005). http://dx.doi.org/10.1021/nl051586w. 25

[13] H. E. Unalan, Y. Zhang, P. Hiralal, S. Dalal, D. Chu, G. Eda, K. B. K. Teo, M. Chhowalla, W. I. Milne, G. A. J. Amaratunga, "Zinc Oxide Nanowire Networks for Macroelectronic Devices", *Appl. Phys. Lett.*, **94**, 163501 (2009). http://dx.doi.org/10.1063/1.3120561. 25

[14] J. B. Baxter, E. S. Aydil, "Nanowire-Based Dye-Sensitized Solar Cells", *Appl. Phys. Lett.*, **86**, 053114 (2005). http://dx.doi.org/10.1063/1.1861510. 25, 26

[15] R. Katoh, A. Furube, T. Yoshihara, K. Hara, G. Fujihashi, S. Takano, S. Murata, H. Arakawa, M. Tachiya, "Efficiencies of Electron Injection from Excited N3 Dye into Nanocrystalline Semiconductor (ZrO_2, TiO_2, ZnO, Nb_2O_5, SnO_2, In_2O_3) Films", *J. Phys. Chem. B*, **108**, 4818 (2004). http://dx.doi.org/10.1021/jp031260g. 25

[16] K. Keis, C. Bauer, G. Boschloo, A. Hagfeldt, K. Westermark, H. Rensmo, H. Siegbahn, "Nanostructured ZnO Electrodes for Dye-sensitized Solar Cell Applications", *J. Photochem. Photobiol., A*, **148**, 57 (2002). http://dx.doi.org/10.1016/S1010-6030(02)00039-4. 25

[17] K. Keis, L. Vayssieres, S.-E. Lindquist, A. Hagfeldt, "Nanostructured ZnO Electrodes for Photovoltaic Applications", *Nanostruct. Mater.*, **12**, 487 (1999). http://dx.doi.org/10.1016/S0965-9773(99)00165-8. 25

[18] M. Law, L. E. Greene, J. C. Johnson, R. Saykally, P. Yang, "Nanowire Dye-Sensitized Solar Cells", *Nat Mater*, **4**, 455 (2005). http://dx.doi.org/10.1038/nmat1387. 25

[19] H. Rensmo, K. Keis, H. Lindstrom, S. Sodergren, A. Solbrand, A. Hagfeldt, S.-E. Lindquist, L. N. Wang, M. Muhammed, "High Light-to-Energy Conversion Efficiencies for Solar Cells Based on Nanostructured ZnO Electrodes", *J. Phys. Chem. B*, **101**, 2598 (1997). http://dx.doi.org/10.1021/jp962918b. 25

[20] H. Kind, H. Q. Yan, B. Messer, M. Law, P. D. Yang, "Nanowire Ultraviolet Photodetectors and Optical Switches", *Adv. Mater.*, **14**, 158 (2002). http://dx.doi.org/10.1002/1521-4095(20020116)14:2<158::AID-ADMA158>3.0.CO;2-W. 25

[21] M. H. Huang, S. Mao, H. Feick, H. Yan, Y. Wu, H. Kind, E. Weber, R. Russo, P. Yang, "Room-Temperature Ultraviolet Nanowire Nanolasers", *Science*, **292**, 1897 (2001). http://dx.doi.org/10.1126/science.1060367. 25, 26

[22] R. F. Service, "Materials Science: Will UV Lasers Beat the Blues?", *Science*, **276**, 895 (1997). http://dx.doi.org/10.1126/science.276.5314.895. 25

[23] H. Yan, R. He, J. Johnson, M. Law, R. J. Saykally, P. Yang, "Dendritic Nanowire Ultraviolet Laser Array", *J. Am. Chem. Soc.*, **125**, 4728 (2003). http://dx.doi.org/10.1021/ja034327m. 25

[24] S. J. Jiao, Z. Z. Zhang, Y. M. Lu, D. Z. Shen, B. Yao, J. Y. Zhang, B. H. Li, D. X. Zhao, X. W. Fan, Z. K. Tang, "ZnO p-n Junction Light-Emitting Diodes Fabricated on Sapphire Substrates", *Appl. Phys. Lett.*, **88**, 031911 (2006). http://dx.doi.org/10.1063/1.2166686. 25

[25] Y. Ryu, T.-S. Lee, J. A. Lubguban, H. W. White, B.-J. Kim, Y.-S. Park, C.-J. Youn, "Next Generation of Oxide Photonic Devices: ZnO-Based Ultraviolet Light Emitting Diodes", *Appl. Phys. Lett.*, **88**, 241108 (2006). http://dx.doi.org/10.1063/1.2210452. 25

[26] A. Tsukazaki, M. Kubota, A. Ohtomo, T. Onuma, K. Ohtani, H. Ohno, S. F. Chichibu, M. Kawasaki, "Blue Light-Emitting Diode Based on ZnO", *Jpn. J. Appl. Phys.*, **44**, L643 (2005). http://dx.doi.org/10.1143/JJAP.44.L643. 25

[27] A. Tsukazaki, A. Ohtomo, T. Onuma, M. Ohtani, T. Makino, M. Sumiya, K. Ohtani, S. F. Chichibu, S. Fuke, *et al.*, "Repeated Temperature Modulation Epitaxy For P-type Doping and Light-Emitting Diode based on ZnO", *Nat. Mater.*, **4**, 42 (2005). http://dx.doi.org/10.1038/nmat1284. 25, 26

[28] Q. H. Li, Q. Wan, Y. J. Chen, T. H. Wang, H. B. Jia, D. P. Yu, "Stable Field Emission from Tetrapod-Like ZnO Nanostructures", *Appl. Phys. Lett.*, **85**, 636 (2004). http://dx.doi.org/10.1063/1.1773613. 25, 26

[29] Y. B. Li, Y. Bando, D. Golberg, "ZnO Nanoneedles with Tip Surface Perturbations: Excellent Field Emitters", *Appl. Phys. Lett.*, **84**, 3603 (2004). http://dx.doi.org/10.1063/1.1738174. 25, 26

[30] Q. Wan, K. Yu, T. H. Wang, C. L. Lin, "Low-Field Electron Emission from Tetrapod-Like ZnO Nanostructures Synthesized by Rapid Evaporation", *Appl. Phys. Lett.*, **83**, 2253 (2003). http://dx.doi.org/10.1063/1.1612899. 25

[31] F. Xu, K. Yu, G. Li, Q. Li, Z. Zhu, "Synthesis and Field Emission of Four Kinds of ZnO Nanostructures: Nanosleeve-Fishes, Radial Nanowire Arrays, Nanocombs and Nanoflowers", *Nanotechnology*, **17**, 2855 (2006). http://dx.doi.org/10.1088/0957-4484/17/12/005. 25, 26

[32] Y. W. Zhu, H. Z. Zhang, X. C. Sun, S. Q. Feng, J. Xu, Q. Zhao, B. Xiang, R. M. Wang, D. P. Yu, "Efficient Field Emission from ZnO Nanoneedle Arrays", *Appl. Phys. Lett.*, **83**, 144 (2003). http://dx.doi.org/10.1063/1.1589166. 25

[33] Y. Zhang, K. Yu, S. Ouyang, Z. Zhu, "Selective-Area Growth and Field Emission Properties of Zinc Oxide Nanowire Micropattern Arrays", *Phys. B*, **382**, 76 (2006). http://dx.doi.org/10.1016/j.physb.2006.02.001. 25

[34] C. Agashe, O. Kluth, G. Schöpe, H. Siekmann, J. Hüpkes, B. Rech, "Optimization of the Electrical Properties of Magnetron Sputtered Aluminum-Doped Zinc Oxide Films for Opto-Electronic Applications", *Thin Solid Films*, **442**, 167 (2003). http://dx.doi.org/10.1016/S0040-6090(03)00966-0. 25, 26

[35] T. Minami, H. Nanto, S. Takata, "Highly Conductive and Transparent Aluminum Doped Zinc Oxide Thin Films Prepared by RF Magnetron Sputtering", *Jpn. J. Appl. Phys.*, **23**, L280 (1984). http://dx.doi.org/10.1143/JJAP.23.L280. 25

[36] S. J. Chang, Y. K. Su, Y. P. Shei, "High Quality ZnO Thin Films on InP Substrates Prepared by Radio Frequency Magnetron Sputtering. II. Surface Acoustic Wave Device Fabrication", *J. Vac. Sci. Technol., A*, **13**, 385 (1995). http://dx.doi.org/10.1116/1.579368. 25

[37] Y. Qin, X. Wang, Z. L. Wang, "Microfibre-Nanowire Hybrid Structure for Energy Scavenging", *Nature*, **451**, 809 (2008). http://dx.doi.org/10.1038/nature06601. 25

[38] J. Song, J. Zhou, Z. L. Wang, "Piezoelectric and Semiconducting Coupled Power Generating Process of a Single ZnO Belt/Wire. A Technology for Harvesting Electricity from the Environment", *Nano Lett.*, **6**, 1656 (2006). http://dx.doi.org/10.1021/nl060820v. 25

[39] S. C. Minne, S. R. Manalis, C. F. Quate, "Parallel Atomic Force Microscopy using Cantilevers with Integrated Piezoresistive Sensors and Integrated Piezoelectric Actuators", *Appl. Phys. Lett.*, **67**, 3918 (1995). http://dx.doi.org/10.1063/1.115317. 25

[40] T. Shibata, K. Unno, E. Makino, Y. Ito, S. Shimada, "Characterization of Sputtered ZnO Thin Film as Sensor and Actuator for Diamond AFM Probe", *Sens. Actuators, A*, **102**, 106 (2002). http://dx.doi.org/10.1016/S0924-4247(02)00339-4. 25

[41] F. Chaabouni, M. Abaab, B. Rezig, "Metrological Characteristics of ZnO Oxygen Sensor at Room Temperature", *Sensors and Actuators B,: Chemical*, **100**, 200 (2004). http://dx.doi.org/10.1016/j.snb.2003.12.059. 25

[42] C. H. Kwon, H.-K. Hong, D. H. Yun, K. Lee, S.-T. Kim, Y.-H. Roh, B.-H. Lee, "Thick-Film Zinc-Oxide Gas Sensor for the Control of Lean Air-to-Fuel Ratio in Domestic Combustion Systems", *Sens. Actuators, B*, **25**, 610 (1995). http://dx.doi.org/10.1016/0925-4005(95)85134-8. 25, 26

[43] C. Baratto, G. S. berveglieri, A. Onischuk, B. Caruso, S. di Stasio, "Low Temperature Selective NO_2 Sensors by Nanostructured Fibres of ZnO", *Sens. Actuators, B*, **100**, 261 (2004). http://dx.doi.org/10.1016/j.snb.2003.12.045. 25

[44] S. T. Shishiyanu, T. S. Shishiyanu, O. I. Lupan, "Sensing Characteristics of Tin-doped ZnO Thin Films as NO_2 Gas Sensor", *Sens. Actuators, B*, **107**, 379 (2005). http://dx.doi.org/10.1016/j.snb.2004.10.030. 25, 26

[45] H. Gong, J. Hu, J. Wang, C. Ong, F. Zhu, "Nano-Crystalline Cu-doped ZnO Thin Film Gas Sensor for CO", *Sens. Actuators, B*, **115**, 247 (2006). http://dx.doi.org/10.1016/j.snb.2005.09.008. 25, 26

[46] S. Kim, B. S. Kang, F. Ren, K. Ip, Y. W. Heo, D. P. Norton, S. J. Pearton, "Sensitivity of Pt/ZnO Schottky Diode Characteristics to Hydrogen", *Appl. Phys. Lett.*, **84**, 1698 (2004). http://dx.doi.org/10.1063/1.1664012. 25

[47] C. S. Rout, A. Raju, A. Govindaraj, C. Rao, "Hydrogen Sensors based on ZnO Nanoparticles", *Solid State Commun.*, **138**, 136 (2006). http://dx.doi.org/10.1016/j.ssc.2006.02.016. 25

[48] K. D. Mitzner, J. Sternhagen, D. W. Galipeau, "Development of a Micromachined Hazardous Gas Sensor Array", *Sens. Actuators, B*, **93**, 92 (2003). Proceedings of the Ninth International Meeting on Chemical Sensors, http://dx.doi.org/10.1016/S0925-4005(03)00244-2. 25

[49] C. Wang, X. Chu, M. Wu, "Detection of H_2S down to ppb Levels at Room Temperature using Sensors based on ZnO Nanorods", *Sens. Actuators, B*, **113**, 320 (2006). http://dx.doi.org/10.1016/j.snb.2005.03.011. 25

[50] G. S. T. Rao, D. T. Rao, "Gas Sensitivity of ZnO Based Thick Film Sensor to NH_3 at Room Temperature", *Sens. Actuators, B*, **55**, 166 (1999). http://dx.doi.org/10.1016/S0925-4005(99)00049-0. 25

[51] G. Sberveglieri, S. Groppelli, P. Nelli, A. Tintinelli, G. Giunta, "A Novel Method for the Preparation of NH_3 Sensors Based on ZnO-in Thin Films", *Sens. Actuators, B*, **25**, 588 (1995). http://dx.doi.org/10.1016/0925-4005(95)85128-3. 25

[52] F. Paraguay, M. Miki-Yoshida, J. Morales, J. Solis, W. E. L., "Influence of Al, In, Cu, Fe and Sn Dopants on the Response of Thin Film ZnO Gas Sensor to Ethanol Vapour", *Thin Solid Films*, **373**, 137 (2000). http://dx.doi.org/10.1016/S0040-6090(00)01120-2. 25, 26

[53] S. A. Kumar, S.-M. Chen, "Nanostructured Zinc Oxide Particles in Chemically Modified Electrodes for Biosensor Applications", *Anal. Lett.*, **41**, 141 (2008). http://dx.doi.org/10.1080/00032710701792612. 25

[54] P. R. Solanki, A. Kaushik, A. A. Ansari, B. D. Malhotra, "Nanostructured Zinc Oxide Platform for Cholesterol Sensor", *Appl. Phys. Lett.*, **94**, 143901 (2009). http://dx.doi.org/10.1063/1.3111429. 25, 26

[55] S.-M. Lee, G. Grass, G.-M. Kim, C. Dresbach, L. Zhang, U. Gösele, M. Knez, "Low-Temperature ZnO Atomic Layer Deposition on Biotemplates: Flexible Photocatalytic ZnO Structures from Eggshell Membranes", *Phys. Chem. Chem. Phys.*, **11**, 3608 (2009). http://dx.doi.org/10.1039/b820436e. 25, 26

[56] N. Padmavathy, R. Vijayaraghavan, "Enhanced Bioactivity of ZnO Nanoparticles - an Antimicrobial Study", *Sci. Technol. Adv. Mater.*, **9**, 035004 (7pp) (2008). http://dx.doi.org/10.1088/1468-6996/9/3/035004. 25

[57] S. Y. Myong, S. J. Baik, C. H. Lee, W. Y. Cho, K. S. Lim, "Extremely Transparent and Conductive ZnO:Al Thin Films Prepared by Photo-Assisted Metalorganic Chemical Vapor Deposition (photo-MOCVD) Using $AlCl_3(6H_2O)$ as New Doping Material", *Jpn. J. Appl. Phys.*, **36**, L1078 (1997). http://jjap.ipap.jp/link?JJAP/36/L1078/. 25

[58] B. M. Ataev, A. M. Bagamadova, A. M. Djabrailov, V. V. Mamedov, R. A. Rabadanov, "Highly Conductive and Transparent Ga-Doped Epitaxial ZnO Films on Sapphire by CVD", *Thin Solid Films*, **260**, 19 (1995). http://dx.doi.org/10.1016/0040-6090(94)09485-3. 25

[59] S. J. Henley, M. N. R. Ashfold, D. Cherns, "The Growth of Transparent Conducting ZnO Films by Pulsed Laser Ablation", *Surf. Coat. Technol.*, **177-178**, 271 (2004). http://dx.doi.org/10.1016/j.surfcoat.2003.09.005. 25, 26

[60] D. C. Look, B. Claflin, "p-type Doping and Devices based on ZnO", *phys. stat. sol. (b)*, **241**, 624 (2004). http://dx.doi.org/10.1002/pssb.200304271. 25

[61] Y. R. Ryu, S. Zhu, D. C. Look, J. M. Wrobel, H. M. Jeong, H. W. White, "Synthesis of p-Type ZnO Films", *J. Cryst. Growth*, **216**, 330 (2000). http://dx.doi.org/10.1016/S0022-0248(00)00437-1. 25, 26

[62] T. Aoki, Y. Hatanaka, D. C. Look, "ZnO Diode Fabricated by Excimer-Laser Doping", *Appl. Phys. Lett.*, **76**, 3257 (2000). http://dx.doi.org/10.1063/1.126599. 25

[63] K.-K. Kim, H.-S. Kim, D.-K. Hwang, J.-H. Lim, S.-J. Park, "Realization of p-Type ZnO Thin Films via Phosphorus Doping and Thermal Activation of the Dopant", *Appl. Phys. Lett.*, **83**, 63 (2003). http://dx.doi.org/10.1063/1.1591064. 25

[64] D. C. Look, D. C. Reynolds, C. W. Litton, R. L. Jones, D. B. Eason, G. Cantwell, "Characterization of Homoepitaxial p-type ZnO Grown by Molecular Beam Epitaxy", *Appl. Phys. Lett.*, **81**, 1830 (2002). http://dx.doi.org/10.1063/1.1504875. 25, 26

[65] J. M. Bian, X. M. Li, X. D. Gao, W. D. Yu, L. D. Chen, "Deposition and Electrical Properties of N-In-codoped p-Type ZnO Films by Ultrasonic Spray Pyrolysis", *Appl. Phys. Lett.*, **84**, 541 (2004). http://dx.doi.org/10.1063/1.1644331. 25, 26

[66] M. Joseph, H. Tabata, T. Kawai, "p-Type Electrical Conduction in ZnO Thin Films by Ga and N codoping", *Jpn. J. Appl. Phys.*, **38**, L1205 (1999). http://dx.doi.org/10.1143/JJAP.38.L1205. 25

[67] A. B. Djurisic, Y. H. Leung, "Optical Properties of ZnO Nanostructures", *Small*, **2**, 944 (2006). http://dx.doi.org/10.1002/smll.200600134. 25, 26

[68] C. X. Xu, X. W. Sun, X. H. Zhang, L. Ke, S. J. Chua, "Photoluminescent Properties Of Copper-Doped Zinc Oxide Nanowires", *Nanotechnology*, **15**, 856 (2004). http://dx.doi.org/10.1088/0957-4484/15/7/026. 25

[69] B. Zhu, C. Xie, J. Wu, D. Zeng, A. Wang, X. Zhao, "Influence of Sb, In and Bi Dopants on the Response of ZnO Thick Films to VOCs", *Mater. Chem. Phys.*, **96**, 459 (2006). http://dx.doi.org/10.1016/j.matchemphys.2005.07.044. 26

[70] J. M. Ntep, S. Said Hassani, A. Lusson, A. Tromson-Carli, D. Ballutaud, G. Didier, R. Triboulet, "ZnO Growth by Chemical Vapour Transport", *J. Cryst. Growth*, **207**, 30 (1999). http://dx.doi.org/10.1016/S0022-0248(99)00363-2. 26

[71] E. Ohshima, H. Ogino, I. Niikura, K. Maeda, M. Sato, M. Ito, T. Fukuda, "Growth of the 2-in-size Bulk ZnO Single Crystals by the Hydrothermal Method", *J. Cryst. Growth*, **260**, 166 (2004). http://dx.doi.org/10.1016/j.jcrysgro.2003.08.019. 26

[72] E. A. Meulenkamp, "Synthesis and Growth of ZnO Nanoparticles", *J. Phys. Chem. B*, **102**, 5566 (1998). http://dx.doi.org/10.1021/jp980730h. 26, 27

[73] L. Spanhel, M. A. Anderson, "Semiconductor Clusters in the Sol-Gel Process - Quantized Aggregation, Gelation, and Crystal-Growth in Concentrated ZnO Colloids", *J. Am. Chem. Soc.*, **113**, 2826 (1991). http://dx.doi.org/10.1021/ja00008a004. 26

[74] Z. L. Wang, "Nanostructures of Zinc Oxide", *Mater. Today*, **7**, 26 (2004). http://dx.doi.org/10.1016/S1369-7021(04)00286-X. 26

[75] E. Matijevic, "Monodispersed Metal (Hydrous) Oxides - A Fascinating Field of Colloid Science", *Acc. Chem. Res.*, **14**, 22 (1981). http://dx.doi.org/10.1021/ar00061a004. 26

[76] M. Monge, M. L. Kahn, A. Maisonnat, B. Chaudret, "Room-Temperature Organometallic Synthesis of Soluble and Crystalline ZnO Nanoparticles of Controlled Size and Shape", *Angew. Chem., Int. Ed.*, **42**, 5321 (2003). http://dx.doi.org/10.1002/anie.200351949. 26, 34

[77] C. Pacholski, A. Kornowski, H. Weller, "Self-Assembly of ZnO: From Nanodots, to Nanorods", *Angew. Chem., Int. Ed.*, **41**, 1188 (2002). http://dx.doi.org/10.1002/1521-3773(20020402)41:7<1188::AID-ANIE1188>3.0.CO;2-5. 26, 27, 34

[78] X. Wang, C. J. Summers, Z. L. Wang, "Large-Scale Hexagonal-Patterned Growth of Aligned ZnO Nanorods for Nano-optoelectronics and Nanosensor Arrays", *Nano Lett.*, **4**, 423 (2004). http://dx.doi.org/10.1021/nl035102c. 26

[79] P. X. Gao, C. S. Lao, W. L. Hughes, Z. L. Wang, "Three-Dimensional Interconnected Nanowire Networks of ZnO", *Chem. Phys. Lett.*, **408**, 174 (2005). http://dx.doi.org/10.1016/j.cplett.2005.04.024. 26

[80] B. D. Yao, Y. F. Chan, N. Wang, "Formation of ZnO Nanostructures by a Simple Way of Thermal Evaporation", *Appl. Phys. Lett.*, **81**, 757 (2002). http://dx.doi.org/10.1063/1.1495878. 26

[81] H. J. Fan, B. Fuhrmann, R. Scholz, F. Syrowatka, A. Dadgar, A. Krost, M. Zacharias, "Well-Ordered ZnO Nanowire Arrays on GanN Substrate Fabricated via Nanosphere Lithography", *J. Cryst. Growth*, **287**, 34 (2006). http://dx.doi.org/10.1016/j.jcrysgro.2005.10.038. 26

[82] Y. Tong, Y. Liu, C. Shao, Y. Liu, C. Xu, J. Zhang, Y. Lu, D. Shen, X. Fan, "Growth and Optical Properties of Faceted Hexagonal ZnO Nanotubes", *J. Phys. Chem. B*, **110**, 14714 (2006). http://dx.doi.org/10.1021/jp056654h. 26

[83] R. Xie, D. Li, H. Zhang, D. Yang, M. Jiang, T. Sekiguchi, B. Liu, Y. Bando, "Low-Temperature Growth of Uniform ZnO Particles with Controllable Ellipsoidal Morphologies and Characteristic Luminescence Patterns", *J. Phys. Chem. B*, **110**, 19147 (2006). http://dx.doi.org/10.1021/jp0605449. 26

[84] T. Andelman, Y. Gong, M. Polking, M. Yin, I. Kuskovsky, G. Neumark, S. O'Brien, "Morphological Control and Photoluminescence of Zinc Oxide Nanocrystals", *J. Phys. Chem. B*, **109**, 14314 (2005). http://dx.doi.org/10.1021/jp050540o. 26

[85] F. Li, Y. Ding, P. Gao, X. Xin, Z. L. Wang, "Single-Crystal Hexagonal Disks and Rings of ZnO: Low-Temperature, Large-Scale Synthesis and Growth Mechanism", *Angew. Chem., Int. Ed.*, **43**, 5238 (2004). http://dx.doi.org/10.1002/anie.200460783. 26

[86] Y. Peng, A. W. Xu, B. Deng, M. Antonietti, H. Colfen, "Polymer-Controlled Crystallization of Zinc Oxide Hexagonal Nanorings and Disks", *J. Phys. Chem. B*, **110**, 2988 (2006). http://dx.doi.org/10.1021/jp056246d. 26

[87] L.-C. Chao, P.-C. Chiang, S.-H. Yang, J.-W. Huang, C.-C. Liau, J.-S. Chen, C.-Y. Su, "Zinc Oxide Nanodonut Prepared by Vapor-Phase Transport Process", *Appl. Phys. Lett.*, **88**, 251111 (2006). http://dx.doi.org/10.1063/1.2214146. 26

[88] C. X. Xu, X. W. Sun, Z. L. Dong, M. B. Yu, "Zinc Oxide Nanodisk", *Appl. Phys. Lett.*, **85**, 3878 (2004). http://dx.doi.org/10.1063/1.1811380. 26

[89] J. Joo, S. G. Kwon, J. H. Yu, T. Hyeon, "Synthesis of ZnO Nanocrystals with Cone, Hexagonal Cone, and Rod Shapes via Non-Hydrolytic Ester Elimination Sol-Gel Reactions", *Adv. Mater.*, **17**, 1873 (2005). http://dx.doi.org/10.1002/adma.200402109. 26, 27, 32, 36

[90] X. Ren, D. Han, D. Chen, F. Tang, "Large-Scale Synthesis of Hexagonal Cone-Shaped ZnO Nanoparticles with a Simple Route and their Application to Photocatalytic Degradation", *Mater. Res. Bull.*, **42**, 807 (2007). http://dx.doi.org/10.1016/j.materresbull.2006.08.030. 26, 27

[91] P. X. Gao, Y. Ding, W. Mai, W. L. Hughes, C. Lao, Z. L. Wang, "Conversion of Zinc Oxide Nanobelts into Superlattice-Structured Nanohelices", *Science*, **309**, 1700 (2005). http://dx.doi.org/10.1126/science.1116495. 26

[92] X. Y. Kong, Z. L. Wang, "Spontaneous Polarization-Induced Nanohelixes, Nanosprings, and Nanorings of Piezoelectric Nanobelts", *Nano Lett.*, **3**, 1625 (2003). http://dx.doi.org/10.1021/nl034463p. 26

[93] H. Q. Yan, R. R. He, J. Pham, P. D. Yang, "Morphogenesis of One-Dimensional ZnO Nano- and Microcrystals", *Adv. Mater.*, **15**, 402 (2003). http://dx.doi.org/10.1002/adma.200390091. 26

[94] B. Liu, H. C. Zeng, "Fabrication of ZnO "Dandelions" via a Modified Kirkendall Process", *J. Am. Chem. Soc.*, **126**, 16744 (2004). http://dx.doi.org/10.1021/ja044825a. 26

[95] M. Mo, J. C. Yu, L. Zhang, S. K. A. Li, "Self-Assembly of ZnO Nanorods and Nanosheets into Hollow Microhemispheres and Microspheres", *Adv. Mater.*, **17**, 756 (2005). http://dx.doi.org/10.1002/adma.200401477. 26

[96] G. H. Du, F. Xu, Z. Y. Yuan, G. V. Tendeloo, "Flowerlike ZnO Nanocones and Nanowires: Preparation, Structure, and Luminescence.", *Appl. Phys. Lett.*, **88**, 243101 (2006). http://dx.doi.org/10.1063/1.2211007. 26

[97] P. Feng, Q. Wan, T. H. Wang, "Contact-Controlled Sensing Properties of Flowerlike ZnO Nanostructures.", *Appl. Phys. Lett.*, **87**, 213111 (2005). http://dx.doi.org/10.1063/1.2135391. 26

[98] T. Zhang, W. Dong, M. Keeter-Brewer, S. Konar, R. N. Njabon, Z. R. Tian, "Site-Specific Nucleation and Growth Kinetics in Hierarchical Nanosyntheses of Branched ZnO Crystallites", *J. Am. Chem. Soc.*, **128**, 10960 (2006). http://dx.doi.org/10.1021/ja0631596. 26

[99] Z. Zhang, Y. Liu, D. Liu, S. Luo, J. Shen, L. Liu, W. Ma, Y. Ren, Y. Xiang, *et al.*, "Secondary Growth of Small ZnO Tripodlike Arms on the End of Nanowires", *Appl. Phys. Lett.*, **91**, 013106 (2007). http://dx.doi.org/10.1063/1.2752605. 26

[100] L. E. Greene, M. Law, D. H. Tan, M. Montano, J. Goldberger, G. Somorjai, P. D. Yang, "General Route to Vertical ZnO Nanowire Arrays using Textured ZnO Seeds", *Nano Lett.*, **5**, 1231 (2005). http://dx.doi.org/10.1021/nl050788p. 26

[101] L. E. Greene, B. D. Yuhas, M. Law, D. Zitoun, P. Yang, "Solution-Grown Zinc Oxide Nanowires", *Inorg. Chem.*, **45**, 7535 (2006). http://dx.doi.org/10.1021/ic0601900. 26

[102] M. Guo, P. Diao, S. Cai, "Hydrothermal Growth of Perpendicularly Oriented ZnO Nanorod Array Film and its Photoelectrochemical Properties", *Appl. Surf. Sci.*, **249**, 71 (2005). http://dx.doi.org/10.1016/j.apsusc.2004.11.053. 26

[103] L. Vayssieres, "Growth of Arrayed Nanorods and Nanowires of ZnO from Aqueous Solutions", *Adv. Mater.*, **15**, 464 (2003). http://dx.doi.org/10.1002/adma.200390108. 26

[104] L. Vayssieres, K. Keis, S.-E. Lindquist, A. Hagfeldt, "Purpose-Built Anisotropic Metal Oxide Material: 3D Highly Oriented Microrod Array of ZnO", *J. Phys. Chem. B*, **105**, 3350 (2001). http://dx.doi.org/10.1021/jp010026s. 26

[105] H. Yu, Z. Zhang, M. Han, X. Hao, F. Zhu, "A General Low-Temperature Route for Large-Scale Fabrication of Highly Oriented ZnO Nanorod/Nanotube Arrays", *J. Am. Chem. Soc.*, **127**, 2378 (2005). http://dx.doi.org/10.1021/ja043121y. 26

[106] R. A. Laudise, A. A. Ballman, "Hydrothermal Synthesis of Zinc Oxide and Sulfide", *J. Phys. Chem.*, **64**, 688 (1960). http://dx.doi.org/10.1021/j100834a511. 26, 36

[107] W. J. Li, E. W. Shi, W. Z. Zhong, Z. W. Yin, "Growth Mechanism and Growth Habit of Oxide Crystals", *J. Cryst. Growth*, **203**, 186 (1999). http://dx.doi.org/10.1016/S0022-0248(99)00076-7. 26, 36

[108] E. M. Dodson, J. A. Savage, "Vapour Growth of Single-Crystal Zinc Oxide", *J. Mater. Sci.*, **3**, 19 (1968). http://dx.doi.org/10.1007/BF00550885. 26

[109] A. Moustaghfir, E. Tomasella, A. Rivaton, B. Mailhot, M. Jacquet, J. L. Gardette, J. Cellier, "Sputtered Zinc Oxide Coatings: Structural Study and Application to the Photoprotection of the Polycarbonate", *Surf. Coat. Technol.*, **180-181**, 642 (2004). http://dx.doi.org/10.1016/j.surfcoat.2003.10.109. 26

[110] M. Grundmann, H. v. Wenckstern, R. Pickenhain, T. Nobis, A. Rahm, M. Lorenz, "Electrical Properties of ZnO Thin Films and Optical Properties of ZnO-Based Nanostructures", *Superlattices Microstruct.*, **38**, 317 (2005). http://dx.doi.org/10.1016/j.spmi.2005.08.026. 26

[111] X. Q. Wei, Z. Zhang, Y. X. Yu, B. Y. Man, "Comparative Study on Structural and Optical Properties of ZnO Thin Films Prepared by PLD using ZnO Powder Target and Ceramic Target", *Opt. Laser Technol.*, **41**, 530 (2009). http://dx.doi.org/10.1016/j.optlastec.2008.11.009. 26

[112] J. A. Libera, J. W. Elam, M. J. Pellin, "Conformal ZnO Coatings on High Surface Area Silica Gel using Atomic Layer Deposition", *Thin Solid Films*, **516**, 6158 (2008). http://dx.doi.org/10.1016/j.tsf.2007.11.044. 26

[113] D. Bao, H. Gu, A. Kuang, "Sol-gel-Derived c-Axis Oriented ZnO Thin Films", *Thin Solid Films*, **312**, 37 (1998). http://dx.doi.org/10.1016/S0040-6090(97)00302-7. 26

[114] L. Spanhel, "Colloidal ZnO Nanostructures and Functional Coatings: A Survey", *J. Sol-Gel Sci. Technol.*, **39**, 7 (2006). http://dx.doi.org/10.1007/s10971-006-7302-5. 26

[115] S. Baruah, J. Dutta, "Hydrothermal growth of ZnO nanostructures", *Science and Technology of Advanced Materials*, **10**, 013001 (18pp) (2009). http://dx.doi.org/10.1088/1468-6996/10/1/013001. 26

[116] S. K. N. Ayudhya, P. Tonto, O. Mekasuwandumrong, V. Pavarajarn, P. Praserthdam, "Solvothermal Synthesis of ZnO with Various Aspect Ratios Using Organic Solvents", *Cryst. Growth Des.*, **6**, 2446 (2006). http://dx.doi.org/10.1021/cg050345z. 26, 27

[117] L. Yang, G. Wang, C. Tang, H. Wang, L. Zhang, "Synthesis and Photoluminescence of Corn-Like ZnO Nanostructures under Solvothermal-Assisted Heat Treatment", *Chem. Phys. Lett.*, **409**, 337 (2005). http://dx.doi.org/10.1016/j.cplett.2005.05.015. 26, 27

[118] Y. Chen, M. Kim, G. Lian, M. B. Johnson, X. Peng, "Side Reactions in Controlling the Quality, Yield, and Stability of High Quality Colloidal Nanocrystals", *J. Am. Chem. Soc.*, **127**, 13331 (2005). http://dx.doi.org/10.1021/ja053151g. 26, 27, 32

[119] H. Du, F. Yuan, S. Huang, J. Li, Y. Zhuy, "A New Reaction to ZnO Nanoparticles", *Chem. Lett.*, **33**, 770 (2004). http://dx.doi.org/10.1246/cl.2004.770. 26, 27, 32

[120] X. Zhou, D. Zhang, Y. Zhu, Y. Shen, X. Guo, W. Ding, Y. Chen, "Mechanistic Investigations of PEG-Directed Assembly of One-Dimensional ZnO Nanostructures", *J. Phys. Chem. B*, **110**, 25734 (2006). http://dx.doi.org/10.1021/jp0643855. 26

[121] M. Epifani, J. Arbiol, R. Diaz, M. J. Peralvarez, P. Siciliano, J. R. Morante, "Synthesis of SnO $_2$ and ZnO Colloidal Nanocrystals from the Decomposition of Tin(II) 2-Ethylhexanoate and Zinc(II) 2-Ethylhexanoate", *Chem. Mater.*, **17**, 6468 (2005). http://dx.doi.org/10.1021/cm051642u. 26

[122] C. Fauteux, R. Longtin, J. Pegna, D. Therriault, "Fast Synthesis of ZnO Nanostructures by Laser-Induced Decomposition of Zinc Acetylacetonate", *Inorg. Chem.*, **46**, 11036 (2007). http://dx.doi.org/10.1021/ic700915z. 26, 36

[123] S. A. Studenikin, N. Golego, M. Cocivera, "Fabrication of Green and Orange Photoluminescent, Undoped ZnO Films using Spray Pyrolysis", *Journal of Applied Physics*, **84**, 2287 (1998). http://dx.doi.org/10.1063/1.368295. 26

[124] I. Bilecka, I. Djerdj, M. Niederberger, "One-minute Synthesis of Crystalline Binary and Ternary Metal Oxide Nanoparticles", *Chem. Commun.*, pp. 886–888 (2008). http://dx.doi.org/10.1039/b717334b. 26

[125] I. Bilecka, P. Elser, M. Niederberger, "Kinetic and Thermodynamic Aspects in the Microwave-Assisted Synthesis of ZnO Nanoparticles in Benzyl Alcohol", *ACS Nano*, **3**, 467 (2009). http://dx.doi.org/10.1021/nn800842b. 26, 33

[126] A. Lagashetty, V. Havanoor, S. Basavaraja, S. D. Balaji, A. Venkataraman, "Microwave-Assisted Route for Synthesis of Nanosized Metal Oxides", *Sci. Technol. Adv. Mater.*, **8**, 484 (2007). http://dx.doi.org/10.1016/j.stam.2007.07.001. 26

[127] S. J. Pearton, W. H. Heo, M. Ivill, D. P. Norton, T. Steiner, "Dilute Magnetic Semiconducting Oxides", *Semicond. Sci. Technol.*, **19**, R59 (2004). http://dx.doi.org/10.1088/0268-1242/19/10/R01. 26

[128] W. Prellier, A. Fouchet, B. Mercey, "Oxide-Diluted Magnetic Semiconductors: A Review of the Experimental Status", *J. Phys.: Condens. Matter*, **15**, R1583 (2003). http://dx.doi.org/10.1088/0953-8984/15/37/R01. 26

[129] T. Meron, G. Markovich, "Ferromagnetism in Colloidal Mn^{2+}-Doped ZnO Nanocrystals", *J. Phys. Chem. B*, **109**, 20232 (2005). http://dx.doi.org/10.1021/jp0539775. 26

[130] P. V. Radovanovic, N. S. Norberg, K. E. McNally, D. R. Gamelin, "Colloidal Transition-Metal-doped ZnO Quantum Dots", *J. Am. Chem. Soc.*, **124**, 15192 (2002). http://dx.doi.org/10.1021/ja028416v. 26

[131] D. A. Schwartz, N. S. Norberg, Q. P. Nguyen, J. M. Parker, D. R. Gamelin, "Magnetic Quantum Dots: Synthesis, Spectroscopy, and Magnetism of Co^{2+}- and Ni^{2+}-doped ZnO Nanocrystals", *J. Am. Chem. Soc.*, **125**, 13205 (2003). http://dx.doi.org/10.1021/ja036811v. 26

[132] R. Viswanatha, S. Sapra, S. Sen Gupta, B. Satpati, P. V. Satyam, B. N. Dev, D. D. Sarma, "Synthesis and Characterization of Mn-Doped ZnO Nanocrystals", *J. Phys. Chem. B*, **108**, 6303 (2004). http://dx.doi.org/10.1021/jp049960o. 26

[133] B. D. Yuhas, D. O. Zitoun, P. J. Pauzauskie, R. R. He, P. D. Yang, "Transition-Metal-doped Zinc Oxide Nanowires", *Angew. Chem., Int. Ed.*, **45**, 420 (2006). http://dx.doi.org/10.1002/anie.200503172. 26

[134] X. F. Wang, J. B. Xu, N. Ke, J. G. Yu, J. Wang, Q. Li, H. C. Ong, R. Zhang, "Imperfect Oriented Attachment: Direct Activation of High-Temperature Ferromagnetism in Diluted Magnetic Semiconductor Nanocrystals", *Appl. Phys. Lett.*, **88**, 223108 (2006). http://dx.doi.org/10.1063/1.2208554. 27

[135] X. F. Wang, J. B. Xu, B. Zhang, H. G. Yu, J. Wang, X. Zhang, J. G. Yu, Q. Li, "Signature of Intrinsic High-Temperature Ferromagnetism in Cobalt-doped Zinc Oxide Nanocrystals", *Adv. Mater.*, **18**, 2476 (2006). http://dx.doi.org/10.1002/adma.200600396. 27

[136] R. D. Yang, S. Tripathy, Y. Li, H.-J. Sue, "Photoluminescence and Micro-Raman Scattering in ZnO Nanoparticles: The Influence of Acetate Adsorption", *Chem. Phys. Lett.*, **411**, 150 (2005). http://dx.doi.org/10.1016/j.cplett.2005.05.125. 27

[137] I. Djerdj, G. Garnweitner, D. Arcon, P. M., J. Zvonko, M. Niederberger, "Diluted Magnetic Semiconductors: Mn/Co-doped ZnO Nanorods as Case Study", *J. Mater. Chem.*, **18**, 5208 (2008). http://dx.doi.org/10.1039/b808361d. 27

[138] D. Chu, Y. Zeng, D. Jiang, "Solution-Based, High-Yield Synthesis of Cobalt-Doped Zinc Oxide Nanorods", *J. Am. Ceram. Soc.*, **90**, 2269 (2007). http://dx.doi.org/10.1111/j.1551-2916.2007.01687.x. 27

[139] K. C. Barick, M. Aslam, V. P. Dravid, D. Bahadur, "Self-Aggregation and Assembly of Size-Tunable Transition Metal Doped ZnO Nanocrystals", *J. Phys. Chem. C*, **112**, 15163 (2008). http://dx.doi.org/10.1021/jp802361r. 27

[140] S. Cimitan, S. Albonetti, L. Forni, F. Peri, D. Lazzari, "Solvothermal Synthesis and Properties Control of Doped ZnO Nanoparticles", *J. Colloid Interface Sci.*, **329**, 73 (2009). http://dx.doi.org/10.1016/j.jcis.2008.09.060. 27

[141] Y. Guo, X. Cao, X. Lan, C. Zhao, X. Xue, Y. Song, "Solution-Based Doping of Manganese into Colloidal ZnO Nanorods", *J. Phys. Chem. C*, **112**, 8832 (2008). http://dx.doi.org/10.1021/jp800106v. 27

[142] X. Qiu, G. Li, X. Sun, L. Li, X. Fu, "Doping Effects of Co^{2+} Ions on ZnO Nanorods and their Photocatalytic Properties", *Nanotechnology*, **19**, 215703 (8pp) (2008). http://dx.doi.org/10.1088/0957-4484/19/21/215703. 27

[143] S. Thota, T. Dutta, J. Kumar, "On the Sol-Gel Synthesis and Thermal, Structural, and Magnetic Studies of Transition Metal (Ni, Co, Mn) Containing ZnO Powders", *J. Phys.: Condens. Matter*, **18**, 2473 (2006). http://dx.doi.org/10.1088/0953-8984/18/8/012. 27

[144] B. D. Yuhas, S. Fakra, M. A. Marcus, P. Yang, "Probing the Local Coordination Environment for Transition Metal Dopants in Zinc Oxide Nanowires", *Nano Lett.*, **7**, 905 (2007). http://dx.doi.org/10.1021/nl0626939. 27

[145] R. S. Anderson, "Lattice-Vibration Effects in the Spectra of ZnO:Ni and ZnO:Co", *Phys. Rev.*, **164**, 398 (1967). http://dx.doi.org/10.1103/PhysRev.164.398. 31

[146] P. Y. Emelie, J. D. Phillips, B. Buller, U. D. Venkateswaran, "Free Carrier Absorption and Lattice Vibrational Modes in Bulk ZnO", *J. Electron. Mater.*, **35**, 525 (2006). http://dx.doi.org/10.1007/s11664-006-0094-0. 31

[147] S. Hayashi, N. Nakamori, H. Kanamori, Y. Yodogawa, K. Yamamoto, "Infrared Study of Surface Phonon Modes in ZnO, CdS And BeO Small Crystals", *Surf. Sci.*, **86**, 665 (1978). http://dx.doi.org/10.1016/0039-6028(79)90447-3. 31

[148] R. Ruppin, R. Englman, "Optical phonons of small crystals", *Rep. Prog. Phys.*, **33**, 149 (1970). http://dx.doi.org/10.1088/0034-4885/33/1/304. 31

[149] M. Tzolov, N. Tzenov, D. Dimova-Malinovska, M. Kalitzova, C. Pizzuto, G. Vitali, G. Zollo, I. Ivanov, "Vibrational Properties and Structure of undoped and Al-doped ZnO Films Deposited by RF Magnetron Sputtering", *Thin Solid Films*, **379**, 28 (2000). http://dx.doi.org/10.1016/S0040-6090(00)01413-9. 31

[150] M. A. Andres-Verges, A. Mifsud, C. J. Serna, "Formation of Rod-Like Zinc-Oxide Microcrystals in Homogeneous Solutions", *J. Chem. Soc., Dalton Trans.*, **86**, 959 (1990). http://dx.doi.org/10.1039/FT9908600959. 31, 32, 34

[151] M. Andres-Verges, M. Martinez-Gallego, "Spherical and Rod-Like Zinc Oxide Microcrystals: Morphological Characterization and Microstructural Evolution with Temperature", *J. Mater. Sci.*, **27**, 3756 (1992). http://dx.doi.org/10.1007/BF00545452. 31

[152] M. Andres-Verges, C. J. Serna, "Morphological Characterization of ZnO Powders by X-Ray and IR Spectroscopy", *J. Mater. Sci.*, **7**, 970 (1988). http://dx.doi.org/10.1007/BF00720745. 31

[153] S. Music, D. Dragcevic, M. Maljkovic, S. Popovic, "Influence of Chemical Synthesis on the Crystallization and Properties of Zinc Oxide", *Mater. Chem. Phys.*, **77**, 521 (2003). http://dx.doi.org/10.1016/S0254-0584(02)00088-3. 31

[154] S. Music, S. Popovic, M. Maljkovic, D. Dragcevic, "Influence of Synthesis Procedure on the Formation and Properties of Zinc Oxide", *J. Alloys Compd.*, **347**, 324 (2002). http://dx.doi.org/10.1016/S0925-8388(02)00792-2. 31

[155] F. A. Sigoli, M. R. Davolos, M. Jafelicci, "Morphological Evolution of Zinc Oxide originating from Zinc Hydroxide Carbonate", *J. Alloys Compd.*, **262-263**, 292 (1997). http://dx.doi.org/10.1016/S0925-8388(97)00404-0. 31

[156] M. Niederberger, G. Garnweitner, "Organic Reaction Pathways in the Nonaqueous Synthesis of Metal Oxide Nanoparticles", *Chem. Eur. J.*, **12**, 7282 (2006). http://dx.doi.org/10.1002/chem.200600313. 32

[157] N. Pinna, M. Niederberger, "Surfactant-free Nonaqueous Synthesis of Metal Oxide Nanostructures", *Angew. Chem. Int. Ed.*, **47**, 5292 (2008). http://dx.doi.org/10.1002/anie.200704541. 32, 34

[158] M. Niederberger, N. Pinna, *Metal Oxide Nanoparticles in Organic Solvents*, Engineering Materials and Processes (Springer, 2009). ISBN: 978-1-84882-670-0. 32, 34

[159] N. Pinna, "The "Benzyl Alcohol Route": an Elegant Approach Towards Organic-Inorganic Hybrid Nanomaterials", *J. Mater. Chem.*, **17**, 2769 (2007). http://dx.doi.org/10.1039/b702854g. 34

[160] N. Pinna, G. Garnweitner, P. Beato, M. Niederberger, M. Antonietti, "Synthesis of Yttria-Based Crystattine and Lamellar Nanostructures and their Formation Mechanism", *Small*, **1**, 112 (2005). http://dx.doi.org/10.1002/smll.200400014. 34

[161] Z. Hu, J. F. Herrera Santos, G. Oskam, P. C. Searson, "Influence of the Reactant Concentrations on the Synthesis of ZnO Nanoparticles", *J. Colloid Interface Sci.*, **288**, 313 (2005). http://dx.doi.org/10.1016/j.jcis.2005.02.058. 34

[162] J. Park, K. J. An, Y. S. Hwang, J. G. Park, H. J. Noh, J. Y. Kim, J. H. Park, N. M. Hwang, T. Hyeon, "Ultra-Large-Scale Syntheses of Monodisperse Nanocrystals", *Nat. Mater.*, **3**, 891 (2004). http://dx.doi.org/10.1038/nmat1251. 40

Chapter III:

Cobalt and Manganese Doped ZnO Dopant environment and Magnetic properties

Contents

III.1 Introduction

III.1.1 Doped ZnO context

Since 2000 and the paper of Dietl et al.[1] predicting room ferromagnetism in zinc oxide doped by manganese, a lot of controversial works were published on the magnetic properties of ZnO doped by different dopants and combination of dopants[2–8]. A picture of the controversy is given by the tableIII.1 which reports some studies on Co- and Mn-doped ZnO. From this table, one can see that, for the same dopant, the magnetic behaviors go from paramagnetic to ferromagnetic or spin glass behavior. In fact, many of the claims of high-temperature ferromagnetism in DMS systems are questionable owing to the tendency of these materials to phase-separate into a semiconductor matrix laced with ferromagnetic metal or oxide domains[9–18]. Consequently, the main point of any new study relies on the exclusion of any secondary phase as the origin of the ferromagnetism. This point is critical for nanoscale systems as they tend to expel the doping atoms from the nanocrystals core. In fact, during synthesis, dopant can form many secondary phases that possess magnetic ordering (cf. tableIII.2). Thus, homogenous doping is particularly important in the comprehensive study of DMS.

However, even if sometime the presence of a second phase can be excluded, there is still a discrepancy between the intrinsic magnetism reported. In fact, the exact origin of the magnetism in DMS is yet not understood and subject of active debate[4,8,19–23]. It appears that for homogeneous systems the magnetic properties seems to be strongly dependent on dopant/matrix interaction, carrier concentration, defects, and thus on synthesis conditions. Indeed, many authors agree with the important role played by defects in the magnetic properties and, it was found that Zn interstitial, oxygen vacancies or free carriers introduced by co-doping (Li, N, H, Sn) are able to induce or enhance ferromagnetism[4,16,21,24–30].

In view of all the facts mentioned above, we conducted meticulous characterizations of the doped nanoparticles obtained, with emphasis on the homogeneity as well as the

	Dopant content x ($Zn_{1-x}M_{Tx}O$)	Synthesis	Form	Magnetic State	Ref
Mn	0.02-0.06	Decomposition	Bulk	Para	[31]
Mn	0.05-0.1	Solid state	Bulk	Para	[32]
Mn	0.02-0.05	Solid state	Bulk	Para	[33]
Mn	0.02	Solid state	Bulk	Ferro T_C>420 K	[34]
Mn	0.05	PLD	Film on sapphire	Para	[35]
Mn	0.1-0.3	MBE	Film on sapphire	Ferro T_C = 30-45 K	[36]
Mn	0.36	PLD	Film on sapphire	Spin glass T_F = 13 K	[37]
Mn	0.07	Sputtering	Film on sapphire	Para	[38]
Mn	0.02	PLA	Film on fused quartz	Ferro T_C>400 K	[39]
Mn	0.002	Solution	Film on fused silica	Ferro T_C>300 K	[40]
Mn	0.01-0.04	VLS	Nanowires on Si	Ferro T_C>400 K	[41]
Mn	<0.01	CVD	Nanorods on sapphire	Ferro T_C>350 K	[42]
Mn	0.04	Solution	Nanocrystals	Ferro T_C>300 K	[43]
Mn	0.002-0.02	Sol-gel	Nanocrystals	Ferro T_C>350 K	[44]
Mn	0.02-0.25	Combustion	Nanowires	Para	[45]
Co	0.02-0.15	Decomposition	Bulk	Para	[46]
Co	0.05-0.15	Decomposition	Bulk	Para	[47]
Co	0.02	Solid state	Bulk	Para	[33]
Co	0.05	Sol-gel	Bulk	Para	[48]
Co	0.1	Hydrothermal	Bulk	Para	[49]
Co	0.05-0.25	PLD	Film on sapphire	Ferro T_C~300 K	[50]
Co	0.01-0.25	PLD	Film on sapphire	Ferro T_C>300 K	[35]
Co	0.25	PLD	Film on sapphire	Spin glass T_F = 8K	[51]
Co	0.016-0.05	PLD at 500°C	Film on Al_2O_3	Ferro T_C~300 K	[52]
Co	0.016-0.05	PLD at 700°C	Film on Al_2O_3	Para	[52]
Co	0.05	PLD	Film on Si	Ferro T_C>300 K	[53]
Co	0.01-0.02	Electrodeposition	Nanowires on Si	Ferro T_C>300 K	[54]
Co	0.01-0.08	Solution	Nanocrystals	Ferro T_C>350 K	[55]
Co	0.056	Solvothermal	Nanocrystals	Ferro T_C>300 K	[56]
Co	0.01-0.1	Solution	Nanocrystals	Para	[57]

Table III.1: Magnetic behaviors of doped ZnO: Overview of some published results (VLS stands for vapor-liquid-solid).

local environment of the magnetic ions diluted into the matrix before to interpret the magnetic properties: this will be presented in this chapter.

Phase	**Form**	**Magnetic ordering**	**Transition Temperature (K)**	**Refs**
Mn	-	Antiferro	100	[27]
MnO	Bulk	Antiferro	≈120	[58–61]
	NPs	Ferro	10-30	[59,62]
MnO_2 (α; β; λ)	Bulk	Antiferro	25; 92; 32	[63–66]
	NPs	Antiferro	13; 98 & 30-50; 17	[63–65,67]
αMn_2O_3	Bulk	Antiferro	80-90 & 25	[58,68]
	Diluted NPs	Superpara	≈35	[69]
Mn_3O_4	Bulk	Ferri	42	[70]
	NPs	Ferri	≈40	[58–60,71]
	Diluted NPs	Superpara	41	[72]
$ZnMn_2O_4$	-	Ferro	1298	[5]
MnZn	-	Ferro	150	[5]
Co	Bulk	Ferro	1373	[5,15]
	NPs	Superpara	10 to RT	[73,74]
	Diluted NPs	Superpara	9-13	[75]
CoO	-	Antiferro	287	[76]
Co_3O_4	Bulk	Antiferro	40	[76,77]
	NPs	Antiferro	30-35	[78]
	Diluted NPs	Superpara	10-20	[78]
CoZn	Bulk	Ferro	≈400	[9,79]

Table III.2: Possible secondary phases formed by the dopant with their magnetic properties as bulk and nanoparticles (NPs).

III.1.2 Case of Co- and Mn-doped ZnO from trioctylamine route

The works reported in this manuscript follows closely the study of Dr. Zitoun on the synthesis and characterization of manganese and cobalt doped ZnO nanowires synthesized by a surfactant assisted route[80,81]. The results obtained will be introduced here as they will be compared to our results all along this chapter.

The Co- and Mn-doped zinc oxide nanowires were grown from a solution phase synthesis by the thermal decomposition of the metal precursors (zinc acetate, cobalt acetate or manganese oleate) in a coordinating solvent, the trioctylamine, between 280-310 °C. The nanowires, average 30 nm in diameter, can grow as long as 3-4 μm. The Mn-doped ZnO displays a paramagnetic state even after annealing and the appearance of a Mn rich precipitate while Co-doped ZnO exhibits mainly a ferromagnetic behavior till 350K, and display high magnetic moment values (1.3 μ_B/Co at 300K). The dopant distribution in the wurtzite lattice, ensured by EDX, EPR, EELS and photoluminescence experiments, was uniform with no detectable phase impurities or clustering. Even though no secondary phase was observed, amine is able to reduce metals at high temperature; therefore, the use of another solvent less reductive such as alcohol and lower temperature is more likely to avoid any possible reduction or segregation of the magnetic dopants.

III.2 Dopant environment

After determining the morphology, purity and dopant concentration (cf. chapter II) we ascertained the local environment of the cobalt using electronic spectroscopy and paramagnetic resonance.

III.2.1 UV/Visible reflectance

Diffuse reflectance UV-Visible measurements of pure ZnO and ZnO doped with Co and Mn are shown in figure 1. The spectrum of pure ZnO exhibits typical exciton band-gap absorption around 3.3 eV. Co-doped ZnO spectra synthesized in pure BA and in BA/anisole (5/95%) show the same additional optical absorptions at 2.18, 2.03 and 1.9 eV. These features are due to the $^4A_2(F) \rightarrow {}^2A_1(G)$, $^4A_2(F) \rightarrow {}^4T_1(P)$, $^4A_2(F) \rightarrow {}^2E(G)$ transitions, characteristic of Co^{2+} in a tetrahedral crystal field[82–84]. A modification of the excitonic peak emerges after doping, which is usually attributed as a red shift of the band gap due to sp-d exchange interactions[16,85,86]. However, we assume that this modification is probably caused by a charge transfer as explained by Gamelin et al.[55,87,88]. Indeed, the band gap edge of ZnO is still present at 3.3 eV and is only partially overlapping with this new band at around 3 eV. The spectrum of the Mn-doped sample depicts a broad absorption peak centered at 2.7eV. Such a band is often attributed to the Mn^{2+} transition $^6A_1 \rightarrow {}^4T_1(G)$[31,89]. However, manganese II (d5) should not present any (or very weak) absorption as they are forbidden by parity and spin. Thus, the exact origin of this band is not unequivocally assigned and by considering the width of this absorption it is justifiable to attribute it to a charge-transfer[40,90,91]. Finally, electron spectroscopy is consistent with Co- and Mn-doped ZnO presenting a homogeneous distribution of the dopants in a tetrahedral environment, i.e. at the Zn site.

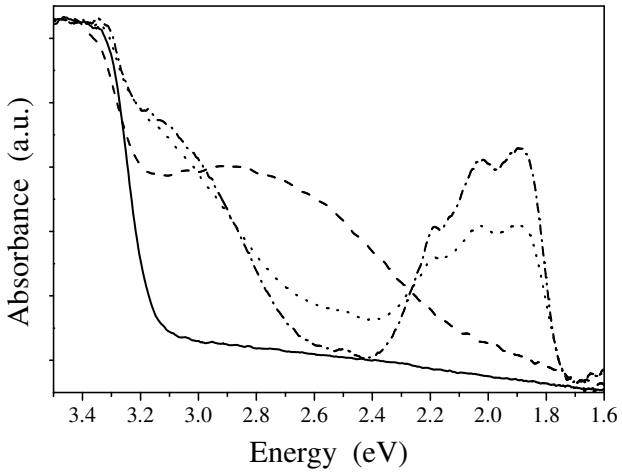

Figure III.1: Diffuse reflectance UV-Visible of pure ZnO (—) and 0.81% Co-doped ZnO (···) synthesized in BA/anisole (5/95%), 0.77% Co-doped ZnO (·–) synthesized in pure BA and 0.66% Mn-doped ZnO (- - -) synthesized in BA/anisole (5/95%).

III.2.2 Electron paramagnetic resonance spectroscopy

We complemented the study of the dopant distribution and environment with electron paramagnetic resonance spectroscopy (EPR). This technique is a very efficient tool to determine environment of paramagnetic species in a host lattice and was used to investigate Mn in several II-VI semiconductors[92–95] and Co in SnO_2 or ZnSe[96,97].

Manganese

EPR was used to probe manganese in ZnO as films, single crystals, colloids and powders[40,80,98–100]. It appears that isolated manganese in the tetrahedral environment of zinc oxide has a g-factor value close to 2 with a hyperfine coupling constant (^{55}Mn nucleus, I = 5/2) of A = 76x10^{-4} cm^{-1}[98–101] whereas the presence of surface state Mn^{2+} atoms presents a hyperfine coupling of A = 89x10^{-4} cm^{-1}[40,100].

EPR measurements were performed on powders and the spectra obtained are independent of the solvent used. Below 1.0% Mn doping, the spectrum shows two features at a g-factor ∼2: (i) A broad resonance resulting from exchange interactions between Mn^{2+}

ions and (ii) a sextuplet from isolated spins (Fig.2). The observed hyperfine splitting (a = 76 Gauss, A = 72x10^{-4} cm^{-1}) (Fig.3) is in close agreement with the bulk value for diluted Mn in ZnO matrix and precludes the occurrence of surface state Mn^{2+} atoms. In the present case the manganese ions are distributed substitutionally in tetrahedral sites. EPR spectra were also recorded at different temperatures between 100 and 300 K (Fig.2). The linewidth (peak-to-peak) of the broad resonance is constant over this range of temperature, indicating an absence of spin correlation. Moreover, the intensity decreases with increasing temperature following, as expected for isolated paramagnetic ions, a Curie's law. Plotting the inverse of the intensity versus temperature (Fig.4), it is possible to determine a Curie-Weiss temperature of θ = -55.5 K, the minus sign indicating antiferromagnetic exchanges between interacting neighboring manganese. At higher Mn concentration, only the broad signal is observable. Similar behavior of the signal with the concentration of Mn has been observed for sample synthesized with trioctylamine[80].

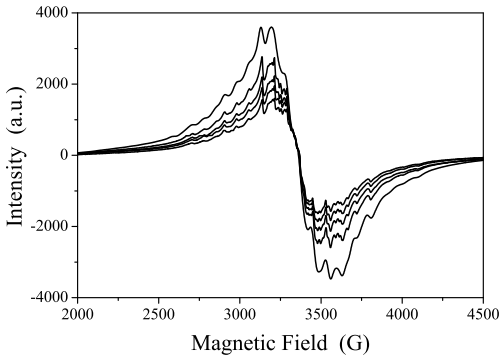

Figure III.2: Temperature-dependent EPR spectra (intensity decreases with increasing temperature, T = 100, 150, 200, 250 and 300 K) of 0.56% Mn doped ZnO synthesized in benzyl alcohol.

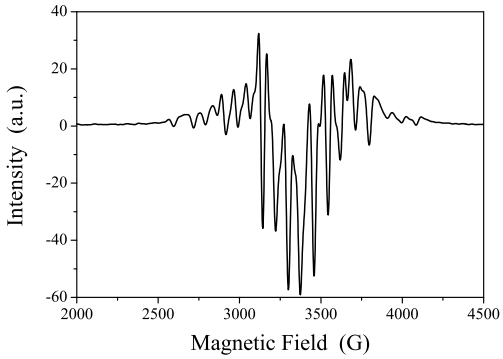

Figure III.3: First derivative of the spectrum in figure 2 collected at T = 100 K.

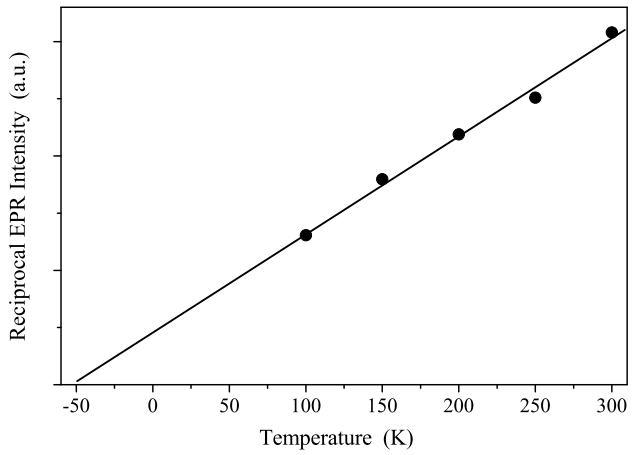

Figure III.4: Reciprocal EPR intensity versus temperature of 0.56% Mn-doped ZnO synthesized in BA.

Cobalt

Cobalt in ZnO present below 100 K two bands with a g-factor value of $g_{\parallel}$= 2.25 and $g_{eff\perp}$ = 4.5 and a corresponding hyperfine coupling value (^{59}Co nucleus, I = 7/2) of $A_{\parallel}$ = 16x10^{-4} and $A_{\perp}$ = 3x10^{-4} cm^{-1} [81,98,102–104].

For particles synthesized in pure benzyl alcohol and in anisole with traces of benzyl alcohol a series of EPR spectra was recorded as a function of temperature (Fig.5 and Fig.6). At room temperature, the samples do not display any resonance. At low temperature (below 100 K) the spectra, for the two type of samples, are dominated by an intense broad resonance (H = 1500 Gauss, g = 4.46) and a weaker band (H = 3000 Gauss, g = 2.23). The hyperfine structure is resolved for the band at g = 2.23 (Fig.7). The octet is separated by 15.9 Gauss (A = 14x10^{-4} cm^{-1}), a value close to the one found in the literature[98,102]. All these results are indications for a homogeneous substitutional doping of cobalt in ZnO. However, a deep analysis of the EPR data relies also on the exclusion of other cobalt species possibly present in the ZnO.

For Co-doped ZnO quantum dots, it was found that interstitial octahedral cobalt give rise to resonances at $g_{eff\parallel}$ ∼3 and $g_{eff\perp}$ ∼5[103]. Such features do not appear in our

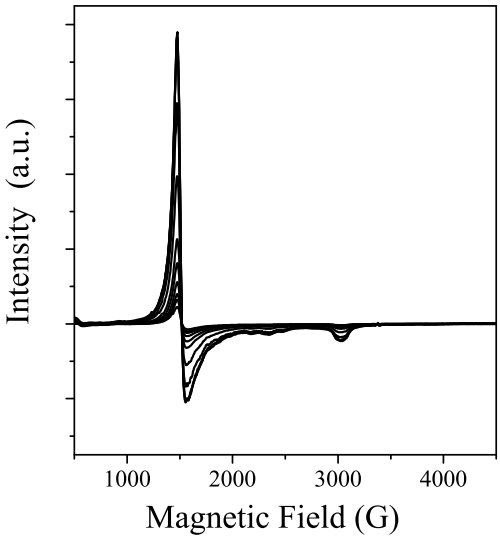

Figure III.5: Temperature-dependent EPR spectra (intensity decreases with increasing temperature) of 0.65% Co-doped ZnO synthesized in anisole with traces of benzyl alcohol in the temperature range 2.8-70 K.

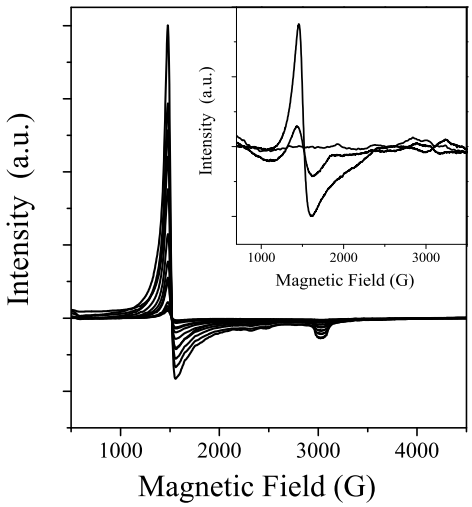

Figure III.6: Temperature-dependent EPR spectra (intensity decreases with increasing temperature) of 3.88% Co-doped ZnO synthesized in pure BA in the range of temperature 3.7-82.8 K. (inset) Spectra collected at T = 100, 150 and 300 K.

spectra. Even though the occurrence of isolated small clusters cannot grant for the observed ferromagnetic ordering at room temperature (cf. next section), the need to rule out cobalt clustering stands as the main focus of this study. In particular, the cobalt oxidation state needs to be enlightened by the study of Co (0) clusters to preclude any metal clustering in the ZnO matrix. There are few examples in the literature on the use of EPR to fully characterize cobalt based molecular clusters. The study of $[Co_6(\mu_3\text{-}S)_8(PEt_3)6](PF_6)]$ by EPR spectroscopy reveals a fine resonance interpreted by a g tensor [$g_x = 2.35$, $g_y = 2.04$, $g_z = 1.95$][105]. Other studies on $[Co_5MoN(CO)_{14}]^{2-}$ and $[Co_5MoN(CO)_{14}AuPPh_3]^-$ show similar results[106]. However, the samples studied in the present work do not exhibit any resonance at room temperature (inset Fig.6). Therefore, the EPR data rule out the presence of molecular or metal clusters. For Co nanoparticles, high-frequency ferromagnetic resonance was reported in the superparamagnetic regime as a function of the temperature for particles of 1.5 and 1.9 nm

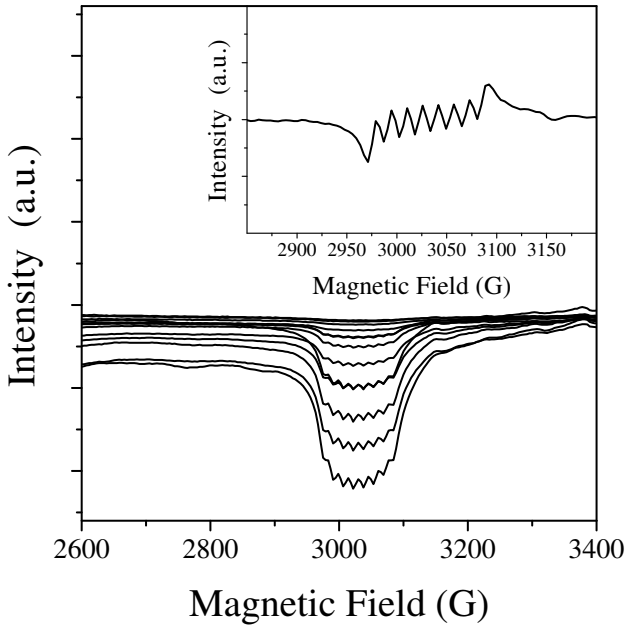

Figure III.7: Magnification of the band of g-factor value = 2.25 with in inset the first derivative of the EPR spectrum recorded at 5 K of 3.88% Co-doped ZnO synthesized in pure BA.

dispersed in polymer[107]. The polymer matrix interacted poorly with the surface of the particles and the low concentration of clusters prevented the presence of dipolar interactions between neighboring particles, which made easy the interpretation of the magnetic measurements[74,75,107,108]. The uncorrected values of g_{eff} ∼2.38 found at room temperature were well above the bulk values, 2.06 and 2.18 for fcc and hcp crystalline structures, respectively. The g_{eff} and ΔB increased as the inverse of temperature. At 100 K, the cobalt nanoparticles displayed a resonance centered at g_{eff} = 2.6 with ΔB = 1750 Gauss. At 10K, according to the behavior observed between 100 and 298 K, the cobalt clusters would display a resonance centered at g_{eff} = 5.5 with ΔB >2000 Gauss. The observed ferromagnetic resonance for the small cobalt clusters in a matrix is found to be drastically different from the observed one for cobalt doped ZnO nanoparticles. In the latter case, the g-factor values do not vary with temperature and the linewidth is ΔB = 80-90 Gauss for all samples, a very low value compared to

Co clusters. Therefore, the EPR study would preclude as well the occurrence of isolated cobalt nanoparticles.

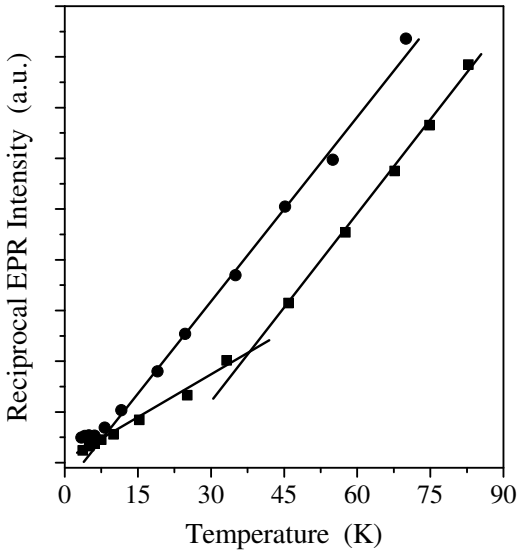

Figure III.8: Reciprocal EPR intensity versus temperature of 0.65% Co doped ZnO synthesized in anisole with traces of benzyl alcohol (circles) and 3.88% Co doped ZnO in pure benzyl alcohol (squares).

The reciprocal EPR intensity versus temperature is plotted in figure 8. Curie's Law predicts that this would be a straight line for isolated paramagnetic Co^{2+} ions. Samples synthesized in anisole with only traces of benzyl alcohol do not show any discrepancy from a Curie's law (Fig.8 circles). On the contrary, we observe a deviation for samples synthesized in pure benzyl alcohol in the temperature range 35-40 K (Fig.8 squares), suggesting that these samples are not paramagnetic. As a matter of fact, Co-doped ZnO synthesized in trioctylamine which are ferromagnetic, display also a deviation from the Curie's law in the same range of temperature[81].

III.3 Magnetic properties

With the environment of the metal dopant determined and preclusion of any clustering and/or dopant reduction, we next examined the magnetic properties with a SQUID magnetometer.

III.3.1 Manganese

In the case of manganese, for all concentrations and all synthesis conditions, the pristine samples never show any deviation from a paramagnetic behavior. The ZFC-FC measurements show no deviation from Curie's law (not shown). Figure 9 shows magnetization vs. Field (M-H) measurement for a Mn-doped ZnO sample synthesized in pure BA. The magnetic moment per atom does not saturate and reaches 4 μ_B/Mn for an applied field of 5 T. The absence of saturation due to some Mn^{2+} antiferromagnetically coupled, as revealed by EPR, could explain the discrepancy between the measurement and the expected effective moments for Mn^{2+} (5.92 μ_B/Mn) and the small coercive field (1 mT) observed (inset Fig.9).

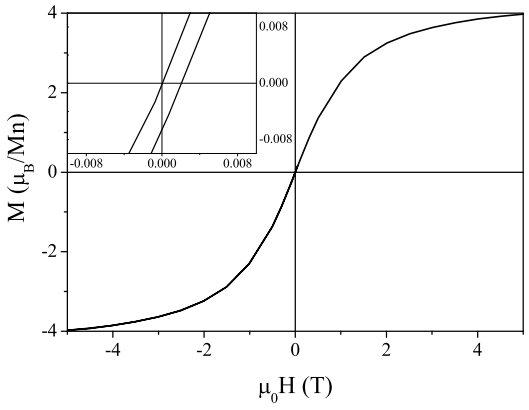

Figure III.9: Magnetization versus field loop at 2 K of 0.56% Mn-doped ZnO synthesized in pure benzyl alcohol.

III.3.2 Cobalt

The magnetic properties of cobalt doped samples were investigated as a function of Co concentration and synthesis solvent. Magnetization versus field (M-H) measurements at 2 K are depicted in figures 10 and 11 for synthesis in different solvent ratio. The nanoparticles synthesized in BA/anisole (5/95%) do not exhibit magnetic hysteresis for any concentration (Fig.10). At μ_0H = 5.0 T, the magnetization does not saturate and reaches values from 2.1 to 3.6 μ_B/Co atom depending on the cobalt concentration. The maximum is found for 1.16% doping (Fig.10 dashed-line). The Langevin fit gives an estimated value of M_S = 3.6 μ_B/Co, close to the expected value for isolated Co^{2+} (3.87 μ_B/Co). The lower magnetization observed in some samples is probably due to an antiferromagnetic coupling between a small fraction of Co^{2+} ions. Samples synthesized in pure benzyl alcohol (Fig.11) display lowest magnetic moment values at μ_0H = 5.0 T with no saturation. The most doped sample has a coercive field of 25 mT (Fig.11 dotted-line).

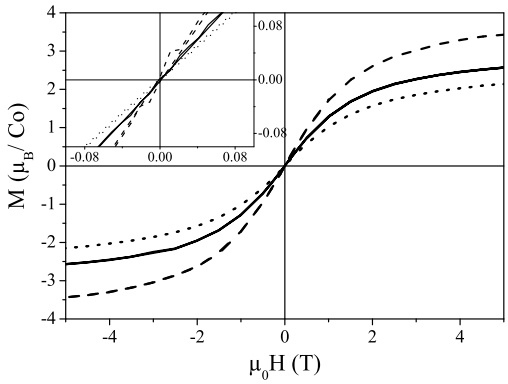

Figure III.10: Magnetization versus field loops at 2 K of 0.81% (—), 1.16% (- - -) and 4.09% (···) Co-doped ZnO synthesized in BA/anisole (5/95%).

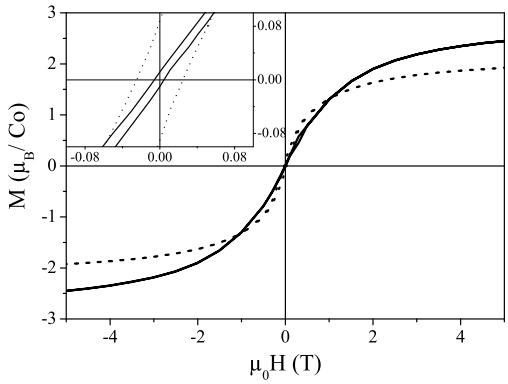

Figure III.11: Magnetization versus field loops at 2 K of 0.77% (—) and 3.88% (···) Co-doped ZnO in pure BA.

At room temperature, all samples synthesized in anisole are paramagnetic (Fig.12). However, the samples synthesized in pure benzyl alcohol exhibit a square loop with a

coercive field of 17 mT. The magnetic moment per cobalt atom is still reaching the value of 0.80 μ_B/Co for an applied field of μ_0H = 1.0 T (Fig.13 full-line).

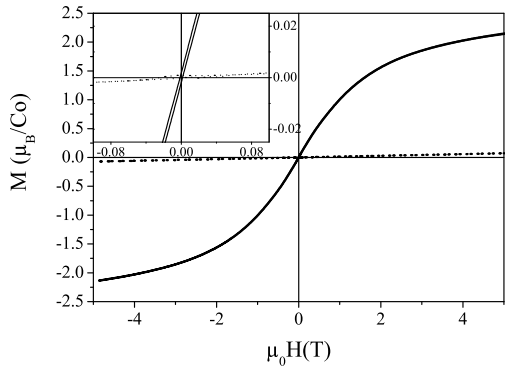

Figure III.12: Magnetization versus field of 4.09% Co-doped ZnO synthesized in BA/anisole (5/95%) at 2 K (—) and 300 K (···).

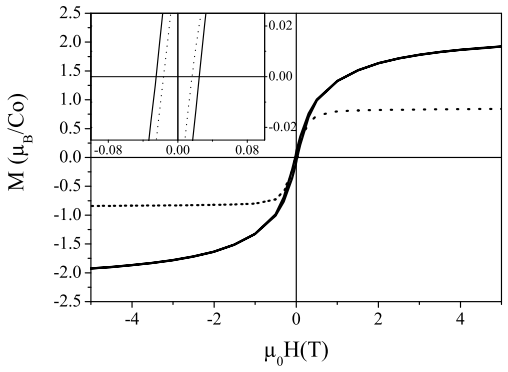

Figure III.13: Magnetization versus Field of 3.88% Co-doped ZnO synthesized in pure BA at 2 K (—) and 300 K (···).

We have also measured susceptibility versus temperature (ZFC-FC curves) (Fig.14). The ZFC-FC measurements show no deviation from Curie's law for nanoparticles synthesized in benzyl alcohol/anisole (5/95%) (Fig.14 full-line and dotted-line). However, in the case of the synthesis in pure benzyl alcohol, the ZFC-FC curves deviate from the Curie's law, as already deduced from EPR measurements. Indeed, for temperatures around 25-30 K the magnetization begins to deviate from paramagnetism, as determined from a plot of the inverse magnetic susceptibility versus temperature (not shown). Above this temperature the magnetic moment is stable at a non zero value (Fig.14 dashed-line and dot-dot-dashed-line). The temperature dependence displays a behavior typical of the coexistence of ferromagnetic and paramagnetic phases. Therefore, the magnetic behavior of these nanoparticles can be most reasonably ascribed to a paramagnetic phase (isolated Co^{2+}) and a ferromagnetic phase (coupled Co^{2+}). The exchange mechanism remains unclear although the reaction conditions play a key role on the magnetic properties and in particular on the exchange interaction.

As room-temperature ferromagnetism has been reported for pure ZnO particles [109–112],

a controlled experiment on pure ZnO was performed to rule out any ferromagnetism originated from point defects (Fig.15). In this case, the expected diamagnetism is only compensated at low temperature by a paramagnetism that certainly results from paramagnetic species absorbed on surface or intrinsic defects[113]. Moreover, the paramagnetism observed is at least three orders of magnitude lower than in cobalt doped samples.

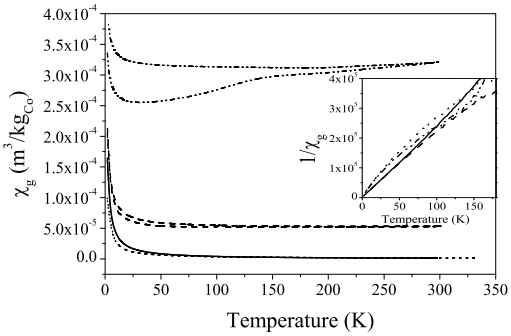

Figure III.14: ZFC-FC susceptibility curves of 0.81% (—) and 4.09% (···) Co-doped ZnO synthesized in BA/anisole (5/95%), 0.77% (- - -) and 3.88% (··–) Co-doped ZnO synthesized in pure BA and (inset) the inverse of magnetization for all samples (pure benzyl alcohol samples have been corrected from theirs ferromagnetic contribution).

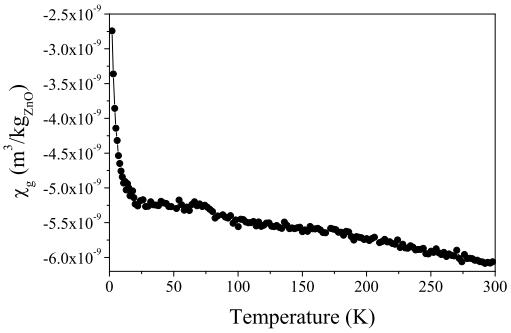

Figure III.15: ZFC susceptibility curve of pure ZnO synthesized in benzyl alcohol.

High temperature magnetization studies have been performed on samples synthesized in pure BA with a Vibrating Sample Magnetometer (VSM). The room temperature ferromagnetism is persistent up to 900 K and the decreasing of the magnetization with temperature is sensitive to the cobalt content (Fig.16). The behavior of magnetization shows a non-Brillouin type temperature dependence, for various cobalt concentrations which could arise from an intrinsic magnetic effect or from thermal changes in the state of the sample with annealing temperature. Finally, it is rather intriguing and promising that the Curie temperature can be so high in an intrinsic DMS system.

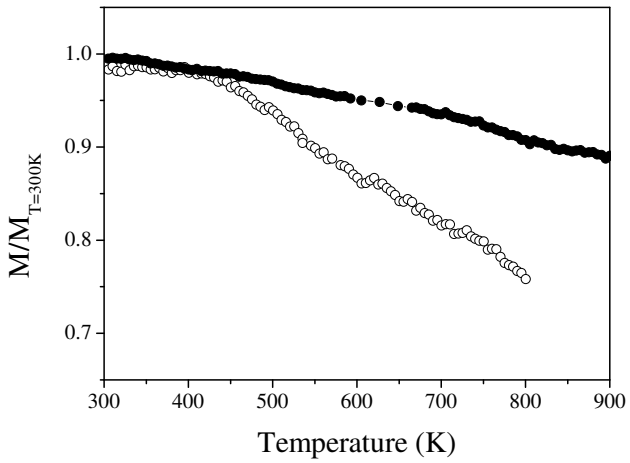

Figure III.16: High temperature magnetization curves of 0.77% (unfilled round) and 3.88% (filled round) Co-doped ZnO synthesized in pure BA (data are normalized to the magnetic moment at 300 K).

III.3.3 Discussion on the magnetic properties

The ferromagnetism observed for Co-doped samples synthesized in pure benzyl alcohol appears to be related to the doping of zinc oxide and not to a secondary phase. Indeed, the only phase that can be responsible for such magnetic behavior would be metallic cobalt. However, EPR measurements exclude the presence of cobalt clusters or particles. Furthermore, the magnetic moment obtained at room temperature (0.84 μ_B/Co) would imply that half cobalt (48.8%) is present as metallic cobalt (Ms = 1.72 μ_B/Co for bulk at RT)[74,114] with a large particle size to achieve the high Curie temperature found. Such proportion of cobalt should have been detected by another technique of characterization. In addition, the magnetic properties observed are comparable to those found when the synthesis is performed in trioctylamine; same doping ion and temperature dependence. The only discrepancy lies on the spontaneous magnetic moment per cobalt at room temperature, which seems to be higher in the case of synthesis in trioctylamine.

In spite of this, for the same cobalt concentration the synthesis in pure benzyl alco-

hol route leads to a ferromagnetic material unlike the one in benzyl alcohol/anisole (5/95%). In the other hand, the paramagnetic contribution for each sample is quantitatively related to the cobalt content and not to the solvent (inset Fig.14). The nature of the solvent is only relevant to the sign of the exchange interaction between the spins; antiferromagnetic coupling for anisole and ferromagnetic coupling for benzyl alcohol (cf. TableIII.3). Hence, the solvent plays an important role in the magnetic state and two hypotheses may arise from this statement. (i) The solvent may act as a reducing agent; amines and, to a less extent, alcohols are reducing agents. Co (0) is unlikely to be present as already discussed from EPR measurements. The cobalt would then be stabilized in two different oxidation states: Co^{2+} and Co^{+}. Co (I) (valence shell $3d^74s^1$) does not present any paramagnetic resonance due to its spin parity. In this case the formation of Co^{+} might mediate the interactions between the Co^{2+} centers[20]. (ii) On the other hand, benzyl alcohol could also act as strong σ-donor ligand on the surface. The carrier concentration would then increase from the particles synthesized in anisole to the ones in pure benzyl alcohol. Some results on nanoparticles have shown the effect of varying the carrier concentration by chemisorption of various reagents including amines, phosphines and sulfonates[115–119]. The chemical manipulation of magnetic state in ZnO has been claimed to depend only on the carrier concentration. These results would then be in agreement with the Zener model[1]. Based on the conclusion of studies presented above, we conducted several thermal treatments in presence of the solvents used in the synthesis. The samples synthesized by the benzyl alcohol route were refluxed in anisole for 48 hours in an autoclave. Their magnetic properties at room temperature are displayed in figure 17. The samples still exhibit a ferromagnetic behavior with no noticeable change. On the other hand, a sample synthesized following the benzyl alcohol/anisole route has been heated in benzyl alcohol at 250 °C for 48 hours; the collected material still displays a paramagnetic behavior as shown on figure 18. Based on these results, we assume that the magnetic properties observed in our material are not sensitive to the surface state. The observance of ferromagnetism

appears to be clearly related to the core properties of cobalt doped ZnO nanocrystals.

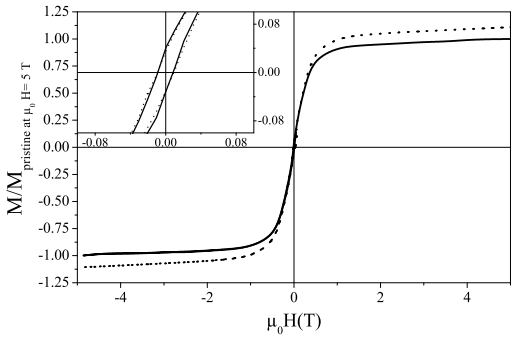

Figure III.17: Magnetization versus field at 300 K of 3.88% Co-doped ZnO synthesized in pure BA (—) and after thermal treatment in anisole (···) (data are normalized to the magnetic moment of pristine sample at μ_0H = 5 T).

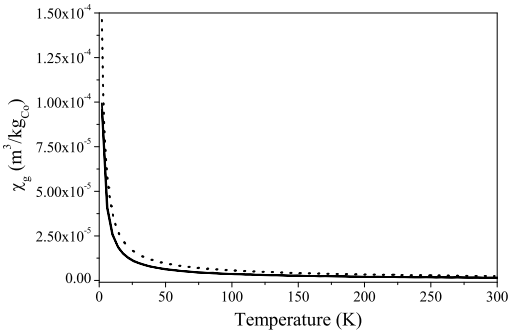

Figure III.18: ZFC-FC susceptibility curves of 4.09% Co-doped ZnO synthesized in BA/anisole (5/95%) (—) and after reflux in BA (···).

Solvents	**Dopants**	**Effective doping(%)**	**Magnetic coupling**
BA	Co	0.77	Ferromagnetic
BA	Co	3.88	Ferromagnetic
BA	Mn	0.56	Antiferromagnetic
A/BA (95/5 %)	Co	0.81	Antiferromagnetic
A/BA (95/5 %)	Co	1.16	Antiferromagnetic
A/BA (95/5 %)	Co	4.09	Antiferromagnetic
A/BA (95/5 %)	Mn	0.66	Antiferromagnetic
A/BA (95/5 %)	Mn	0.86	Antiferromagnetic
A + traces of BA	Co	0.65	Antiferromagnetic

Table III.3: Magnetic results for Mn- and Co-doped ZnO.

After the publication of the results presented here[120], another group has reported a very close work in which Co- and Mn-doped ZnO nanorods were also synthesized using

benzyl alcohol but with acetylacetonate precursors[121]. They evaluated the successful incorporation of the dopant in the ZnO matrix by XRD with Rietveld refinement and EPR. They found relatively the same result, i.e. manganese doping lead to a phase mainly paramagnetic and the cobalt to ferromagnetism till room temperature. However, their samples present at 300 K a higher magnetic moment at saturation; Ms = 4.86 emu/g for ∼5% Co-doped ZnO compared to the 2.23 emu/g (0.84 μ_B/Co) found here for 3.88% Co-doped sample. Nevertheless, this work confirms the potential of using non-hydrolytic sol-gel and in particular the benzyl alcohol route to obtain doped oxide nanostructures.

III.4 Conclusion

In summary, we have synthesized cobalt and manganese doped zinc oxide nanoparticles using a new solvent directed synthesis. The dopant substitutes onto zinc sites in the wurtzite lattice uniformly, with no detectable phase impurities or clustering. Mn-doped nanoparticles display paramagnetism for all temperature range. On the other hand, Co-doped nanoparticles exhibit a dependence of the magnetic behavior in function of the solvent used (cf. tableIII.3). When they are synthesized in pure benzyl alcohol they show a hysteresis effect through a wide temperature range, and display mainly ferromagnetic behavior. The magnetic moment at room temperature reaches the extremely high value of 0.8 μ_B for very low field. The complete EPR and magnetic studies on Co-doped ZnO allow to ensure that the ferromagnetic behavior is due to Co^{2+} ions. Finally, the present work brings new insights on the nature of ferromagnetism in Co-doped ZnO along with the ability of elaborating very large scale amount of DMS materials without any inorganic or organic impurity.

III.5 Experimental details

Diffuse reflectance UV/Visible was performed on Jasco V-560 UV/Vis spectrophotometer. The EPR experiments were performed at X band ∼9.5 GHz on a Brucker ESP300 spectrometer with microwave powers between 0.02 and 200 mW. Temperature studies from 4.2 to 300 K were carried out using an Oxford gas-flow cryostat. Magnetic properties were measured using a SuperQuantum Interference Design (SQUID) magnetometer MPMS XL7, in the range of temperature 2-350 K and of field 0-5 T. The temperature-dependent susceptibility was measured using DC procedure. The sample was cooled to 1.8 K under zero magnetic field, low magnetic field (5-50 mT) was then applied and data collected from 2 K to 350 K (zero-field cooled, ZFC). Field Cooled (FC) measurements were performed from 2K to 350K with an applied field during the cooling. High temperature magnetic measurements were performed on a Vibrating Sample Magnetometer (VSM) from Maglab Oxford Instrument operating at T = 300-1000K under a field of μ_0H = 2 T.

Bibliography

[1] T. Dietl, H. Ohno, F. Matsukura, J. Cibert, D. Ferrand, "Zener Model Description of Ferromagnetism in Zinc-Blende Magnetic Semiconductors", *Science*, **287**, 1019 (2000). http://dx.doi.org/10.1126/science.287.5455.1019. 57, 73

[2] T. Fukumura, Y. Yamada, H. Toyosaki, T. Hasegawa, H. Koinuma, M. Kawasaki, "Exploration of Oxide-Based Diluted Magnetic Semiconductors toward Transparent Spintronics", *Appl. Surf. Sci.*, **223**, 62 (2004). http://dx.doi.org/10.1016/S0169-4332(03)00898-5. 57

[3] C. Liu, F. Yun, H. Morkoc, "Ferromagnetism of ZnO and GaN: A Review", *J. Mater. Sci.: Mater. Electron.*, **16**, 555 (2005). http://dx.doi.org/10.1007/s10854-005-3232-1. 57

[4] F. Pan, C. Song, X. Liu, Y. Yang, F. Zeng, "Ferromagnetism and Possible Application in Spintronics of Transition-Metal-Doped ZnO Films", *Mater. Sci. Eng., R*, **62**, 1 (2008). http://dx.doi.org/10.1016/j.mser.2008.04.002. 57

[5] S. J. Pearton, W. H. Heo, M. Ivill, D. P. Norton, T. Steiner, "Dilute Magnetic Semiconducting Oxides", *Semicond. Sci. Technol.*, **19**, R59 (2004). http://dx.doi.org/10.1088/0268-1242/19/10/R01. 57, 59

[6] W. Prellier, A. Fouchet, B. Mercey, "Oxide-Diluted Magnetic Semiconductors: A Review of the Experimental Status", *J. Phys.: Condens. Matter*, **15**, R1583 (2003). http://dx.doi.org/10.1088/0953-8984/15/37/R01. 57

[7] R. Seshadri, "Zinc Oxide-Based Diluted Magnetic Semiconductors", *Curr. Opin. Solid State Mater. Sci.*, **9**, 1 (2005). http://dx.doi.org/10.1016/j.cossms.2006.03.002. 57

[8] M. Snure, D. Kumar, A. Tiwari, "Progress in ZnO-based Diluted Magnetic Semiconductors", *J. Miner. Met. Mater. Soc.*, **61**, 72 (2009). http://dx.doi.org/10.1007/s11837-009-0092-9. 57

[9] T. C. Kaspar, T. Droubay, S. M. Heald, M. H. Engelhard, P. Nachimuthu, S. A. Chambers, "Hidden Ferromagnetic Secondary Phases in Cobalt-doped ZnO Epitaxial Thin Films", *Phys. Rev. B*, **77**, 201303 (2008). http://dx.doi.org/10.1103/PhysRevB.77.201303. 57, 59

[10] J. H. Park, M. G. Kim, H. M. Jang, S. Ryu, Y. M. Kim, "Co-metal Clustering as the Origin of Ferromagnetism in Co-doped ZnO Thin Films", *Appl. Phys. Lett.*, **84**, 1338 (2004). http://dx.doi.org/10.1063/1.1650915. 57

[11] J. L. Costa-Kramer, F. Briones, J. F. Fernandez, A. C. Caballero, M. Villegas, M. Diaz, M. A. Garcia, A. Hernando, "Nanostructure and Magnetic Properties of the MnZnO System, a Room Temperature Magnetic Semiconductor?", *Nanotechnol.*, **16**, 214 (2005). http://dx.doi.org/10.1088/0957-4484/16/2/006. 57

[12] J. Blasco, F. Bartolome, L. M. Garcia, J. Garcia, "Extrinsic Origin of Ferromagnetism in Doped ZnO", *J. Mater. Chem.*, **16**, 2282 (2006). http://dx.doi.org/10.1039/b518418e. 57

[13] H. J. von Bardeleben, N. Jedrecy, J. L. Cantin, "Ferromagnetic Resonance Signature of Metallic Co Clusters in Ferromagnetic ZnCoO Thin Films", *Appl. Phys. Lett.*, **93**, 142505 (2008). http://dx.doi.org/10.1063/1.2998309. 57

[14] K. Rode, R. Mattana, A. Anane, V. Cros, E. Jacquet, J.-P. Contour, F. Petroff, A. Fert, M.-A. Arrio, *et al.*, "Magnetism of (Zn,Co)O Thin Films Probed by X-ray Absorption Spectroscopies", *Appl. Phys. Lett.*, **92**, 012509 (2008). http://dx.doi.org/10.1063/1.2829610. 57

[15] D. P. Norton, M. E. Overberg, S. J. Pearton, K. Pruessner, J. D. Budai, L. A. Boatner, M. F. Chisholm, J. S. Lee, Z. G. Khim, *et al.*, "Ferromagnetism in Cobalt-Implanted ZnO", *Appl. Phys. Lett.*, **83**, 5488 (2003). http://dx.doi.org/10.1063/1.1637719. 57, 59

[16] S. Deka, P. A. Joy, "Electronic Structure and Ferromagnetism of Polycrystalline $Zn_{1-x}Co_xO$ ($0 \leq x \leq 0.15$)", *Solid State Commun.*, **134**, 665 (2005). http://dx.doi.org/10.1016/j.ssc.2005.03.013. 57, 61

[17] S.-J. Han, T.-H. Jang, Y. B. Kim, B.-G. Park, J.-H. Park, Y. H. Jeong, "Magnetism in Mn-doped ZnO Bulk Samples prepared by Solid State Reaction", *Appl. Phys. Lett.*, **83**, 920 (2003). http://dx.doi.org/10.1063/1.1597414. 57

[18] R. K. Zheng, H. Liu, X. X. Zhang, V. A. L. Roy, A. B. Djurisic, "Exchange Bias and the Origin of Magnetism in Mn-doped ZnO Tetrapods", *Appl. Phys. Lett.*, **85**, 2589 (2004). http://dx.doi.org/10.1063/1.1795366. 57

[19] S. Chambers, T. Droubay, C. Wang, K. Rosso, S. Heald, D. Schwartz, K. Kittilstved, D. Gamelin, "Ferromagnetism in Oxide Semiconductors", *Mater. Today*, **9**, 28 (2006). http://dx.doi.org/10.1016/S1369-7021(06)71692-3. 57

[20] K. R. Kittilstved, W. K. Liu, D. R. Gamelin, "Electronic Structure Origins of Polarity-Dependent High-T_C Ferromagnetismin Oxide-Diluted Magnetic Semiconductors", *Nat. Mater.*, **5**, 291 (2006). http://dx.doi.org/10.1038/nmat1616. 57, 73

[21] X. J. Liu, X. Y. Zhu, J. T. Luo, F. Zeng, F. Pan, "Grain Boundary Defects-Mediated Room Temperature Ferromagnetism in Co-doped ZnO Film", *J. Alloys Compd.*, **482**, 224 (2009). http://dx.doi.org/10.1016/j.jallcom.2009.03.162. 57

[22] A. Quesada, M. A. Garcia, M. Andres, A. Hernando, J. F. Fernandez, A. C. Caballero, M. S. Martin-Gonzalez, F. Briones, "Ferromagnetism in Bulk Co-Zn-O", *J. Appl. Phys.*, **100**, 113909 (2006). http://dx.doi.org/10.1063/1.2399884. 57

[23] B. W. Wessels, "Ferromagnetic Semiconductors and the Role of Disorder", *New J. Phys.*, **10**, 055008 (2008). http://dx.doi.org/10.1088/1367-2630/10/5/055008. 57

[24] N. Khare, M. Kappers, M. Wei, M. G. Blamire, J. MacManus-Driscoll, "Defect-Induced Ferromagnetism in Co-doped ZnO", *Adv. Mater.*, **18**, 1449 (2006). http://dx.doi.org/10.1002/adma.200502200. 57

[25] K. R. Kittilstved, D. R. Gamelin, "Manipulating Polar Ferromagnetism in Transition-Metal-doped ZnO: Why Manganese is Different from Cobalt", *J. Appl. Phys.*, **99**, 08M112 (2006). http://dx.doi.org/10.1063/1.2167638. 57

[26] H. Liu, X. Zhang, L. Li, Y. X. Wang, K. H. Gao, Z. Q. Li, R. K. Zheng, S. P. Ringer, B. Zhang, X. X. Zhang, "Role of point defects in room-temperature ferromagnetism of Cr-doped ZnO", *Appl. Phys. Lett.*, **91**, 072511 (2007). http://dx.doi.org/10.1063/1.2772176. 57

[27] D. P. Norton, S. J. Pearton, A. F. Hebard, N. Theodoropoulou, L. A. Boatner, R. G. Wilson, "Ferromagnetism in Mn-Implanted ZnO : Sn Single Crystals", *Appl. Phys. Lett.*, **82**, 239 (2003). http://dx.doi.org/10.1063/1.1537457. 57, 59

[28] A. L. Rosa, R. Ahuja, "Tuning the Ferromagnetism in Mn-Zn-O by Intrinsic Defects", *J. Phys.: Condens. Matter*, **19**, 386232 (2007). http://dx.doi.org/10.1088/0953-8984/19/38/386232. 57

[29] D. Rubi, J. Fontcuberta, A. Calleja, L. Aragones, X. G. Capdevila, M. Segarra, "Reversible Ferromagnetic Switching in ZnO:(Co, Mn) Powders", *Phys. Rev. B*, **75**, 155322 (2007). http://dx.doi.org/10.1103/PhysRevB.75.155322. 57

[30] D. A. Schwartz, D. R. Gamelin, "Reversible 300 K Ferromagnetic Ordering in a Diluted Magnetic Semiconductor", *Adv. Mater.*, **16**, 2115 (2004). http://dx.doi.org/10.1002/adma.200400456. 57

[31] C. N. R. Rao, F. L. Deepak, "Absence of Ferromagnetism in Mn- and Co-doped ZnO", *J. Mater. Chem.*, **15**, 573 (2005). http://dx.doi.org/10.1039/b412993h. 58, 61

[32] S. W. Yoon, S.-B. Cho, S. C. We, S. Yoon, B. J. Suh, H. K. Song, Y. J. Shin, "Magnetic Properties of ZnO-based Diluted Magnetic Semiconductors", *J. Appl. Phys.*, **93**, 7879 (2003). http://dx.doi.org/10.1063/1.1556126. 58

[33] S. Kolesnik, B. Dabrowski, "Absence of Room Temperature Ferromagnetism in Bulk Mn-doped ZnO", *J. Appl. Phys.*, **96**, 5379 (2004). http://dx.doi.org/10.1063/1.1755428. 58

[34] P. Sharma, A. Gupta, F. J. Owens, A. Inoue, K. V. Rao, "Room Temperature Spintronic Material–Mn-doped ZnO Revisited", *J. Magn. Magn. Mater.*, **282**, 115 (2004). http://dx.doi.org/10.1016/j.jmmm.2004.04.028. 58

[35] M. Venkatesan, C. B. Fitzgerald, J. G. Lunney, J. M. D. Coey, "Anisotropic Ferromagnetism in Substituted Zinc Oxide", *Phys. Rev. Lett.*, **93**, 177206 (2004). http://dx.doi.org/10.1103/PhysRevLett.93.177206. 58

[36] S. W. Jung, S.-J. An, G.-C. Yi, C. U. Jung, S.-I. Lee, S. Cho, "Ferromagnetic Properties of $Zn_{1-x}Mn_xO$ Epitaxial Thin Films", *Appl. Phys. Lett.*, **80**, 4561 (2002). http://dx.doi.org/10.1063/1.1487927. 58

[37] T. Fukumura, Z. W. Jin, M. Kawasaki, T. Shono, T. Hasegawa, S. Koshihara, H. Koinuma, "Magnetic Properties of Mn-doped ZnO", *Appl. Phys. Lett.*, **78**, 958 (2001). http://dx.doi.org/10.1063/1.1348323. 58

[38] X. M. Cheng, C. L. Chien, "Magnetic Properties of Epitaxial Mn-doped ZnO Thin Films", *J. Appl. Phys.*, **93**, 7876 (2003). http://dx.doi.org/10.1063/1.1556125. 58

[39] J.-H. Guo, A. Gupta, P. Sharma, K. V. Rao, M. A. Marcus, C. L. Dong, J. M. O. Guillen, S. M. Butorin, M. Mattesini, *et al.*, "X-ray Spectroscopic Study of the Charge State and Local Ordering of Room-temperature Ferromagnetic Mn-doped ZnO", *J. Phys.: Condens. Matter*, **19**, 172202 (2007). http://dx.doi.org/10.1088/0953-8984/19/17/172202. 58

[40] N. S. Norberg, K. R. Kittilstved, J. E. Amonette, R. K. Kukkadapu, D. A. Schwartz, D. R. Gamelin, "Synthesis of Colloidal Mn^{2+}: ZnO Quantum Dots and High-T_C Ferromagnetic Nanocrystalline Thin Films", *J. Am. Chem. Soc.*, **126**, 9387 (2004). http://dx.doi.org/10.1021/ja048427j. 58, 61, 62

[41] U. Philipose, S. V. Nair, S. Trudel, C. F. de Souza, S. Aouba, R. H. Hill, H. E. Ruda, "High-Temperature Ferromagnetism in Mn-doped ZnO Nanowires", *Appl. Phys. Lett.*, **88**, 263101 (2006). http://dx.doi.org/10.1063/1.2217707. 58

[42] J. M. Baik, J. L. Lee, "Fabrication of Vertically Well-Aligned (Zn,Mn)O Nanorods with Room Temperature Ferromagnetism", *Adv. Mater.*, **17**, 2745 (2005). http://dx.doi.org/10.1002/adma.200500776. 58

[43] T. Meron, G. Markovich, "Ferromagnetism in Colloidal Mn^{2+}-Doped ZnO Nanocrystals", *J. Phys. Chem. B*, **109**, 20232 (2005). http://dx.doi.org/10.1021/jp0539775. 58

[44] J. B. Wang, G. J. Huang, X. L. Zhong, L. Z. Sun, Y. C. Zhou, E. H. Liu, "Raman Scattering and High Temperature Ferromagnetism of Mn-doped ZnO Nanoparticles", *Appl. Phys. Lett.*, **88**, 252502 (2006). http://dx.doi.org/10.1063/1.2208564. 58

[45] S. Deka, P. Joy, "Synthesis and Magnetic Properties of Mn Doped ZnO Nanowires", *Solid State Commun.*, **142**, 190 (2007). http://dx.doi.org/10.1016/j.ssc.2007.02.017. 58

[46] G. Lawes, A. S. Risbud, A. P. Ramirez, R. Seshadri, "Absence of Ferromagnetism in Co and Mn Substituted Polycrystalline ZnO", *Phys. Rev. B*, **71**, 045201 (2005). http://dx.doi.org/10.1103/PhysRevB.71.045201. 58

[47] A. S. Risbud, N. A. Spaldin, Z. Q. Chen, S. Stemmer, R. Seshadri, "Magnetism in Polycrystalline Cobalt-substituted Zinc Oxide", *Phys. Rev. B*, **68**, 205202 (2003). http://dx.doi.org/10.1103/PhysRevB.68.205202. 58

[48] A. Manivannan, P. Dutta, G. Glaspell, M. S. Seehra, "Nature of Magnetism in Co- and Mn-doped ZnO Prepared by Sol-Gel Technique", *J. Appl. Phys.*, **99**, 08M110 (2006). http://dx.doi.org/10.1063/1.2166598. 58

[49] M. Bouloudenine, N. Viart, S. Colis, A. Dinia, "Bulk $Zn_{1-x}Co_xO$ Magnetic Semiconductors Prepared by Hydrothermal Technique", *Chem. Phys. Lett.*, **397**, 73 (2004). http://dx.doi.org/10.1016/j.cplett.2004.08.064. 58

[50] K. Ueda, H. Tabata, T. Kawai, "Magnetic and electric properties of transition-metal-doped ZnO films", *Appl. Phys. Lett.*, **79**, 988 (2001). http://dx.doi.org/10.1063/1.1384478. 58

[51] J. H. Kim, H. Kim, D. Kim, Y. E. Ihm, W. K. Choo, "Magnetic Properties of Epitaxially Grown Semiconducting $Zn_{1-x}Co_xO$ Thin Films by Pulsed Laser Deposition", *J. Appl. Phys.*, **92**, 6066 (2002). http://dx.doi.org/10.1063/1.1513890. 58

[52] A. Fouchet, W. Prellier, B. Mercey, "Influence of the Microstructure on the Magnetism of Co-doped ZnO Thin Films", *J. Appl. Phys.*, **100**, 013901 (2006). http://dx.doi.org/10.1063/1.2206091. 58

[53] Q. Liu, C. L. Gan, C. L. Yuan, G. C. Han, "Role of Metallic Cobalt in Room Temperature Dilute Ferromagnetic Semiconductor $Zn_{0.95}Co_{0.05}O_{1-\delta}$", *Appl. Phys. Lett.*, **92**, 032501 (2008). http://dx.doi.org/10.1063/1.2835702. 58

[54] J. Cui, Q. Zeng, U. J. Gibson, "Synthesis and Magnetic Properties of Co-doped ZnO Nanowires", *J. Appl. Phys.*, **99**, 08M113 (2006). http://dx.doi.org/10.1063/1.2169411. 58

[55] D. A. Schwartz, N. S. Norberg, Q. P. Nguyen, J. M. Parker, D. R. Gamelin, "Magnetic Quantum Dots: Synthesis, Spectroscopy, and Magnetism of Co^{2+}- and Ni^{2+}-doped ZnO Nanocrystals", *J. Am. Chem. Soc.*, **125**, 13205 (2003). http://dx.doi.org/10.1021/ja036811v. 58, 61

[56] X. F. Wang, J. B. Xu, N. Ke, J. G. Yu, J. Wang, Q. Li, H. C. Ong, R. Zhang, "Imperfect Oriented Attachment: Direct Activation of High-Temperature Ferromagnetism in Diluted Magnetic Semiconductor Nanocrystals", *Appl. Phys. Lett.*, **88**, 223108 (2006). http://dx.doi.org/10.1063/1.2208554. 58

[57] P. Lommens, P. F. Smet, C. de Mello Donega, A. Meijerink, L. Piraux, S. Michotte, S. Mátéfi-Tempfli, D. Poelman, Z. Hens, "Photoluminescence Properties of Co^{2+}-doped ZnO Nanocrystals", *J. Lumin.*, **118**, 245 (2006). http://dx.doi.org/10.1016/j.jlumin.2005.08.020. 58

[58] T. Ahmad, K. V. Ramanujachary, S. E. Lofland, A. K. Ganguli, "Nanorods of Manganese Oxalate: a Single Source Precursor to Different Manganese Oxide Nanoparticles (MnO, Mn_2O_3, Mn_3O_4)", *J. Mater. Chem.*, **14**, 3406 (2004). http://dx.doi.org/10.1039/b409010a. 59

[59] W. S. Seo, H. H. Jo, K. Lee, B. Kim, S. J. Oh, J. T. Park, "Size-Dependent Magnetic Properties of Colloidal Mn_3O_4 and MnO Nanoparticles", *Angew. Chem., Int. Ed.*, **43**, 1115 (2004). http://dx.doi.org/10.1002/anie.200352400. 59

[60] I. Djerdj, D. Arcon, Z. Jaglicic, M. Niederberger, "Nonaqueous Synthesis of Manganese Oxide Nanoparticles, Structural Characterization, and Magnetic Properties", *J. Phys. Chem. C*, **111**, 3614 (2007). http://dx.doi.org/10.1021/jp067302t. 59

[61] D. Zitoun, N. Pinna, N. Frolet, C. Belin, "Single Crystal Manganese Oxide Multipods by Oriented Attachment", *J. Am. Chem. Soc.*, **127**, 15034 (2005). http://dx.doi.org/10.1021/ja0555926. 59

[62] G. H. Lee, S. H. Huh, J. W. Jeong, B. J. Choi, S. H. Kim, H.-C. Ri, "Anomalous Magnetic Properties of MnO Nanoclusters", *J. Am. Chem. Soc.*, **124**, 12094 (2002). http://dx.doi.org/10.1021/ja027558m. 59

[63] J. B. Yang, X. D. Zhou, W. J. James, S. K. Malik, C. S. Wang, "Growth and Magnetic Properties of $MnO_{2-\delta}$ Nanowire Microspheres", *Appl. Phys. Lett.*, **85**, 3160 (2004). http://dx.doi.org/10.1063/1.1805699. 59

[64] G. Wang, B. Tang, L. Zhuo, J. Ge, M. Xue, "Facile and Selected-Control Synthesis of β-MnO_2 Nanorods and Their Magnetic Properties", *Eur. J. Inorg. Chem.*, **2006**, 2313 (2006). http://dx.doi.org/10.1002/ejic.200500983. 59

[65] L. W. Guo, D. L. Peng, H. Makino, T. Hanada, S. K. Hong, K. Sumiyama, T. Yao, K. Inaba, "Structural Characteristics and Magnetic Properties of λ-MnO_2 Films Grown by Plasma-Assisted Molecular Beam Epitaxy", *J. Appl. Phys.*, **90**, 351 (2001). http://dx.doi.org/10.1063/1.1377303. 59

[66] J. E. Greedan, N. P. Raju, A. S. Wills, C. Morin, S. M. Shaw, J. N. Reimers, "Structure and Magnetism in λ-MnO2. Geometric Frustration in a Defect Spinel", *Chem. Mater.*, **10**, 3058 (1998). http://dx.doi.org/10.1021/cm9801789. 59

[67] L. W. Guo, H. Makino, H. J. Ko, Y. F. Chen, T. Hanada, D. L. Peng, K. Inaba, T. Yao, "Structural Characteristic and Magnetic Properties of Mn Oxide Films Grown by Plasma-Assisted MBE", *J. Cryst. Growth*, **227-228**, 955 (2001). http://dx.doi.org/10.1016/S0022-0248(01)00936-8. 59

[68] R. W. Grant, S. Geller, J. A. Cape, G. P. Espinosa, "Magnetic and Crystallographic Transitions in the α-Mn_2O_3-Fe_2O_3 System", *Phys. Rev.*, **175**, 686 (1968). http://dx.doi.org/10.1103/PhysRev.175.686. 59

[69] S. Mukherjee, A. K. Pal, S. Bhattacharya, J. Raittila, "Magnetism of Mn_2O_3 Nanocrystals Dispersed in a Silica Matrix: Size Effects and Phase Transformations", *Phys. Rev. B*, **74**, 104413 (2006). http://dx.doi.org/10.1103/PhysRevB.74.104413. 59

[70] K. Dwight, N. Menyuk, "Magnetic Properties of Mn_3O_4 and the Canted Spin Problem", *Phys. Rev.*, **119**, 1470 (1960). http://dx.doi.org/10.1103/PhysRev.119.1470. 59

[71] L.-X. Yang, Y.-J. Zhu, H. Tong, W.-W. Wang, G.-F. Cheng, "Low Temperature Synthesis of Mn_3O_4 Polyhedral Nanocrystals and Magnetic Study", *J. Solid State Chem.*, **179**, 1225 (2006). http://dx.doi.org/10.1016/j.jssc.2006.01.033. 59

[72] B. Folch, J. Larionova, Y. Guari, C. Guerin, A. Mehdi, C. Reye, "Formation of Mn_3O_4 Nanoparticles from the Cluster $[Mn_{12}O_{12}(C_2H_5COO)_{16}(H_2O)_3]$ Anchored to Hybrid Mesoporous Silica", *J. Mater. Chem.*, **14**, 2703 (2004). http://dx.doi.org/10.1039/b404967e. 59

[73] J.-I. Park, N.-J. Kang, Y.-W. Jun, S. J. Oh, H.-C. Ri, J. Cheon, "Superlattice and Magnetism Directed by the Size and Shape of Nanocrystals", *ChemPhysChem*, **3**, 543 (2002). http://dx.doi.org/10.1002/1439-7641(20020617)3:6<543::AID-CPHC543>3.0.CO;2-E. 59

[74] J. Osuna, D. deCaro, C. Amiens, B. Chaudret, E. Snoeck, M. Respaud, J. M. Broto, A. Fert, "Synthesis, Characterization, and Magnetic Properties of Cobalt Nanoparticles from an Organometallic Precursor", *J. Phys. Chem.*, **100**, 14571 (1996). http://dx.doi.org/10.1021/jp961086e. 59, 66, 72

[75] M. Respaud, J. M. Broto, H. Rakoto, A. R. Fert, L. Thomas, B. Barbara, M. Verelst, E. Snoeck, P. Lecante, *et al.*, "Surface Effects on the Magnetic Properties of Ultrafine Cobalt Particles", *Phys. Rev. B*, **57**, 2925 (1998). http://dx.doi.org/10.1103/PhysRevB.57.2925. 59, 66

[76] A. S. Risbud, L. P. Snedeker, M. M. Elcombe, A. K. Cheetham, R. Seshadri, "Wurtzite CoO", *Chem. Mater.*, **17**, 834 (2005). http://dx.doi.org/10.1021/cm0481269. 59

[77] P. Dutta, M. S. Seehra, S. Thota, J. Kumar, "A Comparative Study of the Magnetic Properties of Bulk and Nanocrystalline Co_3O_4", *J. Phys.: Condens. Matter*, **20**, 015218 (2008). http://dx.doi.org/10.1088/0953-8984/20/01/015218. 59

[78] M. Sato, S. Kohiki, Y. Hayakawa, Y. Sonda, T. Babasaki, H. Deguchi, M. Mitome, "Dilution Effect on Magnetic Properties of Co_3O_4 Nanocrystals", *J. Appl. Phys.*, **88**, 2771 (2000). http://dx.doi.org/10.1063/1.1287769. 59

[79] T. Hori, H. Shiraish, Y. Ishii, "Magnetic Properties of β-MnCoZn Alloys", *J. Magn. Magn. Mater.*, **310**, 1820 (2007). http://dx.doi.org/10.1016/j.jmmm.2006.10.582. 59

[80] G. Clavel, N. Pinna, D. Zitoun, "Magnetic Properties of Cobalt and Manganese doped ZnO Nanowires", *Phys. Status Solidi A*, **204**, 118 (2007). http://dx.doi.org/10.1002/pssa.200673025. 60, 62, 63

[81] B. D. Yuhas, D. O. Zitoun, P. J. Pauzauskie, R. R. He, P. D. Yang, "Transition-Metal-doped Zinc Oxide Nanowires", *Angew. Chem., Int. Ed.*, **45**, 420 (2006). http://dx.doi.org/10.1002/anie.200503172. 60, 64, 67

[82] P. Koidl, "Optical absorption of Co^{2+} in ZnO", *Phys. Rev. B*, **15**, 2493 (1977). http://dx.doi.org/10.1103/PhysRevB.15.2493. 61

[83] H. A. Weakliem, "Optical Spectra of Ni^{2+}, Co^{2+}, and Cu^{2+} in Tetrahedral Sites in Crystals", *J. Chem. Phys.*, **36**, 2117 (1962). http://dx.doi.org/10.1063/1.1732840. 61

[84] R. Pappalardo, D. L. Wood, J. R. C. Linares, "Optical Absorption Study of Co-Doped Oxide Systems. II", *J. Chem. Phys.*, **35**, 2041 (1961). http://dx.doi.org/10.1063/1.1732208. 61

[85] C. B. Fitzgerald, M. Venkatesan, J. G. Lunney, L. S. Dorneles, J. M. D. Coey, "Cobalt-doped ZnO - a Room Temperature Dilute Magnetic Semiconductor", *Appl. Surf. Sci.*, **247**, 493 (2005). http://dx.doi.org/10.1016/j.apsusc.2005.01.043. 61

[86] J. H. Kim, H. Kim, D. Kim, S. G. Yoon, W. K. Choo, "Optical and Magnetic Properties of Laser-Deposited Co-doped ZnO Thin Films", *Solid State Commun.*, **131**, 677 (2004). http://dx.doi.org/10.1016/j.ssc.2004.06.033. 61

[87] M. A. White, S. T. Ochsenbein, D. R. Gamelin, "Colloidal Nanocrystals of Wurtzite $Zn_{1-X}Co_xO$ (0≤X≤1): Models of Spinodal Decomposition in an Oxide Diluted Magnetic Semiconductor", *Chem. Mater.*, **20**, 7107 (2008). http://dx.doi.org/10.1021/cm802280g. 61

[88] W. K. Liu, G. M. Salley, D. R. Gamelin, "Spectroscopy of Photovoltaic and Photoconductive Nanocrystalline Co^{2+}-doped ZnO Electrodes", *J. Phys. Chem. B*, **109**, 14486 (2005). http://dx.doi.org/10.1021/jp0518781. 61

[89] Z. W. Jin, T. Fukumura, M. Kawasaki, K. Ando, H. Saito, T. Sekiguchi, Y. Z. Yoo, M. Murakami, Y. Matsumoto, *et al.*, "High Throughput Fabrication of Transition-Metal-doped Epitaxial ZnO Thin Films: A Series of Oxide-Diluted Magnetic Semiconductors and Their Properties", *Appl. Phys. Lett.*, **78**, 3824 (2001). http://dx.doi.org/10.1063/1.1377856. 61

[90] T. Fukumura, Z. W. Jin, A. Ohtomo, H. Koinuma, M. Kawasaki, "An Oxide-Diluted Magnetic Semiconductor: Mn-doped ZnO", *Appl. Phys. Lett.*, **75**, 3366 (1999). http://dx.doi.org/10.1063/1.125353. 61

[91] J. K. Furdyna, "Diluted Magnetic Semiconductors", *J. Appl. Phys.*, **64**, R29 (1988). http://dx.doi.org/10.1063/1.341700. 61

[92] P. A. G. Beermann, B. R. McGarvey, S. Muralidharan, R. C. W. Sung, "EPR Spectra of Mn^{2+}-doped ZnS Quantum Dots", *Chem. Mater.*, **16**, 915 (2004). http://dx.doi.org/10.1021/cm030435w. 62

[93] N. Feltin, L. Levy, D. Ingert, M. P. Pileni, "Magnetic Properties of 4-nm $Cd_{1-y}Mn_yS$ Nanoparticles Differing by Their Compositions, y", *J. Phys. Chem. B*, **103**, 4 (1999). http://dx.doi.org/10.1021/jp981241k. 62

[94] D. Magana, S. C. Perera, A. G. Harter, N. S. Dalal, G. F. Strouse, "Switching-On Superparamagnetism in Mn/CdSe Quantum Dots", *J. Am. Chem. Soc.*, **128**, 2931 (2006). http://dx.doi.org/10.1021/ja055785t. 62

[95] N. Samarth, J. K. Furdyna, "Electron Paramagnetic Resonance in $Cd_{1-x}Mn_xS$, $Cd_{1-x}Mn_xSe$, and $Cd_{1-x}Mnx$Te", *Phys. Rev. B*, **37**, 9227 (1988). http://dx.doi.org/10.1103/PhysRevB.37.9227. 62

[96] S. K. Misra, S. I. Andronenko, K. M. Reddy, J. Hays, A. Punnoose, "Magnetic Resonance Studies of Co^{2+} Ions in Nanoparticles of SnO_2 Processed at Different Temperatures", *J. Appl. Phys.*, **99**, 08M106 (2006). http://dx.doi.org/10.1063/1.2165146. 62

[97] M. Luo, N. Y. Garces, N. C. Giles, U. N. Roy, Y. Cui, A. Burger, "Optical and Electron Paramagnetic Resonance Spectroscopies of Diffusion-doped Co^{2+}:ZnSe", *J. Appl. Phys.*, **99**, 073709 (2006). http://dx.doi.org/10.1063/1.2188030. 62

[98] A. O. Ankiewicz, M. C. Carmo, N. A. Sobolev, W. Gehlhoff, E. M. Kaidashev, A. Rahm, M. Lorenz, M. Grundmann, "Electron Paramagnetic Resonance in Transition Metal-doped ZnO Nanowires", *J. Appl. Phys.*, **101**, 024324 (2007). http://dx.doi.org/10.1063/1.2402095. 62, 64

[99] M. Diaconu, H. Schmidt, A. Poppl, R. Bottcher, J. Hoentsch, A. Klunker, D. Spemann, H. Hochmuth, M. Lorenz, M. Grundmann, "Electron Paramagnetic Resonance of $Zn_{1-x}Mn_xO$ Thin Films and Single Crystals", *Phys. Rev. B*, **72**, 085214 (2005). http://dx.doi.org/10.1103/PhysRevB.72.085214. 62

[100] H. Zhou, D. M. Hofmann, A. Hofstaetter, B. K. Meyer, "Magnetic Resonance Investigation of Mn^{2+} in ZnO Nanocrystals", *J. Appl. Phys.*, **94**, 1965 (2003). http://dx.doi.org/10.1063/1.1586986. 62

[101] E. Chikoidze, H. J. von Bardeleben, Y. Dumont, P. Galtier, J. L. Cantin, "Magnetic interactions in $Zn_{1-x}Mn_xO$ studied by electron paramagnetic resonance spectroscopy", *J. Appl. Phys.*, **97**, 10D316 (2005). http://dx.doi.org/10.1063/1.1850372. 62

[102] N. Jedrecy, H. J. von Bardeleben, Y. Zheng, J. L. Cantin, "Electron Paramagnetic Resonance Study of $Zn_{1-x}Co_xO$: A Predicted High-temperature Ferromagnetic Semiconductor", *Phys. Rev. B*, **69**, 041308 (2004). http://dx.doi.org/10.1103/PhysRevB.69.041308. 64

[103] P. Lommens, F. Loncke, P. F. Smet, F. Callens, D. Poelman, H. Vrielinck, Z. Hens, "Dopant Incorporation in Colloidal Quantum Dots: A Case Study on Co^{2+} Doped ZnO", *Chem. Mater.*, **19**, 5576 (2007). http://dx.doi.org/10.1021/cm071623f. 64

[104] I. Ozerov, F. Chabre, W. Marine, "Incorporation of Cobalt into ZnO Nanoclusters", *Mater. Sci. Eng., C*, **25**, 614 (2005). http://dx.doi.org/10.1016/j.msec.2005.07.007. 64

[105] A. Bencini, C. A. Ghilardi, A. Orlandini, S. Midollini, C. Zanchini, "Electronic-Structure of Paramagnetic Clusters of Transition-Metal Ions .2. Crystal and Molecular-Structure, Single-Crystal EPR-Spectra, and Magnetic-Properties of $[Co_6(\mu_3\text{-}S)_8(PEt_3)_6](PF_6)$", *J. Am. Chem. Soc.*, **114**, 9898 (1992). http://dx.doi.org/10.1021/ja00051a023. 65

[106] R. Della Pergola, A. Fumagalli, F. F. de Biani, L. Garlaschelli, F. Laschi, M. C. Malatesta, M. Manassero, E. Roda, M. Sansoni, P. Zanello, "Carbonyl-Nitrido Mixed-Metal Clusters: Synthesis, Reactivity, Electrochemical Behavior and Solid-State Structure of $[Co_5MoN(CO)_{14}]^{-2}$ and $[Co_5MoN(CO)_{14}AuPPh_3]^{-}$", *Eur. J. Inorg. Chem.*, **2004**, 3901 (2004). http://dx.doi.org/10.1002/ejic.200400104. 65

[107] M. Respaud, M. Goiran, J. M. Broto, F. H. Yang, T. Ould-Ely, C. Amiens, B. Chaudret, "High-Frequency Ferromagnetic Resonance on Ultrafine Cobalt Particles", *Phys. Rev. B*, **59**, R3934 (1999). http://dx.doi.org/10.1103/PhysRevB.59.R3934. 66

[108] D. Zitoun, M. Respaud, M. C. Fromen, M. J. Casanove, P. Lecante, C. Amiens, B. Chaudret, "Magnetic Enhancement in Nanoscale CoRh Particles", *Phys. Rev. Lett.*, **89**, 037203 (2002). http://dx.doi.org/10.1103/PhysRevLett.89.037203. 66

[109] D. Gao, Z. Zhang, J. Fu, Y. Xu, J. Qi, D. Xue, "Room Temperature Ferromagnetism of Pure ZnO Nanoparticles", *J. Appl. Phys.*, **105**, 113928 (2009). http://dx.doi.org/10.1063/1.3143103. 70

[110] M. A. Garcia, J. M. Merino, E. Fernandez Pinel, A. Quesada, J. de la Venta, M. L. Ruiz Gonzalez, G. R. Castro, P. Crespo, J. Llopis, *et al.*, "Magnetic Properties of ZnO Nanoparticles", *Nano Lett.*, **7**, 1489 (2007). http://dx.doi.org/10.1021/nl070198m. 70

[111] A. Sundaresan, R. Bhargavi, N. Rangarajan, U. Siddesh, C. N. R. Rao, "Ferromagnetism as a Universal Feature of Nanoparticles of the otherwise Nonmagnetic Oxides", *Phys. Rev. B*, **74**, 161306 (2006). http://link.aps.org/abstract/PRB/v74/e161306. 70

[112] Q. Wang, Q. Sun, P. Jena, "Ligand Induced Ferromagnetism in ZnO Nanostructures", *J. Chem. Phys.*, **129**, 164714 (2008). http://dx.doi.org/10.1063/1.3001925. 70

[113] R. Munoz-Espi, G. Jeschke, I. Lieberwirth, C. M. Gomez, G. Wegner, "ZnO-Latex Hybrids Obtained by Polymer-Controlled Crystallization: A Spectroscopic Investigation", *J. Phys. Chem. B*, **111**, 697 (2007). http://dx.doi.org/10.1021/jp066380d. 71

[114] X. F. Wang, J. B. Xu, B. Zhang, H. G. Yu, J. Wang, X. Zhang, J. G. Yu, Q. Li, "Signature of Intrinsic High-Temperature Ferromagnetism in Cobalt-doped Zinc Oxide Nanocrystals", *Adv. Mater.*, **18**, 2476 (2006). http://dx.doi.org/10.1002/adma.200600396. 72

[115] O. D. Jayakumar, I. K. Gopalakrishnan, S. Kulshreshtha, "Surfactant-Assisted Synthesis of Co- and Li-Doped ZnO Nanocrystalline Samples Showing Room-Temperature Ferromagnetism", *Adv. Mater.*, **18**, 1857 (2006). http://dx.doi.org/10.1002/adma.200502415. 73

[116] O. D. Jayakumar, C. Sudakar, I. K. Gopalakrishnan, "Surfactant-Assisted Synthesis of $Zn_{0.95}Co_{0.05}O$ and $Zn_{0.85}Co_{0.05}Li_{0.10}O$ Nanoparticles Showing Room Temperature Ferromagnetism", *J. Cryst. Growth*, **310**, 3251 (2008). http://dx.doi.org/10.1016/j.jcrysgro.2008.03.038. 73

[117] K. R. Kittilstved, D. R. Gamelin, "Activation of High-T_C Ferromagnetism in Mn^{2+}-doped ZnO using Amines", *J. Am. Chem. Soc.*, **127**, 5292 (2005). http://dx.doi.org/10.1021/ja050723o. 73

[118] K. R. Kittilstved, N. S. Norberg, D. R. Gamelin, "Chemical Manipulation of High-T_C Ferromagnetism in ZnO Diluted Magnetic Semiconductors", *Phys. Rev. Lett.*, **94**, 147209 (2005). http://dx.doi.org/10.1103/PhysRevLett.94.147209. 73

[119] D. Chu, Y. Zeng, D. Jiang, "Solution-Based, High-Yield Synthesis of Cobalt-Doped Zinc Oxide Nanorods", *J. Am. Ceram. Soc.*, **90**, 2269 (2007). http://dx.doi.org/10.1111/j.1551-2916.2007.01687.x. 73

[120] G. Clavel, M. G. Willinger, D. Zitoun, N. Pinna, "Solvent Dependent Shape and Magnetic Properties of Doped ZnO Nanostructures", *Adv. Funct. Mater.*, **17**, 3159 (2007). http://dx.doi.org/10.1002/adfm.200601142. 74

[121] I. Djerdj, G. Garnweitner, D. Arcon, P. M., J. Zvonko, M. Niederberger, "Diluted Magnetic Semiconductors: Mn/Co-doped ZnO Nanorods as Case Study", *J. Mater. Chem.*, **18**, 5208 (2008). http://dx.doi.org/10.1039/b808361d. 75

Chapter IV:

Mn-doped ZrO_2

Contents

IV.1 Introduction

IV.1.1 ZrO_2

Zirconium dioxide, known as zirconia (ZrO_2), is a white and hard oxide of zirconium which possesses three polymorphic forms; the thermodynamically stable monoclinic, the cubic and tetragonal phases[1]. It has gained substantial interest in complementary metal oxide semiconductor (CMOS) technology because of its high dielectric permittivity[2]. Moreover, materials based on zirconia display a good thermal, chemical and mechanical stability and interesting acid-base and redox properties combined with the advantage of a very low cost. As a consequence, zirconia is one of the leading materials for industry with applications in catalysis, ceramics and solid oxide fuel cells[3–6]. In view of applications, the tetragonal and cubic phases are the most suitable. One of the major challenges is therefore to control and tune the crystallographic phase. In general, tetragonal and cubic metastable phases are stabilized at room temperature by addition of several mol% of another cation in the structure. Mainly yttrium but also magnesium, calcium, gadolinium, cadmium are used as dopand, their concentration playing an important role in the stabilization of rather the cubic or tetragonal phase[7–12]. Transition-metal-doped ZrO_2 have been widely studied as catalysts[13,14] but, interestingly, they were rarely considered as potential materials for their electronic properties. Indeed, the study of magnetic properties of zirconia doped with magnetic ions (e.g. Mn, Co, Fe, etc.) was almost completely neglected. In fact, one study only reported on the magnetic properties when zirconia was doped with manganese[15].

Recently, the field of transition metal doped oxides was dominated by the quest for high temperature ferromagnetic diluted magnetic semiconductors (DMS). Most of the theoretical and experimental studies focused on zinc oxide or gallium nitride as they were predicted ferromagnetic above room temperature when doped with magnetic ions. These materials gave rise to further investigation on very large band gap semiconductors. Materials possessing the characteristic required are scarce. As recently predicted

by Ostanin et al.[16], doped ZrO2 should be considered as one of the few suitable materials.

IV.1.2 Theoretical prediction

In their study, Ostanin et al. predicted that cubic zirconia stabilized with several transition metal ions should be ferromagnetic at room temperature in function of the transition metal ion and its oxidation state[16]. The figure 1 shows one of the results reported in their article. This graph presents the Curie temperature as a function of the metal dopant and its oxidation state (number of extra electrons per magnetic impurity). A careful reading of the results reveals that for manganese doping it is expected that zirconia is ferromagnetic for an oxidation state varying from III to IV. Chromium is also a promising dopant as it should be ferromagnetic for an oxidation state II and III.

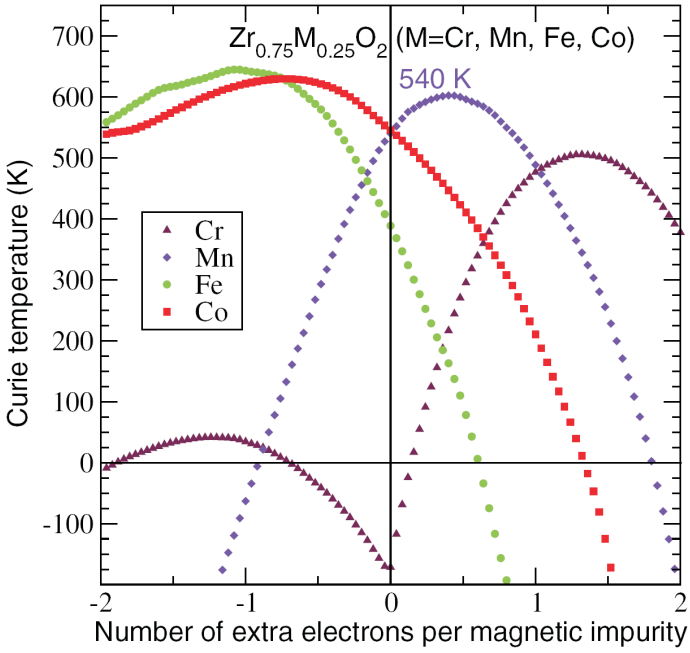

Figure IV.1: Curie temperatures of $Zr_{0.75}M_{0.25}O_2$ (M= Cr, Mn, Fe, Co) from frozen-magnon calculations. The variation of number of extra electrons per magnetic impurity (n) corresponds to modeling extra doping (n=0 corresponds to the nominal electron number), from ref[16]

In view of this result, we extended the "benzyl alcohol route" and used the background acquired with the study of the doping of zinc oxide, to explore this new system. Using our synthetic approach, we expect that the synthesized particles can be used for an experimental verification of the theoretical prediction. This is of special interest in view of recent theoretical investigations aimed at the prediction of new DMS materials.

IV.2 Synthesis and Morphology

IV.2.1 Synthesis

The synthesis of Mn-doped ZrO_2 was achieved by the benzyl alcohol route. In the case of pure zirconia, this approach leads to particles exhibiting a uniformly spherical morphology with a narrow size distribution which can be produced in multigram-scale quantities[17–19]. The condensation reaction leading to the formation of oxide is an ether elimination occurring between zirconium isopropoxide and benzyl alcohol[17]. The same mechanism was previously reported for the formation of HfO_2 which is a material similar to zirconia[20].

Doping of ZrO_2 was performed by the addition of a quantity of manganese(II) acetate or, alternatively, of manganese(III) acetylacetonate to the reaction mixture. In both cases, pale brown powders were obtained. The doping concentration after synthesis was monitored by ICP-AES measurements and was found to range from 1 to 5% (cf. TableVI.1). The effectiveness of the doping is elevated, ranging around 80% for $Mn(ac)_2$ and 90% in the case of $Mn(acac)_3$.

IV.2.2 Morphology

Observation of as-synthesized ZrO_2 by TEM reveals particles of highly homogeneous size and shape (Fig.2), the average diameter of the spherical nanoparticles being 3-4 nm. Upon doping, the particles present a similar shape and size (Fig.4).

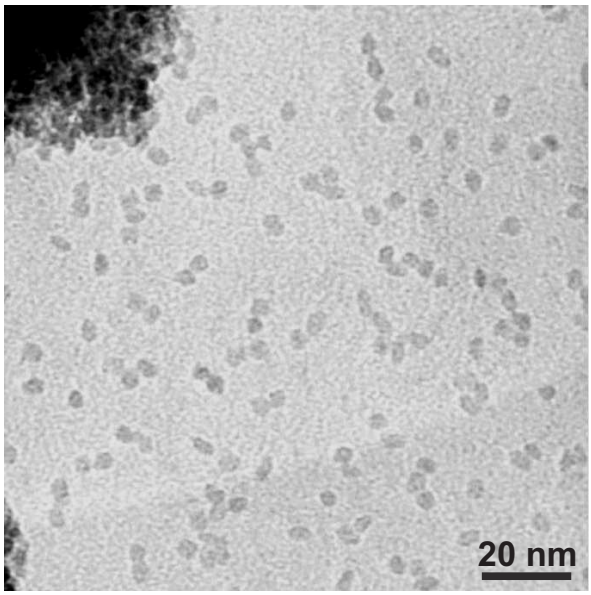

Figure IV.2: TEM image of pure ZrO_2 particles synthesized in BA at 230 °C

IV.3 Characterizations

IV.3.1 Matrix characterizations

X-ray diffraction patterns of the pure and doped zirconia particles are displayed in Figure 3. They show broad diffraction peaks due to the nanometric size of the zirconia crystals. No additional reflections of crystalline impurities are observed even for the most doped sample. An average particle size of approximately 3-4 nm, as deduced by the Scherrer formula, is obtained for both pure and doped zirconia particles, in agreement with TEM observations. As the diffraction peaks are broad, XRD experiments are not suitable to assign univocally the crystalline structure of the nanoparticles. Indeed, lattice parameters of the cubic (JCPDS [27-997]) and tetragonal phase (JCPDS [17-923]) of zirconia are similar and XRD patterns just differ in a few and very close reflections (cf. vertical bar Fig.3). However, based on Rietveld refinement it was demonstrated that this synthesis procedure leads to the cubic phase for pure ZrO_2 [17]. Contrary to the bulk phase, at the nanoscale the cubic or tetragonal structure does not need to be

stabilized by the addition of another ion[21–26].

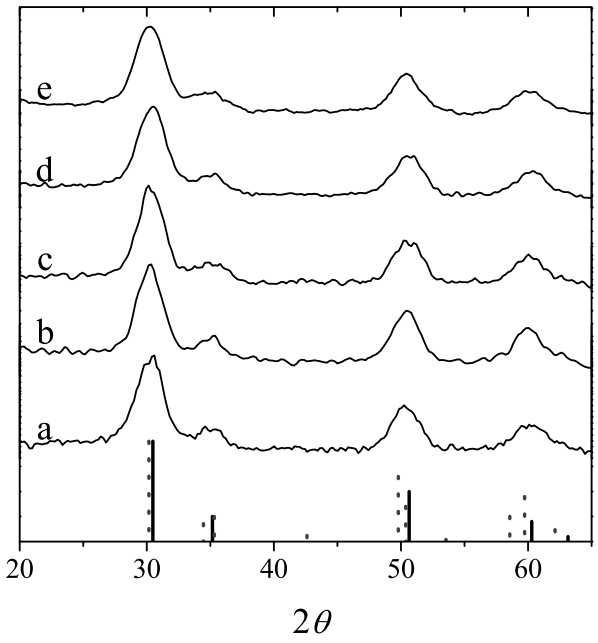

Figure IV.3: XRD patterns of a) undoped zirconia, b) zirconia doped with 1.39% of $Mn(ac)_2$, c) zirconia doped with 1.20% of $Mn(acac)_3$, d) zirconia doped with 4.38% of $Mn(ac)_2$, e) zirconia doped with 4.85% of $Mn(acac)_3$, theoretical reflection of cubic phase (vertical full line) and tetragonal phase (vertical dotted line) are specified.

Figure 4 shows overview and high resolution TEM micrographs as well as the power spectra from single particles in [110] direction. Observing the particles by TEM at high magnification (Fig.4 B, D), the crystalline particles appear at random orientation on the supporting carbon film of the TEM grid and show lattice fringes. The distances and angles between the corresponding lattice planes were abstracted from the Fourier transformed high resolution images and are in good agreement with the cubic ZrO_2 phase, both, for the Mn-doped and the undoped sample. Furthermore, the particles are monocrystalline in nature and do not present any core default. Because of the small size of the particles, the precision in the measurement of the lattice spacing from high

resolution images is limited. Therefore, slight changes in the lattice spacing that might eventually be induced by the dopant can not be detected.

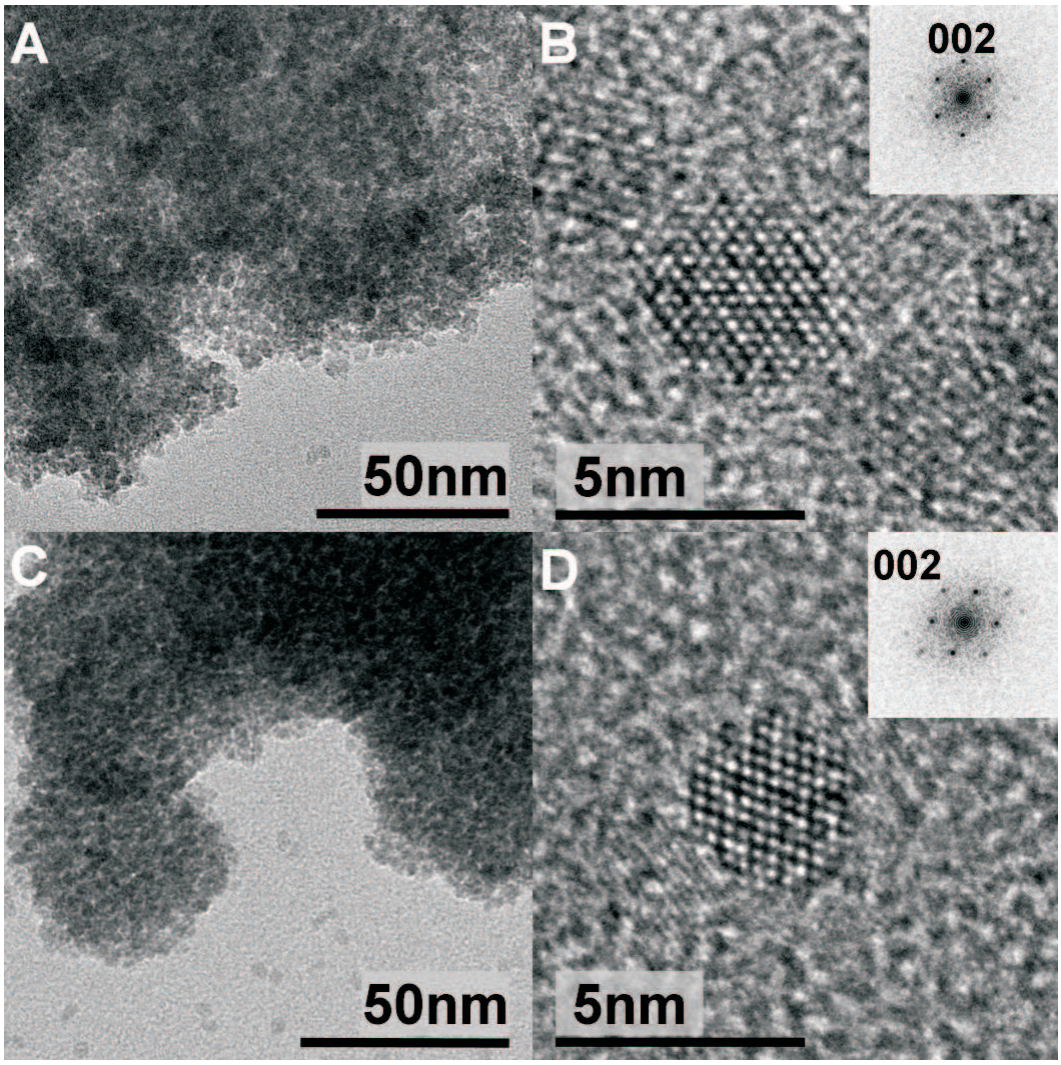

Figure IV.4: (A) TEM overview image showing an agglomeration of 4.38% Mn-doped ZrO_2 doped particles synthesized from $Mn(ac)_2$, (B) corresponding HRTEM image of a particle in [110] orientation with the respective power spectrum (inset), (C) TEM image of pure zirconia sample and (D) corresponding HRTEM picture, showing a single particle in [110] orientation and its power spectrum.

IV.3.2 Dopant environment

EELS

In order to investigate the distribution of manganese, electron energy loss spectrometry (EELS) was applied. EELS is a very sensitive technique and perfectly suitable for analyzing the chemical composition of materials at the nanometer scale. EELS spectra recorded in the energy range covering the oxygen K edge at around 530 eV and the manganese $L_{2,3}$ edges at 638 eV (L_3) and 649 eV (L_2), respectively, are presented in Figure 5. The spectra were recorded from sample III (high doping) at different regions, containing varying numbers of particles in order to draw conclusions about the homogeneity of the Mn distribution (Fig.5, A-C). In all presented spectra, the background was removed and zero-loss deconvolution for the removal of intensity due to plural inelastic scattering was performed. A clear manganese $L_{2,3}$ edge is visible in all the obtained spectra, although, according to the ICP-AE measurements, only 4.38% of the zirconium atoms were replaced by manganese. In general, the relative intensities of the Mn L_2 and L_3 edges and their integrated intensities are a sensible measure for the manganese oxidation state and its quantity [27], in the present case, the low amount of Mn in combination with the small particle size result in a bad signal to noise ratio preventing a precise determination of these quantities.

Besides the low signal to noise ratios, also the background removal and deconvolution are responsible for most of the observed differences in the spectra. This is due to the fact that both, background subtraction and zero-loss deconvolution were done for spectra that were recorded under non ideal conditions, i.e. from regions containing inhomogeneous distributions of particles. Nevertheless, based on the presence of the manganese $L_{2,3}$ edges in all spectra, independently of the amount of particles from which the signal was recorded, a homogeneous distribution of manganese in the particles is concluded.

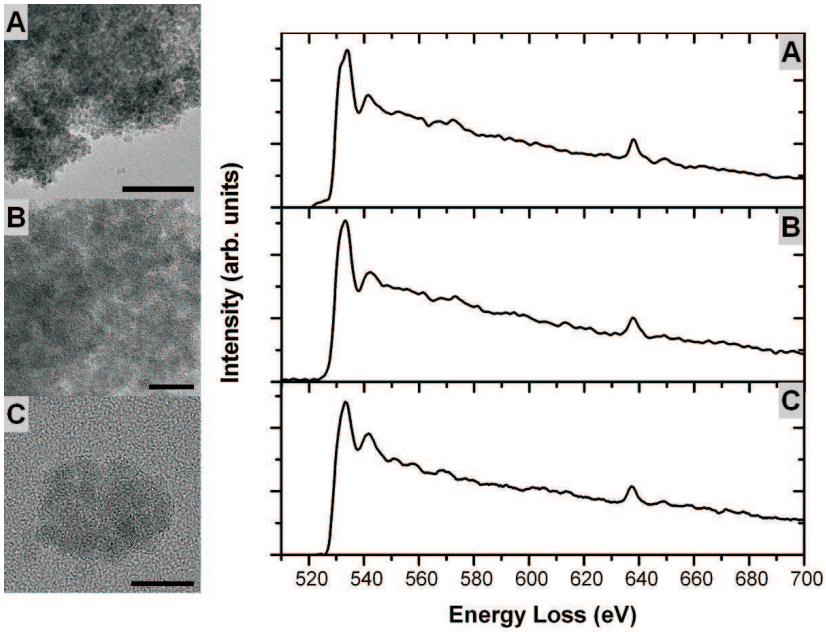

Figure IV.5: EELS spectra recorded from different agglomerations of particles (A), (B) and (C). The TEM images show the amount of particles that have contributed to each spectrum. Scale bars correspond to 50nm, 10nm and 10nm for A, B and C, respectively.

EPR

The local environment and oxidation state of the Mn ions was probed on powder samples with electron paramagnetic resonance (EPR), which provides information about the oxidation state, the local symmetry and the spin-spin interactions. EPR is a sensitive probe and has previously been used for the investigation of local environment of stabilizing ions in zirconia[28–30] and of transition metal impurities on surfaces or in dilute solid solutions[10,31–33].

In zirconia, the manganese ions can exist or co-exist in three different oxidation states (II, III and IV). Mn^{2+} and Mn^{4+} show similar, but discernable resonances, whereas the Mn^{3+} ion is EPR "silent"[32]. The lack of signals for Mn^{3+} is due to the large value of the zero-field splitting, occurring for most of the local environments (i.e. crystal fields), which shift the EPR signal out of the energy regime of conventional X-band spectrometers[34].

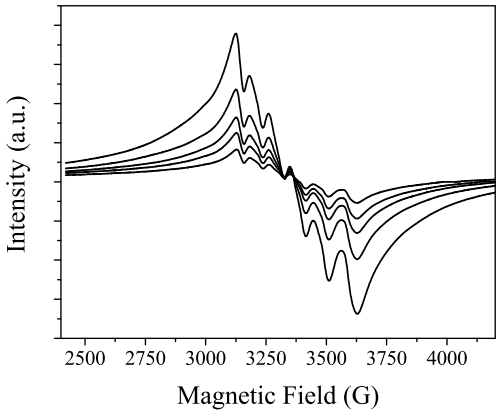

Figure IV.6: Temperature-dependent EPR spectra (intensity decreases with increasing temperature, T = 100, 150, 200, 250 and 300 K) of 1.20% Mn-doped ZrO_2 synthesized from $Mn(acac)_3$ precursor.

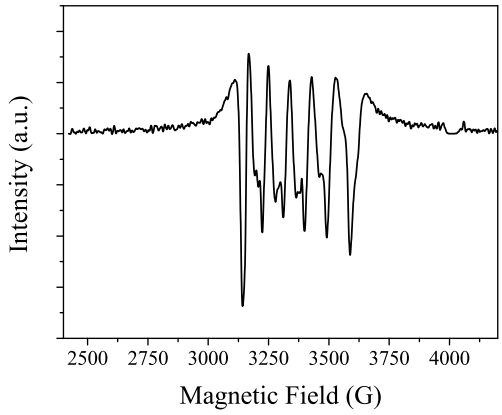

Figure IV.7: First derivative of the spectrum in figure 6 collected at T = 300 K.

Figure 6 shows EPR spectra recorded from 300 K down to 100 K for the most diluted sample synthesized from Mn(acac)3 precursor. They are characteristic of spectra recorded for the different types of samples, that is, whatever the precursor used or its quantity. The EPR spectra display two contributions centered at g = 2.020 (Fig.6): (i) a broad resonance resulting from magnetic interactions of Mn ions and (ii) a sextuplet from isolated spins. The observed hyperfine splitting (Fig.7) of 86 Gauss (A = 80x10^{-4} cm^{-1}) corresponds to the usual values for Mn^{2+} in cubic zirconia[32,33]. The g factor of Mn^{2+} ($3d^5$, g_0 = 2.00) and Mn^{4+} ($3d^3$, g_0 = 1.98) are very close to each other. However, the hyperfine value is usually found to be lower in the case of Mn^{4+} (a = 78 Gauss, A = 72x10^{-4} cm^{-1}) and allows to distinguish the two oxidation states. Therefore, taking into account the g-factor and the hyperfine values, the EPR signal is then assumed to be mainly dominated by the contribution of Mn^{2+}. This analysis is in agreement with a previous study where EPR analysis revealed that Mn^{2+} and Mn^{3+} can be introduced in cubic zirconia and not Mn^{4+} [32]. In a set of experiments, the temperature was varied from 300 K down to 100 K. No change in the spectrum, except for an increase of the signal amplitude, was observed (Fig.6). The absence of linewidth broadening with

temperature implies a lack of spin correlation, i.e. the lack of a magnetic order. Figure 8 presents a typical spectrum obtained for the highly doped samples. Surprisingly, the sextuplet characteristic of isolated ions is still present. In general, with an increase of the dopant concentration the signal appears as a single broad band due to exchanges between interacting neighboring manganese.

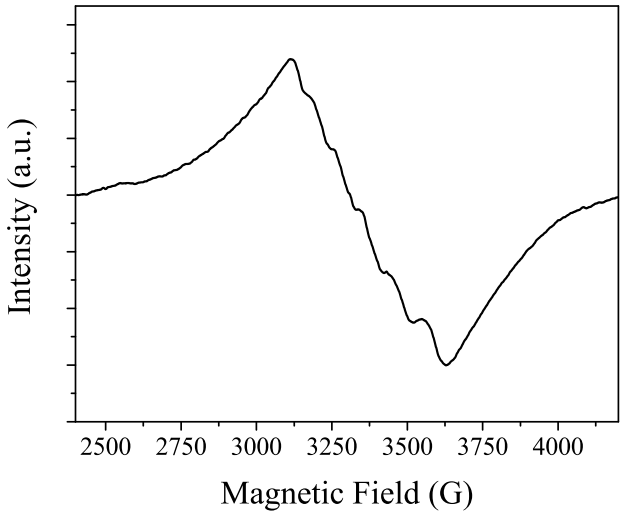

Figure IV.8: EPR spectrum recorded at room temperature for 4.85% Mn-doped ZrO_2 synthesized from $Mn(acac)_3$ precursor.

A manganese salt (manganese(II)acetate, hydrated) diluted in a matrix and Mn-doped ZnO sample were used as references to perform quantitative EPR analysis. Mn-doped zinc oxide is a suitable reference as it is a DMS itself which contains Mn in a 2+ oxidation state[35]. The nominal content of Mn^{2+} in ZrO_2 was evaluated from the double integral of the respective EPR signals after a baseline correction. In all cases, the amount of Mn^{2+} was found to be lower than the manganese total concentration derived from ICP measurements. The amount of Mn^{3+} was therefore deduced by a simple subtraction (cf. Table IV.1).

A first order analysis of the data therefore reveals the presence of manganese in two

oxidation states (II and III). An interesting point is the relation between the manganese concentration and its oxidation state. For the most diluted samples, the Mn(II) is predominant, independently of the oxidation state of the precursor used (Table IV.1). From this it follows that for the highly diluted samples each Mn atom in the zirconia matrix should be associated to one oxygen vacancy. An increase of the Mn concentration from 1 to 5 atomic % leads to a decrease of the paramagnetic signal. This can be attributed to the oxidation of some Mn(II) towards the EPR silent Mn(III). The estimated Mn(III) content is larger than that of the Mn(II) for the most concentrated samples (Table IV.1). In order to confirm this hypothesis, a technique suitable for the characterization of the Mn oxidation state, such as XPS, should be used.

Mn precursor	%Mn (ICP-AES)	% Mn^{2+} (EPR)	% Mn^{3+} (EPR)	Msat (μ_B/Mn)
$Mn(acac)_3$	1.20	69±2	31±2	4.33
$Mn(ac)_2$	1.39	61±2	39±2	4.27
$Mn(ac)_2$	4.38	9±2	91±2	3.55
$Mn(acac)_3$	4.85	8±2	92±2	3.40

Table IV.1: Dopant concentration, oxidation state and magnetic moment of Mn-doped ZrO_2 samples. Magnetic moments at saturation (Msat) were determined from a Langevin fit of the magnetization curves.

IV.4 Magnetism

After providing evidence on the homogeneity of doping and the absence of any secondary phase, the magnetic properties of the DMS can now be safely discussed. The magnetic measurements were performed at low and high field as a function of manganese concentration and oxidation state of the metal-organic precursor used. The susceptibility was investigated using a zero field cooled/field cooled routine at low field

(μ_0H = 5.0 mT). Figures 9 and 10 show the results for two different Mn concentrations. The susceptibility is plotted as both a function of temperature and, in the inset, as a function of inverse temperature. All samples display a paramagnetic behavior. For the more diluted sample (1.20% of Mn from $Mn(acac)_3$, Fig.9), the inverse of susceptibility follows a Curie's law with a parameter C = 8.85 10^{-4} emu.K/g_{Mn} and a Curie-Weiss temperature of θ = -0.4 +/- 0.2 K. For a sample with the higher Mn concentration (4.38% of Mn from $Mn(ac)_2$, Fig.10), the same parameters reach the values of C = 1.16 10^{-3} emu.K/g_{Mn} and θ = -50 +/- 2 K, respectively. From the Curie constants, the spontaneous moment per Mn atom can be determined at M_S = 4.4(1) and 3.8(1) μ_B/Mn, respectively.

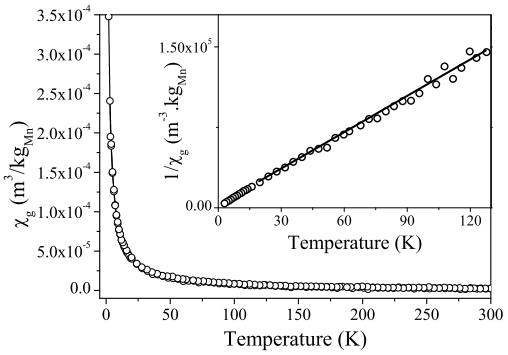

Figure IV.9: ZFC/FC curves measured in a field of 50 Oe for a diluted sample from $Mn(acac)_3$ with 1.20% of Mn (inset shows the inverse of the susceptibility and a linear fit).

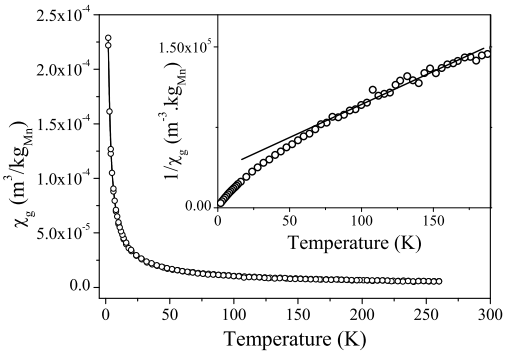

Figure IV.10: ZFC/FC curves measured in a field of 50 Oe for a concentrated sample from $Mn(ac)_2$ with 4.38% of Mn (inset shows the inverse of the susceptibility and a linear fit).

As the samples showed a pure paramagnetic behavior at room temperature, additional high field measurements M(H) were performed at low temperature (T = 2 K). The results are plotted in Bohr magnetons per manganese atom (μ_B/Mn) for the samples synthesized from $Mn(acac)_3$ and $Mn(ac)_2$ in Figure 11 and 12, respectively. All doped samples display a hysteresis. The coercive field reaches 1.7 mT for the 4.38% Mn-doped sample and 0.4 mT for the 1.39% Mn-doped sample. The observed hysteresis results from antiferromagnetic coupling between the manganese atoms. At high field (μ_0H =

5 T), the magnetic moment per atom reaches 3.90 μ_B/Mn and 3.68 μ_B/Mn for the most diluted samples (1.20 and 1.39% of Mn, respectively) and 2.80 μ_B/Mn and 2.74 μ_B/Mn for the most concentrated ones (4.38 and 4.85% of manganese, respectively). As a general trend, the magnetization does not reach saturation even at an applied field of 5 T. The magnetic moments at saturation determined from the fitting of the experimental curves with a Langevin function (cf. Table IV.1) are very close to the values determined from Curie constants obtained from susceptibility measurements (up to 4.4 μ_B/Mn for the most diluted sample).

The high magnetization of diluted samples is clearly an evidence for the presence of a majority of manganese in a low oxidation state (Mn^{2+}, $3d^5$ or Mn^{3+}, $3d^4$). In the case of more concentrated samples, the magnetization does not allow any conclusion as the values are lower than expected for any oxidation state. The expected effective moments are: Mn^{2+} (5.92 μ_B), Mn^{3+} (4.90 μ_B) and Mn^{4+} (3.87 μ_B). This result therefore supports the hypothesis of a coexistence of different manganese oxidation states in the zirconium matrix.

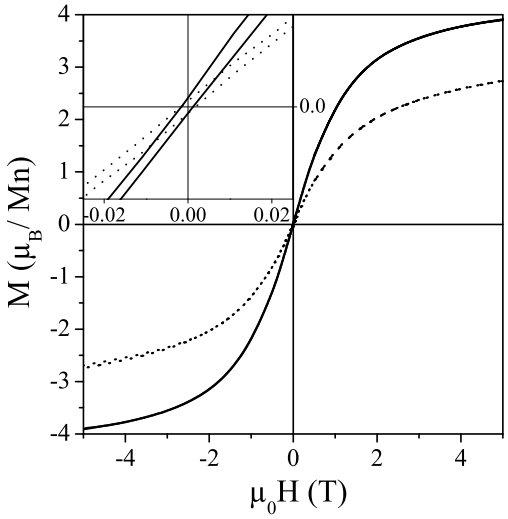

Figure IV.11: Hysteresis loops at T = 2 K for samples from $Mn(acac)_3$ with 1.20% of Mn (—) and 4.85% of Mn (···).

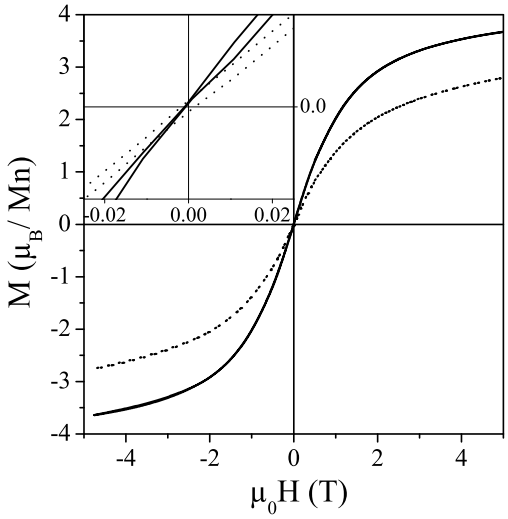

Figure IV.12: Hysteresis loops at T = 2 K for samples from $Mn(ac)_2$ with 1.39% of Mn (—) and 4.38% of Mn (···).

The low field and high field magnetic measurements provide clear evidence for a paramagnetic behavior with antiferromagnetic interactions that increase with the dopant concentrations from ∼1% to ∼5%. The manganese oxidation state is difficult to determine from the collected magnetic data. A purely Mn^{4+} or Mn^{3+} dopant state was already excluded based on the EPR measurements. Interestingly, the observed magnetic properties are not sensitive to the nature of the molecular source of manganese, i.e. $Mn(ac)_2$ or $Mn(acac)_3$. This surprising result may be related to the synthetic route. It was already shown that the synthesis of Mn oxides by the "benzyl alcohol route" always leads to the formation of a secondary phase which is MnO for the case of Mn_3O_4 and vice-versa[36]. In our case the presence of Mn^{2+} in the samples synthesized from $Mn(acac)_3$ can be explained by the soft reducing power of the benzyl alcohol. Furthermore, from quantitative EPR measurements and the derived magnetic moment, it follows that Mn^{2+} is not the only species obtained from the $Mn(ac)_2$ precursor. As each Mn^{2+} diluted in zirconia requires the generation of one oxygen vacancy, manganese at higher oxidation state is more likely to substitute a zirconium atom for large concentrations.

IV.5 Conclusions

In the search for high temperature ferromagnetic diluted magnetic semiconductors zirconia doped with up to 5% of manganese was synthesized by the "benzyl alcohol route". The synthetic approach led to the formation of homogeneously doped single crystalline nanoparticles of 3-4 nm in diameter. As a positive side effect of the nanoscale, the cubic structure does not need to be stabilized by the addition of another cation. The environment of the manganese diluted into the zirconia matrix was probed by EPR. It was found that Mn(II) and Mn(III) coexist and that their ratio depends only on the manganese concentration. Magnetic measurements show mainly a paramagnetic behavior of the diluted spins in the matrix. For larger Mn concentration, a small amount of an-

tiferromagnetic interactions is found. The ferromagnetism predicted by the theoretical work of Ostanin et al.[16] was not found even at low temperature. This can be explained by the low oxidation state of the manganese which, in our case, was estimated to be between (II) and (III). In fact, a larger oxidation state is more likely to give rise to ferromagnetic interactions[16]. Furthermore, the same theoretical study predicts that the Curie temperature increases with the concentration of manganese. In order to confirm or refute the theoretical results, a careful control of the manganese oxidation state and of the amount of oxygen vacancies, as well an increase of the manganese concentration is required.

Perspective of the work

The continuation of this work has been entrusted to another PhD student. The working plan followed was: (i) The synthesis of highly doped zirconia as a ferromagnetic behavior is expected upon increasing the concentration. (ii) The control of the oxidation state of manganese by post annealing in different atmospheres and by chemical oxidations have been tested in order to enhance higher oxidation states. (iii) Chromium is also a promising dopant as it should give ferromagnetic for an oxidation state (II) and (III). Similar approach for the synthesis and the characterization of Cr-doped ZrO_2 has been developed. (iv) Hafnia (HfO_2), which has been recently predicted to give rise to ferromagnetism at room temperature[37], has been explored. As zirconia and hafnia have very similar physical, chemical and structural properties, their joint study might permit to elucidate the matrix effect on the magnetic properties. Furthermore, as for zirconia, 3-5 nm nanoparticles of hafnia[20] can be synthesized by the "benzyl alcohol route"and up to now their doping was not investigated. (v) For all materials, the magnetic data have been compared to the theoretical study[16,37] and discussed also together with the group of theoreticians, in order to gain a better understanding of the origin of ferromagnetism in diluted magnetic semiconductors.

What appears from this study is that the largest effective doping concentration was ob-

tained for HfO_2 from $Mn(acac)_3$ (17% Mn). From post-synthetic annealing treatments under controlled atmospheres, it turned out that it is a rather delicate step as post-synthetic annealing can induce segregation and clustering at relatively low temperature (i.e., above 600-700 °C), as well as phase transformations. So, the annealing has to be performed below 650 °C to preserve the nanocrystals size and the crystallographic structure. Magnetic measurements reveal three different behaviors. (i) a paramagnetic state for ZrO_2- and HfO_2-doped samples for all studied transition metal contents, (ii) clustering of ferromagnetic Mn_3O_4 in the case of Mn-doped samples after calcination, (iii) a ferromagnetic phase below 43 K for calcined Cr-doped ZrO_2, which has been attributed to the intrinsic DMS behavior. The detailed results can be found in ref[38]. Further EXAFS experiments are currently conducted in order to investigate the local atomic environment, oxidation state and coordination and to obtain a complete and comprehensive picture on the origin of the observed magnetism.

IV.6 Experimental part

Synthesis

Zirconium(IV) isopropoxide isopropanol complex 99.9%, Manganese(II) acetate 98%, Manganese(III) acetylacetonate and benzyl alcohol 99%, were purchased from Aldrich, stored in a glovebox and used as received. All the syntheses were performed in a glove box. In a typical reaction, a Teflon cup of 45 ml inner volume was filled with 1.29 mmol of Zirconium(IV) isopropoxide isopropanol complex, 20 ml of benzyl alcohol and an adequate quantity of dopand. The cup was slide into a steel autoclave, sealed, removed from the glove box and then heated at 230 °C for 2 days in a furnace. The resulting suspensions were centrifuged and the resulting precipitates were meticulously washed with ethanol and acetone and afterwards dried in air at 80 °C. The reaction produced nanocrystals with a yield greater that 80%, as a white powder for pure ZrO_2 or slightly brown when Mn(II) and Mn(III) doping were added.

Experimental details

Inductively Coupled Plasma-Atomic Emission Spectrometry (ICP-AES) was realized in the Analytical Laboratories of University of Aveiro. Transmission electron microscopy (TEM) was carried out on a Hitachi H-9000 microscope operating at 300 kV, high resolution microscopy and EELS measurements were performed on a CM200FEG (Philips) microscope, operated at 200 kV and equipped with a field emission gun. The X-ray powder diffraction (XRD) data were collected on an X'Pert MPD Philips diffractometer (CuKα X-radiation at 40 kV and 50 mA). Samples were prepared by depositing a drop of a suspension of particles in ethanol on a copper grid coated with an amorphous carbon film. The EPR experiments were performed at X band ∼9.5 GHz on a Brucker ESP300 spectrometer with microwave powers between 0.02 and 200 mW. Temperature studies from 6 to 300 K were carried out using an Oxford gas-flow cryostat. Magnetic properties were measured using a SuperQuantum Interference Design (SQUID) magnetometer MPMS XL7, in the range of temperature 2-350 K and of field 0-5 T. The temperature-dependent susceptibility was measured using DC procedure. The sample was cooled to 2 K under zero magnetic field, a low magnetic field (5 mT) was then applied and the data collected from 2 K to 350 K (zero-field cooled, ZFC). Field Cooled (FC) measurements were performed from 2 K to 350 K with an applied field during the cooling.

Bibliography

[1] J. K. Dewhurst, J. E. Lowther, "Relative Stability, Structure, and Elastic Properties of Several Phases of Pure Zirconia", *Phys. Rev. B*, **57**, 741 (1998). http://dx.doi.org/10.1103/PhysRevB.57.741. 89

[2] G. D. Wilk, R. M. Wallace, J. M. Anthony, "High-kappa Gate Dielectrics: Current Status and Materials Properties Considerations", *J. Appl. Phys.*, **89**, 5243 (2001). http://dx.doi.org/10.1063/1.1361065. 89

[3] S. P. S. Badwal, "Stability of Solid Oxide Fuel Cell Components", *Solid State Ion.*, **143**, 39 (2001). http://dx.doi.org/10.1016/S0167-2738(01)00831-1. 89

[4] D. S. Lee, W. S. Kim, S. H. Choi, J. Kim, H. W. Lee, J. H. Lee, "Characterization of ZrO_2 co-doped with Sc_2O_3 and CeO_2 Electrolyte for the Application of IntermediateTemperature SOFCs", *Solid State Ion.*, **176**, 33 (2005). http://dx.doi.org/10.1016/j.ssi.2004.07.013. 89

[5] G. D. Yadav, J. J. Nair, "Sulfated Zirconia and its Modified Versions as Promising Catalysts for Industrial Processes", *Microporous Mesoporous Mat.*, **33**, 1 (1999). http://dx.doi.org/10.1016/S1387-1811(99)00147-X. 89

[6] R. M. Ormerod, "Solid Oxide Fuel Cells", *Chem. Soc. Rev.*, **32**, 17 (2003). http://dx.doi.org/10.1039/b105764m. 89

[7] D. Gazzoli, G. Mattei, M. Valigi, "Raman and X-ray Investigations of the Incorporation of Ca^{2+} and Cd^{2+} in the ZrO_2 Structure", *J. Raman Spectrosc.*, **38**, 824 (2007). http://dx.doi.org/10.1002/jrs.1708. 89

[8] M. S. Khan, M. S. Islam, D. R. Bates, "Cation Doping and Oxygen Diffusion in Zirconia: a Combined Atomistic Simulation and Molecular Dynamics Study", *J. Mater. Chem.*, **8**, 2299 (1998). http://dx.doi.org/10.1039/a803917h. 89

[9] P. Li, I. W. Chen, J. E. Penner-Hahn, "X-ray Absorption Studies of Zirconia Polymorphs. I. Characteristic Local Structures", *Phys. Rev. B*, **48**, 10063 (1993). http://dx.doi.org/10.1103/PhysRevB.48.10063. 89

[10] K. Sasaki, J. Maier, "Re-Analysis of Defect Equilibria and Transport Parameters in Y_2O_3-stabilized ZrO_2 using EPR and Optical Relaxation", *Solid State Ion.*, **134**, 303 (2000). http://dx.doi.org/10.1016/S0167-2738(00)00766-9. 89, 96

[11] E. V. Stefanovich, A. L. Shluger, C. R. A. Catlow, "Theoretical Study of the Stabilization of Cubic-Phase ZrO_2 by Impurities", *Phys. Rev. B*, **49**, 11560 (1994). http://dx.doi.org/10.1103/PhysRevB.49.11560. 89

[12] M. Yashima, K. Ohtake, M. Kakihana, H. Arashi, M. Yoshimura, "Determination of Tetragonal-Cubic Phase Boundary of $Zr_{1-x}R_xO_{2-x/2}$ (R = Nd, Sm, Y, Er and Yb) by Raman Scattering", *J. Phys. Chem. Solids*, **57**, 17 (1996). http://dx.doi.org/10.1016/0022-3697(95)00085-2. 89

[13] E. F. Lopez, V. S. Escribano, C. Resini, J. M. Gallardo-Amores, G. Busca, "A Study of Coprecipitated Mn-Zr Oxides and their Behaviour as Oxidation Catalysts", *Appl. Catal., B*, **29**, 251 (2001). http://dx.doi.org/10.1016/S0926-3373(00)00206-X. 89

[14] A. Keshavaraja, A. V. Ramaswamy, "3d Transition-metal Oxide-stabilized Zirconia as Novel Catalysts for Complete Oxidation of Hydrocarbons", *Chem. Commun.*, pp. 397–398 (1996). http://dx.doi.org/10.1039/CC9960000397. 89

[15] M. Valigi, D. Gazzoli, R. Dragone, A. Marucci, G. Mattei, "Manganese Oxide Zirconium Oxide Solid Solutions. An X-ray Diffraction, Raman Spectroscopy, Thermogravimetry and Magnetic Study", *J. Mater. Chem.*, **6**, 403 (1996). http://dx.doi.org/10.1039/JM9960600403. 89

[16] S. Ostanin, A. Ernst, L. M. Sandratskii, P. Bruno, M. Dane, I. D. Hughes, J. B. Staunton, W. Hergert, I. Mertig, J. Kudrnovsky, "Mn-Stabilized Zirconia: From Imitation Diamonds to a New Potential High-T_C Ferromagnetic Spintronics Material", *Phys. Rev. Lett.*, **98**, 016101 (2007). http://dx.doi.org/10.1103/PhysRevLett.98.016101. 90, 103

[17] G. Garnweitner, L. M. Goldenberg, O. V. Sakhno, M. Antonietti, M. Niederberger, J. Stumpe, "Large-Scale Synthesis of Organophilic Zirconia Nanoparticles and their Application in Organic-Inorganic Nanocomposites for Efficient Volume Holography", *Small*, **3**, 1626 (2007). http://dx.doi.org/10.1002/smll.200700075. 91, 92

[18] G. Garnweitner, M. Niederberger, "Nonaqueous and Surfactant-Free Synthesis Routes to Metal Oxide Nanoparticles", *J. Am. Ceram. Soc.*, **89**, 1801 (2006). http://dx.doi.org/10.1111/j.1551-2916.2006.01005.x. 91

[19] M. Niederberger, G. Garnweitner, J. Buha, J. Polleux, J. Ba, N. Pinna, "Nonaqueous Synthesis of Metal Oxide Nanoparticles: Review and Indium Oxide as Case Study for the Dependence of Particle Morphology on Precursors and Solvents", *J. Sol-Gel Sci. Technol.*, **40**, 259 (2006). http://dx.doi.org/10.1007/s10971-006-6668-8. 91

[20] N. Pinna, G. Garnweitner, M. Antonietti, M. Niederberger, "Non-Aqueous Synthesis of High-Purity Metal Oxide Nanopowders using an Ether Elimination Process", *Adv. Mater.*, **16**, 2196 (2004). http://dx.doi.org/10.1002/adma.200400460. 91, 103

[21] R. C. Garvie, "Stabilization of the Tetragonal Structure in Zirconia Microcrystals", *J. Phys. Chem.*, **82**, 218 (1978). http://dx.doi.org/10.1021/j100491a016. 93

[22] R. C. Garvie, "The Occurrence of Metastable Tetragonal Zirconia as a Crystallite Size Effect", *J. Phys. Chem.*, **69**, 1238 (1965). http://dx.doi.org/10.1021/j100888a024. 93

[23] M. Gateshki, V. Petkov, T. Hyeon, J. Joo, M. Niederberger, Y. Ren, "Interplay Between the Local Structural Disorder and the Length of Structural Coherence in Stabilizing the Cubic Phase in Nanocrystalline ZrO_2", *Solid State Commun.*, **138**, 279 (2006). http://dx.doi.org/10.1016/j.ssc.2006.03.013. 93

[24] J. Joo, T. Yu, Y. W. Kim, H. M. Park, F. Wu, J. Z. Zhang, T. Hyeon, "Multigram Scale Synthesis and Characterization of Monodisperse Tetragonal Zirconia Nanocrystals", *J. Am. Chem. Soc.*, **125**, 6553 (2003). http://dx.doi.org/10.1021/ja034258b. 93

[25] J. C. Valmalette, M. Isa, "Size Effects on the Stabilization of Ultrafine Zirconia Nanoparticles", *Chem. Mater.*, **14**, 5098 (2002). http://dx.doi.org/10.1021/cm021233n. 93

[26] F. Zhang, P. J. Chupas, S. L. A. Lui, J. C. Hanson, W. A. Caliebe, P. L. Lee, S. W. Chan, "In Situ Study of the Crystallization from Amorphous to Cubic Zirconium Oxide: Rietveld and Reverse Monte Carlo Analyses", *Chem. Mater.*, **19**, 3118 (2007). http://dx.doi.org/10.1021/cm061739w. 93

[27] G. H. Du, Z. Y. Yuan, G. V. Tendeloo, "Transmission Electron Microscopy and Electron Energy-Loss Spectroscopy Analysis of Manganese Oxide Nanowires", *Appl. Phys. Lett.*, **86**, 063113 (2005). http://dx.doi.org/10.1063/1.1861963. 95

[28] P. J. Alonso, R. Alcala, J. Casas-Gonzalez, R. Cases, V. M. Orera, "Spectroscopy Of Chromium (III) In Yttrium-Stabilized ZrO_2", *J. Phys. Chem. Solids*, **50**, 1185 (1989). http://dx.doi.org/10.1016/0022-3697(89)90029-2. 96

[29] G. Bacquet, J. Dugas, C. Escribe, F. Fabre, "Electron Paramagnetic Resonance or Rare Earth Ions in Calcia Stabilized Zirconia: Gd^{3+} and Yb^{3+}", *J. Phys. C*, **6**, 1432 (1973). http://dx.doi.org/10.1088/0022-3719/6/8/010. 96

[30] G. Bacquet, J. Dugas, C. Escribe, J. M. Gaite, J. Michoulier, "Comparative Electron Paramagnetic Resonance Study of Fe^{3+} and Gd^{3+} Ions in Monoclinic Zirconia", *J. Phys. C*, **7**, 1551 (1974). http://dx.doi.org/10.1088/0022-3719/7/8/019. 96

[31] F. C. Jentoft, A. Hahn, J. Krohnert, G. Lorenz, R. E. Jentoft, T. Ressler, U. Wild, R. Schlogl, C. Haner, K. Kohler, "Incorporation of Manganese and Iron into the Zirconia Lattice in Promoted Sulfated Zirconia Catalysts", *J. Catal.*, **224**, 124 (2004). http://dx.doi.org/10.1016/j.jcat.2004.02.012. 96

[32] M. Occhiuzzi, D. Cordischi, R. Dragone, "Manganese Ions in the Monoclinic, Tetragonal and Cubic Phases of Zirconia: an XRD and EPR Study", *Phys. Chem. Chem. Phys.*, **5**, 4938 (2003). http://dx.doi.org/10.1039/b311123g. 96, 97

[33] E. A. Zhilinskaya, V. N. Lazukin, I. V. Chepeleva, V. V. Osiko, "EPR Investigation of Stabilized ZrO_2 Single Crystals Doped with Chromium and Manganese", *phys. stat. sol. (b)*, **98**, 419 (1980). http://dx.doi.org/10.1002/pssb.2220980203. 96, 97

[34] J. Krzystek, J. Telser, L. A. Pardi, D. P. Goldberg, B. M. Hoffman, L. C. Brunel, "High-Frequency and -Field Electron Paramagnetic Resonance of High-Spin Manganese(III) in Porphyrinic Complexes", *Inorg. Chem.*, **38**, 6121 (1999). http://dx.doi.org/10.1021/ic9901970. 96

[35] G. Clavel, M. G. Willinger, D. Zitoun, N. Pinna, "Solvent Dependent Shape and Magnetic Properties of Doped ZnO Nanostructures", *Adv. Funct. Mater.*, **17**, 3159 (2007). http://dx.doi.org/10.1002/adfm.200601142. 98

[36] I. Djerdj, D. Arcon, Z. Jaglicic, M. Niederberger, "Nonaqueous Synthesis of Manganese Oxide Nanoparticles, Structural Characterization, and Magnetic Properties", *J. Phys. Chem. C*, **111**, 3614 (2007). http://dx.doi.org/10.1021/jp067302t. 102

[37] I. V. Maznichenko, S. Ostanin, A. Ernst, I. Mertig, "First-principles Study of Manganese-stabilized Hafnia", *J. Magn. Magn. Mater.*, **321**, 913 (2009). http://dx.doi.org/10.1016/j.jmmm.2008.11.054. 103

[38] A. Pucci, G. Clavel, M.-G. Willinger, D. Zitoun, N. Pinna, "Transition Metal-Doped ZrO_2 and HfO_2 Nanocrystals", *J. Phys. Chem. C*, **113**, 12048 (2009). http://dx.doi.org/10.1021/jp9029375. 104

Chapter V:

Magnetic Hetero-Structures

Contents

V.1 Introduction

In the previous chapters, we intended to develop a synthetic route towards homogeneous multifunctional materials. The DMS combine semi-conducting, ferromagnetic and even optical properties arising from the same material. Multifunctional magnetic materials can also be obtained through the elaboration of hetero-structures[1–4]. This is another strategy to combine multiple properties and functionalities in a material. For example, ferromagnetic nanoparticles surrounded by an insulating layer can display magneto-resistive properties[5,6]. As well, composites of ferroelectric or piezoelectric and ferromagnetic oxides have led to multiferroic materials[7,8]. The hetero-structures studied during this work are magnetic nanoparticles of cobalt ferrite ($CoFe_2O_4$) distributed into a semiconducting and dielectric material, namely ZnO or TiO_2. Cobalt ferrite is a well-known hard magnetic material, which has been studied in detail due to its high coercivity and moderate saturation magnetization (about 80 emu/g) as well as its remarkable chemical stability and mechanical hardness[4,9]. Homogeneous particles can be easily synthesized by thermal decomposition in the presence of stabilizing ligands[4,10–12]. ZnO and TiO_2 are piezoelectric and dielectric wide band gap semiconductors, respectively. We have previously established a new process for the deposition of TiO_2 by Atomic Layer Deposition[13]. This research is composed of four distinct steps/challenges:

(i) synthesis of uniform magnetic nanoparticles,

(ii) deposition of the particles as a film on substrate,

(iii) covering of the particles by an oxide matrix,

(iV) characterization of the obtained assembly.

The aim of this study is the investigation of the properties of the different phases and most importantly, the interaction between the nanoparticles and the matrix and between the particles through the oxide host. The deposition of the solution phase processed magnetic nanocrystals will be attempted through Langmuir-Blodgett (LB) film

formation. LB is a room temperature deposition process that may be used to deposit monolayer and multilayer films of materials, either molecular or nanoscale, to form Self Assembled Monolayers (SAMs)[4,14–19]. The deposition of the oxide matrix will be made using an Atomic Layer Deposition (ALD) process, which permits a complete and homogemeous coating of the particles[20,21]. These two methods permit the manipulation of molecules/particles on the nanometer scale, thereby allowing intriguing superlatticed architectures to be assembled. The properties of the different phases, as well as the interaction between the particles and the film or between the particles through the film will be carefully studied.

V.2 $CoFe_2O_4$ particles

V.2.1 Synthesis

The synthesis of cobalt ferrite consists in the thermal decomposition at high temperature of metal oleates in the presence of surfactant such as oleic acid. This procedure has already been successfully used to synthesize homogeneous oxide nanoparticles such as Fe_3O_4, cobalt ferrite, CoO, MnO[10,22–25], with an accurate control of the size. Temperature, concentration of surfactant and synthesis duration are the key parameters that dictate the size of the particles[22]. Furthermore, the complexation state of the oleate precursors slightly influences the size, shape and homogeneity of the particles as it changes the decomposition temperature of the oleate complex[26].

Taking into account all these parameters, we developed a synthesis to obtain 10 nm particles. The precursors used, $Co(oleate)_2$ and $Fe(oleate)_3$, were prepared from their chloride counterpart by reaction with sodium oleate. A molecular ratio of 1:1 between the surfactant (oleic acid) and the precursors was used and the reaction was performed at 300 °C for one hour. A particle size of 10 nm was chosen because it is a good compromise between a size small enough to permit a good covering by ALD and a size large enough to obtain a ferromagnetic behavior at room temperature, i.e. a high

blocking temperature. After synthesis, the surface of the particles is covered by a certain amount of surfactant and even after meticulous washing the particles are obtained as a waxy brown solid.

V.2.2 Characterizations

TEM observations reveal spherical particles of around 8-10 nm, homogeneous in shape and with a narrow size distribution (Fig.1). High magnification shows that the particles are monocrystalline and randomly oriented on the TEM grid. A high resolution TEM image of a particle oriented along the [1-1-2] direction is presented in figure 1 (top right). Its corresponding power spectrum (Fig.1 bottom right) can be indexed to the cubic spinel structure of $CoFe_2O_4$ (JCPDS Card No 22-1086). The composition of the nanoparticles was verified by EDX recorded in the TEM. For the conditions of synthesis used, the ratio of Co/Fe appears to be exactly one Co for two Fe (Fig.2).

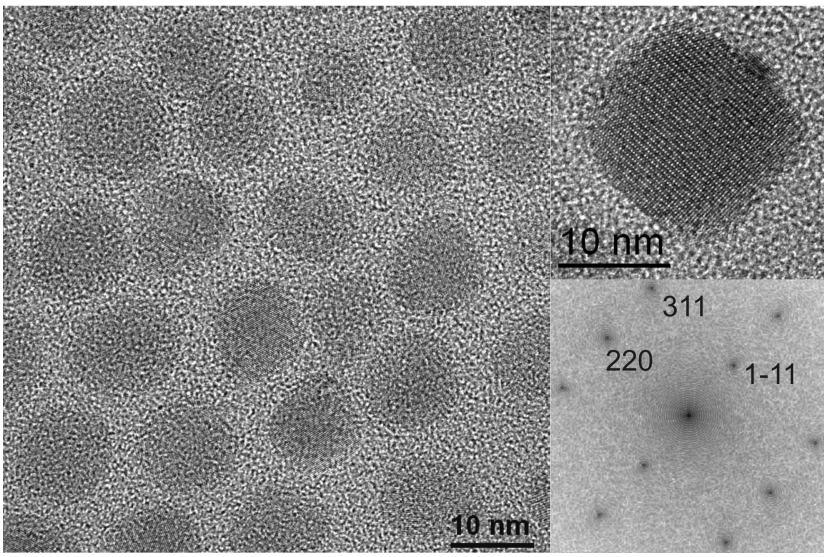

Figure V.1: High resolution TEM of a set of particles of cobalt ferrite. Top right : a particle showing clear lattice fringes. Bottom right: power spectrum of the particles displayed above.

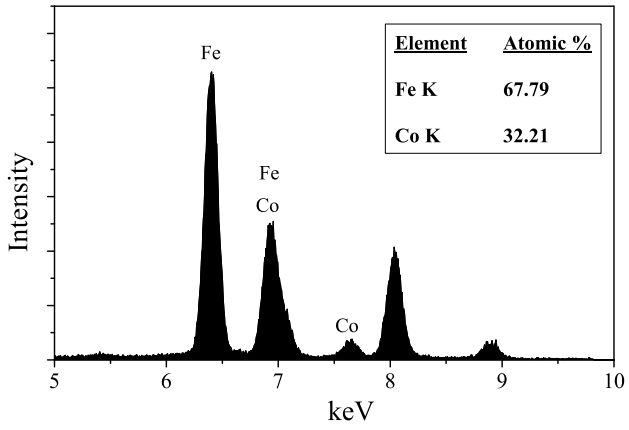

Figure V.2: EDX spectrum taken from a collection of particles, (inset) atomic percent of Fe and Co in the particles.

V.2.3 Magnetic properties

The magnetic properties of the waxy powder were studied using a SQUID magnetometer by current (dc) and alternating current (ac) modes. The susceptibility versus temperature plot, using the zero-field cooling (ZFC) and field cooling (FC) procedures between 2 and 350 K, shows that the material is magnetic until room temperature (the blocking temperature (T_B) is just above 300 K) (Fig.3). The separation of the ZFC and FC curves happens very close to the maxima of the ZFC curve (i.e. the blocking temperature) indicating that the particles are homogeneous in size. The anisotropy constant K estimated by the relation: $K \approx 25 \times k_B \times T_B / \langle V \rangle$, where k_B is the Boltzmann constant and $\langle V \rangle$ the means volume of particles, is about 2.80 x 10^5 J/m^3 (2.80 x 10^6 erg/cm^3). This value is consistent with the value for bulk cobalt ferrite (1.8 to 3.0 x 10^6 erg/cm^3)[27–29].

Magnetization versus field measurements are plotted in figure 4. At 2K the magnetization does not saturated with an applied field of $\mu_0 H = 5.0$ T and reaches the value of 28 emu/g. The magnetization at saturation for bulk cobalt ferrite is ∼90 emu/g[9]. The total magnetic moment of a magnetic single-domain nanoparticle (i.e. the magnetization

at saturation extracted from M-H experiments) should be, in principle, directly proportional to the number of magnetic atoms in the particle. However, the magnetization at saturation measured for nanoparticles is often lower than expected[9,30,31,31–33]. This is principally due to two reasons in the case of oxides: i) the reduction of the particle size results in a large amount of magnetic atoms on the surface of the particle. These atoms have fewer nearest neighbors to which they can interact. Therefore, it is more likely that their moment become randomly oriented at the surface (spin-canting) and that higher applied fields are needed to align them parallel to it. ii) Moreover, when the syntheses are performed in the presence of surfactants a large amount of organic species are present at the particle surface and can contribute to 30% or more of the total weight of the sample[34]. Therefore, the magnetization is artificially lowered by the weight fraction of these impurities. At 2 K the particles show a very high coercivity of 1.8 T and a ratio of the remanent to saturation magnetizations (Mr/Ms) of 0.7, as expected for 8-10 nm particles[32,35,36]. The coercivity decreases rapidly while increasing the temperature (0.33 T at 150 K and 4.5 mT at 300 K) but the magnetization remains relatively constant (Fig.4).

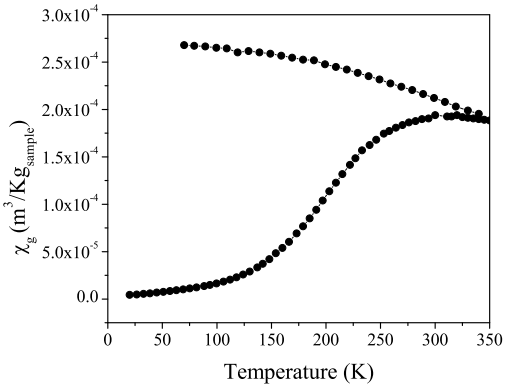

Figure V.3: ZFC-FC susceptibility curves of cobalt ferrite nanoparticles powder with an applied field of 500 Oe.

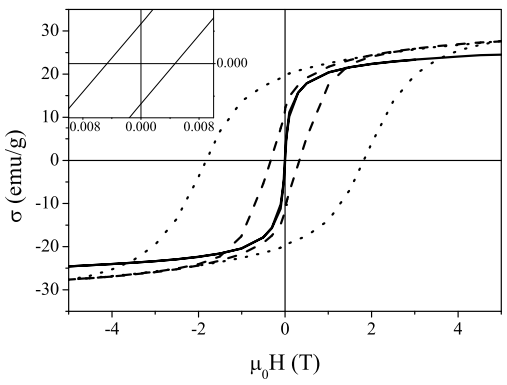

Figure V.4: Magnetization versus field loops at 2 K (···), 150 K (- - -) and 300 K (—) for cobalt ferrite nanoparticles powder.

The superparamagnetic behavior of the particles was further investigated by alternat-

ing current (ac) susceptibility measurements made in a zero external field with different frequencies ranging from 10 to 1000 Hz. The temperature dependence of the in-phase (χ') and out-of-phase (χ") components is plotted in figure 5. Both χ' and χ" responses shift towards higher temperature when the frequency increases. The frequency dependence of the peaks of χ" susceptibility can be analyzed by the Arrhenius law, $\tau = \tau_0 \exp(\Delta E/k_B T)$ in which ΔE is the average energy barrier and is given by $\Delta E = KV$ (K being the anisotropy energy constant and V the particle volume). Although the pre-exponential factor τ_0 can be determined from the line in figure 6, its value does not stand for an isolated nanocrystal as the system is not diluted and the particles are in interaction. Nevertheless, ΔE was estimated and the anisotropy constant calculated was 4.85 x 10^5 J/m^3. This value is slightly higher that the one extracted from the ZFC/FC curves but of the same order of magnitude.

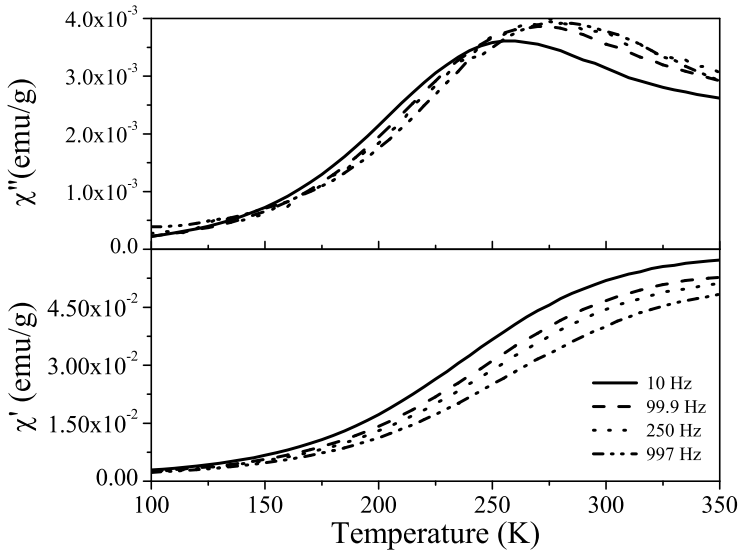

Figure V.5: Temperature dependence of the in-phase (χ') and out-of-phase (χ") components of the ac susceptibility of cobalt ferrite particles powder.

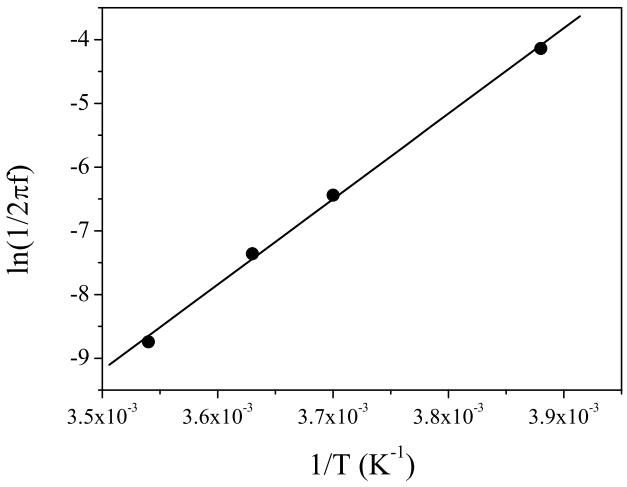

Figure V.6: Thermal variation of the relaxation time according to the Arrhenius law from temperature dependence of the maxima of (χ") component curves (Fig.5).

V.3 Films of particles

V.3.1 Deposition and characterizations

The Langmuir-Blodgett technique was used to deposit film of particles on silicon wafers or glass substrates by dip-coating in a LB cell. For this purpose, a stable dispersion of the particles in a highly volatile solvent was prepared. After synthesis and meticulous washing, the particles were dispersed in the minimum amount of chloroform and the resulting dispersion passed through a PTFE filter to remove any dusts, aggregated particles or precipitates. Some drops of the dispersion were then spread onto water of a Langmuir trough. The surfactant that remains after synthesis at the surface of the particles, allows obtaining a floating Langmuir monolayer at the air/water interface without further surface modification of the particles. After spreading the dispersion and evaporation of the solvent, the film was compressed (rate of compression was 5 mm/min) by two mobile barriers to ensure a symmetrical compression. By closing the barriers (decrease of the water area), the particles pass from an uncompressed state (large distance between particles) to "liquid"and "solid"phases in which the par-

ticles come closer until they are orderly packed. These phenomena can be followed by recording the pressure at the water/air interface. Figure 7 presents the obtained pressure-area isotherm for our particles (surface pressure versus water surface area). It presents a plateau at very low-pressure immediately followed by a rapid pressure increase until 50 mN/m with some discontinuities. Even for low water surface area, the pressure analysis gave no evidence of collapsing (no decrease of the pressure) of the particle film into three-dimensional structures. However, we observed cracks and wrinkling of the film at the surface of the water, after a pressure of 20 mN/m.

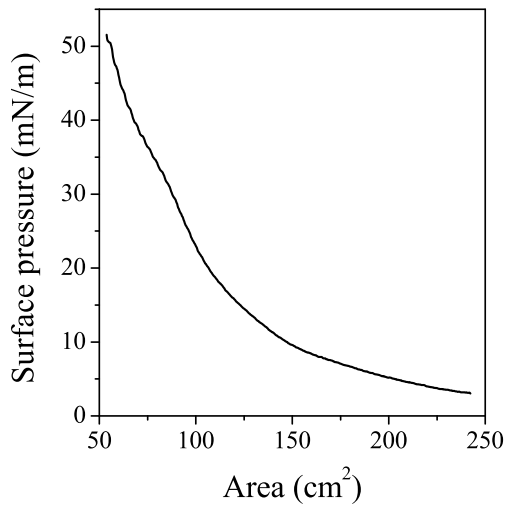

Figure V.7: Surface pressure versus surface area isotherm obtained on spreading oleic acid coated $CoFe_2O_4$ nanoparticles on water surface.

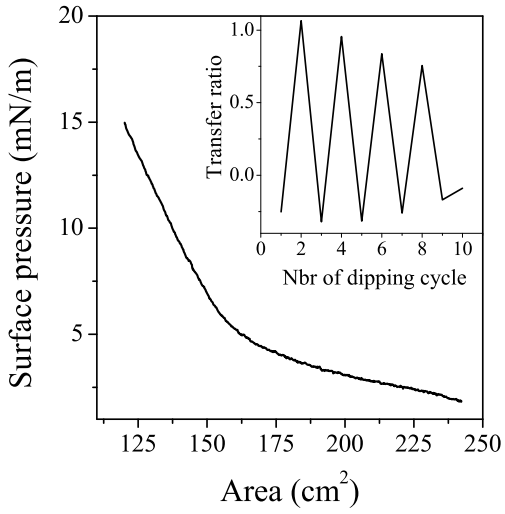

Figure V.8: Part of the isotherm where the dipping is performed. Inset: Transfer ratio vs. dipping cycles (position down and up of the dipper).

As the film has to be rigid enough to be transferred onto the substrates, the depositions were made at a constant pressure of 15 mN/m (Fig.8). Films were transferred onto silicon or glass by dipping the substrates through the monolayer upward (rate of vertical transfer was 3 mm/min). While normally the direction of dipping is dictated by the hydrophobicity of the substrate/particles, we do not observed difference between Si substrate, with and without SiO_2 native layer, and glass. The transfer ratio (ratio between the decrease in monolayer area during a deposition and the area of the

substrate) is high and, up to 4 layers can be deposited with the same Langmuir film (Fig.8 inset).

In order to study the effect of the magnetic particles coverage, mono- bi- and tri-layer films were prepared. The successful deposition of multilayers films was monitored by UV-visible spectroscopy on the glass-deposited samples. From the linear increase of the absorbance versus the number of dipping cycles (Fig.9 inset), it appears that for each layer the same amount of materials is deposited.

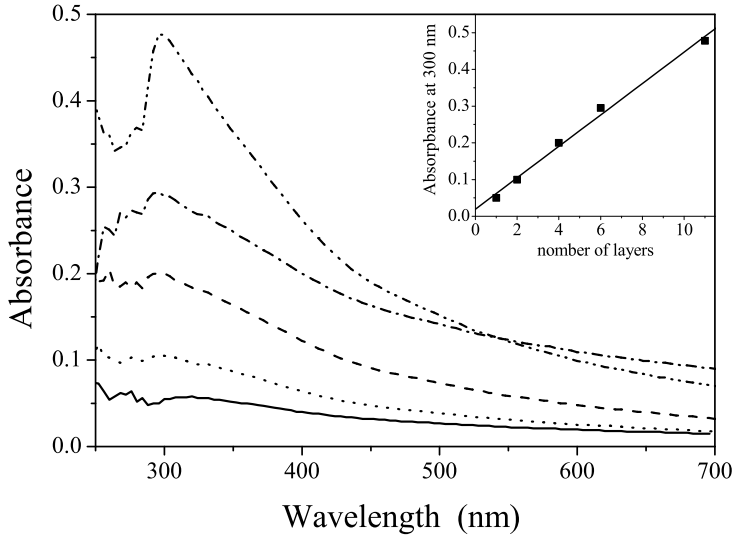

Figure V.9: UV-Visible of cobalt ferrite particles films deposited onto glass substrates, for 1 (—), 2 (- - -), 4 (· · ·), 6 (· –) and 11 (· · –) layers. The curves were corrected for the contribution of the glass substrate. Inset: absorbance at 300 nm in function of the number of layer deposited.

SEM pictures of a single layer deposited on silicon wafer are shown in figure 10. The particles are organized in chains and form interdigitated islands. The formed domains are homogenous over several hundred nanometers. Furthermore, it is clear from SEM images that only one layer has been transferred on the substrate.

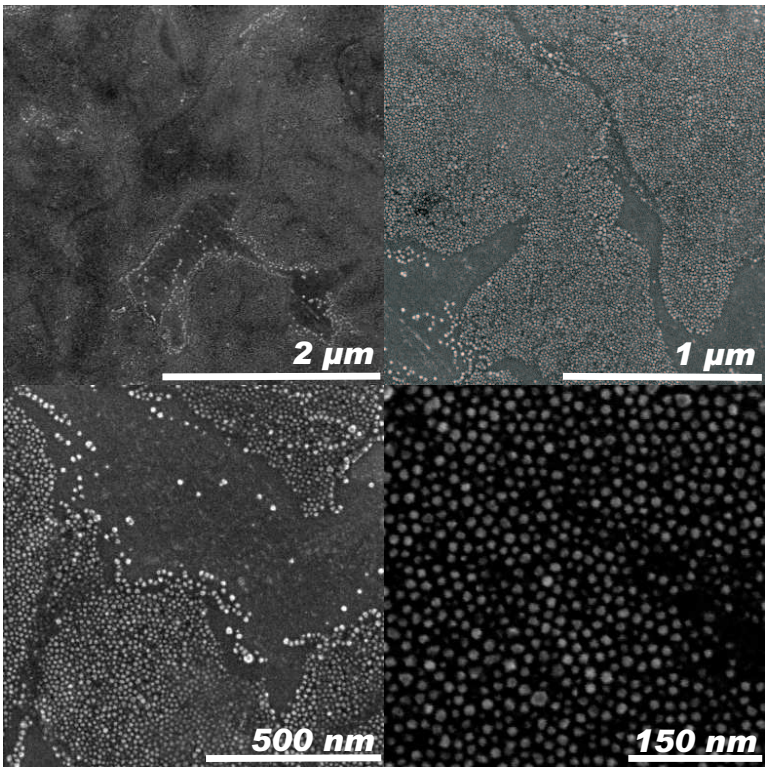

Figure V.10: SEM images at different magnifications of a monolayer film of $CoFe_2O_4$ nanoparticles deposited on Si substrate.

V.3.2 Calcinations and characterizations

In order to remove the surfactant from the surface of the particles, we have performed post-deposition calcination. Oleic acid is usually strongly grafted at the surface of nanoparticles and high temperature is needed for its complete removal. For example, a temperature of 400 °C in vacuum is needed to eliminate oleic acid at the surface of Co metal and 600 °C in N_2 atmosphere for oleic acid coated cobalt ferrite[37,38]. However, a temperature superior to 400 °C or a long calcination time leads to the shrinking of the film and segregation of the particles (Fig.11). To overcome this problem, rapid thermal annealing was used to perform short time calcination under controlled atmosphere (vacuum and O_2). Different conditions were tested and infrared spectroscopy used to examine the removal of the oleic acid (Fig.12). An annealing of 2 min at 400 °C (slope of 47 °C/s) in vacuum or O_2 was not sufficient for a complete elimination (Fig.12 dot-

dot-dashed and dot-dashed lines) neither when, in the same condition, vacuum and O_2 were used successively (Fig.12 solid-line). In fact, the use of higher temperature (450 °C) or a slower heating slope (1.3 °C/s) is needed (Fig.12 doted-line and dashed-line, respectively). Since a temperature of 450 °C induced aggregation of the particles, the films that have been used in the following studies were calcined at 400 °C with a slow heating slope.

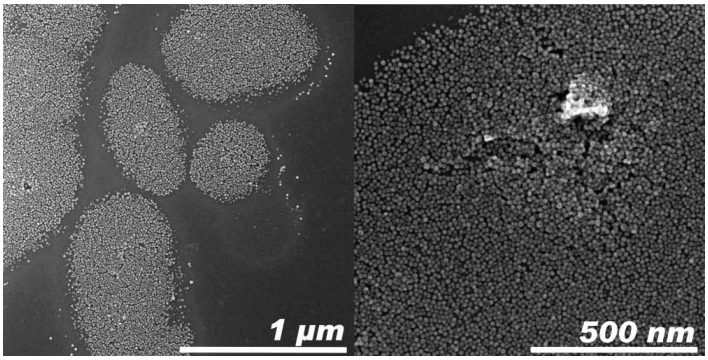

Figure V.11: SEM images of a monolayer film of particles calcined under non-ideal condition (15 min at 380 °C).

SEM images, taken before (Fig.13 A-B) and after (Fig.13 C-D) annealing, illustrate the effect of the calcination on the film. In the annealing condition used, the film does not shrink and the particles are not aggregated. On the contrary, the film seems to be more homogenous forming micrometers long areas.

V.3.3 Magnetic properties

The magnetic properties of films of nanoparticles deposited on silicon wafers and glass substrates are presented in figure 14-15 and 16-17, respectively. Zero-field cooled - field-cooled (ZFC-FC) measurements (susceptibility versus temperature) made on samples deposited on silicon substrate (Fig.14) show that, like the powder, the films are ferri-magnetic until 300 K. Furthermore, the difference of susceptibility between the ZFC and FC curves is twice as large for the film made of two layers of particles (Fig.14 cir-

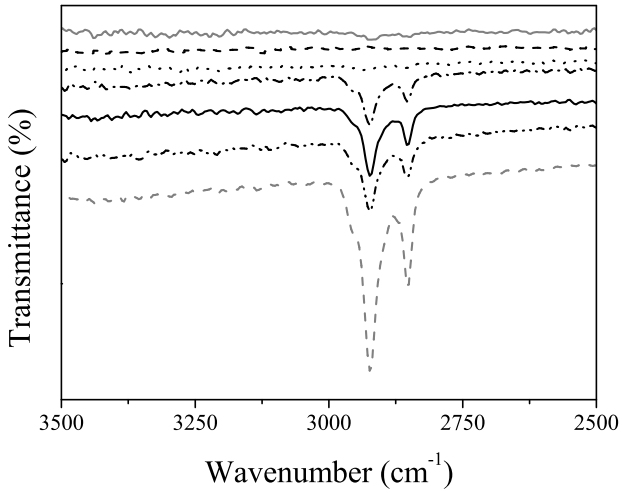

Figure V.12: IR spectra of monolayer film deposited on glass substrate and calcined at 400 °C (heating slope of 47 °C/s) under vacuum (· · –), under oxygen (· –), under successive vacuum and O_2 (—), annealed at 450 °C in vacuum then oxygen (· · ·) and at 400 °C with a heating slope of 1.3 °C/s (- - -). Grey curves are spectra of pristine sample (- - -) and glass substrate (—), respectively.

cles) compared to the one composed of a monolayer only (Fig.14 squares), confirming the successful deposition of multilayer. When the films are annealed, we observed a slight decrease of the susceptibility, but the gap between the ZFC-FC curves remains constant (Fig.14 triangles).

In the case of films of particles deposited on glass substrate (Fig.16), the ZFC-FC curves are dominated by the paramagnetism coming from impurities of the glass. However, here again the susceptibility shows a dependence of the number of layers deposited (Fig.16 inset).

The magnetization versus field measurements display, for all samples deposited on Si wafer (Fig.15), a weak hysteresis at very low field that is compensated at high field by the diamagnetism of the substrates. The magnetization versus field (M-H) measurements at 2 K, for the samples deposited on glass substrates, show hysteresis loops (Fig.17). The magnetizations at saturation and coercitive fields decrease while increasing the number of layers. Surprisingly, the hystereses are not centered on zero and are

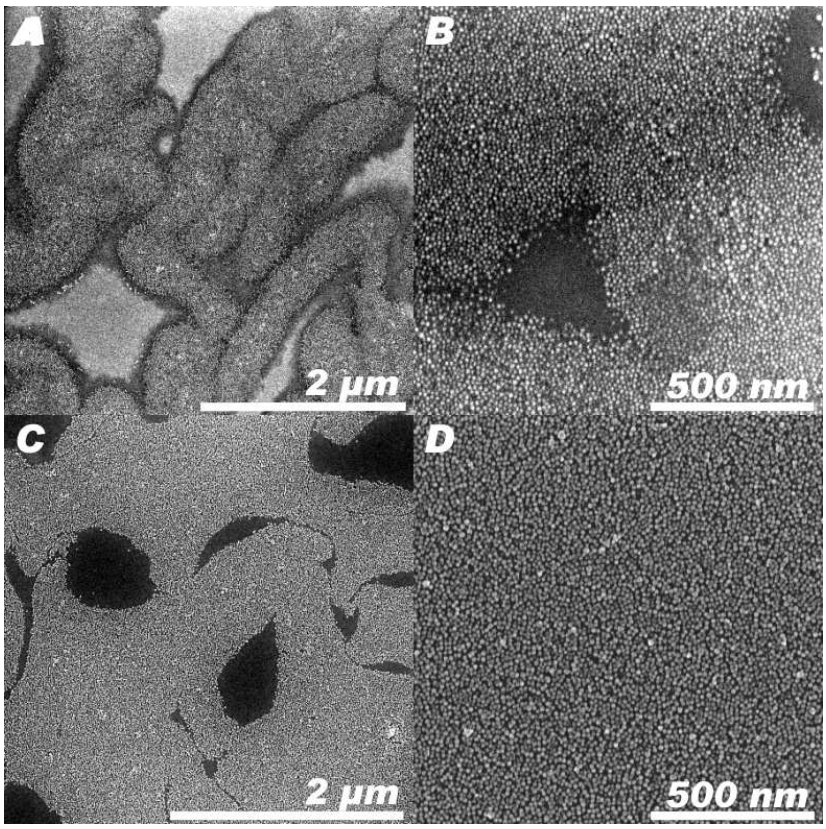

Figure V.13: SEM images of a $CoFe_2O_4$ nanoparticles film deposited on Si substrate, A and B before calcination, C and D after calcination with a slow heating slope at 400 °C under vacuum and oxygen.

inverted, i.e. clockwise loops. This effect, already observed for 2D layers, has been attributed to dipolar interactions between blocked and superparamagnetic nanoparticles in the literature[39], the reversal of superparamagnetic nanoparticles is prevented in the vicinity of blocked nanoparticles, the dipolar field being larger than the external field. Nevertheless, in the present study the effect was observed at very low temperature (T = 2 K) where all particle are assumed to be in the blocked state, the observed behavior is more probably attributable to the non-zero magnetic state of the films. The large anisotropy and size of the particles leads to a non randomly dispersed state for the particles. This non random distribution of the anisotropy easy axes could explain the observed hysteresis, even if a detailed simulation is needed to accredit this assumption.

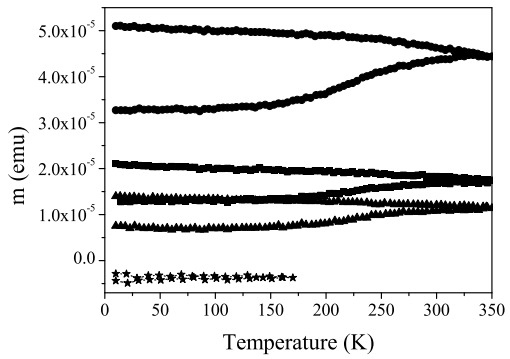

Figure V.14: Susceptibility versus temperature for films of particles on Si substrate composed of 2 layers (circles), 1 layer (squares) and 1 layer after calcination (triangles), (stars) Si substrate only.

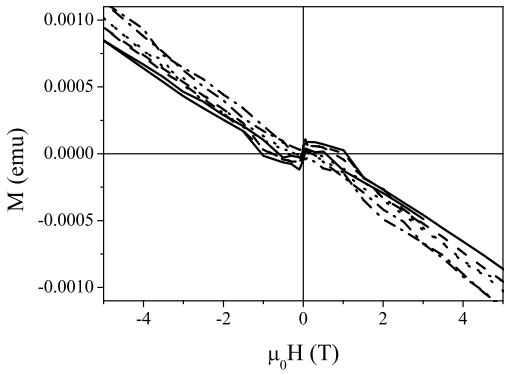

Figure V.15: Magnetization versus field at 2 K for bi-layer film (—), monolayer film (···) and calcined bilayer film (·–) and at 300 K for bi-layer film (- - -).

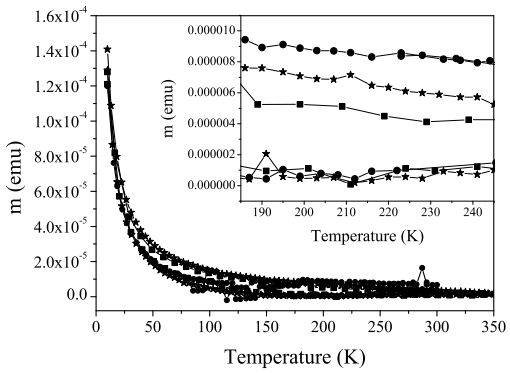

Figure V.16: Magnetization versus temperature for films of 1 layer (squares), 2 layers (stars) and 3 layers (circles) of particles on glass substrate.

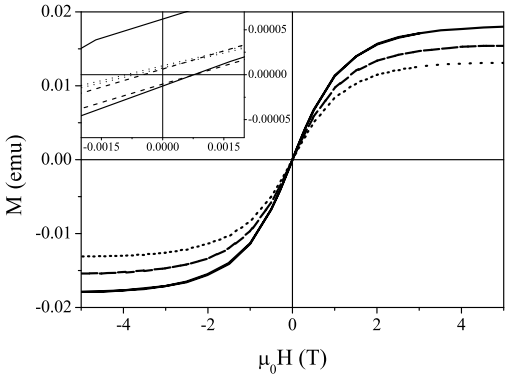

Figure V.17: Magnetization versus field at 2 K for 1 layer (—), 2 layers (- - -) and 3 layers (···) films of particles deposited on glass substrate.

V.4 Deposition of the oxide film

V.4.1 Deposition

The deposition of the oxide matrixes has been made using an atomic layer deposition process. This technique permits a whole and homogeneous coating of the particles. Zinc oxide films were made in collaboration with the group of Dr. Mato Knez (Max Planck Institute of Microstructure Physics, Halle, Germany). Using a low temperature

process based on the reaction of diethylzinc and water[40], 20, 50 and 100 nm of ZnO were deposited on mono and bi-layer films. To deposit TiO_2, we employed a method that was developed in our group. The process is based on the reaction of a carboxylic acid with a metal alkoxide. The advantages of this method are mainly due to the new chemistry taking place during the metal oxide thin film formation such as: (i) the metal oxide network takes place without the formation of intermediate hydroxyl groups under the elimination of an organic ester. (ii) A real self-limiting ALD growth can be achieved with titanium and also hafnium alkoxide even at very low temperature (50 °C) and this self-limiting ALD growth is obtained over a large range of temperatures (i.e. a large ALD window). (iii) Inherent to the chemistry of the process is a low amount of carbon impurities left in the metal oxide film. (iv) The as-grown films show an excellent uniformity and possess good dielectric properties[13]. Following this approach, films of particles coated with 20 and 27 nm of amorphous TiO_2 have been realized.

V.4.2 Characterizations

The thickness of the oxide layer was measured by X-ray reflectometry (XRR). Figures 18-19 present the patterns obtained for pure oxide films, film of particles and a composite film. Pure TiO_2 films (Fig.18) display various periodic well-defined oscillations proving that the films have a homogenous thickness. From the distance between minima the thicknesses were evaluated to be 20 and 27 nm respectively. In contrast, the film constitued by a monolayer of particles shows less defined oscillations denoting a lower thickness and a higher roughness of the film. This is due to the shape of the particles and the inhomogeneity of the deposition at the surface Fig.19 (dashed line). The pattern of the composite film (Fig.19 solid line) presents intense oscillations that are not periodic; this stressed the presence of two films with a different thickness. Indeed, the non periodicity is due to the fact that the observed signals is the superposition of two signals characterized by different position of the oscillations.

SEM images of composite films are shown in figure 20. For both, TiO_2 and ZnO, the

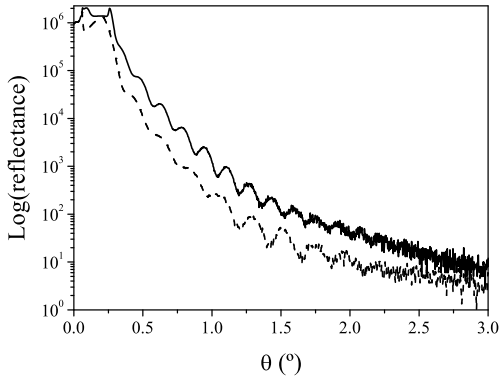

Figure V.18: XRR patterns of pure TiO_2 film of 20 nm (- - -) and 27 nm (—).

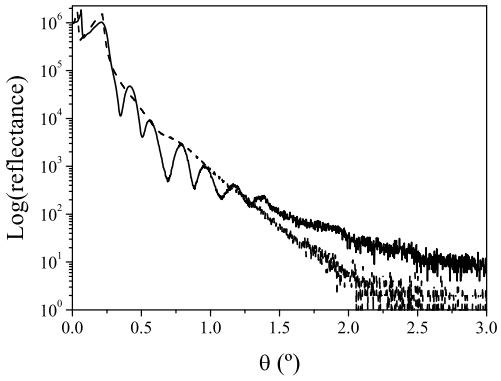

Figure V.19: XRR patterns of 1 monolayer film of particles (- - -) and monolayer film of particles covered by 27 nm of TiO_2 (—).

coating is uniform along the whole surface and the underneath film of particles are still visible.

The surface of ZnO films were also monitored by atomic force microscopy (AFM). Non-contact mode AFM image of 100 nm pure ZnO is presented figure 21. The film consists of nanocrystallites of around 10 nm in size. This behavior was expected for ZnO since, as it was already reported, the growth of ZnO by ALD from diethylzinc and water leads to a nanocrystalline film even at low temperature (i.e. T <100 °C)[40]. Moreover, it was shown that the nanocrystallite size could be tuned by the deposition temperature. On the other hand the roughness of the TiO_2 films is much lower (cf. XRR studies) because the as deposited films are amorphous even at deposition temperatures above 200 °C.

V.4.3 Magnetic properties

Susceptibility versus temperature measurements are depicted in figure 22 for films made of a monolayer of nanoparticles covered with TiO_2 and ZnO. The ZFC-FC curves are similar to the one of uncoated film of particles. Indeed, the blocking temperature of the magnetic phase still takes place slightly above 300 K. The magnetic properties are not affected by the oxide growth and, as depicted before from SEM and AFM, the

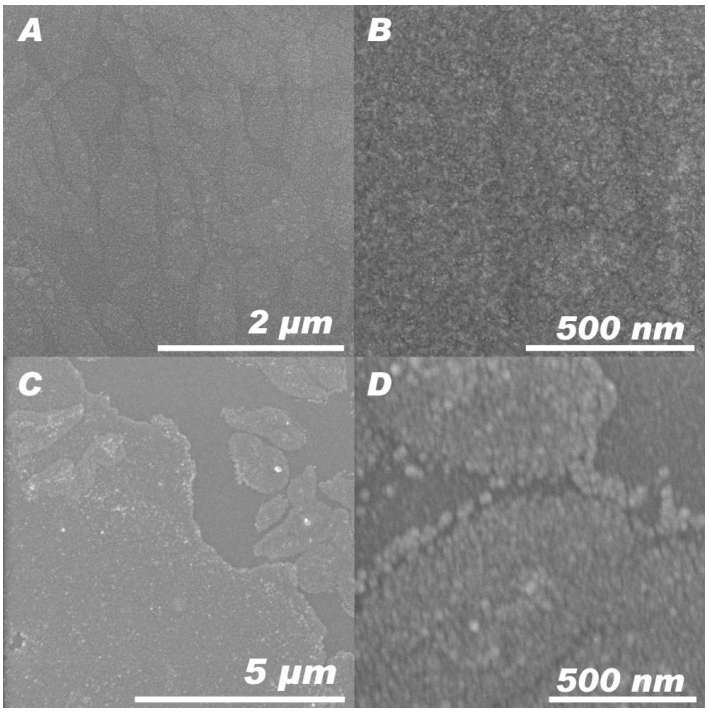

Figure V.20: SEM images of cobalt ferrite monolayer film covered by 50 nm of ZnO (A-B) and bilayer film covered by 27 nm of TiO_2 (C-D).

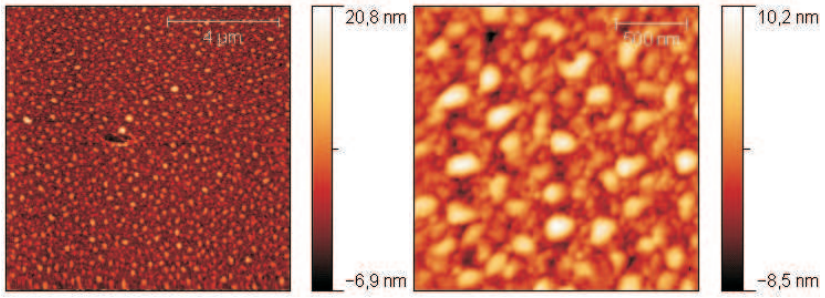

Figure V.21: AFM images of 100 nm pure ZnO film.

particles size is kept constant during the process. This confirms that the experimental approach is suitable to obtain a composite superlattice with a quasi-monodisperse layer of ferrimagnetic nanoparticles.

To characterize the film and know if there is interactions between the particles through the oxide film, one can measure the relaxation time by ac mode magnetic measurement. Unfortunately, due to the weak signal of the system we did not yet succeed to measure

such phenomenon with a Squid magnetometer, even when using a reciprocating sample (RSO) measurement system.

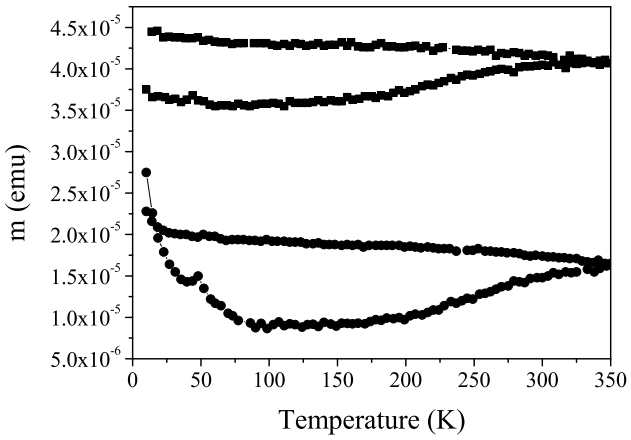

Figure V.22: Susceptibility versus temperature of monolayer film of particles coated with 100 nm of ZnO (filled circles) and 20 nm of TiO_2 (filled squares) on silicon.

V.5 Summary and Conclusions

Nanoparticles of cobalt ferrite (composition $CoFe_2O_4$) have been synthesized by a decomposition method in the presence of surfactant. This procedure led to 8-10 nm spherical monocrystalline particles homogeneous in size and shape which present a typical superparamagnetic behavior above 310 K. Below this temperature, the particles are blocked and display a high coercivity. Mono- bi- and tri-layer films of the cobalt ferrite particles were successfully deposited by a Langmuir-Blodgett technique onto glass and silicon substrates. A careful annealing of the films permits the removing of the surfactant that were used for controlling the size and shape of the particles during synthesis and that also allowed their deposition by LB, without deterioration of the films. Homogeneous domains of particles could be obtained over several nanometer areas. Magnetic measurements performed on the films confirmed the successful deposition of

multilayer. Furthermore, the films show a ferrimagnetic behavior up to room temperature as for the as-synthesized nanoparticles. The covering of the particles by oxide materials (ZnO and TiO_2) was realized in a controlled way by ALD. The resulting hetero-structures present well calibrated thickness and could be used as model systems for the investigation of the magnetic interactions between magnetic particles through the continuous oxide thin films. Unfortunately, the magnetic properties of the resulting hetero-structures could not be explored in details so far. However, some analyses are still in progress. For example, ferromagnetic resonance experiments are underway to obtain information on the magnetic properties of particles embedded in oxide matrices. Other experiments such as magnetoresistance measurements of the composite film under an applied film, could bring light on the interaction of the magnetic particles with the oxide film. Finally, the results presented here are the starting point in a project devoted to the synthesis of hetero-structured materials and they should be seen as the basis for numerous future works.

V.6 Experimental part

Precursors and particles syntheses

Iron (III) chloride hexahydrate 98%, cobalt (II) chloride hexahydrate 98%, Oleic acid 90% (cis-9-Octadecenoic acid) and 1-Octadecene 90% were purchased from Aldrich and used as received.

Iron and cobalt oleate complexes were synthesized from their metal chloride counterpart using modified known procedures[22,41]. In a typical experiment, 60 mmol of oleaic acid were mixed to 65 mmol of NaOH in a solution of H_2O/ethanol/hexane (40/40/80 ml). After addition of 20 mmol of the metal chloride, the solution has been heated at 60 °C for 1 hour. After cooling at room temperature, the organic phase was extrated in a separotory funnel and then washed 3 times with water. Evaporation of the hexane leads to a orange oily solution for the iron oleate or a air-sensitive purple solid for

cobalt oleate.

The particles were obtained by the thermal decomposition of the metal oleates in the presence of oleic acid. In a round-bottom flask, 0.85 g (0.94 mmol) of iron oleate, 0.44 g (0.7 mmol) of cobalt oleate, 0.45 g (1.6 mmol) of oleic acid and 10 ml of octadecene are heated at around 5 °C/min under vigorous stirring. Above 250 °C the solution turns black. The reaction is then kept at 300 °C for one hour. After cooling down, the nanoparticles are separated from the solution by centrifugation and thoroughly washed with ethanol, hexane and dichloromethane. A dark waxy powder is obtained.

Langmuir-Blodgett films

A laboratory Langmuir-Blodgett trough made of PTFE (trough width 7.5 cm, area 242.25 cm^2) equipped with two mobile barriers was used for the deposition of the film. A Wilhelmy balance measured the interfacial pressure during deposition. Milli-Q water and chloroform were used as subphase and spreading solvent, respectively. The cobalt ferrite nanoparticles were dispersed in the minimum of chloroform just after their synthesis/washing. Before use, the solution is passed through a PTFE filter.

After the spreading of few drops of the solution onto the water surface, 15 min were allowed for solvent evaporation. The film was compressed at a rate of 5 mm/min to a pressure of 15 mN/m. The transfer was performed using a vertical dipper at a rate of 3 mm/min and at a constant pressure (maintained by a feedback loop). A waiting time of 30 to 60 minutes was given to the system to reach equilibrium prior the transfer. 25 x 25 mm glass substrates (1 mm thick) and 15 x 20 mm Si wafer (0.5 mm thick) were used as film supports. Some of the Si substrates were previously washed with a diluted solution of HF in order to remove the native SiO_2 layer. For all substrates, the transfer occurred only when dipped upward, i.e. from the subphase to air.

TiO_2 deposition

Films were deposited using titanium isopropoxide (Aldrich, 99.99%) and acetic acid (Fluka 99.8%). Pure nitrogen was used as carrier and purging gas. Precursor and acid vapors were generated in external reservoirs preheated at 80 °C and 40 °C , respectively. They were introduced into the reactor through an ALD valve. All tubes of the circuit were maintained at 100 °C during the deposition process. The substrate temperature was maintained at 200 °C and nitrogen gas flow at 5 sccm. In a typical experiment the valves were opened for 0.02 s for carboxylic acid and 1 s for the metal alkoxides while the residence and purging periods were 20s and 15s, respectively.

Experimental details

TEM and EDX were carried out on a JEOL 2200 FS microscope operating at 200 kV and equipped with an in-column energy filter. Samples were prepared by depositing a drop of a solution of particles in ethanol on a copper grid coated with an amorphous carbon film. Magnetic properties were measured using a SuperQuantum Interference Design (SQUID) magnetometer MPMS XL7, in the range of temperature 2-350 K and of field 0-5 T. The temperature-dependent susceptibility was measured using DC procedure. The sample was cooled to 1.8 K under zero magnetic field, magnetic field was then applied and data collected from 2 K to 350 K (zero-field cooled, ZFC). Field Cooled (FC) measurements were performed from 2 K to 350 K with an applied field during the cooling. AC susceptibility was measured in a zero external field with different frequencies ranging from 10 to 1000 Hz. UV-vis spectra were recorded with a Unicam UV 4 spectrophotometer. SEM images were performed without carbon coating using a FEG-SEM Hitachi S4100 microscope operating from 5 to 25 kV. Rapid Thermal Annealing was carried out on a JIPELEC JETFIRST 100 instrument. FTIR spectra were measured on a Matson 7000 FTIR spectrometer. XRR data were collected on an X'Pert MPD Philips diffractometer (CuKα X-radiation at 40 kV and 50 mA).

Bibliography

[1] A. R. de Moraes, C. K. Saul, D. H. Mosca, J. Varalda, P. Schio, A. J. A. de Oliveira, M. A. Canesqui, V. Garcia, D. Demaille, *et al.*, "Magnetoresistance in Granular Magnetic Tunnel Junctions with Fe Nanoparticles Embedded in ZnSe Semiconducting Epilayer", *J. Appl. Phys.*, **103**, 123714 (2008). http://dx.doi.org/10.1063/1.2938071. 111

[2] F. M. Yang, T. C. Chang, P. T. Liu, P. H. Yeh, Y. C. Yu, J. Y. Lin, S. M. Sze, J. C. Lou, "Memory Characteristics of Co Nanocrystal Memory Device with HfO_2 as Blocking Oxide", *Appl. Phys. Lett.*, **90**, 132102 (2007). http://dx.doi.org/10.1063/1.2716845. 111

[3] H. Zeng, S. Sun, "Syntheses, Properties, and Potential Applications of Multicomponent Magnetic Nanoparticles", *Adv. Funct. Mater.*, **18**, 391 (2008). http://dx.doi.org/10.1002/adfm.200701211. 111

[4] U. Jeong, X. Teng, Y. Wang, H. Yang, Y. Xia, "Superparamagnetic Colloids: Controlled Synthesis and Niche Applications", *Adv. Mater.*, **19**, 33 (2007). http://dx.doi.org/10.1002/adma.200600674. 111, 112

[5] R. P. Tan, J. Carrey, C. Desvaux, J. Grisolia, P. Renaud, B. Chaudret, M. Respaud, "Transport in Superlattices of Magnetic Nanoparticles: Coulomb Blockade, Hysteresis, and Switching Induced by a Magnetic Field", *Phys. Rev. Lett.*, **99**, 176805 (2007). http://dx.doi.org/10.1103/PhysRevLett.99.176805. 111

[6] X. Batlle, A. Labarta, "Finite-size Effects in Fine Particles: Magnetic and Transport Properties", *J. Phys. D: Appl. Phys.*, **35**, R15 (2002). http://dx.doi.org/10.1088/0022-3727/35/6/201. 111

[7] H. Zheng, J. Wang, S. E. Lofland, Z. Ma, L. Mohaddes-Ardabili, T. Zhao, L. Salamanca-Riba, S. R. Shinde, S. B. Ogale, *et al.*, "Multiferroic $BaTiO_3$-$CoFe_2O_4$ Nanostructures", *Science*, **303**, 661 (2004). http://dx.doi.org/10.1126/science.1094207. 111

[8] S. Mornet, C. Elissalde, O. Bidault, F. Weill, E. Sellier, O. Nguyen, M. Maglione, "Ferroelectric-Based Nanocomposites: Toward Multifunctional Materials", *Chem. Mater.*, **19**, 987 (2007). http://dx.doi.org/10.1021/cm0616735. 111

[9] M. Grigorova, H. J. Blythe, V. Blaskov, V. Rusanov, V. Petkov, V. Masheva, D. Nihtianova, L. M. Martinez, J. S. Munoz, M. Mikhov, "Magnetic Properties and Mossbauer Spectra of Nanosized $CoFe_2O_4$ Powders", *J. Magn. Magn. Mater.*, **183**, 163 (1998). http://dx.doi.org/10.1016/S0304-8853(97)01031-7. 111, 114, 115

[10] J. Park, J. Joo, S. Kwon, Y. Jang, T. Hyeon, "Synthesis of Monodisperse Spherical Nanocrystals", *Angew. Chem., Int. Ed.*, **46**, 4630 (2007). http://dx.doi.org/10.1002/anie.200603148. 111, 112

[11] X. Jia, D. Chen, X. Jiao, T. He, H. Wang, W. Jiang, "Monodispersed Co, Ni-Ferrite Nanoparticles with Tunable Sizes: Controlled Synthesis, Magnetic Properties, and Surface Modification", *J. Phys. Chem. C*, (2008). http://dx.doi.org/10.1021/jp077019+. 111

[12] T. Hyeon, "Chemical synthesis of magnetic nanoparticles", *Chem. Commun.*, pp. 927–934 (2003). http://dx.doi.org/10.1039/b207789b. 111

[13] E. Rauwel, G. Clavel, M.-G. Willinger, P. Rauwel, N. Pinna, "Non-aqueous routes to metal oxide thin films by atomic layer deposition", *Angew. Chem., Int. Ed.*, **47**, 3592 (2008). http://dx.doi.org/10.1002/anie.200705550. 111, 125

[14] S. Lefebure, C. Menager, V. Cabuil, M. Assenheimer, F. Gallet, C. Flament, "Langmuir Monolayers of Monodispersed Magnetic Nanoparticles Coated with a Surfactant", *J. Phys. Chem. B*, **102**, 2733 (1998). http://dx.doi.org/10.1021/jp980403+. 112

[15] P. Masse, S. Ravaine, "The Langmuir-Blodgett Technique: A Powerful Tool to Elaborate Multilayer Colloidal Crystals", *Colloids Surf., A*, **270-271**, 148 (2005). http://dx.doi.org/10.1016/j.colsurfa.2005.05.056. 112

[16] S. Bordacs, A. Agod, Z. Horvolgyi, "Compression of Langmuir Films Composed of Fine Particles: Collapse Mechanism and Wettability", *Langmuir*, **22**, 6944 (2006). http://dx.doi.org/10.1021/la060696v. 112

[17] M. Clemente-Leon, H. Soyer, E. Coronado, C. Mingotaud, C. J. Gomez-Garcia, P. Delhaes, "Langmuir-Blodgett Films of Single-Molecule Nanomagnets", *Angew. Chem., Int. Ed.*, **37**, 2842 (1998). http://dx.doi.org/10.1002/(SICI)1521-3773(19981102)37:20<2842::AID-ANIE2842>3.0.CO;2-B. 112

[18] T. Fried, G. Shemer, G. Markovich, "Ordered Two-Dimensional Arrays of Ferrite Nanoparticles", *Adv. Mater.*, **13**, 1158 (2001). http://dx.doi.org/10.1002/1521-4095(200108)13:15<1158::AID-ADMA1158>3.0.CO;2-6. 112

[19] P. Poddar, T. Telem-Shafir, T. Fried, G. Markovich, "Dipolar Interactions in Two- and Three-Dimensional Magnetic Nanoparticle Arrays", *Phys. Rev. B*, **66**, 060403 (2002). http://dx.doi.org/10.1103/PhysRevB.66.060403. 112

[20] M. Knez, K. Nielsch, L. Niinisto, "Synthesis and Surface Engineering of Complex Nanostructures by Atomic Layer Deposition", *Adv. Mater.*, **19**, 3425 (2007). http://dx.doi.org/10.1002/adma.200700079. 112

[21] M. Leskela, M. Kemell, K. Kukli, V. Pore, E. Santala, M. Ritala, J. Lu, "Exploitation of Atomic Layer Deposition for Nanostructured Materials", *Mater. Sci. Eng., C*, **27**, 1504 (2007). http://dx.doi.org/10.1016/j.msec.2006.06.006. 112

[22] J. Park, K. J. An, Y. S. Hwang, J. G. Park, H. J. Noh, J. Y. Kim, J. H. Park, N. M. Hwang, T. Hyeon, "Ultra-Large-Scale Syntheses of Monodisperse Nanocrystals", *Nat. Mater.*, **3**, 891 (2004). http://dx.doi.org/10.1038/nmat1251. 112, 129

[23] W. W. Yu, J. C. Falkner, C. T. Yavuz, V. L. Colvin, "Synthesis of Monodisperse Iron Oxide Nanocrystals by Thermal Decomposition of Iron Carboxylate Salts", *Chem. Commun.*, pp. 2306–2307 (2004). http://dx.doi.org/10.1039/b409601k. 112

[24] N. R. Jana, Y. Chen, X. Peng, "Size- and Shape-Controlled Magnetic (Cr, Mn, Fe, Co, Ni) Oxide Nanocrystals via a Simple and General Approach", *Chem. Mater.*, **16**, 3931 (2004). http://dx.doi.org/10.1021/cm049221k. 112

[25] K. An, N. Lee, J. Park, S. C. Kim, Y. Hwang, J. G. Park, J. Y. Kim, J. H. Park, M. J. Han, *et al.*, "Synthesis, Characterization, and Self-Assembly of Pencil-Shaped CoO Nanorods", *J. Am. Chem. Soc.*, **128**, 9753 (2006). http://dx.doi.org/10.1021/ja0608702. 112

[26] L. M. Bronstein, X. Huang, J. Retrum, A. Schmucker, M. Pink, B. D. Stein, B. Dragnea, "Influence of Iron Oleate Complex Structure on Iron Oxide Nanoparticle Formation", *Chem. Mater.*, **19**, 3624 (2007). http://dx.doi.org/10.1021/cm062948j. 112

[27] T. Meron, Y. Rosenberg, Y. Lereah, G. Markovich, "Synthesis and Assembly of High-Quality Cobalt Ferrite Nanocrystals Prepared by a Modified Sol-Gel Technique", *J. Magn. Magn. Mater.*, **292**, 11 (2005). http://dx.doi.org/10.1016/j.jmmm.2004.10.084. 114

[28] T. Hyeon, Y. Chung, J. Park, S. S. Lee, Y.-W. Kim, B. H. Park, "Synthesis of Highly Crystalline and Monodisperse Cobalt Ferrite Nanocrystals", *J. Phys. Chem. B*, **106**, 6831 (2002). http://dx.doi.org/10.1021/jp026042m. 114

[29] A. J. Rondinone, A. C. S. Samia, Z. J. Zhang, "Characterizing the Magnetic Anisotropy Constant of Spinel Cobalt Ferrite Nanoparticles", *Appl. Phys. Lett.*, **76**, 3624 (2000). http:/dx.doi.org/10.1063/1.126727. 114

[30] C. Liu, A. J. Rondinone, Z. J. Zhang, "Synthesis of Magnetic Spinel Ferrite $CoFe_2O_4$ Nanoparticles from Ferric Salt and Characterization of the Size-Dependent Superparamagnetic Properties", *Pure Appl. Chem.*, **72**, 37 (2000). http://dx.doi.org/10.1351/pac200072010037. 115

[31] M. Rajendran, R. C. Pullar, A. K. Bhattacharya, D. Das, S. N. Chintalapudi, C. K. Majumdar, "Magnetic Properties of Nanocrystalline $CoFe_2O_4$ Powders Prepared at Room Temperature: Variation with Crystallite Size", *J. Magn. Magn. Mater.*, **232**, 71 (2001). http://dx.doi.org/10.1016/S0304-8853(01)00151-2. 115

[32] A. T. Ngo, M. P. Pileni, "Nanoparticles of Cobalt Ferrite: Influence of the Applied Field on the Organization of the Nanocrystals on a Substrate and on Their Magnetic Properties", *Adv. Mater.*, **12**, 276 (2000). http://dx.doi.org/10.1002/(SICI)1521-4095(200002)12:4<276::AID-ADMA276>3.0.CO;2-D. 115

[33] B. Toksha, S. E. Shirsath, S. Patange, K. Jadhav, "Structural Investigations and Magnetic Properties of Cobalt Ferrite Nanoparticles Prepared by Sol-Gel Auto-combustion Method", *Solid State Commun.*, **147**, 479 (2008). http://dx.doi.org/10.1016/j.ssc.2008.06.040. 115

[34] F. X. Redl, C. T. Black, G. C. Papaefthymiou, R. L. Sandstrom, M. Yin, H. Zeng, C. B. Murray, S. P. O'Brien, "Magnetic, Electronic, and Structural Characterization of Nonstoichiometric Iron Oxides at the Nanoscale", *J. Am. Chem. Soc.*, **126**, 14583 (2004). http://dx.doi.org/10.1021/ja046808r. 115

[35] E. Tirosh, G. Shemer, G. Markovich, "Optimizing Cobalt Ferrite Nanocrystal Synthesis using a Magneto-optical Probe", *Chem. Mater.*, **18**, 465 (2006). http://dx.doi.org/10.1021/cm052401p. 115

[36] A. Hutlova, D. Niznansky, J. L. Rehspringer, C. Estournes, M. Kurmoo, "High Coercive Field for Nanoparticles of $CoFe_2O_4$ in Amorphous Silica Sol-Gel", *Adv. Mater.*, **15**, 1622 (2003). http://dx.doi.org/10.1002/adma.200305305. 115

[37] V. Perez-Dieste, O. M. Castellini, J. N. Crain, M. A. Eriksson, A. Kirakosian, J.-L. Lin, J. L. McChesney, F. J. Himpsel, C. T. Black, C. B. Murray, "Thermal Decomposition of Surfactant Coatings on Co and Ni Nanocrystals", *Appl. Phys. Lett.*, **83**, 5053 (2003). http://dx.doi.org/10.1063/1.1633971. 120

[38] S.-Y. Zhao, D. K. Lee, C. W. Kim, H. G. Cha, Y. H. Kim, Y. S. Kang, "Synthesis of Magnetic Nanoparticles of Fe_3O_4 and $CoFe_2O_4$ and Their Surface Modification by Surfactant Adsorption", *Bull. Korean Chem. Soc.*, **27**, 237 (2006). http://newjournal.kcsnet.or.kr/main/j_search/j_abstract_view.htm?code=B060215. 120

[39] J. Y. Yang, J. H. Kim, J. S. Lee, S. J. Woo, J. S. Kwak, J. P. Hong, M. H. Jung, "Inverted Hysteresis Loops Observed in a Randomly Distributed Cobalt Nanoparticle System", *Phys. Rev. B*, **78**, 094415 (2008). http://dx.doi.org/10.1103/PhysRevB.78.094415. 123

[40] S.-M. Lee, G. Grass, G.-M. Kim, C. Dresbach, L. Zhang, U. Gösele, M. Knez, "Low-Temperature ZnO Atomic Layer Deposition on Biotemplates: Flexible Photocatalytic ZnO Structures from Eggshell Membranes", *Phys. Chem. Chem. Phys.*, **11**, 3608 (2009). http://dx.doi.org/10.1039/b820436e. 125, 126

[41] H. Funakoshi, "Gas Absorption by Cobalt Soaps", *Bull. Chem. Soc. Jpn.*, **35**, 1025 (1962). http://dx.doi.org/10.1246/bcsj.35.1025. 129

Conclusion

In this work, we intended to make non-magnetic oxides become magnetic.

The first approach followed was to use doping to induce ferromagnetism in semiconductor materials (Chapter II, III and IV). We have developed non-aqueous sol-gel routes, leading to well controlled oxide nanomaterials, to the synthesis of transition-metal doped oxides (ZnO, ZrO_2). Homogeneous doping is particularly important in the comprehensive study of diluted magnetic semiconductors (DMSs). One of the main points of this study was to ascertain the oxidation state and local structure of the dopant ions and to preclude the formation of additional magnetic phases that could be responsible for, or interfere with, the magnetic properties observed.

Doped zinc oxide nanoparticles were synthesized by reacting zinc acetate and a transition metal precursor with benzyl alcohol at 250 °C. This solvothermal method enables the incorporation of several dopants into the ZnO matrix, such as Mn and Co. Moreover, by varying the amount of benzyl alcohol with anisole as inert co-solvent, the morphology of the particles can be tuned. For example, Co-doped ZnO synthesized in benzyl alcohol/anisole (95/5%) yields small rods whereas particles are obtained for Mn-doped ZnO synthesized in pure benzyl alcohol. Surprisingly, the use of anisole affects the magnetic behavior as well. Mn-doped ZnO always display a paramagnetic behavior while cobalt doped particles are paramagnetic or ferromagnetic depending on the solvent used. For both cobalt and manganese doped zinc oxide, independently of the synthesis condition, we could show that the dopant substitutes onto zinc sites in the wurtzite lattice, with no detectable phase impurities or clustering. Hence, the observance of ferromagnetism appears to be clearly related to the core properties of cobalt doped ZnO nanocrystals.

The synthesis of Mn-doped zirconia, also achieved by the benzyl alcohol route, led to high quality spherical nanocrystals of 3-4 nm. The particles are monocrystalline in nature and do not present any core default. Previous theoretical calculations on zirconia indicate that the ferromagnetic interactions are closely related to the oxidation state of the magnetic ion. EPR experiments of the Mn-doped samples reveal the coexistence of manganese oxidation state (II) and (III), their ratio depending on the manganese concentration. The magnetic measurements show mainly a paramagnetic behavior. The synthesis routes explored on DMS enable a state of the art control of any parameter that influences the electronic properties of transition metal doped oxides. We expect that the synthesized particles can be used for an experimental verification of the theoretical prediction.

The second approach pursued in order to obtain ferromagnetic materials was to realize hetero-structures composed of oxide films and magnetic nanoparticles (Chapter V). The hetero-systems studied were magnetic nanoparticles of cobalt ferrite distributed into a semiconducting or dielectric material, namely ZnO or TiO_2.

Nanoparticles of cobalt ferrite have been synthesized by a decomposition method in the presence of oleic acid as surfactant. This procedure led to 8-10 nm spherical monocrystalline particles homogeneous in size and shape. These nanoparticles present a superparamagnetic behavior above 310 K. Mono- bi- and tri-layer films of the cobalt ferrite particles were successfully deposited by Langmuir-Blodgett technique onto glass and silicon substrates. Homogeneous domains of particles could be obtained over several micrometers. An annealing of the films was performed to remove the surfactant grafted at their surface. Magnetic measurements confirmed the successful deposition of multilayer film on glass and silicon substrates. Furthermore, the films show a ferrimagnetic behavior up to room temperature as for the as-synthesized nanoparticles. The coating of the particles by oxide materials (ZnO and TiO_2) was realized by ALD. The obtained hetero-structures were characterized by AFM, SEM and preliminary magnetic studies

show that the magnetic properties do not differ greatly from the one of the nanoparticles films. Finally, this work is the starting point for future studies devoted to the combination of solution routes for the fabrication of assembly of nanoparticles and low temperature gas phase deposition approaches for the formation of multifunctional hetero-structures.

Appendices

Appendice A:

French Abstract

Les travaux présentés dans ce mémoire ont été obtenus dans le cadre de la thèse intitulée "Magnetic Impurities in nanostructured materials" réalisés conjointement sous la direction du Dr. Nicola Pinna à l'Université de Aveiro (Portugal) et du Dr. David Zitoun à l'Université Montpellier II.

A.1 Introduction

L'électronique de spin (spintronique) est un domaine émergent de l'électronique qui vise à exploiter le spin de l'électron en plus de sa charge. L'utilisation de porteurs polarisés promet d'offrir plusieurs avantages par rapport aux dispositifs traditionnels (basés sur le transport des électrons seulement), par exemple, une meilleure puissance de traitement des informations, une réponse rapide, une faible consommation d'énergie ainsi qu'une plus grande intégration/miniaturisation. Dans ce travail, nous avons projeté de rendre des oxydes non-magnétiques magnétiques afin d'obtenir des matériaux pouvant correspondre aux attentes de la spintronique. L'objectif de cette thèse a donc été la synthèse et la caractérisation de matériaux associant des propriétés magnétiques et semi-conductrices. Nous nous sommes concentrés sur des oxydes synthétisés par des voies de chimie douce et en particulier par des procédés de sol gel non-hydrolytique

(NHSG).

La première approche suivie a été l'étude de semi-conducteurs magnétiques dilués (DMSs). Les DMSs sont une classe de semi-conducteurs, pour lesquels une faible fraction de leurs cations est remplacée par des ions magnétiques afin d'induire un ordre ferromagnétique. Nous avons fait usage de procédés NHSG pour synthétiser des oxydes semi-conducteurs (ZnO, ZrO_2) dopés par des métaux de transition. Un dopage homogène est particulièrement important dans l'étude de ces semi-conducteurs magnétiques dilués et le point principal de cette étude était de déterminer l'état d'oxydation et la structure locale du dopant et d'exclure l'existence d'une phase secondaire comme origine du magnétisme. La partie A est consacrée à la synthèse, la caractérisation morphologique et structurale, l'étude de l'environnement du dopant et les résultats magnétiques du ZnO dopé par le manganèse et le cobalt ainsi que du ZrO_2 par le manganèse. Cette partie regroupe donc le chapitre II, III et IV du mémoire.

Une autre possibilité pour combiner plusieurs propriétés et fonctionnalités dans un même matériau est l'élaboration d'hétéro-structures. En conséquence, outre les travaux sur les DMSs, nous avons étudié les propriétés magnétiques d'hétéro-système composé de nanoparticules magnétiques dispersées dans une matrice d'oxyde. Les matériaux étudiés sont des nanoparticules de ferrite de cobalt déposées sous forme de film et recouvertes d'un oxyde semi-conducteur ou diélectrique, à savoir ZnO ou TiO_2. La synthèse de ces matériaux s'est déroulée en trois étapes distinctes : (i) la synthèse de nanoparticules magnétiques uniformes, (ii) le dépôt des particules obtenues sous forme de film par la technique de Langmuir-Blodgett et (iii) la déposition de la matrice d'oxyde par ALD (atomic layer deposition). Les résultats expérimentaux obtenus sur ces hétéro-structures sont donnés et discutés dans la partie B (correspondant au résumé du chapitre V).

A.2 Partie A : Semi-conducteurs magnétiques dilués

A.2.1 État de l'art

Les DMSs sont des semi-conducteurs, principalement de type III-V et II-VI, dont une partie de leurs cations ont été aléatoirement substitués par des ions magnétiques (Fig.1). Ces matériaux combinent donc propriétés semi-conductrices et magnétiques. La réémergence, ces dix dernières années, de recherches dans ce domaine est principalement due à l'hypothèse que le magnétisme est réellement promu par les porteurs de charge du semi-conducteur hôte et que le ferromagnétisme peut persister jusqu'à température ambiante.

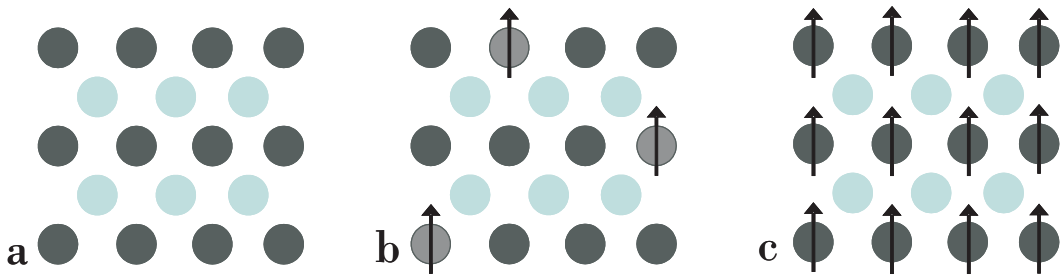

FIGURE A.1: Représentation schématique de a) un semi-conducteur non-magnétique, b) un semi-conducteur magnétique dilué composé d'un semi-conducteur non-magnétique dopé par des atomes magnétiques et c) un semi-conducteur magnétique contenant un réseau périodique d'éléments magnétiques.

En effet, basé sur le modèle de Zener, Dietl et al. ont prédit que les semi-conducteurs à large band-gap tel que GaN et ZnO dopés manganèse seraient ferromagnétiques avec une température de Curie supérieure à la température ambiante[1]. Depuis cette prédiction, des travaux théoriques[2–8] et expérimentaux ont été abondamment publiés sur l'oxyde de zinc[9–14] et le nitrure de gallium[15–18]. Toutefois, ces matériaux ont donné lieu à une étude plus approfondie sur les oxydes dopés et en particulier sur l'oxyde de titane[15,19]. Récemment Ostanin et al. ont prédit que ZrO_2 et HfO_2[20,21] dopés avec différents ions de métaux de transition serait ferromagnétiques à température am-

biante en fonction du degré d'oxydation du métal de transition. La figure 2 montre l'un des résultats obtenu sur l'oxyde de zirconium présenté dans leur article[21]. Ce graphique présente la température de Curie en fonction du dopant et son état d'oxydation (nombre d'électrons supplémentaires par impureté magnétique). Une lecture des résultats montre que pour le manganèse, la zircone est ferromagnétique à température ambiante pour un état d'oxydation allant de III à IV.

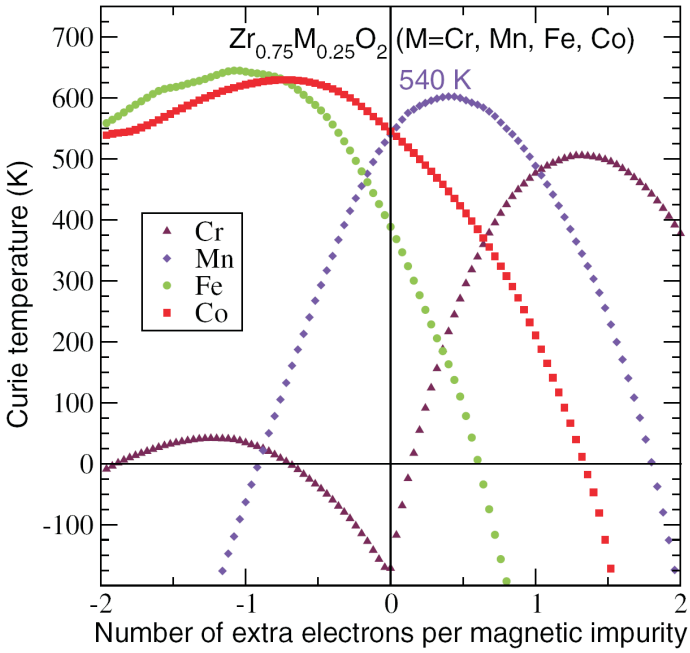

FIGURE A.2: Température de Curie de $Zr_{0.75}M_{0.25}O_2$ (M = Cr, Mn, Fe, Co) d'après frozen-magnon calcul. (n) nombre d'extra électrons par impureté magnétique (n = 0 correspond au nombre nominal d'électrons) d'après ref[21]

Bien que des progrès significatifs ont été accomplis dans la synthèse et sur les propriétés magnétiques des DMSs, des questions demeurent, en particulier une importante controverse existe sur l'origine du ferromagnétisme dans les DMSs[10,14,16,22–25]. Ceci vient du fait que les températures de Curie reportées sont souvent discordantes et le doute est mis sur la nature, intrinsèque ou extrinsèque, du ferromagnétisme[10,26]. Par conséquent, le point principal de toute nouvelle étude repose sur l'exclusion de toute

phase secondaire comme origine du ferromagnétisme. De plus, la nature des mécanismes d'échanges qui stabilisent la phase ferromagnétique dans les DMSs n'est pas bien comprise[11,13,14,25,27–29] et le lien entre la concentration de porteurs de charge et ferromagnétisme n'a pas encore été clairement établi[2,4,11,22,26]. Cependant, il semble que pour des systèmes homogènes les propriétés magnétiques semblent être fortement dépendantes de l'interaction matrice/dopant, la concentration des porteurs de charge, des défauts du semi-conducteur, et donc des conditions de synthèse.

Dans ce travail, nous avons fait usage de procédés non aqueux pour synthétiser des oxydes dopés. Les synthèses en solution et en particulier le procédé sol-gel non-aqueux sont attrayantes pour la préparation de nanoparticules d'oxydes métalliques de taille et forme contrôlées, offrant de nombreux avantages tels que une bonne cristallinité des oxydes même synthétisés à basse température et une excellente reproductibilité[30–33].

A.2.2 Résultats et discussions

Nanoparticules d'oxyde de zinc dopé cobalt et manganèse

L'oxyde de zinc dopé a été synthétisé à partir d'acétate de zinc et d'alcool benzylique en présence d'un précurseur de dopant (acétate de cobalt (II) ou oléate de manganèse (II)). Des concentrations allant jusqu'à 5% pour le cobalt et 1% pour le manganèse ont été étudiées. Le mécanisme de la réaction a été étudié en analysant la composition du mélange après réaction par résonance magnétique nucléaire (RMN). La solution après réaction contient une large quantité d'acétate de benzyle et le mécanisme suivant a été proposé : une première étape consistant en la solvolyse du précurseur de zinc par l'alcool benzylique conduit à la formation d'un intermédiaire hydroxylé (Fig.3.A). Cette étape est suivie de réactions de condensation (Fig.3.B) formant l'oxyde de zinc. La taille et la structure cristalline des particules ont été caractérisées à Aveiro par diffraction des rayons X (DRX), microscopie électronique à transmission (MET), microscopie électronique à balayage (MEB) et spectroscopie infrarouge.

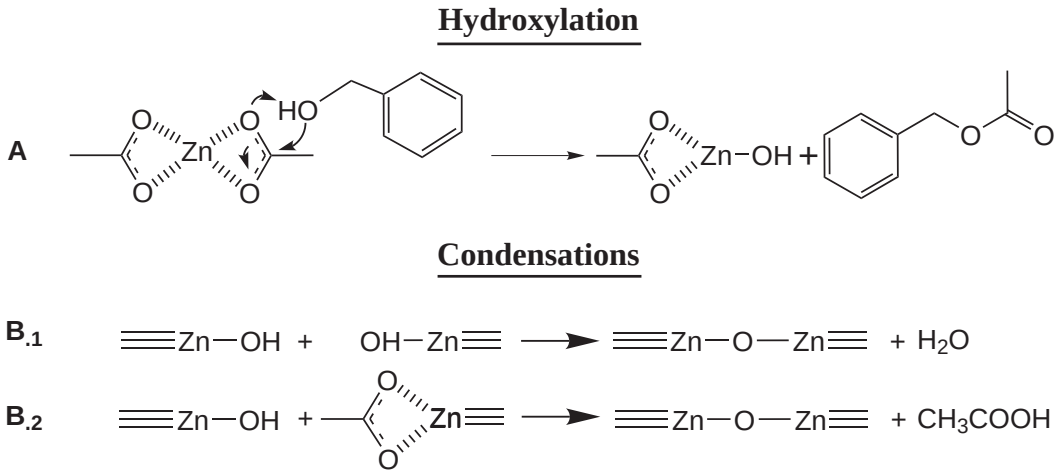

FIGURE A.3: Réactions entre alcool benzylique et acétate de zinc. (A) hydroxylation de l'acétate de zinc, (B) Condensations possibles, ≡ représente tout type de ligand coordiné à l'atome de Zn (OH, acétate, O-Zn).

La synthèse dans l'alcool benzylique pur produit un échantillon hétérogène où co-existent des particules sphériques, triangulaires et allongées pour l'oxyde de zinc pur et dopé manganèse (Fig.4.A), tandis que des petits bâtonnets sont obtenus pour ZnO dopé cobalt. Afin d'améliorer la taille et la forme des particules obtenues, la concentration en alcool benzylique a été contrôlée par l'utilisation d'un co-solvant inerte ; l'anisole. Pour 5% d'alcool benzylique dans l'anisole, des bâtonnets d'environ 400 x 100 nm sont obtenus pour ZnO dopé Co (Fig.4.C). Une plus faible quantité en alcool benzylique améliore le ratio d'aspect (Fig.4.B) ; cependant, une baisse drastique des rendements de la réaction est observée. En conséquence, nous avons concentré cette étude sur des échantillons synthétisés avec au moins 5% d'alcool benzylique dans l'anisole. Pour tous les échantillons étudiés, les particules sont monocristallines (Fig.4.D insert) et présentent une structure hexagonale de type Wurtzite. De plus, aucune phase secondaire (précipité ou inclusion) a été observée par DRX et MET haute résolution même pour les particules comportant la plus grande quantité de dopant.

L'homogénéité et la structure locale du dopant dans la matrice de ZnO ont été caractérisées par spectrométrie UV-VIS en réflexion diffuse, microscopie à haute résolution (HRTEM) et par résonance paramagnétique électronique (RPE). Pour le cobalt et le

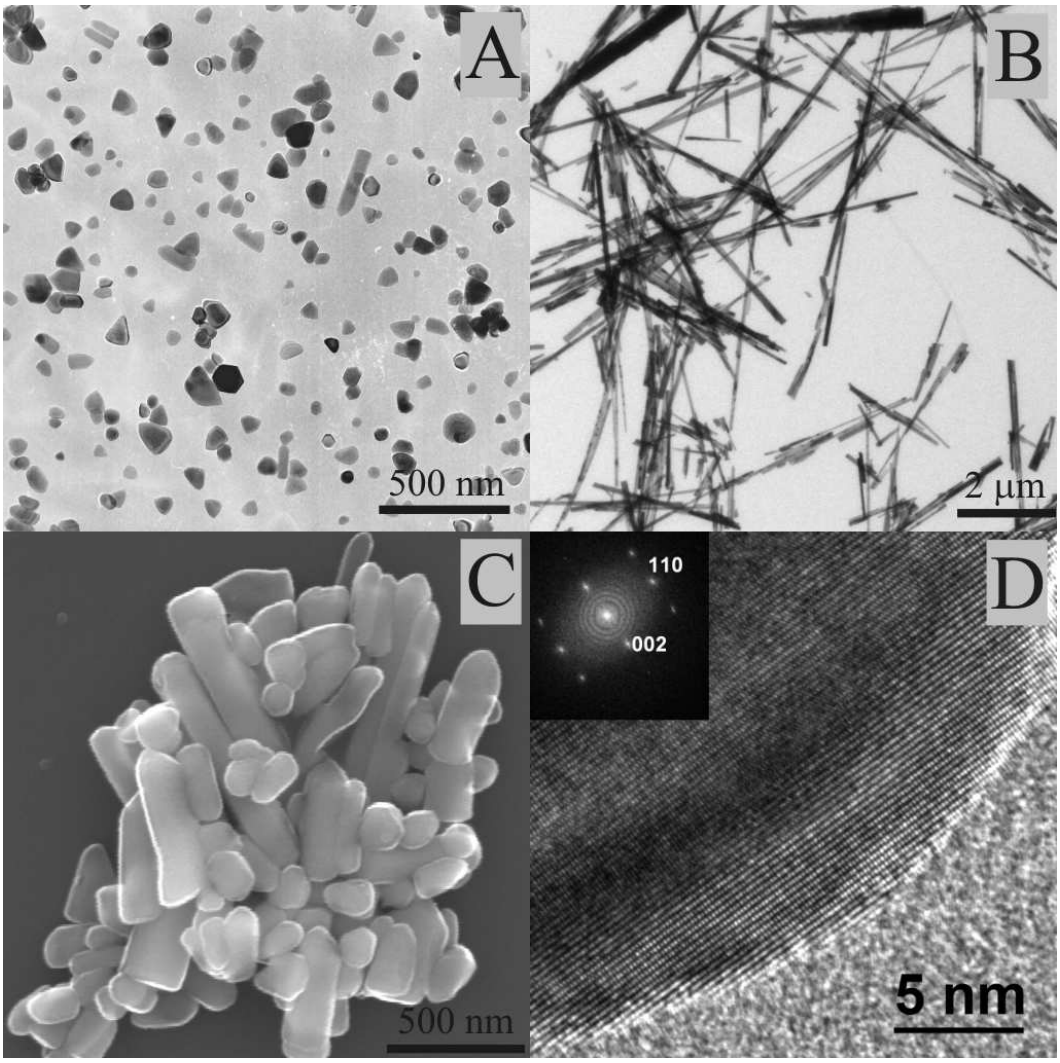

FIGURE A.4: Images MET de : (A) ZnO dopé avec 0.56% de Mn synthetisé dans l'alcool benzylique pur et (B) ZnO dopé Co à 0.65% obtenu dans l'anisole avec traces d'alcool benzylique, image MEB (C) et MET haute résolution (D) avec la transformée de Fourier correspondante (insert) de ZnO dopé Co synthétisé dans un mélange anisole/alcool benzylique (95/5%).

manganèse, nous avons pu montrer que le dopant substitue le zinc dans la structure Wurtzite de manière homogène. En particulier, la RPE a permit d'exclure formellement la présence de phases secondaires.

Les propriétés magnétiques ont été mesurées sur magnétomètres SQUID et VSM à l'Université de Montpellier. Pour les échantillons dopés manganèse un comportement paramagnétique a été observé. Dans le cas du cobalt, les propriétés magnétiques dé-

pendent fortement du solvant de synthèse. Pour toute concentration, ZnO dopé Co synthétisé dans un mélange alcool benzylique/anisole (5/95%) est paramagnétique et ne présente aucun écart par rapport à une loi de Curie (Fig.5). Dans le cas des synthèses effectuées seulement avec l'alcool benzylique, ZnO dopé Co présente un comportement ferromagnétique avec une déviation par rapport à une loi de Curie au-delà de 30 K (Fig. 5). Un moment magnétique à température ambiante de 0,8 μ_B à très faible champ a été mesuré. Les particules présentent un comportement ferromagnétique typique, similaire à ceux publiés pour d'autres particules de ZnO dopé Co. Par exemple, Zitoun et al. ont reporté pour des nanofils de ZnO dopé Co, synthétisés par décomposition de l'acétate de zinc dans la trioctylamine, un comportement ferromagnétique au dessus de 20 K qui persiste jusqu'à température ambiante[34,35]. Si les propriétés magnétiques dépendent du solvant utilisé pour la synthèse, en revanche la contribution paramagnétique pour chaque échantillon est quantitativement liée à la teneur en cobalt (Fig5). La nature du solvant n'est pertinente que pour le signe d'interaction d'échanges entre les spins.

En résumé, nous avons synthétisé des nanoparticules d'oxyde de zinc dopé cobalt et manganèse en utilisant un procédé sol-gel non-hydrolytique. Le dopant se substitue au zinc uniformément, aucune phase secondaire ou cluster n'a été détecté. Le dopage par le manganèse conduit à un comportement paramagnétique. D'autre part, les nanoparticules dopées cobalt présentent une dépendance du comportement magnétique en fonction du solvant utilisé. Synthétisés dans l'alcool benzylique pur, les échantillons ont un comportement essentiellement ferromagnétique et montrent un effet d'hystérésis à travers une large gamme de températures. L'étude EPR a permit de s'assurer que le comportement ferromagnétique est dû aux ions Co^{2+}.

Nanoparticules d'oxyde de zirconium dopées manganèse.

La synthèse de l'oxyde de zirconium consiste en la réaction de l'alcool benzylique avec un alkoxide de métal. La réaction est une condensation entre l'alcool benzylique et isopropoxyde de zirconium appelée élimination d'éther. Cette approche conduit à la

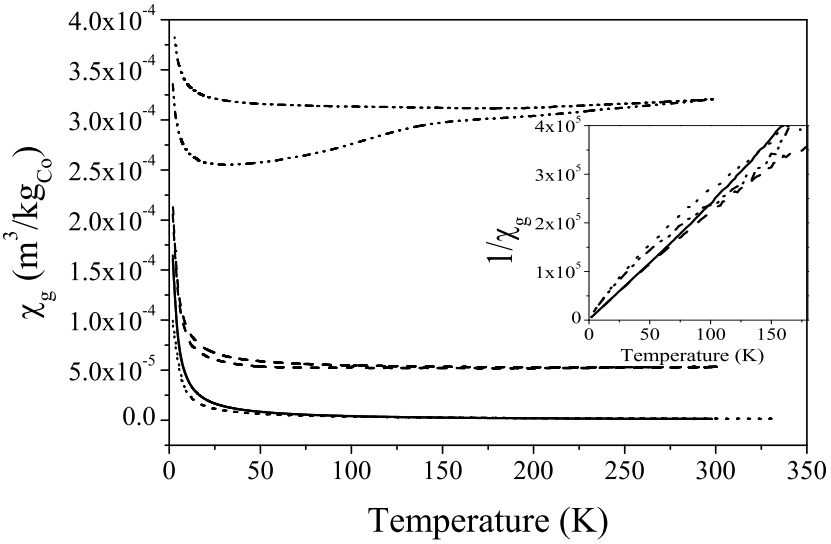

FIGURE A.5: Courbes de magnétisation en fonction de la température (ZFC-FC) de ZnO dopé synthétisé dans un mélange anisole/alcool benzylique (95/5%) avec 0.81% (—) et 4.09% (···) de cobalt, ZnO dopé synthétisé dans l'alcool benzylique pure avec 0.77% (---) et 3.88% (··–) de cobalt. En insert, l'inverse de la magnétisation en fonction de la température pour les 4 échantillons (les échantillons ferromagnétiques étant corrigés de leur contribution ferromagnétique).

formation de nanocristaux sphériques de 3-4 nm de diamètre (Fig.6.A). Les nanoparticules sont monocristallines et ne présentent pas de défauts (Fig.6.B).

Le dopage a été effectué par l'addition d'une quantité de manganèse (II) acétate ou de manganèse (III) acetylacetonate directement dans le mélange réactionnel. La concentration du dopant a été déterminée à l'échelle macroscopique par analyse chimique (ICP-SEA) et à l'échelle nanométrique par spectrométrie EELS (electron energy loss spectroscopy). L'efficacité du dopage est élevée variant autour de 80%-90% pour la gamme de concentration étudiée, c'est-à-dire de 1 à 5%. La phase cristallographique a été étudiée par XRD et microscopie. L'oxyde de zirconium pur et dopé synthétisé par cette approche cristallise dans le système cubique. Contrairement au bulk, à l'échelle nanométrique la structure cubique métastable n'a pas besoin d'être stabilisée[36].

Nous avons effectué une caractérisation méticuleuse du dopant en mettant l'accent sur l'homogénéité, l'environnement local et le degré d'oxydation de l'ion magnétique dans

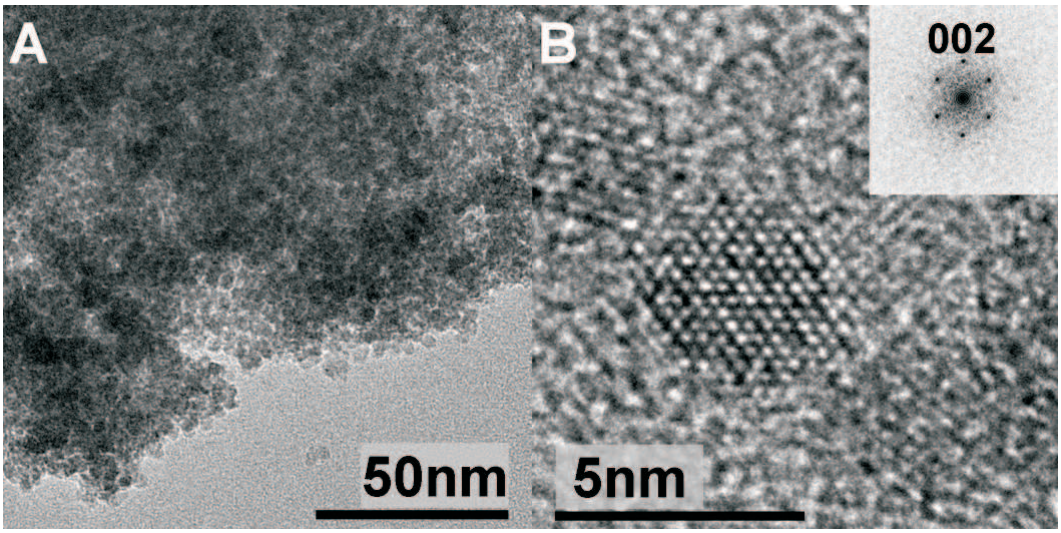

FIGURE A.6: (A) image MET et (B) image MET en haute résolution avec la transformée de Fourier correspondante (insert) de ZrO_2 dopé Mn

la matrice par RPE qui est une technique sensible au degré d'oxydation, à la symétrie et aux interactions spin-spin de centres paramagnétiques. Les calculs théoriques sur la zircone indiquent que les interactions ferromagnétiques sont étroitement liées au degré d'oxydation des ions magnétiques. Les expériences de RPE des échantillons dopés Mn révèlent la coexistence de deux degrés d'oxydation du manganèse ; (II) et (III). Leur quantité est fonction de la concentration de manganèse et non du précurseur utilisé (Table 1). Mn (II) est prédominant pour les échantillons les plus dilués et Mn (III) pour les plus dopés. La présence de Mn^{2+} dans les échantillons synthétisés à partir de $Mn(acac)_3$ peut être expliquée par le faible pouvoir réducteur de l'alcool benzylique. Toutefois, comme chaque Mn^{2+} entraîne la génération d'une lacune d'oxygène, un manganèse dans un plus grand état d'oxydation est plus susceptible de remplacer un atome de zirconium pour des concentrations importantes.

Les mesures magnétiques montrent principalement un comportement paramagnétique (Fig.7). Néanmoins, pour les plus fortes concentrations de dopant, des interactions antiferromagnétiques émergent sur les courbes ZFC/FC (Fig.7). Le ferromagnétisme prédit par le travail théorique de Ostanin[21] et al. n'a pas été observé, même à basse

Précurseurs Mn	%Mn (SEA)	% Mn^{2+} (RPE)	% Mn^{3+} (RPE)	Msat (μ_B/Mn)
$Mn(acac)_3$	1.20	69±2	31±2	4.33
$Mn(ac)_2$	1.39	61±2	39±2	4.27
$Mn(ac)_2$	4.38	9±2	91±2	3.55
$Mn(acac)_3$	4.85	8±2	92±2	3.40

TABLE A.1: échantillons dopés manganèse étudiés dans ce travail. Le tableau montre les précurseurs inorganiques utilisés, la concentration atomique de Mn dans la zircone ($Zr_{(1-x)}Mn_xO_y$), l'état d'oxydation du manganèse selon les mesures de RPE et les moments magnétiques à saturation (Ms), déterminé à partir des courbes de magnétisation ajustées par un fonction de Langevin.

température. Ceci peut être expliqué par le faible état d'oxydation du manganèse qui, dans notre cas, a été estimé être entre (II) et (III). En fait, un état d'oxydation plus grand est davantage susceptible de donner lieu à des interactions ferromagnétiques[21].

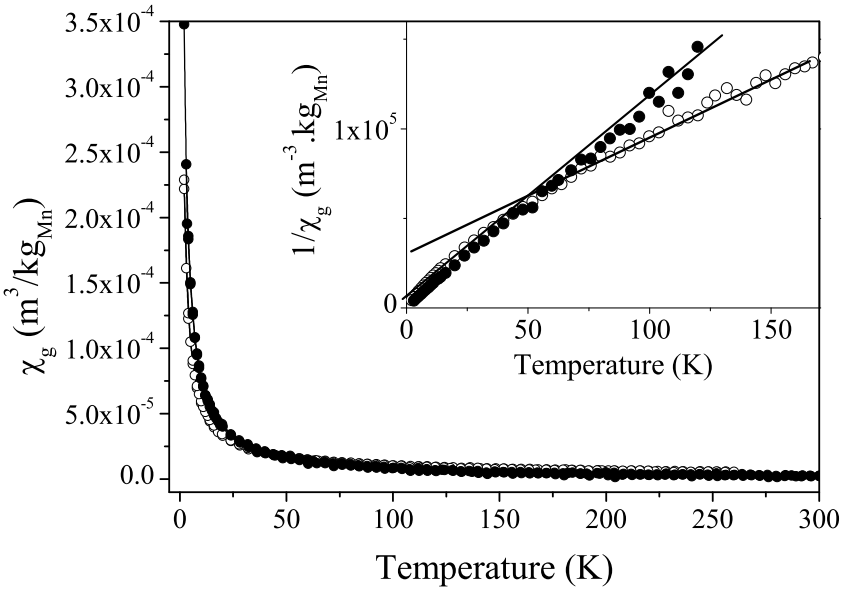

FIGURE A.7: Courbes ZFC/FC mesurées avec un champs magnétique de 50 Oe pour l'échantillon dopé avec 1.20% de Mn (ratio Mn^{2+}/Mn^{3+} de 70/30%) (cercles pleins) et 4.38% de Mn (ratio Mn^{2+}/Mn^{3+} de 10/90%) (cercles vides). En insert, l'inverse de la susceptibilité en fonction de la température et les régressions linéaires correspondantes.

Pour conclure, des nanoparticules de ZrO_2 dopé manganèse ont été synthétisées par une approche non-hydrolytique. Les nanocristaux sont de forme et taille uniformes et une répartition homogène des ions magnétiques a été obtenue. L'environnement du manganèse dilué dans la matrice de zircone a été examiné par RPE. Il a été constaté que le manganèse existe sous deux degrés d'oxydation ; (II) et (III). Les mesures magnétiques montrent principalement un comportement paramagnétique en accord avec les calculs théoriques qui indique un comportement ferromagnétique pour un état d'oxydation de III à IV.

A.3 Partie B : Hétéro-structures magnétiques

A.3.1 État de l'art

Dans la partie précédente, nous avons mis au point une voie de synthèse vers des matériaux homogènes et multifonctionnels. Les DMSs combinent des propriétés semi-conductrices et ferromagnétiques provenant du même matériau. Des matériaux magnétiques et multifonctionnels peuvent aussi être obtenus par l'élaboration d'hétéro-structures[37–40]. Par exemple, des nanoparticules ferromagnétiques entourées d'une couche isolante peuvent montrer des propriétés magnéto-résistives[41,42] et la réalisation de composite d'oxydes ferroélectriques (ou piézoélectriques) et ferromagnétiques est une manière efficace d'obtenir des matériaux multiferroïques[43–45].

Les hétéro-structures étudiées dans ce travail sont des nanoparticules magnétiques de ferrite de cobalt dispersées dans un matériau semi-conducteur ou diélectrique (ZnO ou TiO_2). Le ferrite de cobalt ($CoFe_2O_4$) est un matériau magnétique dur qui a été étudié en détail en raison de sa grande coercivité et aimantation à saturation (environ 80 emu/g) ainsi que sa remarquable stabilité chimique et la dureté mécanique[38,46]. Des particules homogènes peuvent facilement être synthétisées par décomposition ther-

mique en présence d'agent de surface[38,47,48]. La synthèse de ces structures a été réalisée en trois étapes distinctes :

(i) La synthèse de nanoparticules magnétiques uniformes.

(ii) Le dépôt de ces particules sous forme de film.

(iii) Le recouvrement de ces particules par un oxyde.

Le dépôt des nanocristaux magnétique a été réalisé par la technique de Langmuir-Blodgett (LB). Cette technique est un processus de dépôt à température ambiante qui peut être utilisée pour déposer des monocouches et multicouches de matériaux moléculaires ou nanométriques[38,49–54]. ZnO et de TiO_2 ont été déposés par ALD. Pour l'oxyde de titane, nous avons utilisé une nouvelle procédure récemment établie dans notre groupe[55]. L'ALD est par sa nature un procédé qui devrait conduire à un revêtement complet et homogène des particules[56,57]. Ces deux méthodes de dépôt permettent la manipulation de molécules ou particules à l'échelle nanométrique permettant ainsi l'assemblage de superstructures. L'objectif de cette étude était l'investigation des propriétés des différentes phases ainsi que des interactions entre les particules et le film ou entre les particules à travers le film.

A.3.2 Résultats et discussions

Synthèse et caractérisation des nanoparticules de ferrite de cobalt

La synthèse de ferrite de cobalt consiste en la décomposition thermique des précurseurs, Co(oléate)$_2$ et Fe(oléate)$_3$ en présence d'acide oléique. Cette procédure déjà utilisée avec succès pour la synthèse de nanoparticules de ferrite de cobalt permet un contrôle précis de la taille des nanocristaux[47]. Nous avons adapté cette synthèse afin d'obtenir des particules de 10 nm. Les précurseurs utilisés, Co (oléate)$_2$ et Fe(oléate)$_3$, ont été préparés à partir des chlorures de métaux correspondant par réaction avec l'oléate de sodium. Un rapport moléculaire de 1 :1 entre le tensio-actif (acide oléique) et les précurseurs a été utilisé et la réaction a été effectuée à 300 °C pendant une heure. Des particules

de 10 nm de diamètre ont été choisies car c'est un bon compromis entre une taille suffisamment petite pour permettre un bon recouvrement par ALD et suffisamment importante pour obtenir un comportement ferromagnétique à température ambiante. Après la synthèse, la surface des particules est couverte par une quantité incontestable de tensio-actif et, même après un lavage méticuleux, les particules sont obtenues sous la forme d'un solide pâteux. Les observations par MET révèlent des particules sphériques de l'ordre de 8-10 nm, monocristallines, homogène en forme et avec une distribution de taille étroite (Fig.8). L'image haute résolution d'une particule orientée selon le plan (1-1-2) est présenté figure 8 (en haut à droite). Sa transformée de Fourier (power spectra) (en bas à droite) peut être indexé à la structure cubique spinelle de $CoFe_2O_4$. La composition des nanoparticules a été vérifiée par EDX, pour les conditions de synthèse utilisées, le ratio Co/Fe semble être exactement de un Co pour deux Fe.

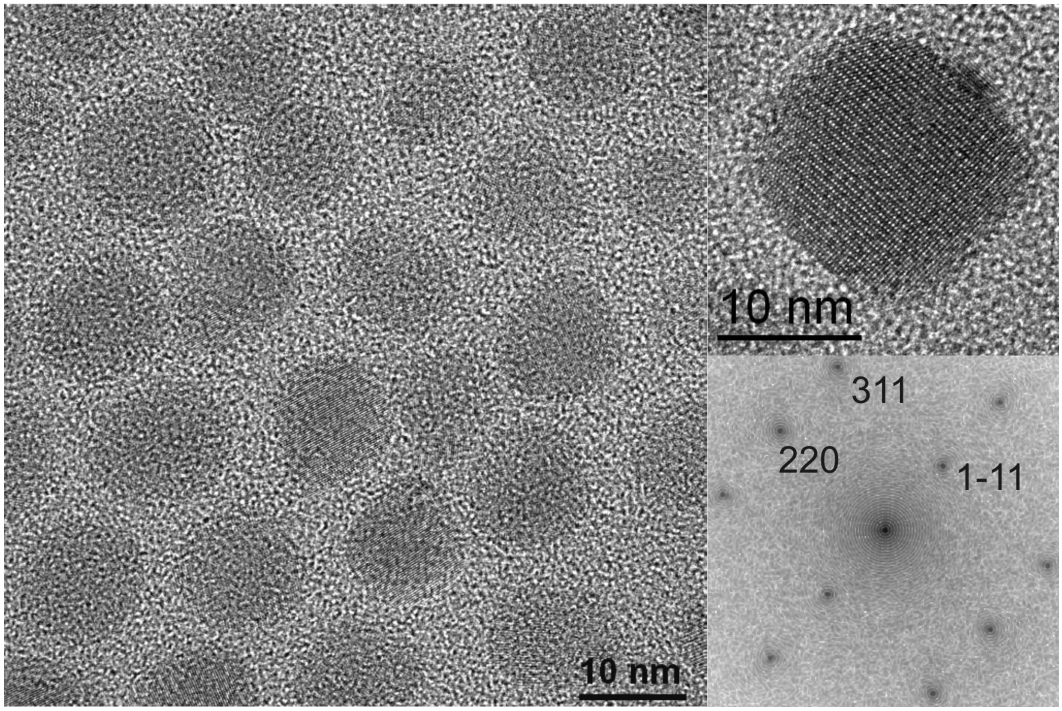

FIGURE A.8: A gauche : image MET d'un ensemble de particules de ferrite de cobalt. A droite : image d'une particule montrant des plans réticulaires croisés (en haut) et la transformée de Fourier correspondante (en bas).

Les propriétés magnétiques de ces particules sous forme de poudre ont été étudiées au moyen d'un magnétomètre SQUID en courant continu (dc) et courant alternatif (ac). Les particules montrent un comportement superparamagnétique. La mesure de l'aimantation en fonction de la température (procédure ZFC/FC) indique que le matériau est magnétique jusqu'à température ambiante, la température de blocage (T_B) étant juste au-dessus 300 K (Fig.9). À 2 K les particules présentent une très grande valeur de champ coercitif (1.8 T), l'aimantation ne sature pas et atteint la valeur de 28 emu/g pour un champ magnétique de $\mu_0 H = 5$ T.

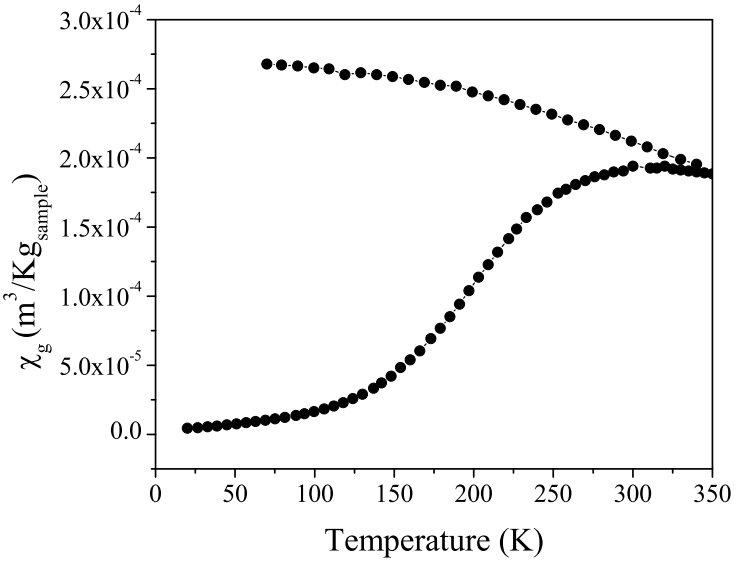

FIGURE A.9: Courbes d'aimantation ZFC-FC du ferrite de cobalt sous un champ magnétique appliqué de 500 Oe.

Dépôt de film de particules par la technique de Langmuir-Blodgett

Pour obtenir des mono- et multi-couches de film de particules, nous avons utilisé la technique de Langmuir-Blodgett. A cet effet, une dispersion stable des particules dans un solvant très volatil a été préparée. Quelques gouttes de la dispersion ont ensuite

été réparties à la surface d'une cuve de Langmuir contenant de l'eau extra pure. Le tensioactif qui reste en surface des particules après la synthèse, a permis d'obtenir un film de Langmuir flottant à l'interface air/eau. Ce film a ensuite été transféré sur du silicium ou de verre en plongeant le substrat à travers la monocouche. Des films comportant deux ou trois couches de particules ont été préparés par dépôts successifs. Les films obtenus ont été contrôlés par MEB et spectroscopie UV-visible. La figure 10 (A et B) montre des micrographes MEB caractéristiques d'une monocouche déposée sur substrat de silicium. Les particules sont organisées sur des domaines homogènes de plusieurs centaines de nanomètres.

Afin d'éliminer l'agent de surface de la surface des particules, nous avons effectué après dépôt une calcination sous vide et sous oxygène. La spectroscopie infrarouge a permis de conclure que l'élimination des molécules organiques est totale pour une température de 400 °C. Les images MEB prises avant (Fig.10.A.B) et après (Fig.10.C.D) le recuit illustrent l'effet de la calcination sur le film. Pour un temps de recuit court, les particules ne forment pas d'agrégats et au contraire, le film semble être plus homogène formant des zones organisées sur quelques micromètres.

Les propriétés magnétiques des particules déposées sur silicium montrent que les films, comme la poudre, sont ferrimagnétiques jusqu'à 300 K (Fig. 11). De plus, la différence de susceptibilité magnétique entre les courbes ZFC et FC est deux fois plus grand pour le film composée de deux couches de particules (Fig.11 cercles) comparé à celui composé d'une monocouche uniquement (Fig.11 carrés), confirmant qu'une même quantité de particule a été déposée couche après couche. Lorsque les films sont recuits, on observe une légère diminution de la susceptibilité, mais l'écart entre les courbes ZFC-FC reste constant (Fig.11 triangles). Dans le cas des films de particules sur substrat de verre (Fig.12), les courbes ZFC-FC sont dominées par le paramagnétisme des impuretés présentes dans le verre. Toutefois, ici encore, la susceptibilité montre clairement une dépendance à l'égard du nombre de couches déposées (Fig.12 insert).

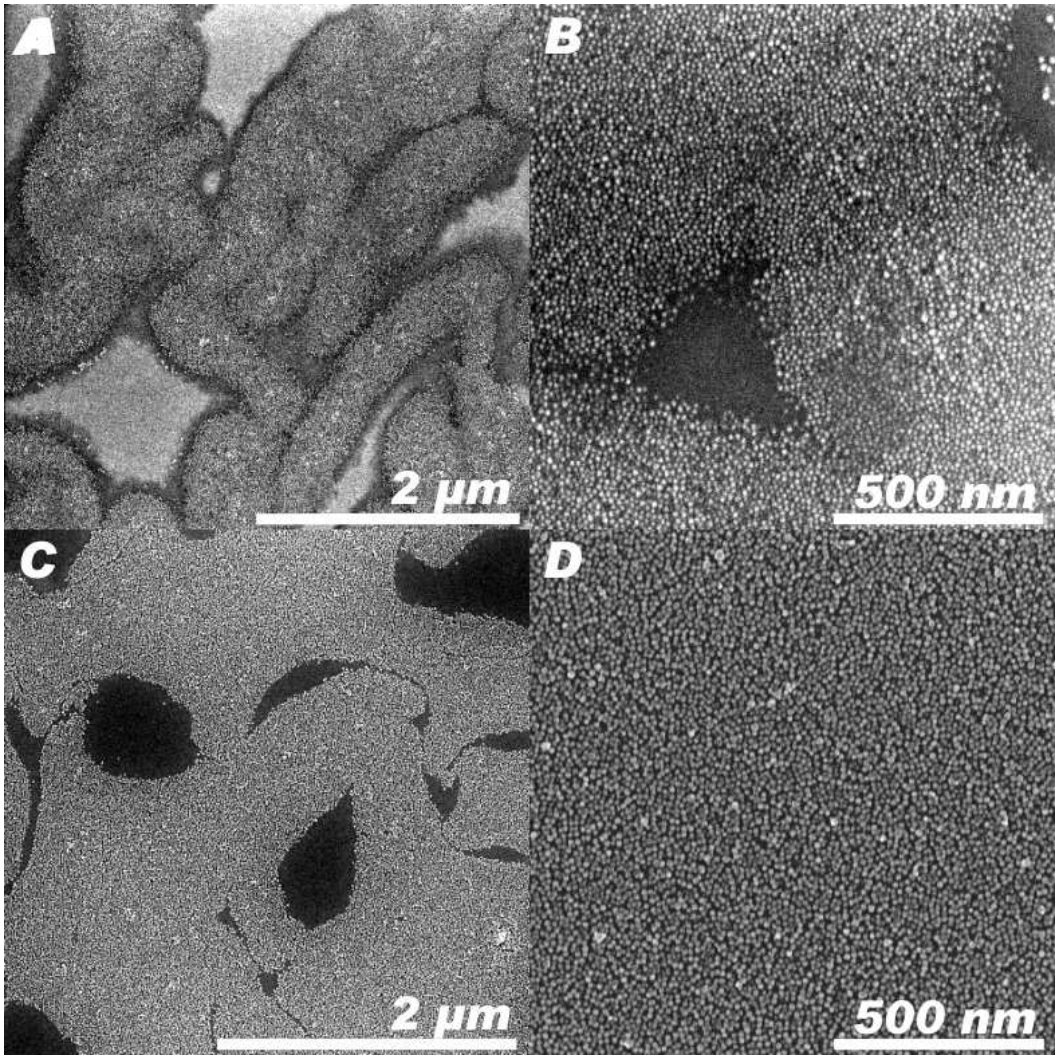

FIGURE A.10: Micrographes MEB d'un film de nanoparticules de $CoFe_2O_4$ déposées sur Si avant calcination, A et B, et après calcination à 400 °C, C et D.

Dépôt de couches minces d'oxyde

Le dépôt des matrices d'oxydes a été réalisé en utilisant un procédé ALD. Cette technique permet un revêtement homogène de l'ensemble des particules.

Les films d'oxyde de zinc ont été déposés en collaboration avec le groupe du Dr. Mato Knez (Max Planck, Halle, Allemagne), à basse température et en utilisant un procédé basé sur la réaction du diéthylzinc avec de l'eau[58]. Des films de 20, 50 et 100 nm de ZnO ont été déposés sur des mono- et bi-couche de particules. Pour la déposition de TiO_2,

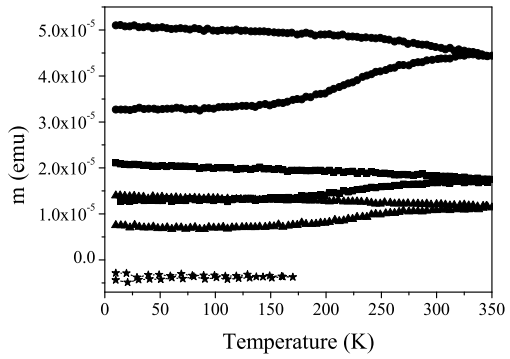

FIGURE A.11: Susceptibilité en fonction de la température des films de particules sur substrat de silicium pour 1 couche (carrés), 2 couches (cercles) et 1 couche après calcination (triangles). (étoiles) Substrat de silicium seul.

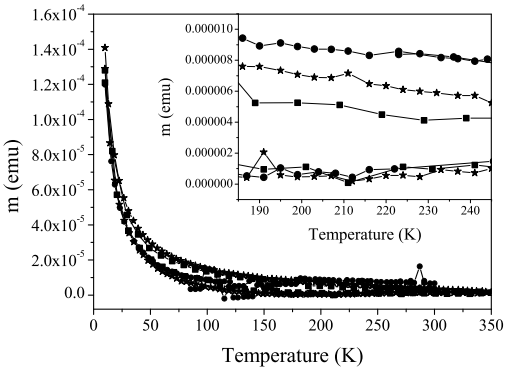

FIGURE A.12: Susceptibilité en fonction de la température pour des films de 1 couche (carrés), 2 couches (étoiles) et 3 couches (cercles) de particules sur substrat de verre.

nous avons utilisé une méthode qui a été développée dans notre groupe. L'approche est basée sur la réaction d'un acide carboxylique avec un alkoxide de métal. L'épaisseur de la couche d'oxyde a été mesurée par réflectométrie des rayons X. Pour le TiO_2 des films de 20 et 27 nm ont été déposés. Des micrographes MEB des l'hétéro-structures sont présentés figure 13. Pour les deux oxides, TiO_2 et ZnO, le revêtement est uniforme sur toute la surface et le film de particule est toujours observable en dessous.

Les mesures de susceptibilité en fonction de la température sont présentées figure 14 pour des films composés d'une monocouche de nanoparticules et recouverts de TiO_2 et ZnO. Les courbes sont similaires à celles des films sans couche d'oxyde. En effet, la température de blocage de la phase magnétique a toujours lieu légèrement au-dessus de 300 K. Les propriétés magnétiques ne sont pas affectées par la croissance d'oxyde et, comme le confirme la microscopie, la taille des particules est maintenue constante durant les différentes étapes de synthèses. Par conséquent, l'approche expérimentale suivie est adaptée pour l'élaboration d'hétéro-structure composée d'une couche quasi-monodisperses de nanoparticules magnetiques.

Pour caractériser les films et savoir si il existe des interactions entre les particules à travers la couche d'oxyde, des mesures magnétiques de temps de relaxation peuvent être

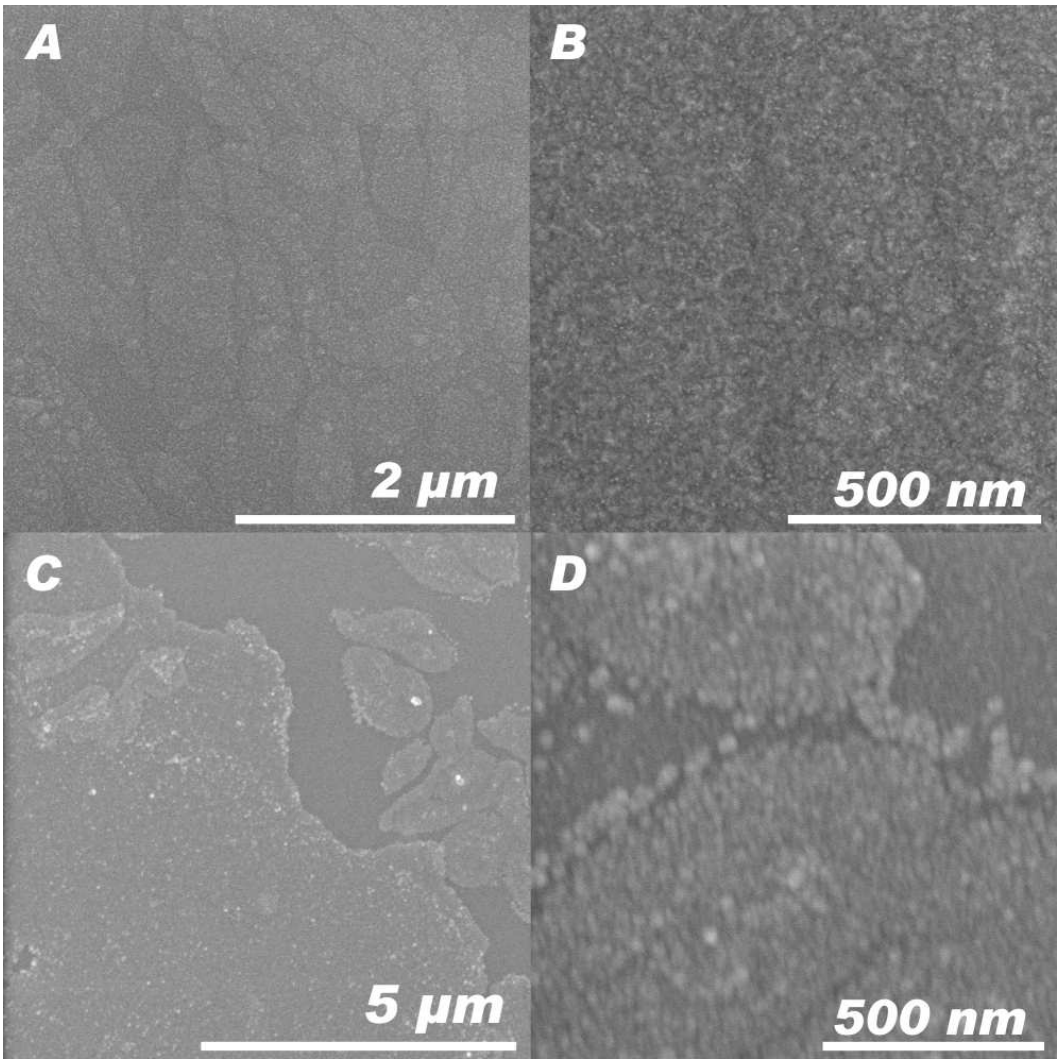

FIGURE A.13: Image MEB de films de ferrite de cobalt recouverts par 50 nm de ZnO (A-B) et 27 nm de TiO_2 (C-D).

mesurées en mode alternatif. Malheureusement, en raison du faible signal du système nous n'avons pas encore réussi à mesurer ce phénomène avec un magnétomètre Squid, même en utilisant un système de mesure RSO.

En résumé, des nanoparticules de ferrite de cobalt ($CoFe_2O_4$) ont été synthétisées par décomposition de précurseurs oléates en présence d'acide oléique. Cette procédure a permis d'obtenir des particules de 8-10 nm, sphériques, monocristallines et homogènes en taille et forme qui présentent un comportement superparamagnétiques en dessus de

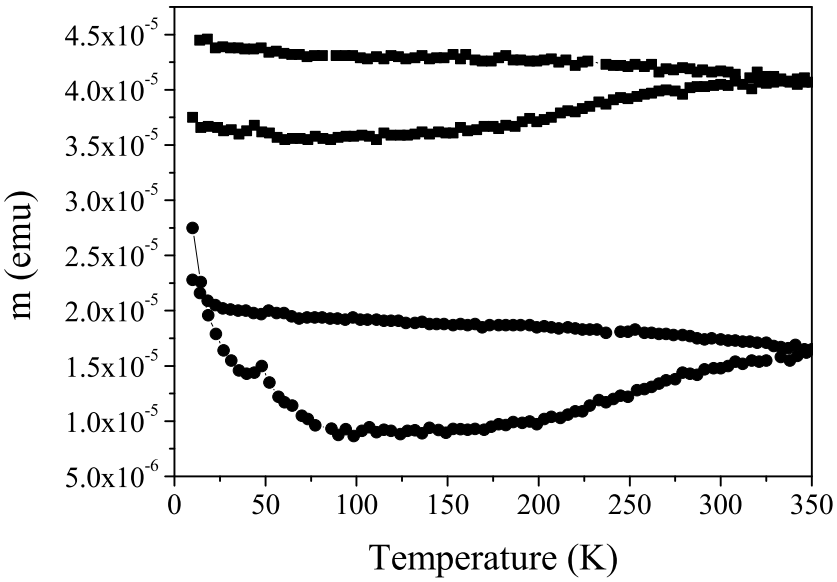

FIGURE A.14: Susceptibilité en fonction de la température de monocouches de particules déposés sur silicium et recouvertes de 100 nm de ZnO (cercles) et 20 nm de TiO_2 (carrés).

310 K. En dessous de cette température, les particules sont dans un état bloqué et presentent une grande coercivité. Des films de particules de ferrite de cobalt ont été déposés avec succès par la technique de Langmuir-Blodgett sur substrats de silicium et verre. Un recuit des films a permis la suppression de l'agent de surface sans détérioration des films. Des domaines de particules homogènes sur plusieurs nanomètres ont pu être obtenues. Les mesures magnétiques réalisées sur les films ont confirmé le succès de dépôts de multicouches. En outre, les films montrent un comportement ferromagnétique à température ambiante comme pour les poudres de nanoparticules. Le revêtement des particules par une matrice d'oxydes (ZnO ou TiO_2) a été réalisé de manière contrôlée par ALD. Les structures résultantes ont une épaisseur bien contrôlée et pourraient donc être utilisées comme systèmes modèles pour l'étude des interactions magnétiques entre particules magnétiques à travers une couche continue d'oxyde.

Malheureusement, les propriétés magnétiques des l'hétéro-structures n'ont pas pu être étudiées en détail à ce jour. Toutefois, certaines analyses sont encore en cours. Par

exemple, des expériences de résonance ferromagnétique sont en cours pour obtenir des informations sur les propriétés magnétiques des particules dispersées dans les matrices d'oxyde. D'autres expériences telles que des mesures de magnétorésistance du composite pourraient apporter quelque lumière sur l'interaction des particules magnétiques avec le film d'oxyde. Enfin, les résultats présentés ici sont juste le point de départ d'un projet consacré à la synthèse de matériaux structurés.

A.4 Conclusion

L'objectif de cette thèse était la synthèse et la caractérisation de matériaux associant des propriétés magnétiques et semi-conductrices. Nous nous sommes concentrés sur des oxydes synthétisés par des voies de chimie douce et en particulier par des procédés de sol gel non-hydrolytique (NHSG). Dans un premier temps nous avons étudié des semi-conducteurs dopés par des impuretés magnétiques afin d'obtenir des semi-conducteurs magnétiques dilués (DMSs). Les voies de synthèses explorées offrent la possibilité de produire des nanoparticules dopées de manière homogène par des métaux de transition. Comme le magnétisme des DMSs est fortement dépendant de l'interaction matrice/dopant, la concentration des porteurs de charge et des défauts du semi-conducteur ; des caractérisations adéquates, mettant l'accent sur l'homogénéité du dopant et sur son environnement local dans la matrice, ont été développées. Ces caractérisations ont été effectuées à l'Université d'Aveiro et à l'Université de Montpellier. En utilisant notre approche, nous souhaitions que les particules synthétisées soient utilisées pour une vérification expérimentale des prédictions théoriques publiées. Ceci est d'un intérêt particulier en raison des récentes recherches théoriques visant à la prédiction de nouveaux DMSs. La seconde approche poursuivie en vue d'obtenir des matériaux ferromagnétiques a été la réalisation d'hétéro-structures composées de couche d'oxyde et de nanoparticules magnétiques. Ce travail est le point de départ pour de futures études consacré à la combinaison de synthèse en solution et de dépôt en phase gazeuse

pour la synthèse de nanoparticules, leur assemblage et la formation d'hétéro-structures multifonctionnelles.

Bibliographie

[1] T. Dietl, H. Ohno, F. Matsukura, J. Cibert, D. Ferrand, "Zener Model Description of Ferromagnetism in Zinc-Blende Magnetic Semiconductors", *Science*, **287**, 1019 (2000). http://dx.doi.org/10.1126/science.287.5455.1019. 145

[2] T. Dietl, "Origin and Control of Ferromagnetism in Dilute Magnetic Semiconductors and Oxides (invited)", *J. Appl. Phys.*, **103**, 07D111 (2008). http://dx.doi.org/10.1063/1.2832613. 145, 147

[3] T. Chanier, M. Sargolzaei, I. Opahle, R. Hayn, K. Koepernik, "LSDA + U versus LSDA : Towards a Better Description of the Magnetic Nearest-neighbor Exchange Coupling in Co- and Mn-doped ZnO", *Phys. Rev. B*, **73**, 134418 (2006). http://dx.doi.org/10.1103/PhysRevB.73.134418. 145

[4] J. M. D. Coey, M. Venkatesan, C. B. Fitzgerald, "Donor Impurity Band Exchange in Dilute Ferromagnetic Oxides", *Nat. Mater.*, **4**, 173 (2005). http://dx.doi.org/10.1038/nmat1310. 145, 147

[5] K. Sato, H. Katayama-Yoshida, "First Principles Materials Design for Semiconductor Spintronics", *Semicond. Sci. Technol.*, **17**, 367 (2002). http://dx.doi.org/10.1088/0268-1242/17/4/309. 145

[6] N. A. Spaldin, "Search for Ferromagnetism in Transition-metal-doped Piezoelectric ZnO", *Phys. Rev. B*, **69**, 125201 (2004). http://dx.doi.org/10.1103/PhysRevB.69.125201. 145

[7] A. Walsh, J. L. F. D. Silva, S.-H. Wei, "Theoretical Description of Carrier Mediated Magnetism in Cobalt Doped ZnO", *Phys. Rev. Lett.*, **100**, 256401 (2008). http://dx.doi.org/10.1103/PhysRevLett.100.256401. 145

[8] Q. Wang, Q. Sun, P. Jena, Y. Kawazoe, "Carrier-mediated Ferromagnetism in N Codoped (Zn,Mn)O $(10\overline{1}0)$ Thin Films", *Phys. Rev. B*, **70**, 052408 (2004). http://dx.doi.org/10.1103/PhysRevB.70.052408. 145

[9] U. Ozgur, I. A. Ya, C. Liu, A. Teke, M. A. Reshchikov, S. Dogan, V. Avrutin, S. J. Cho, H. Morkoc, "A Comprehensive Review of ZnO Materials and Devices", *J. Appl. Phys.*, **98**, 041301 (2005). http://dx.doi.org/10.1063/1.1992666. 145

[10] R. Seshadri, "Zinc Oxide-Based Diluted Magnetic Semiconductors", *Curr. Opin. Solid State Mater. Sci.*, **9**, 1 (2005). http://dx.doi.org/10.1016/j.cossms.2006.03.002. 145, 146

[11] S. Chambers, T. Droubay, C. Wang, K. Rosso, S. Heald, D. Schwartz, K. Kittilstved, D. Gamelin, "Ferromagnetism in Oxide Semiconductors", *Mater. Today*, **9**, 28 (2006). http://dx.doi.org/10.1016/S1369-7021(06)71692-3. 145, 147

[12] T. Fukumura, H. Toyosaki, Y. Yamada, "Magnetic Oxide Semiconductors", *Semicond. Sci. Technol.*, **20**, S103 (2005). http://dx.doi.org/10.1088/0268-1242/20/4/012. 145

[13] K. R. Kittilstved, W. K. Liu, D. R. Gamelin, "Electronic Structure Origins of Polarity-Dependent High-T_C Ferromagnetismin Oxide-Diluted Magnetic Semiconductors", *Nat. Mater.*, **5**, 291 (2006). http://dx.doi.org/10.1038/nmat1616. 145, 147

[14] M. Snure, D. Kumar, A. Tiwari, "Progress in ZnO-based Diluted Magnetic Semiconductors", *J. Miner. Met. Mater. Soc.*, **61**, 72 (2009). http://dx.doi.org/10.1007/s11837-009-0092-9. 145, 146, 147

[15] S. A. Chambers, "Ferromagnetism in Doped Thin-Film Oxide and Nitride Semiconductors and Dielectrics", *Surf. Sci. Rep.*, **61**, 345 (2006). http://dx.doi.org/10.1016/j.surfrep.2006.05.001. 145

[16] C. Liu, F. Yun, H. Morkoc, "Ferromagnetism of ZnO and GaN : A Review", *J. Mater. Sci. : Mater. Electron.*, **16**, 555 (2005). http://dx.doi.org/10.1007/s10854-005-3232-1. 145, 146

[17] A. Bonanni, "Ferromagnetic Nitride-based Semiconductors Doped with Transition Metals and Rare Earths", *Semicond. Sci. Technol.*, **22**, R41 (2007). http://dx.doi.org/10.1088/0268-1242/22/9/R01. 145

[18] S. J. Pearton, C. R. Abernathy, G. T. Thaler, R. M. Frazier, D. P. Norton, F. Ren, Y. D. Park, J. M. Zavada, I. A. Buyanova, *et al.*, "Wide Bandgap GaN-based Semiconductors for Spintronics", *J. Phys. : Condens. Matter*, **16**, R209 (2004). http://dx.doi.org/10.1088/0953-8984/16/7/R03. 145

[19] R. Janisch, P. Gopal, N. A. Spaldin, "Transition Metal-doped TiO_2 and ZnO - Present Status of the Field", *J. Phys. : Condens. Matter*, **17**, R657 (2005). http://dx.doi.org/10.1088/0953-8984/17/27/R01. 145

[20] I. V. Maznichenko, S. Ostanin, A. Ernst, I. Mertig, "First-principles Study of Manganese-stabilized Hafnia", *J. Magn. Magn. Mater.*, **321**, 913 (2009). http://dx.doi.org/10.1016/j.jmmm.2008.11.054. 145

[21] S. Ostanin, A. Ernst, L. M. Sandratskii, P. Bruno, M. Dane, I. D. Hughes, J. B. Staunton, W. Hergert, I. Mertig, J. Kudrnovsky, "Mn-Stabilized Zirconia : From Imitation

Diamonds to a New Potential High-T_C Ferromagnetic Spintronics Material", *Phys. Rev. Lett.*, **98**, 016101 (2007). http://dx.doi.org/10.1103/PhysRevLett.98.016101. 145, 146, 152, 153

[22] S. J. Pearton, W. H. Heo, M. Ivill, D. P. Norton, T. Steiner, "Dilute Magnetic Semiconducting Oxides", *Semicond. Sci. Technol.*, **19**, R59 (2004). http://dx.doi.org/10.1088/0268-1242/19/10/R01. 146, 147

[23] T. Fukumura, Y. Yamada, H. Toyosaki, T. Hasegawa, H. Koinuma, M. Kawasaki, "Exploration of Oxide-Based Diluted Magnetic Semiconductors toward Transparent Spintronics", *Appl. Surf. Sci.*, **223**, 62 (2004). http://dx.doi.org/10.1016/S0169-4332(03)00898-5. 146

[24] W. Prellier, A. Fouchet, B. Mercey, "Oxide-Diluted Magnetic Semiconductors : A Review of the Experimental Status", *J. Phys. : Condens. Matter*, **15**, R1583 (2003). http://dx.doi.org/10.1088/0953-8984/15/37/R01. 146

[25] F. Pan, C. Song, X. Liu, Y. Yang, F. Zeng, "Ferromagnetism and Possible Application in Spintronics of Transition-Metal-Doped ZnO Films", *Mater. Sci. Eng., R*, **62**, 1 (2008). http://dx.doi.org/10.1016/j.mser.2008.04.002. 146, 147

[26] J. Coey, "Dilute Magnetic Oxides", *Curr. Opin. Solid State Mater. Sci.*, **10**, 83 (2006). http://dx.doi.org/10.1016/j.cossms.2006.12.002. 146, 147

[27] B. W. Wessels, "Ferromagnetic Semiconductors and the Role of Disorder", *New J. Phys.*, **10**, 055008 (2008). http://dx.doi.org/10.1088/1367-2630/10/5/055008. 147

[28] X. J. Liu, X. Y. Zhu, J. T. Luo, F. Zeng, F. Pan, "Grain Boundary Defects-Mediated Room Temperature Ferromagnetism in Co-doped ZnO Film", *J. Alloys Compd.*, **482**, 224 (2009). http://dx.doi.org/10.1016/j.jallcom.2009.03.162. 147

[29] A. Quesada, M. A. Garcia, M. Andres, A. Hernando, J. F. Fernandez, A. C. Caballero, M. S. Martin-Gonzalez, F. Briones, "Ferromagnetism in Bulk Co-Zn-O", *J. Appl. Phys.*, **100**, 113909 (2006). http://dx.doi.org/10.1063/1.2399884. 147

[30] M. Niederberger, "Nonaqueous Sol-Gel Routes to Metal Oxide Nanoparticles", *Acc. Chem. Res.*, **40**, 793 (2007). http://dx.doi.org/10.1021/ar600035e. 147

[31] N. Pinna, M. Niederberger, "Surfactant-free Nonaqueous Synthesis of Metal Oxide Nanostructures", *Angew. Chem. Int. Ed.*, **47**, 5292 (2008). http://dx.doi.org/10.1002/anie.200704541. 147

[32] P. H. Mutin, A. Vioux, "Nonhydrolytic Processing of Oxide-Based Materials : Simple Routes to Control Homogeneity, Morphology, and Nanostructure", *Chem. Mater.*, **21**, 582 (2009). http://dx.doi.org/10.1021/cm802348c. 147

[33] M. Niederberger, N. Pinna, *Metal Oxide Nanoparticles in Organic Solvents*, Engineering Materials and Processes (Springer, 2009). ISBN : 978-1-84882-670-0. 147

[34] G. Clavel, N. Pinna, D. Zitoun, "Magnetic Properties of Cobalt and Manganese doped ZnO Nanowires", *Phys. Status Solidi A*, **204**, 118 (2007). http://dx.doi.org/10.1002/pssa.200673025. 150

[35] B. D. Yuhas, D. O. Zitoun, P. J. Pauzauskie, R. R. He, P. D. Yang, "Transition-Metal-doped Zinc Oxide Nanowires", *Angew. Chem., Int. Ed.*, **45**, 420 (2006). http://dx.doi.org/10.1002/anie.200503172. 150

[36] G. Garnweitner, L. M. Goldenberg, O. V. Sakhno, M. Antonietti, M. Niederberger, J. Stumpe, "Large-Scale Synthesis of Organophilic Zirconia Nanoparticles and their Application in Organic-Inorganic Nanocomposites for Efficient Volume Holography", *Small*, **3**, 1626 (2007). http://dx.doi.org/10.1002/smll.200700075. 151

[37] H. Zeng, S. Sun, "Syntheses, Properties, and Potential Applications of Multicomponent Magnetic Nanoparticles", *Adv. Funct. Mater.*, **18**, 391 (2008). http://dx.doi.org/10.1002/adfm.200701211. 154

[38] U. Jeong, X. Teng, Y. Wang, H. Yang, Y. Xia, "Superparamagnetic Colloids : Controlled Synthesis and Niche Applications", *Adv. Mater.*, **19**, 33 (2007). http://dx.doi.org/10.1002/adma.200600674. 154, 155

[39] A. R. de Moraes, C. K. Saul, D. H. Mosca, J. Varalda, P. Schio, A. J. A. de Oliveira, M. A. Canesqui, V. Garcia, D. Demaille, *et al.*, "Magnetoresistance in Granular Magnetic Tunnel Junctions with Fe Nanoparticles Embedded in ZnSe Semiconducting Epilayer", *J. Appl. Phys.*, **103**, 123714 (2008). http://dx.doi.org/10.1063/1.2938071. 154

[40] F. M. Yang, T. C. Chang, P. T. Liu, P. H. Yeh, Y. C. Yu, J. Y. Lin, S. M. Sze, J. C. Lou, "Memory Characteristics of Co Nanocrystal Memory Device with HfO_2 as Blocking Oxide", *Appl. Phys. Lett.*, **90**, 132102 (2007). http://dx.doi.org/10.1063/1.2716845. 154

[41] R. P. Tan, J. Carrey, C. Desvaux, J. Grisolia, P. Renaud, B. Chaudret, M. Respaud, "Transport in Superlattices of Magnetic Nanoparticles : Coulomb Blockade, Hysteresis, and Switching Induced by a Magnetic Field", *Phys. Rev. Lett.*, **99**, 176805 (2007). http://dx.doi.org/10.1103/PhysRevLett.99.176805. 154

[42] X. Batlle, A. Labarta, "Finite-size Effects in Fine Particles : Magnetic and Transport Properties", *J. Phys. D : Appl. Phys.*, **35**, R15 (2002). http://dx.doi.org/10.1088/0022-3727/35/6/201. 154

[43] H. Zheng, J. Wang, S. E. Lofland, Z. Ma, L. Mohaddes-Ardabili, T. Zhao, L. Salamanca-Riba, S. R. Shinde, S. B. Ogale, *et al.*, "Multiferroic $BaTiO_3$-$CoFe_2O_4$ Nanostructures", *Science*, **303**, 661 (2004). http://dx.doi.org/10.1126/science.1094207. 154

[44] S. Mornet, C. Elissalde, O. Bidault, F. Weill, E. Sellier, O. Nguyen, M. Maglione, "Ferroelectric-Based Nanocomposites : Toward Multifunctional Materials", *Chem. Mater.*, **19**, 987 (2007). http://dx.doi.org/10.1021/cm0616735. 154

[45] C.-W. Nan, M. I. Bichurin, S. Dong, D. Viehland, G. Srinivasan, "Multiferroic Magnetoelectric Composites : Historical Perspective, Status, and Future Directions", *J. Appl. Phys.*, **103**, 031101 (2008). http://dx.doi.org/10.1063/1.2836410. 154

[46] M. Grigorova, H. J. Blythe, V. Blaskov, V. Rusanov, V. Petkov, V. Masheva, D. Nihtianova, L. M. Martinez, J. S. Munoz, M. Mikhov, "Magnetic Properties and Mossbauer Spectra of Nanosized $CoFe_2O_4$ Powders", *J. Magn. Magn. Mater.*, **183**, 163 (1998). http://dx.doi.org/10.1016/S0304-8853(97)01031-7. 154

[47] J. Park, J. Joo, S. Kwon, Y. Jang, T. Hyeon, "Synthesis of Monodisperse Spherical Nanocrystals", *Angew. Chem., Int. Ed.*, **46**, 4630 (2007). http://dx.doi.org/10.1002/anie.200603148. 155

[48] X. Jia, D. Chen, X. Jiao, T. He, H. Wang, W. Jiang, "Monodispersed Co, Ni-Ferrite Nanoparticles with Tunable Sizes : Controlled Synthesis, Magnetic Properties, and Surface Modification", *J. Phys. Chem. C*, (2008). http://dx.doi.org/10.1021/jp077019+. 155

[49] P. Masse, S. Ravaine, "The Langmuir-Blodgett Technique : A Powerful Tool to Elaborate Multilayer Colloidal Crystals", *Colloids Surf., A*, **270-271**, 148 (2005). http://dx.doi.org/10.1016/j.colsurfa.2005.05.056. 155

[50] S. Lefebure, C. Menager, V. Cabuil, M. Assenheimer, F. Gallet, C. Flament, "Langmuir Monolayers of Monodispersed Magnetic Nanoparticles Coated with a Surfactant", *J. Phys. Chem. B*, **102**, 2733 (1998). http://dx.doi.org/10.1021/jp980403+. 155

[51] S. Bordacs, A. Agod, Z. Horvolgyi, "Compression of Langmuir Films Composed of Fine Particles : Collapse Mechanism and Wettability", *Langmuir*, **22**, 6944 (2006). http://dx.doi.org/10.1021/la060696v. 155

[52] M. Clemente-Leon, H. Soyer, E. Coronado, C. Mingotaud, C. J. Gomez-Garcia, P. Delhaes, "Langmuir-Blodgett Films of Single-Molecule Nanomagnets", *Angew. Chem., Int. Ed.*, **37**, 2842 (1998). http://dx.doi.org/10.1002/(SICI)1521-3773(19981102)37:20<2842::AID-ANIE2842>3.0.CO;2-B. 155

[53] T. Fried, G. Shemer, G. Markovich, "Ordered Two-Dimensional Arrays of Ferrite Nanoparticles", *Adv. Mater.*, **13**, 1158 (2001). http://dx.doi.org/10.1002/1521-4095(200108)13:15<1158::AID-ADMA1158>3.0.CO;2-6. 155

[54] P. Poddar, T. Telem-Shafir, T. Fried, G. Markovich, "Dipolar Interactions in Two- and Three-Dimensional Magnetic Nanoparticle Arrays", *Phys. Rev. B*, **66**, 060403 (2002). http://dx.doi.org/10.1103/PhysRevB.66.060403. 155

[55] E. Rauwel, G. Clavel, M.-G. Willinger, P. Rauwel, N. Pinna, "Non-aqueous routes to metal oxide thin films by atomic layer deposition", *Angew. Chem., Int. Ed.*, **47**, 3592 (2008). http://dx.doi.org/10.1002/anie.200705550. 155

[56] M. Leskela, M. Kemell, K. Kukli, V. Pore, E. Santala, M. Ritala, J. Lu, "Exploitation of Atomic Layer Deposition for Nanostructured Materials", *Mater. Sci. Eng., C*, **27**, 1504 (2007). http://dx.doi.org/10.1016/j.msec.2006.06.006. 155

[57] M. Knez, K. Nielsch, L. Niinisto, "Synthesis and Surface Engineering of Complex Nanostructures by Atomic Layer Deposition", *Adv. Mater.*, **19**, 3425 (2007). http://dx.doi.org/10.1002/adma.200700079. 155

[58] S.-M. Lee, G. Grass, G.-M. Kim, C. Dresbach, L. Zhang, U. Gösele, M. Knez, "Low-Temperature ZnO Atomic Layer Deposition on Biotemplates : Flexible Photocatalytic ZnO Structures from Eggshell Membranes", *Phys. Chem. Chem. Phys.*, **11**, 3608 (2009). http://dx.doi.org/10.1039/b820436e. 159

Annexe B :

curriculum vitæ

Guylhaine CLAVEL

Universidade de Aveiro
Laboratorio Associado CICECO
Campus Universitario de Santiago
3810-193 Aveiro PORTUGAL
Phone: 0033 631330323
Phone: 00351 912263676
E-mail: clavel@ua.pt

Education

2005-	**PhD.** "Synthesis and Characterization of Nanomaterials containing Magnetic Impurities" Supervisors: **Nicola Pinna** (Universidade de Aveiro, Portugal) and **David Zitoun** (Université Montpellier 2, France)
2004-05	**Postgraduate diploma.** Organic chemistry and solid organization (Université Montpellier 2)
2003-04	**Master.** Organic chemistry (Université Montpellier 2)
2002-03	**Bachelor.** Chemistry (Université Montpellier 2)
2000-02	**2 year university degree in chemistry** (IUT Chimie Sète, Montpellier)
2000	**A levels. Science** (Pézenas, Hérault)

Research experiences

2005	Straining (6 month). Laboratoire de Chimie Moléculaire et Organisation du Solide (UMR 5637, Université Montpellier 2), tutor: Joulia Larionova. "Synthesis of cyano-bridged magnetic nanoparticles using ionic liquid."
2004	Straining (6 month). Laboratoire de Chimie Moléculaire et Organisation du Solide (UMR 5637, Université Montpellier 2), tutor: Joulia Larionova. "Synthesis and characterization of nano-composites based on molecular magnetic nanoparticles."

Languages

French: Native language
English: Fluent
Portuguese: basic knowledge

Publications List

1 - "Formation of Cyano-Bridged Molecule -Based Magnetic Nanoparticles within Hybrid Mesoporous Silica."

G. Clavel, Y. Guari, J. Larionova and C. Guerin, *New J. Chem.*, **2005**, *29*, 275.

http://dx.doi.org/10.1039/b412315h

2 - "Synthesis of Cyano-Bridged Magnetic Nanoparticles Using Room-Temperature Ionic Liquids."

G. Clavel, J. Larionova, Y. Guari, C. Guerin, *Chem. Eur. J.*, **2006**, *12*, 3798.

http://dx.doi.org/10.1002/chem.200500805

3 - "Magnetic Properties of Cobalt and Manganese Doped ZnO Nanowires."

G. Clavel, N. Pinna, D. Zitoun, , *Phys. Status Solidi A*, **2007**, *204*, 118.

http://dx.doi.org/10.1002/pssa.200673025

4 - "Solvent Dependent Shape and Magnetic Properties of Doped ZnO Nanostructures."

G. Clavel, M. G. Willinger, D. Zitoun, N. Pinna, *Adv. Funct. Mater.*, **2007**, *17*, 3159.

http://dx.doi.org/10.1002/adfm.200601142

5 - "Manganese-Doped Zirconia Nanocrystals."

G. Clavel, M. G. Willinger, D. Zitoun, N. Pinna, *Eur. J. Inorg. Chem.*, **2008**, 863.

http://dx.doi.org/10.1002/ejic.200700977

6 - "Non-Aqueous Routes to Metal Oxide Thin Films by Atomic Layer Deposition."

E. Rauwel, **G. Clavel**, M.-G. Willinger, P. Rauwel, N. Pinna, *Angew. Chem. Int. Ed.* **2008**, *47*, 3592 .

http://dx.doi.org/10.1039/b806215c

7 - "Non-Aqueous Sol-Gel Routes Applied to Atomic Layer Deposition of Oxides."

G. Clavel, E. Rauwel, M.-G. Willinger, N. Pinna, *J. Mater. Chem.*, **2009**, *19*, 454.

http://dx.doi.org/10.1039/b806215c

8 - "Transition Metal-Doped ZrO_2 and HfO_2 Nanocrystals."

A. Pucci, **G. Clavel**, M.-G. Willinger, D. Zitoun and N. Pinna, *J. Phys. Chem. C*, **2009**, *113*, 12048.

http://dx.doi.org/10.1021/jp9029375